Ciència i Tecnologia dels Materials

Titanium Dioxide coatings obtained by Thermal Spray technologies and their functional application

by
Marc Gardon Ramos

Prof. Josep Maria Guilemany i Casadamon.

Centre de Projecció Tèrmica, Universitat de Barcelona,
c/Martí i Franquès 1, 08028, Barcelona.

Submitted to the Department of Ciència dels Materials i Enginyeria Metal·lúrgica in Partial Fulfillment of the Requirements for the Degree of Doctor at the Universiat de Barcelona.

Index

0. Motivation and scope

Contribute to Materials Science with an intense engineering point of view is the leitmotif of this Thesis. In order to reach this challenge, it must be entailed an abiding correlation among materials involved, selected technologies and final application of the obtained product. Therefore, for undertaking this commitment and from the kick-off of this doctorate, a permanent quest of coatings that will take a *functional* key role in a device has nurtured the motivation of the project.

Reminding that an initial problem may be solved by means of distinct alternatives; in this survey, real concerns in the industry and in our society are treated with the aim of finding straightforward and worthy solutions using Thermal Spray technologies and Titanium Dioxide feedstock. This text has been considered with the purpose that the reader will depart and land among publications but always correlated around the same concept: get profit of Thermal Spray processes and have a say in the deposition of Titanium Dioxide active layers.

1. Summary

The main subject of this thesis is the fabrication of functional titanium dioxide coatings by means of Atmospheric Plasma Spray (APS) and Cold Gas Spray (CGS). Functional role may be understood as the capacity of TiO_2 surfaces to respond in a determined way under certain conditions. This involved both the understanding of distinct technologies and the real application of the active layers in several fields.

In order to gain a better comprehension about bonding mechanisms on different substrates, the interaction of this metal oxide with plasma jets, combustion flames or nitrogen streams was studied. Most significant achievements in functional Thermal Spray (TS) TiO_2 coatings were reviewed so as to identify new opportunities in recognized lines of research in the last decade and revise detailed technical considerations. It was perceived remarkable occasions regarding APS titanium dioxide coatings in electrochemical applications. Moreover, depositing homogeneous nanostructured anatase layers obtained by CGS would be highly interesting for the photocatalytic degradation of contaminants and also as surface for being used in the biomedical field.

The starting purpose of the doctorate consisted on developing a metal oxide gas sensor based on titanium dioxide using APS. Firstly, conventional coating processes, sensing mechanisms and overall efficiencies were deeply studied. As regards to experimental results, it was observed that H_2 contained in the plasma mixture could reduce TiO_2 towards non stoichiometric or stoichiometric compounds such as titanium sub-oxides (TiO_{2-x}) or Magnéli Phases (Ti_nO_{2n-1}) respectively during the in-flight of the particles. Large accumulation of oxygen vacancies in the crystal lattice of rutile led to a donor level to the conduction band. Therefore, a corrosion-resistant ceramic material with a low electrical resistivity was obtained on ceramic tiles. This unexpected procedure led to deposit APS TiO_{2-x} / Ti_nO_{2n-1} coatings on stainless steel and apply them in electrochemical bi-polar batteries (Engineering and the Environment, University of Southampton). Then, from the created feedback thin stainless steel and aluminium films, carbon-polymer composites or nickel foams as common standard electrode materials were selected and coated.

In all cases, coatings were well-bonded and coated pieces had an increased potential range of operation than uncoated ones. Besides, electric conductivity was boosted, which would decrease the overpotential for electrodeposition and dissolution in lead batteries.

Produce the active layer of a metal oxide gas sensor using APS fed by TiO_2 was still a target to be accomplished. With the aim of offering more innovation to conventional metal oxide sensors, it was determined to build-up the sensing layer on a thin polymeric flexible substrate. It was possible to reach certain spraying conditions that avoided thermal degradation of the polymer. Furthermore, heterogeneous disposition of the coating, where some areas were coated and certain spots uncoated provided electric contact between the electrodes and structure that eased elastic deformation of the film. Satisfactory performances were obtained testing the response of the device in front of a target gas (Group MIND, Universitat de Barcelona). The device had also suitable response as radiation sensor.

Thenceforth, transition to thermally less-aggressive technologies was carried out. Despite some interesting possibilities raised in High Velocity Oxygen Fuel (HVOF), it was decided to focus the efforts on CGS, which does not require melting the material for being deposited. Subsequently, nanostructured anatase was used as feedstock in order to achieve photocatalytic layers with large specific surfaces for applying them in the degradation of different contaminants. It was used a powder able to create chemical bonds with the substrate and among the particles at the impact. Unfortunately, feeding system was repeatedly clogged because of the high agglomerating capacity of the powder. Blends were prepared with copper and microstructured TiO_2 that flowed appropriately so as to avoid the obstruction of the pipelines. First, Cu/nano-TiO_2 coatings were deposited using spraying conditions that favoured the deposition of nanostructured anatase at the top surface, which assured the development of the photocatalytic process. Samples successfully degraded toluene in gaseous phase (Universidad de Las Palmas de Gran Canaria). On the other hand, micro-TiO_2/nano-TiO_2 blend was not suitably deposited onto steel. Ceramic particles may not deform plastically. Thus, chemical bonds with the substrate and among particles had to be boosted for building-up the coatings. Substrate surface

based on APS TiO_{2-x} with controlled roughness provided composition, hardness and required geometry for adhering nano-TiO_2 particles. In this way, CGS nano-TiO_2 coatings were tested for degrading phenol and formic acid in liquid phase. The obtained results equalized or even improved the performance of sol-gel coatings (commercial standard P25® nano-TiO_2).

Attempts to take profit of developing large areas of nano-anatase by CGS were also transferred to biomedical applications. In particular, it was decided to increase the limited bioactivity of Polyetheretherketone (PEEK) implants. However, it was not possible to appropriately bond TiO_2 particles on PEEK. Therefore, metallic Ti coatings were previously deposited onto the polymer by CGS for afterwards spraying nano-TiO_2, following the know-how gained in CGS nano-TiO_2 photocatalysts. Again, lower layer acted as a bond coat between the original substrate and nanostructured anatase. Osteblast cultures were tested on PEEK, CGS Ti on PEEK and CGS nano-TiO_2 deposited on CGS Ti layer (Institut Hospital del Mar d'Investigacions Mèdiques). Higher cell adhesion, proliferation and differentiation were obtained as long as CGS coatings were applied, which leads to an improved bioactivity of polymeric implants.

Below is presented the graphical abstract of this thesis, which includes corresponding publications, unpublished reports and trade secrets.

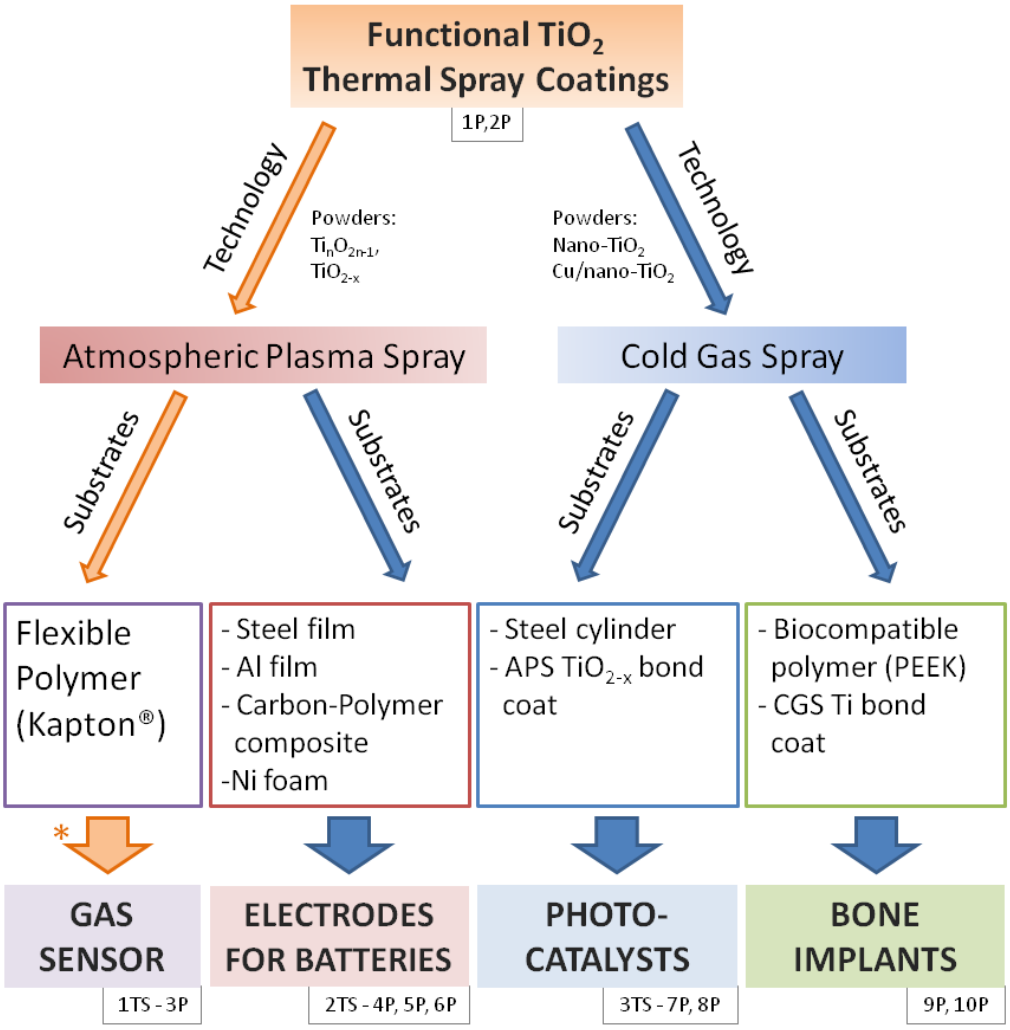

Figure 1. Graphical abstract of the Thesis and related publications, P, and trade secrets, TS (*Starting purpose of the Thesis).

Publications (according figure 1):

[1P] M. Gardon, J.M. Guilemany. "Milestones in functional titanium dioxide thermal spray coatings". Journal of Thermal Spray Technology (2013) Under Review.

[2P] M. Gardon, J.M. Guilemany. “A review on fabrication, sensing mechanisms and performance of metal oxide gas sensors”. Journal of Materials Science: Materials in Electronics 24, 5 (2013) pp. 1410-1421.

[3P] M. Gardon, O. Monereo, G. Vescio, S. Dosta, A. Cirera, J.M. Guilemany. “New procedures for building-up the active layer of gas sensors on flexible polymers”. Surface and Coatings Technology (2013) Under Rerview.

[4P] M. Gardon, J.M. Guilemany. “The influence of titanium sub-oxides in thermal sprayed coatings”. Thermal Spray 2012: Proceedings from the International Thermal Spray Conference and Exposition, May 21-24, Houston, USA. ISBN: 978-1-62708-010-1, pp. 622-626.

[5P] M. Gardon, S. Dosta, J.M. Guilemany, M. Kourasi, B. Mellor, R. Wills. “Improved, high conductivity titanium sub-oxide coated electrodes obtained by Atmospheric Plasma Spray”. Journal of Power Sources 238 (2013) pp. 430-434.

[6P] M. Gardon, S. Dosta, J.M. Guilemany, M. Kourasi, B. Mellor, R. Wills. “Enhanced performance of common electrode materials by means of thermal spray coatings” (2013) To be published.

[7P] M. Gardon, C. Fernández-Rodríguez, M.R. Espino, M. Torrell, S. Dosta, J.M. Guilemany. “Developing photocatalytic Copper/nano-Anatase coatings by Cold Gas Spray”. Surface and Coatings Technology. (2013) Under Review.

[8P] M. Gardon, C. Fernández-Rodríguez, M.R. Espino, M. Torrell, S. Dosta, J.M. Guilemany. “Improved photocatalytic nanostructured anatase coatings obtained by Cold Gas Spray”. (2013) To be published.

[9P] M. Gardon, A. Latorre, M. Torrell, S. Dosta, J. Fernández, J.M. Guilemany. “Cold Gas Spray Titanium coatings onto a biocompatible polymer”. Materials Letters 106 (2013) pp. 97-99.

[10P] M. Gardon, H. Melero, S. Dosta, J. Fernández, J.M. Guilemany. “Enhancing the bioactivity of polymeric implants by means of Cold Gas Spray coatings” (2013) To be published.

Trade Secrets (according figure 1):

1TS M. Gardon, O. Monereo, G. Vescio, A. Cirera, S. Dosta, J. M. Guilemany. "Titanium sub-oxide coatings obtained by Thermal Spray onto a flexible polymer and its application as a gas sensor and radiation sensor". Protected technology: 7th, March 2013. Protocol number: 580.

2TS M. Gardon, J.M. Guilemany, R. Wills. "Titanium oxide coatings obtained by Atmospheric Plasma Spray and its performance as electrodes". Protected technology: 10th, January 2013. Protocol number: 52.

3TS M. Gardon, S. Dosta, J.M. Guilemany. "Photocatalytic nanostructured anatase and copper-anatase coatings obtained by Cold Gas Spray". Protected technology: 2nd, May 2013. Protocol number: 1208.

2. Objectives of the thesis

The foremost objective of this thesis is developing functional titanium dioxide coatings obtained by Thermal Spray processes, whose starting application was intended as gas sensors. Reviewed literature during the thesis and the obtained results drew also the attention to the development of electrodes, photocatalysts and implants. To accomplish this goal, the following key points were reached:

1. Study most significant achievements in functional TiO_2 coatings obtained by Atmospheric Plasma Spray, High-Velocity-Oxygen-Fuel spray and Cold Gas Spray. Determine new opportunities among established lines of research.

2. Revise the fabrication of metal oxide gas sensors and the feasibility of its production using TS technologies and titanium dioxide as feedstock.

3. Understand the sensing mechanisms involved in metal oxide gas sensors and study the viability of reaching commercial levels using TS technologies and titanium dioxide as feedstock.

4. Build-up titanium dioxide coatings by Atmospheric Plasma Spray and study undesired phase transformations.

5. Enhance electric properties of titanium sub-oxide coatings on ceramic tiles.

6. Coat stainless steel substrates and study their performance in simulated batteries.

7. Coat commercial standard electrode materials such as thin stainless steel and aluminium films, carbon-polymer composites and nickel foams. Compare their performance in simulated batteries to uncoated pieces.

8. Study the fabrication of metal oxide gas sensors on a thin polymeric film (Kapton®) by means of APS using TiO_2 as feedstock. Avoid thermal degradation of the polymeric substrate.

9. Develop a surface geometry and disposition of APS coatings that permit the flexible behaviour of the device without decohesion or rupture of the active layer. Test the sensing response in front of gas and radiation.

10. Study nanostructured anatase powders designed for being used in CGS.

11. Blend nano-TiO_2 powder with Cu powder. Study if it provides flowability to the feedstock and spray it using CGS. Enhance the presence of anatase at the top surface of the coatings.

12. Transfer the spraying conditions to a stainless steel cylinder as substrate and test the photocatalytic performance of the samples in liquid or gaseous phase using respectively phenol and toluene as contaminants.

13. Blend nano-TiO_2 powder with microstructured TiO_2 powder. Study if it provides flowability to the feedstock and spray it using CGS. Study its interaction on distinct substrates.

14. Transfer the spraying conditions to a stainless steel cylinder as substrate and test the photocatalytic performance of the samples in liquid phase using phenol and formic acid as contaminants.

15. Use the obtained results in CGS nano-TiO_2 in biomedical applications. Study the feasibility of coating biocompatible polymers in order to boost their bioactivity. Study cell proliferation on the coated samples.

3. Relation of papers

Results and partial discussion chapter of this Thesis is presented as a compilation of papers. Below main reasons that warrant the research associated to each document are compiled:

Paper 1: M. Gardon, J. M. Guilemany. Milestones in functional titanium dioxide thermal spray coatings. Journal of Thermal Spray Technology (2013).

Identifying stablished trends related to active TiO_2 surfaces deposited by thermal spray processes and spot attractive gaps was required for carrying out a Thesis that could provide interesting applications and scientific challenges. Thus, this review was highly useful for guiding the work to topics that can contribute significantly to the state-of-the-art. It was found that titanium sub-oxide coatings obtained by Atmospheric Plasma Spray (APS) and photocatalytic and biomedical applications of nanostructured anatase coatings obtained by Cold Gas Spray (CGS) were researching lines of special interest.

Paper 2: M. Gardon, J. M. Guilemany. A review on fabrication, sensing mechanisms and performance of metal oxide gas sensors. Journal of Materials Science: Materials in Electronics 24, 5 (2013) pp. 1410-1421.

Starting target of the Thesis was based on the development of the active layer in metal oxide gas sensors; thus, competitor technologies in this field, overall sensing mechanisms and performance of these devices had to be deeply studied. In this way, understand how a gas sensor operates and how thermal spray can contribute to this area was priority for suceeding in this objective. It was concluded that Thermal Spray (TS) technologies can provide functional coating materials in this field accomplishing with the required sensing mechanisms.

Paper 3: M. Gardon, J. M. Guilemany. The influence of titanium sub-oxides in thermal spray coatings. Thermal Spray 2012: Proceedings from the International Thermal Spray Conference and Exposition, May 21-24, Houston, USA. ISBN: 978-1-62708-010-1, pp. 622-626.

Thenceforth, research was based on developing electrodes by means of APS. This work focused on understanding and controlling the influence of spraying parameters on electric resistivity of titanium sub-oxide coatings deposited onto ceramic tiles.

Paper 4: M. Gardon, S. Dosta, J. M. Guilemany, M. Kourasi, B. Mellor, R. G. A. Wills. Improved, high conductivity titanium sub-oxide coatings obtained by Atmospheric Plasma Spray. Journal of Power Sources 238 (2013) pp. 430-434.

Know-how gained in the previous work was transferred to stainless steel substrates, which are usually selected as electrodes in batteries. Composition and mechanical properties of the coatings were analyzed. Once proper spraying conditions were selected, coated pieces were used as electrodes in simulated lead batteries and compared with uncoated pieces. This work provided significant data related to how APS TiO_{2-x} coatings may behave in its real application.

Paper 5: M. Gardon, S. Dosta, J. M. Guilemany, M. Kourasi, B. Mellor, R. G. A. Wills. Enhanced performance of common electrode materials by means of Thermal Spray coatings.

Successful performance obtained in Paper 4 encouraged the building-up of coatings onto standard electrode materials commonly used in batteries. Concretely, stainless steel and aluminium thin films, carbon-polymer composites and Ni foams. This work gave the possibility to approach as much as possible APS TiO_{2-x} coatings to standard materials used in this field. Coated and uncoated aluminium sheets were selected for its electrochemical characterization.

Paper 6: M. Gardon, O. Monereo, S. Dosta, G. Vescio, A. Cirera, J. M. Guilemany. New procedures for building-up the active layer of gas sensors on flexible polymers.

The aim of this paper was based on building-up the active layer of a gas sensor correlating all technical considerations given in Paper 2 with experimental results. In this case, it was used a thin flexible polymer as substrate. Main work was focused on avoiding the damage of the substrate and providing a well-bonded active layer. Different concentrations of target gas were tested.

Paper 7: M. Gardon, C. Fernandez, R.M. Espino-Estévez, M. Torrell, S. Dosta, J. M. Guilemany. Developing photocatalytic Copper/nano-Anatase coatings by Cold Gas Spray.

Development of photocatalytic surfaces based on nanostructured anatase is considered to be one of the functional flagship applications in TS processes. Cold Gas Spray avoids undesired phase transformations or growth in the grain size, which makes this technology a suitable solution for building-up these surfaces. However, hard materials such as metal oxides offer many disadvantages as feedstock. Then, blends composed of copper as ductile agent and nano-TiO_2 were prepared and presented in this work, which deals with their deposition using CGS technology. Photocatalytic performance of CGS Cu/nano-TiO_2 coatings was tested for the degradation of toluene in gaseous phase.

Paper 8: M. Gardon, C. Fernández, R. M. Espino-Estévez, S. Dosta, J. M. Guilemany. Improved photocatalytic nanostructured anatase coatings obtained by Cold Gas Spray.

The fabrication of pure nanostructured anatase coatings was presented in this paper. Achieve a complete covering of the substrate by means of CGS nano-TiO_2 particles was the main purpose in order to enlarge the active area of the photocatalyst. Coatings were used for the degradation of phenol and formic acid in aqueous phase and compared to sol gel P25® coatings.

Paper 9: M. Gardon, A. Latorre, M. Torrell, S. Dosta, J. Fernández, J. M. Guilemany. Cold Gas Spray Titanium coatings onto a biocompatible polymer. Materials Letters 106 (2013) pp. 97-99.

Once it was understood how nano-TiO_2 particles could build-up coatings using CGS, findings were transferred to active layers in biomedical applications. Concretely, it was decided to coat polyetheretherketone (PEEK) implants so as to enhance their bioactivity. However, anatase particles were not adequately bonded onto the polymer. Thus, CGS Ti layers were deposited as bond coat. This work compiled the most significant considerations.

Paper 10: M. Gardon, C. Fernández, R. M. Espino-Estévez, S. Dosta, J. M. Guilemany. Enhancing the biocactivity of polymeric implants by means of Cold Gas Spray coatings.

The objective of this paper was providing homogeneous well-bonded CGS nano-TiO_2 coatings on PEEK substrates. Nanostructured anatase particles were sprayed onto Ti layers previously deposited by CGS. Furthermore, it was studied cell adheison, cell proliferation and cell differentiation on PEEK, CGS Ti layers and CGS nano-TiO_2 coatings.

4. Introduction

Before going into more detail regarding TS TiO_2 coatings, some features should be explained. Titanium dioxide crystallizes in three major structures: rutile, anatase and brookite. TiO_2 is commonly used in many different fields as either protecting layer or active surface because of its low cost and chemical stability. Anatase and rutile have been deeply applied as photocatalysts due to its high capacity of generating an electron-hole pair when being irradiated with UV-light. Figure 2 shows Ti-O phase diagram, reduced stoichiometries are highlighted.

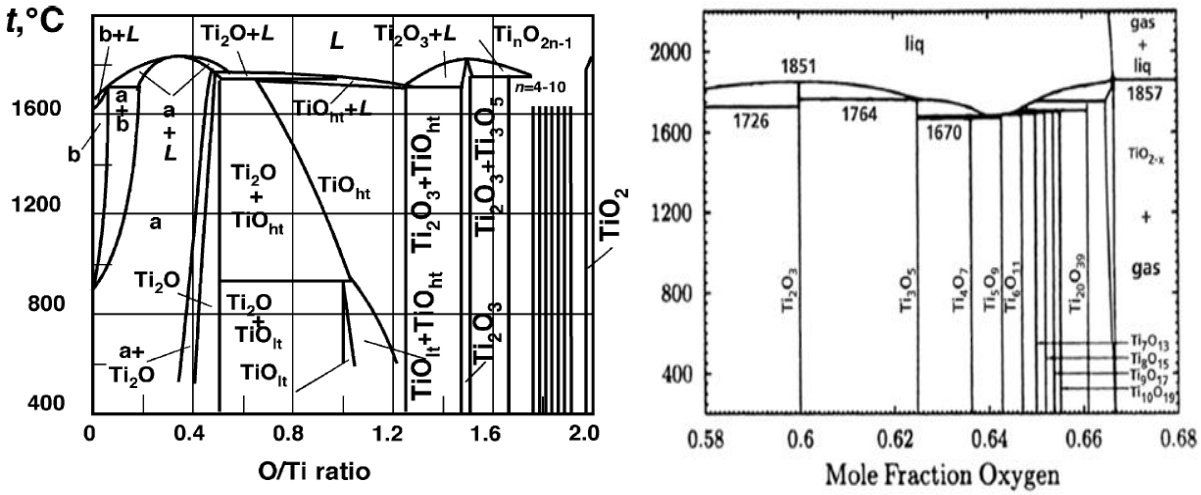

Figure 2. Left: Phase diagram of the Ti-O system [1]. Right: Reduced crystals [2].

Rutile has a large capacity of accumulating oxygen vacancies in its structure. This leads to the creation of a donor level to the conducting band, namely, an increase in the electrical conductivity of the metal oxide. As long as the amount of oxygen vacancies increases, the electrical conductivity is enhanced. Table 1 compiles the electric resistivity for TiO_2 and reduced oxides. Defined stoichiometries below titanium dioxide are known as Magnéli phases (Ti_nO_{2n-1} n=4-10), where the lowest resistivity is found for Ti_4O_7.

Slightly reduced titanium dioxide (titanium sub-oxides: TiO_{2-x}) also carry a stepped decrease of the electrical resistance. The area of existence of this defective non-stoichiometric rutile TiO_{2-x} is very narrow ($x \leq 10^{-2}$) [3]. Even so, it leads to an attractive material with an approximate resistivity of 0,46 Ω·cm [4].

Table 1: Electric resistivity for TiO_2 and reduced oxides [4,5].

Titanium-oxygen phase	TiO_2	Ti_8O_5	Ti_6O_{11}	$Ti_5O_9+Ti_6O_{11}$	Ti_5O_9
Resistivity [Ω·cm]	10^{13}	$4{,}0\cdot10^{-2}$	$1{,}6\cdot10^{-2}$	$2{,}0\cdot10^{-3}$	$1{,}6\cdot10^{-3}$
Titanium-oxygen phase	$Ti_4O_7+Ti_5O_9$	Ti_4O_7	$Ti_3O_5+Ti_4O_7$	Ti_3O_5	
Resistivity [Ω·cm]	$3{,}0\cdot10^{-3}$	$9{,}7\cdot10^{-4}$	$2{,}4\cdot10^{-3}$	$1{,}6\cdot10^{-3}$	

Thus, starting from Ti-O system it is possible to arrive to very distinct materials, which might be of great interest: i) highly efficient photocatalytic surfaces and; ii) electrical conducting ceramic material.

4.1 State-of-the-art

In front of the initial challenge of this thesis, a deep review of the present situation was required. The following document revises the evolution of titanium dioxide coatings obtained by thermal spray processes from its application as passive protecting layers to its use as active surfaces (Paper 1). This survey gave the possibility of recognizing and classifying current synergies in this discipline and considered innovative occasions and scientific gaps that could be filled by the present doctorate.

4.1.1 Paper 1:

M. Gardon, J. M. Guilemany. Milestones in functional titanium dioxide thermal spray coatings, Journal of Thermal Spray Technology.

Milestones in functional Titanium Dioxide Thermal Spray coatings

M. Gardon[1], J. M. Guilemany[1]

[1]Thermal Spray Centre, CPT, University of Barcelona. Martí i franquès 1, 08028, Barcelona, Spain. Contact details: mgardon@cptub.eu - (0034) 634538544

Abstract

The attractive of titanium dioxide coatings from the standpoint of Thermal Spray technologies is explained in this study basing its operation as a functional material. Most significant achievements during the last decade in active layers related to this metal oxide are reviewed in a transition from high-to-low temperatures involved in each technique and the available results are linked with the characteristics of distinct spraying processes. The applications *par excellence* in surface engineering are discussed in comparison to layers deposited by competitor procedures.

Keywords: Functional, coatings, TiO_2, thermal spray, achievements.

1 Introduction

1.1 Metal oxide passive layers

A feasible deposition of metal oxide coatings by Thermal Spray (TS) sourced during the last 20 years from a huge effort in research, which had led to a considerable amount of applications and industrial solutions. Its striking has resided in supplying hardness, wear resistance and corrosion resistance that lacked in certain substrates. Therefore, to provide enhanced mechanical properties to either ductile and more easily oxidizable metals or some ceramics and polymers assured an increase in the working life of the bulk materials. Moreover, the characteristics of TS technologies make possible to achieve it in a cost effective and rapid-manufacturing way, easing the scale-up of the final product.

Quite contributions are available as disclosure patents. J. J. Polidor purposed the protection of refractory parts in machinery used for the casting of steel by means of an Atmospheric Plasma Spray (APS) metal oxide coating [1]. The protecting layer was not only more resistant to the corrosive and erosive effects of molten slag and steel, but also resisted thermal fatigue due to the expansion occurred during the process. A. Makamoto et al. supplied a wear resistance layer that could be applied onto the inside face of the cylinder bore of an engine [2]. Coating composition was based on chromium oxide dispersed into Fe and Mo. In a more detailed way, many authors have reported in scientific journals the deposition of metal oxide coatings by TS for its application as passive-protecting layers. M. Rosso et al. studied the corrosion resistance and properties of metallic pump pistons coated with different percentages of aluminium oxide and titanium dioxide [3]. It was obtained a high corrosion resistance both in saline and acid environment, which could be partly attributed to the inexistence of interconnected pores that do not offer to corrosive media any preferential path to reach the substrate. A slight addition of titania (3%) to alumina provided higher toughness to the coating. Mechanical properties of APS coatings starting from nanostructured Al_2O_3/TiO_2 feedstock were studied by Y. Wang et al. [4].

Surface worn morphologies for powders with nanosized crystallites were smooth without obvious grooves, which may provided substantial improvements in wear resistance compared to standard microstructured powders.

A shift to other spraying technologies and a comparison of the obtained results was also fulfilled. Micro- and nanostructured powders based in alumina and titania were sprayed by Y. Liu et al. using APS and High-Velocity-Oxygen-Fuel Spray (HVOF) [5]. It was observed that HVOF deposited extraordinarily dense coatings, which provided a superior hardness, fracture toughness and abrasion wear resistance compared to APS coatings. Much previously, G. Barbezat et al. had already compared erosion and scuffing resistance of carbide and oxide ceramic coatings obtained by different TS processes [6]. Achieve a satisfactory protection of the bulk material at high temperatures has been also an important market of application. Thus, to improve corrosion resistance of superalloy substrates, such as gas turbine blades, has been a very defined line of research and divulgation [7,8,9]. Besides this, the high electric resistivity of this coatings has been a property exploited for achieving insulating layers in electronics [10,11,12].

In any case, chemical stability at low or high temperatures and mechanical properties of TS metal oxide coatings may not be the only strengths for these materials. Despite its demonstrated behavior as passive coatings, its performance as functional active surfaces in many different fields has also attracted the interest of TS scientists and industrial professionals.

1.2 Titanium dioxide active coatings

Among many metal oxides that can be used as the functional layer in a device, titanium dioxide has drawn a considerable attention. Extracted from minerals like ilmenite, ($FeTiO_3$), rutile and anatase (also with brookite are TiO_2 phases with distinct crystal structures), perovskite ($CaTiO_3$) and titanite ($CaTiSiO_5$), the annual yield of TiO_2 grew approximately above 6 million tons in 2008

and its industrial success is also supported by the lower cost of production compared to other functional metal oxides [13,14]. Only rutile and anatase play a key role in the applications of TiO_2. In both tetragonal structures, a basic building block consists of a titanium atom surrounded by six oxygen atoms in an approximate octahedral disposition. The two bonds between oxygen and titanium at the vertices of the octahedron are slightly longer and in the case of anatase there is a deviation from a 90º bond angle relative among the other four bonds [15]. From a TS perspective, it is a hard material, its melting point is 1870ºC and a phase transformation from anatase (metastable) to rutile can be easily produced in the jets/flames of the TS guns. Titanium dioxide coatings are widely used in distinct applications such as photocatalysis, bone implants, electric devices, renewable energies and gas sensors. Taking this into account, a gradual transition of titanium dioxide coating materials from protecting layers to active functional components has been unsurprisingly welcomed and promoted by all TS industry.

2 Thermal Spray achievements

Temperatures reached in TS processes can develop either undesired phase transformations or alterations in the grain size of the initial TiO_2 powder. Moreover, species like H_2 or O_2 involved in plasma jets or combustion flames change its stoichiometry. Despite this, thermal spray processes have worked in this direction with the aim of achieving functional TiO_2 coatings. Different techniques that are compiled in TS are classified in this work according how the particles are accelerated and if these are bonded in a molten state (e.g. Atmospheric Plasma Spray), semi-molten state (e.g. High-Velocity-Oxygen-Fuel Spray) or solid state (e. g. Cold Gas Spray, CGS). Then, most significant scientific contributions are presented considering the above mentioned classification.

2.1 Atmospheric Plasma Spray

2.1.1 TiO_2 coatings

APS propels molten powder particles towards a substrate by means of a plasma jet. High temperatures up to 28.000ºC are reached and in the case of TiO_2 metastable phases like anatase are transformed to rutile [16]. The starting material is fused and solidified again onto the substrate surface, which leads to an increase in the grain size. The coefficient of thermal expansion (CTE) mismatch of titanium dioxide and typical stainless steel substrates may develop vertical cracks in the cross-section area of the coatings and even complete decohesion that can be avoided with a precise control in the spraying conditions. Besides this, plasma composition plays a key role not just in energy transfer to the particles and the propelling of these, but also in the capacity of altering the stoichiometry of TiO_2. A. Ohmori et al. attributed to H_2 contained in the plasma jet the fact of deoxidizing titanium dioxide during the flight of the particles [17]. Hydrogen may reduce Ti^{4+} to Ti^{3+}, which can lead to the accumulation of a considerable amount of oxygen vacancies. Figure 1 shows a scheme of the operation with anatase-TiO_2 particles in APS process and a typical obtained coating. It is possible to observe how molten particles of titanium dioxide are propelled as droplets by a mixture of gases ($Ar/H_2/He$) that have previously flowed through an electric arc, where the plasma is formed. The possible interaction between the feedstock and the species present in the plasma are also represented. Cross-section area of a representative coating is exhibited; classic lamellar structure can be observed, which is caused by the different oxidation degree of TiO_2. Certain porosity is obtained typical of APS coatings when operating with metal oxides.

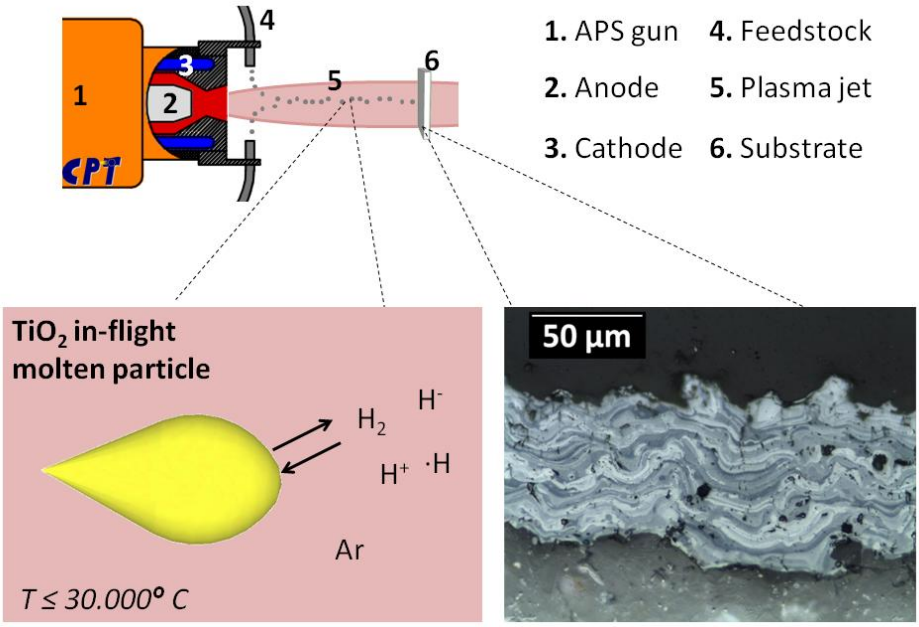

Figure 1. Scheme of an APS gun [18]: interaction between TiO_2 particles and the plasma jet and a representative obtained coating [19].

2.1.2 Applications

a) Photocatalytic degradation of contaminants

Among the distinct systems of photocatalysis, to apply a coating as the active layer is still the most common way for reaching satisfactory efficiencies. Anyhow, forming photoactive layers onto a substrate is not trivial; especially if large functional areas must be coated. With the purpose of solving this, TS processes appeared during the last decade as a group of techniques able to accelerate powder particles towards a substrate in order to build-up photocatalytic coatings with the capacity of degrading pollutants and it has even become the functional flagship application of TS TiO_2.

Since the pioneering paper of A. Fujishima and K. Honda on water splitting by means of the photocatalytic activity of TiO_2 [20], a great amount of research, publication of papers and

patents has been carried out in this field. When irradiating titanium dioxide with UVA-light, holes are photogenerated with a redox potential of +2,53 V versus the standard hydrogen electrode (SHE) in pH 7 solution. Hydroxyl radicals (·OH) are produced after reacting with water (+2,27 V). In addition, the excited electrons have a redox potential of -0,52, which is negative enough to reduce O_2 to O_2^- or H_2O_2 [21]. These highly reactive species formed/adsorbed at the surface of titanium dioxide are then capable to degrade different kind of contaminants in many distinct reaction mechanisms. However, coating processes activated by temperature may carry a decrease in the effectiveness of a photocatalyst because less active phases can be found in the coating. In the case of TiO_2 this is a significant shortcoming due to metastable anatase phase is considered to have an enhanced photocatalytic activity compared to rutile. Thermal condition is also significant when starting feedstock has a nanostructured grain. To work with a crystallite size below 100 nm provides a considerable increase in the specific surface of the coating material, boosting the interaction between the active solid with the species to degrade. Thus, the melting and re-solidification of the powder supposes to increase the grain size of the coating, namely, to decrease the specific area of the active material.

C. Coddet et al. worked in the deposition of TiO_2 by means of APS with the intention of utilize its wear, corrosion and erosion resistance [22-24]. Nonetheless, they also dealt with the purpose of applying the coating material as a photocatalyst and an especial concern rounded the loss of anatase phase and the grain size growth. In a first work starting from a spray dried anatase powder [25], XRD results demonstrated that the amount of the metastable phase in the coatings depended largely on the plasma power and weakly on the nature of the plasma. It was found that the alteration of plasma power with a standard Ar/H_2 mixture and a constant cooling rate increased anatase content from a 35 to a 50%. Later on, in front of the impossibility of boosting the amount of this metastable phase, the same authors selected Suspension Plasma Spray (SPS) for building-up photocatalytic TiO_2 coatings [26]. Feedstock in SPS is a suspension or a powder solution in a liquid, which is radially injected to the plasma jet. In this work, the photocatalytic efficiency of the SPS samples starting from aqueous and alcoholic-based suspensions were evaluated for the degradation of nitrogen oxides. A significant phase

transformation from anatase to rutile and a low decomposition of the pollutants was observed when the coatings were obtained by SPS using an alcoholic-based suspension. However, crystallite size and anatase content were quite preserved in the samples resulting from the aqueous slurry, which led to higher conversion rates of nitrogen oxides (40% NO and 15% NO_x). The same pollutant removal was purposed by C. Coddet et al. in another published article comparing the performance of APS and SPS using spray-dried powders [27]. Plasma-sprayed deposits had an activity below 2%, caused by an almost complete loss of anatase phase. However, SPS samples exhibited activities of 50% and up to 30% in the degradation of NO and NO_x respectively, which were larger than the starting powders and even APS coatings. This was attributed again to the preservation of anatase phase, the elimination of powder impurities (e.g. organic binders) and a cleaning-up of the particle surfaces when crossing the plasma. Other authors have also pointed that the decrease of photocatalytic efficiencies in APS TiO_2 coatings were caused by the loss of anatase in spite of studying the degradation of many different contaminants [28-31].

On the other hand, there are some studies were it has been stated that certain heterogeneous photocatalytic reactions on TiO_2 may not exclusively depend on anatase content. Starting from nanostructured anatase powders, L. Pawlowski et al. obtained SPS rutile coatings with a low content of anatase [32]. No correlation was found between the amount of the metastable phase and the photocatalytic efficiency of the coatings. Moreover, a SPS TiO_2 coating with only an 1,6% of anatase had a specific photocatalytic activity greater than commercial standard material. This discrepancy with the general consensus in the scientific community was attributed by the authors to other factors that may have an influence in TS photocatalytic TiO_2 coatings such as the presence of the hydroxyl radicals and with consideration of coating characteristics like porosity, roughness or thickness (in agreement with P. Ctibor et al. [33]). Furthermore, E. Bannier et al. suggested that the amount of anatase and the photocatalytic efficiency are unsuitable correlated since anatase phase is usually determined by X-Ray Diffraction, which does not correctly represent its value on the top surface of the coating [34].

Visible light photoefficiency is also a remarkable target in TiO_2 coatings. Anion dopant by nitrogen has been extensively studied; absorption to the visible light region is achieved leading to a better exploitation of solar irradiance. Thus, powders with this property are starting to be demanded by TS. Recently, G. Mauer et al. sprayed by SPS anatase powders mixed with TiN milled down to a particle diameter of 5 microns [35]. Photo-thermal deflection spectroscopy of SPS nitrogen-doped shown a higher photoexcitation for doped SPS TiO_2 coatings compared to undoped samples, which is supposed to provide an improved photoactivity. Despite it was not reported any degradation of contaminants, the results opened an interesting path of research in atmospheric and suspension plasma spraying.

A great discussion focused on irreversible anatase-to-rutile phase transformation and efficiencies of APS/SPS anatase photocatalysts has prevailed for the last 10 years. Nevertheless, many scientific works are still being published and the endeavor does not seem to be slowed down [36-38].

b) Bone implants

Although the task of TS titanium dioxide coatings used in biomedical implants does not seem to carry out such a sophisticated interaction similar to the one developed in photocatalysis, it could also be classified as functional. The exceptional anticorrosive and biocompatible properties of titanium are due to the thin protective oxide layer formed onto the metallic surface [39,40]. Therefore, to design bone implants directly with TiO_2 instead of working with Ti has caught the attention of TS. Cells respond to the amount and area of proteins that are available for binding onto an implant [41]. In order to boost this scenario, it had been purposed to use biomaterials coated with TS TiO_2 nanostructured layers. Titanium dioxide nanotextures could provide the formation of a biomimetic structure, where proteins such as fibronectin may be largely anchored. This biomimetism may increase the adhesion strength of osteoblast cells on the

coating surface, which would contribute to enhanced biocompatibilities of TS nano-TiO_2 coatings [42]. Thus, taking into account the importance of the physical structure of a biomaterial surface, much scientific research has focused on its modification. Anyhow, TS processes can skip this step directly providing the above discussed material. Regarding phase composition, J. He et al. found that for a constant nanoroughness, bioactivity of anatase or rutile depended on its hydrophilicity [43]. Anatase phase exhibited better biocompatibility in comparison with rutile, mainly due to its surface wettability. This is also in agreement with D. Yamamoto et al. [44]. In contrast, S. Rossi et al. compared sol-gel-derived anatase- and rutile-structured TiO_2 coatings in soft-tissue environments and no major differences in tissue response were observed [45].

Plasma spray has contributed to this application with successful results particularly using hydroxyapatite (HA) coatings onto titanium implants. However, long-term stability of these coatings may be questionable. Consequently, titanium dioxide has been widely added to hydroxyapatite powders with the aim of improving their mechanical stability. X. B. Zheng et al. fabricated HA/TiO_2 coatings *via* APS and *in vitro* osteoblasts adhesion was analyzed [46]. It was observed that after seven days of culture, osteoblasts completely spread on the coating surface and formed a continuous layer in which individual cells could not be distinguishable. Y. P. Lu et al. also mixed HA and TiO_2 and sprayed it onto a Ti substrate [47]. In this case titanium dioxide was not selected as a material for boosting the interaction with the body fluids/cell, but influencing the mechanical properties of the coatings. TiO_2 acted as obstacles embarrassing stress-induced microcracking, which contributed to the reduction of the near-tip stresses and decreased CTE mismatch. This led to a toughening and strengthening of the coated samples. Besides, the improved bonding may be also caused because of certain hobnobbing of titanium dioxide particles and the oxide layer on the substrate surface. A. Sola et al. worked with a similar intend of HA/TiO_2 coating but with a gradual transition in feedstock composition from TiO_2 to HA [48]. A very good adhesion was obtained at the interface because of the TiO_2-rich region and a more porous disposition was obtained at the top of the coating in the HA-rich region, which is supposed to provide good results as a bone implant. In recent times, M. F.

Morks selected a bio-ceramic material based in titania, zircona and silica [49]. This different alternative suppose to use an APS coating without the poor mechanical properties of APS HA and getting profit from the importance of silicon in bio-active materials for the bonding of bone and muscle as well as cross-linking agent in connective tissues.

Some authors have also chemically treated the obtained APS pure TiO_2 coatings inducing the precipitation of apatite on the surface of TiO_2 sample, which favors biocompatibility of the samples [50,51]. From an industrial point of view, there are also available contributions; R. S. Lima et al. purposed the disclosure of a method for depositing nanostructured TiO_2 powders by means of TS processes that could total or partially melt the particles for its application as bone implants, which includes technologies like Atmospheric Plasma Spray and High-Velocity-Oxygen-Fuel Spray [52].

c) Other applications

Although oxygen vacancies created in the crystal lattice of rutile due to H_2 in the plasma jet may not be a desired phenomenon, it could develop an interesting coating material. Slightly defective nonstoichiometric rutile (TiO_{2-x} $x \leq 0,01$) and reduced stoichiometries such as Magnéli Phases (Ti_nO_{2n-1} n=4-9) may reach very low electric resistivities, especially the latter ones arriving to values comparable with that of graphite [53]. Noticeably, provide layers with a low electric resistivity and maintaining the corrosion resistance of a ceramic material open many possibilities in the electrochemical field. L. M. Berger deeply reviewed this issue highlighting the new opportunities that titanium oxide can offer and the feasibility of using thermal spray processes for acquiring this electrical conducting material as a coating [54]. In addition, it has been also developed the disclosure of various patents. H. Hund et al. prepared by plasma spraying a metal anode based in TiO_{2-x}/Ti_nO_{2n-1} on titanium pieces [55]. The coated samples were used in the electrolysis of alkali chloride as low-cost electrodes able to provide a lifetime far superior than conventional ones. Later on, K. Ellis et al. disclosed also the development of these coated

electrodes [56]. In a preferred embodiment, aluminium sheets were sprayed by APS electrical conducting titanium oxide and it was produced a layer thickness of 120 microns. The coatings were applied as cathodes in electrodeposition of zinc. A successful performance for over 1000 hours of operation was obtained, showing a current density of 450 A/m^2. In a recent publication, J. M. Guilemany et al. got profit of APS rutile coating that contained Magnéli phase Ti_7O_{13} for the solar photoelectrocatalytic degradation of Acid Orange 7 azo dye [57]. Attention has also been centered on the application of reduced stoichiometries in TiO_2 as sliding wear resistant materials [58,59], although its role may not be classified as functional.

2.2 High-Velocity-Oxygen-Fuel Spray

2.2.1 TiO_2 coatings

TS completed a secured step towards a less thermally-aggressive technology with the development of HVOF spray. In this technology, a combustion reaction carried out by either organic substances (propylene, propane or kerosene) and oxygen or hydrogen and oxygen develops a flame (up to 3000ºC) that accelerates the powder particles towards a substrate [16,60]. Lower temperatures compared to APS and higher kinetic energies are crucial concepts for a partial preservation of metastable anatase phase and avoiding grain growth for nanostructured TiO_2 feedstock. Therefore, HVOF guns have deepened in building-up titanium dioxide coatings for its application in active devices.

Figure 2 shows a scheme of the operation with agglomerated nano-TiO_2 particles in HVOF process and a typical obtained coating. In this case, the starting powder is not so influenced by the heat involved in the combustion flame, which leads to in-flight semi-molten particles. Also in this case, interaction with the species present in the flame can be developed and must be taken into account. Cross-section area of a typical HVOF TiO_2 coating onto steel is shown as well. It can be observed that the lamellar structure is not so visible and the greater velocity of the particles has led to a denser coating. A bimodal aspect is also very common

when spraying nanostructured titanium dioxide powders composed by molten zones, where it can be a growth in the grain size and certain anatase-to-rutile phase transformation, and non-molten zones, where the starting material is preserved.

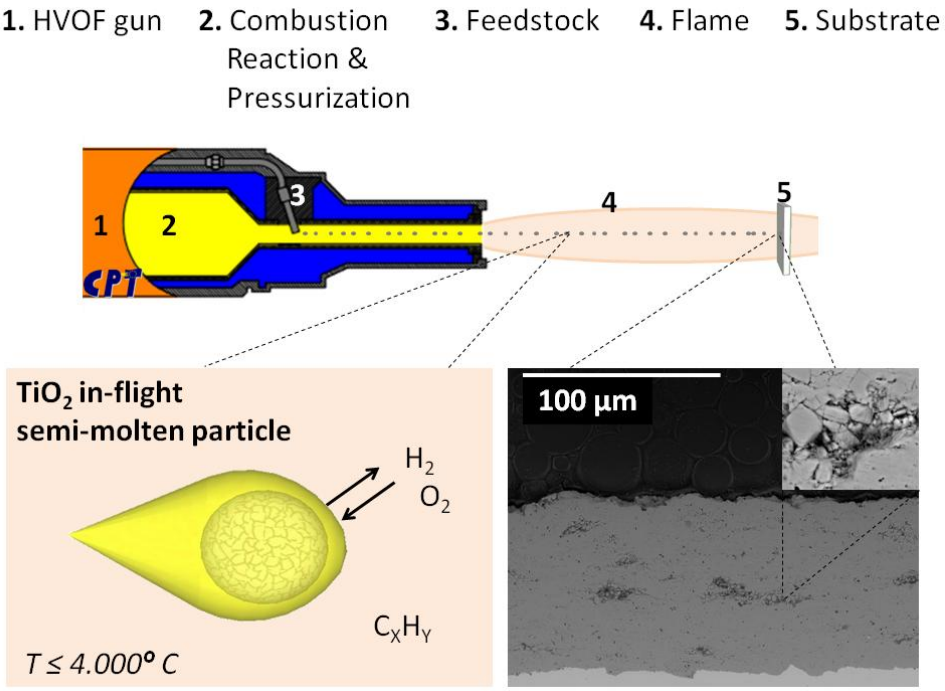

Figure 2. Scheme of the HVOF gun [18]: interaction between TiO_2 particles and the combustion flame and a representative obtained coating (example of a non-molten zone is highlighted).

2.2.2 Applications

a) Photocatalytic degradation of contaminants

Attempts comparing mechanical properties of micro- and nanostructured TiO_2 coatings sprayed by APS and HVOF were carried out in different studies [61,62]. HVOF layers obtained from nanostructured TiO_2 feedstock powders showed enhanced superior abrasion resistance, bond strength, crack propagation resistance and fatigue strength when compared with APS and

HVOF microstructured samples. Consequently, supported from these results, previous or latter obtained outcomes from researching and testing the functional photocatalytic behavior of HVOF nano-TiO_2 are greeted with even more concord. C. Coddet et al. suggested that TiO_2 coatings obtained by HVOF, APS and Vacuum Plasma Spray (VPS) could be used for photocatalytical NO_x removal [63]. In this preliminary study the photocatalytic performance of HVOF coatings was not observed but it was reported that anatase powder provided better photocatalytical activity than the sprayed coatings. The authors attributed again a deep importance to anatase phase but also to the porosity of the samples, which is in command to increase the reactive surfaces and the photocatalytic efficiency. Afterwards, a further study this time focused on nanostructured TiO_2 and Al/TiO_2 coatings built-up by HVOF and its performance degrading NO_x was presented [64]. Ccoatings exhibited firstly poor performances due to an unexpected transformation of anatase phase towards rutile. This was attributed to the axial injection of the powders in the HVOF process. Therefore, a modified HVOF spraying gun was elaborated; concretely the powders were externally injected to the flame. Consequently, an increase of the anatase content in the coatings up to a 65% was found and also the grain size was preserved (18 nm). As regards to the Al/nano-TiO_2 mixture, certain amount of Al_2O_3 was observed and in this case and higher ratio of anatase was obtained. This was explained through the fact that part of the flame heat was used to melt and maybe to vaporize the aluminium particles. NO-NO_x were degraded using nano-TiO_2 and Al/nano-TiO_2 photocatalysts in conversion rates of 24-13% and 43-19% respectively. The authors suggested that aluminium could have contributed to the charges separation during the ultraviolet irradiation enhancing the photocatalytic activity of the coating.

J. Colmenares-Angulo et al. studied the influence of reduced stoichiometries of APS and HVOF titanium dioxide coatings in the photodegradation of 50 mg/L methylene blue [65]. XRD analysis showed that HVOF and APS as-prepared samples showed a presence of Ti_8O_{15} phase, which could indicate the reduction of TiO_2 during the coating process because the existence of reduced phases in the starting feedstock was not reported. Obtained samples were heat treated

in air at 650 °C for a period of 48h to re-oxidize the partially reduced TiO_2, which was confirmed by XRD phase analysis. Then, thermal treated and as-sprayed APS and HVOF samples were tested as photocatalysts. After 48 hours of heterogeneous photocatalysis, non-treated coatings did not exhibit any significant activity. On the other hand, those APS and HVOF samples re-oxidized showed efficiencies of almost 28 and 38% respectively. It was concluded that oxygen vacancies in HVOF and APS TiO_2 coatings are not desired in photocatalytic applications because act as charge recombination centres. The higher efficiency of HVOF sample was attributed to its greater content in anatase. In this way, defect states are re-oxidized increasing the photocatalytic efficiency but anatase-to-rutile phase transformation is also occurred, which may have a negative effect in the desired performance.

A. Ohmori et al. adjusted the spraying conditions in HVOF equipment with the aim of melting partially the starting anatase particles and prove its photocatalytic efficiency [66]. The authors fixed constant oxygen pressure and flow and raised in various steps the fuel gas flow (propane) in order to increase flame temperature. It was found that anatase content was still a 40% when injecting the largest amounts of fuel. In these conditions, the particles were completely molten and impacted on the substrate surface at higher velocities, which led to thinner splats. Then, rapid cooling and solidification may result in the preservation of almost quasi-stable anatase phase. Photocatalytic performance of the samples was tested by means of the degradation of phenol in aqueous phase. Highest rates of pollutant removal were obtained by the coating built-up from the largest ratio of fuel, which had a considerable amount of rutile phase. This dependency was quite different compared to the results reported by other authors. Once again, microstructural features of TiO_2 coatings deposited by TS processes could be playing a key role, although it was not an issue reviewed in this article. Later on, G.-J. Yang et al. tried to clarify which was the dominant microstructural characteristic over photocatalytic activity of HVOF TiO_2 coatings starting from anatase and rutile powders [67]. An increase of the anatase content in the HVOF coatings led to higher photocatalytic activities but in a non-linear relation. Maximum efficiency was obtained starting from anatase powder when operating at low fuel gas

flow, which provided larger amount of anatase in the sprayed material and higher surface area produced by a lower melting of the nanostructured powder. Nevertheless, when starting from rutile powders and operating with high fuel gas flow it was obtained a coating with a 50% of anatase that showed a relative low photocatalytic activity. The authors explained that thermally-powered conditions could: i) transform the upper layer of the coating to rutile, which hinders the area of the material where the expected interaction occurs and; ii) decrease the surface area of the sample. In another work, A. Ohmori et al. compared TiO_2 feedstock based on different grain sizes and studied the photocatalytic degradation of CH_3CHO gas with the obtained HVOF samples [68]. TiO_2 coating using 30nm-agglomerated powder showed higher degradation rate attributed once more to higher anatase content in the coated samples.

In this way, TiO_2 coatings must adequately balance a double effect when adjusting the fuel gas flow in HVOF by means of: a) prevent anatase-to-rutile phase transformation even at the top surface of the coating and; b) provide large specific surface areas. This experimental procedure assures to develop efficient titanium dioxide materials due to the photochemical properties of predominant anatase phase and the existence of more active centres where heterogeneous catatalytic reactions are developed.

HVOF guns can also use feedstock based in suspensions in the same way that SPS does. High Velocity Suspension Fuel Spray (HVSFS) was purposed for pushing once again TS technology to thermally less-aggressive surroundings. However, in this case the suspension was axially injected for avoiding strong flame disturbance causing instabilities in the spray process [69]. R. Gadow et al. successfully deposited nanostructured metal oxide powders like TiO_2, Cr_2O_3, Al_2O_3 and 3YSZ [70]. As regards to TiO_2 samples, from XRD data it could be stated that the coating consisted mainly of anatase (approximately 75%) and the rest of the material was rutile. A further work involved a complete mechanical characterization of the samples and the application of HVSFS nano-TiO_2 coatings as photocatalysts for the degradation of 1 ppm indigo aqueous solution [71]. A significant different microstructure was displayed suggesting 3 different

types of regions: i) fully molten material; ii) well recognizable nanosized particles and; iii) large and thick lamellae with perceivable columnar microstructure. Photocatalytic performance of HVSFS nano-TiO_2 samples was compared to APS and HVOF nano-TiO_2. Results exhibited that those samples fed by suspensions had a superior activity when degrading indigo aqueous solution. Spraying conditions in HSVFS could be adjusted in order to enhance the amount of non-molten nanoparticle agglomerates, which boosted the photocatalytic process. However, lower mechanical and tribological properties were obtained as from these spraying parameters. This was also in agreement with F.-L. Toma et al. [72,73].

b) Bone implants

As it was reported in section 2.1.2, nanotextures present in TiO_2 may increase the adsorption of proteins leading to improved adhesion of osteoblasts, which explains why this material behaves successfully as bone implant. Hence, an expected transition from APS to HVOF in TS TiO_2 coatings was accomplished. Following the tendency observed in APS TiO_2/HA coatings, R. S Lima et al. reinforced HVOF HA coatings with nano-TiO_2 with the purpose of boosting its mechanical properties [74]. Nanostructured TiO_2 + 20 wt.% HA coatings exhibited an adhesive-cohesive failure and had an adhesion value of 68 ± 14 MPa, which was much higher than those values obtained before in TS HA (31 MPa) and HVOF conventional TiO_2 + HA coatings (28 MPa). These results are in agreement with studies carried out by other authors [75,76,77]. R. S. Lima et al. also sprayed separately nano-TiO_2 and HA powders onto Ti-6Al-4V by means of HVOF and APS respectively [78]. Its biocompatibility was compared through osteoblasts cell culture fixed during 15 days in both samples. The results showed that HVOF-sprayed nanostructured titania coated sample exhibited higher osteoblast cell proliferation and adhesion compared to a usual APS HA coating, which may be attributed to TiO_2 nanoroughness present at the top surface of the coating. In a later work, the same authors studied the biocompatible performance of HVOF coatings based in mixtures of nano-TiO_2 and HA [79]. Nano-TiO_2 with a 10 wt.% HA coatings exhibited bond strength levels higher than 77 MPa, which is twice of those

APS HA coatings sprayed onto titanium alloy substrates. Compared to APS HA coatings, results provided strong evidence that HVOF nano-TiO_2 + 10wt.% HA coatings had: i) superior growth and proliferation of cells; ii) commitment towards osteoblastic lineage and, iii) cell/substrate interaction. EDX line scan analysis at the upper layers of the coatings showed microregions containing the existence of Ti, Ca and P atoms. Although XRD did not detect $CaTiO_3$ phase, the authors suggested the possibility of having certain amount of this compound under the sensitivity threshold of XRD analysis. Biological results in this study may be explained by the presence of $CaTiO_3$ because it may help nucleation and growth of apatite, porosity and residual stresses could also play an important role.

Biomedical coatings can also be obtained by HVOF coatings using suspension feedstock in the same sense that photocatalytic applications did. Maybe, this could be moved by assuring nanotextures at the top surface of the samples instead of avoiding anatase-to-rutile phase transformation. Anyhow, remarkable contributions to the state-of-the-art have not been reported yet.

c) Other applications

Reducing fuels such as H_2 are also used in HVOF. Therefore, together with high temperatures, conditions for altering TiO_2 stoichiometry towards TiO_{2-x} or Ti_nO_{2n-1} are reached opening distinct applications in electronics or electrochemistry. L.-M. Berger et al. compared the electric resistivity of coatings obtained by APS and HVOF starting from Ti_5O_9-Ti_6O_{11} powder [54]. It was found that HVOF with hydrogen gas obtained samples with almost half of resistivity compared to APS coatings, which could be attributed to a higher preservation of the O/Ti ratio. This makes HVOF very competitive with APS established procedures in the industry for providing electrical conducting titanium dioxide coatings [80].

Bactericidal effect of HVOF TiO_2 coatings can also be exploited and certain results are available based on the conservation of the photocatalytic performance of the material. Starting from nanostructured anatase powders, B. Jeffery et al. obtained TiO_2 coatings with a 20% of anatase [81]. 50 µL of bacterial cell solution containing Pseudomonas Aeruginosa was pipetted on 304 stainless steel substrate and HVOF TiO_2 coatings. A clear photocatalytic performance was obtained comparing the coated sample with the metallic substrate. However, low killing rate of 24% after 120 min was found. This could be caused by the use of white light, which is less energetic than UV light and the fact that the bacteria could form/embed themselves in a protective biofilm matrix. The authors also attributed the photocatalytic performance of the coatings to anatase phase. Thus, an increase of the performance in the bactericidal effect of the coated samples was expected when optimizing in further studies the amount of anatase phase in the coatings.

2.3 Cold Gas Spray advances

Inevitably, Cold Gas Spray technology is the last stop in this evolution from warm technologies towards thermal spray processes that avoids supplying enough heat to the involved materials for reaching phase transformations or grain growths. CGS does not need temperature for building-up coatings because of particles get adhered on the substrate due to its plastic deformation in solid state. Metallic layers have been successfully attained with the subsequent development of either great amount of research papers or commercial applications. This has been realistic because the plastic deformation of metallic particles at the impact and the locally released heat lead to shear instabilities of the ductile component [82,83]. If the maintenance of the raw microstructure and composition plays a key role in the performance of anatase nanostructured photocatalysts, to use thermal spray non-degrading techniques would be ideal. Thus, CGS appears as an excellent alternative to other conventional TS processes. Nevertheless, it does not seem quite straightforward to produce ceramic coatings by deforming plastically the particles at the impact because of the brittleness of this material.

T. Klassen et al. have dealt with it using titanium dioxide powder as the feedstock material [84]. The ceramic particles were sprayed on titanium, stainless steel, copper and aluminium alloy. It was found that the substrate was plastically deformed at the impact and titanium dioxide particles were mechanically embedded. As long as the ductility of the substrate increased, the metallic jetting between the adhered particles increased and fresh metallic surface was formed. Therefore, *secondary* particles were allowed to bond with these new formed surfaces. A. Ohmori et al. obtained previously very similar results [85]. In a further work, T. Klassen et al. used a powder based in agglomerated crystallites with a size between 5-15 nm [86]. The powder was partly sprayed as-received and another batch was heat treated. The tempered TiO_2 particles bonded more pronouncedly by shear instabilities at substrate sites and the non-tempered behaved more brittle and showed internal fracture. It was concluded that although all the operation parameters influence the formation of the coating, the powder characteristics must be of particular significance. Unfortunately, the impossibility to bond particles among them with the aim of developing layers thicker than the particle diameter results in thin and intermittent coatings. Anyhow, successful applications were reported such as the photocatalytic degradation of dichloroacetic acid carried out using anatase-TiO_2 coatings prepared by APS, HVOF and CGS [87]. It was found that the photocatalytic performance of those coatings obtained by thermally non-agressive techniques like CGS was at least three times higher than HVOF or APS. It was argued that techniques that involved high temperatures converted the anatase content towards rutile, decreasing the efficiency of the photocatalyst. Other applications like the bactericidal effect of CGS anatase coatings were also studied by T. Klassen et al [88]. A kill rate of 99,99% was obtained after 5 minutes of exposing the bacteria Pseudomonas Aeruginosa to UV light with a peak intensity of 360 nm. Certain stagnation of the decay of the bacteria was found, which could be attributed to non-coated areas present due to the impossibility of covering all the surface of the substrate by means of anchoring TiO_2 particles.

Titanium dioxide thick and homogeneous films have successfully been achieved using CGS. M. Fukumoto et al. sprayed 20 micron agglomerated particles of pure anatase with crystalline structure on soft steel, stainless steel and ceramic tile obtaining thicknesses of more than one hundred microns [89]. There was no embedding of the particles into the substrate surface, which suggested a possible chemical bonding. This was ratified by Transmission Electron Microscopy (TEM), where it could be observed that the particles were connected as a single crystal. The nanoscaled structure of the powder led to certain porosity, which developed the breaking down of the particles at the impact in an analogous way that a cold gas sprayed metals are plastically deformed. In a later work, the reactivity and the hardness of different substrate materials were studied in order to understand the deposition behavior [90]. The findings showed that those substrates with a lower standard electrode potential trended to form a thin film of oxide on the surface, which hinders the deposition of the cold sprayed particles. Therefore, substrates with low hardness and reactivity towards oxygen are required properties for reaching a good adhesion in cold sprayed TiO_2 coatings.

M. Fukumoto et al. purposed that the key step for developing TiO_2 powders able to be deposited by CGS was the addition of ammonium sulphate [$(NH_4)_2SO_4$] during the hydrolysis of titanyl sulphate ($TiOSO_4$) and a hydrothermal treatment of the dried powder [91]. When these conditions were applied, it was developed a smoother surface of the metal oxide nanoparticles, which could be attributed to a more uniform agglomeration. Moreover, TEM images revealed a highly oriented aggregated structure. Only TiO_2 with this configuration was capable to reach coating thicknesses about 100 µm by CGS. Stated another way, just the particles produced by this unique chemical route were able to create chemical bonds at the impact. Previously [85], A. Ohmori et al. also gave a considerable importance to the substances used in the agglomeration of the low sized TiO_2 grains assuring that the powder may deform under high transient impact pressure due to the organic binder agglomerating fine particles, which leads to a deformation that may occur similarly to metallic powders in CGS.

Furthermore, S.-Q. Fan et al. deposited nano-TiO_2 powders of 25 nm and 200 nm in diameter by CGS but in this case the material was sprayed in a vacuum chamber (Vacuum Cold Spray, VCS) onto ITO conducting glass and stainless steel for studying the viability of producing Dye Sensitized Solar Cells (DSSC) [92]. Homogeneous nanocrystalline anatase coatings were attained with at thickness of some tens and exhibited good adhesion to the substrate. The coatings were dense but showed certain porosity, which suggested that were formed mainly by agglomeration of small particles upon impact at high velocity. An average Vickers microhardness value much lower than that of sintered TiO_2 bulk was obtained behaving as a ceramic green bodies preform with weak bonding between particles. It was mentioned a preliminary study of DSSC performance that showed high conversion efficiency, but was not included in this survey. Afterwards, photoelectrochemical measurements were carried out under the illumination of a metal halide lamp [93]. Nano-TiO_2 powders were partly sprayed and mixed with poly-ethylene glycol (PEG) before spraying; obtained samples were annealed at 450 ºC. PEG was removed during annealing, which created more porosity. This led to: i) larger pores were the transfer of ions in electrolyte was promoted through diffusion and; ii) increased adsorption of dye per volume of nano-TiO_2 coating. Finally, conversion efficiency of TiO_2 powders mixed with PEG was higher than the values obtained starting from pure TiO_2. In a latter work, the same authors repeated the above experiments but in this case without the presence of PEG [94]. In this survey, annealing was clearly defined to be crucial after building-up the coatings. This post-sintering step improved the contact among the VCS nano-TiO_2 deposited particles and had a considerable effect in the conversion of solar energy. An increase from 2,4% to 4,9% was reached, which suggested how important are sintering steps before spraying in order to boost the interlocking of nano-TiO_2 particles. Apart from these works, no more notable contributions to the state-of-the-art of DSSC are available. Anyhow, cold spray expansion is expected to reach non-traditional markets such as the fabrication of complex conductive patterns in solar cells for photovoltaic applications [95]. Therefore, more attempts are awaited in order to establish motivating performances.

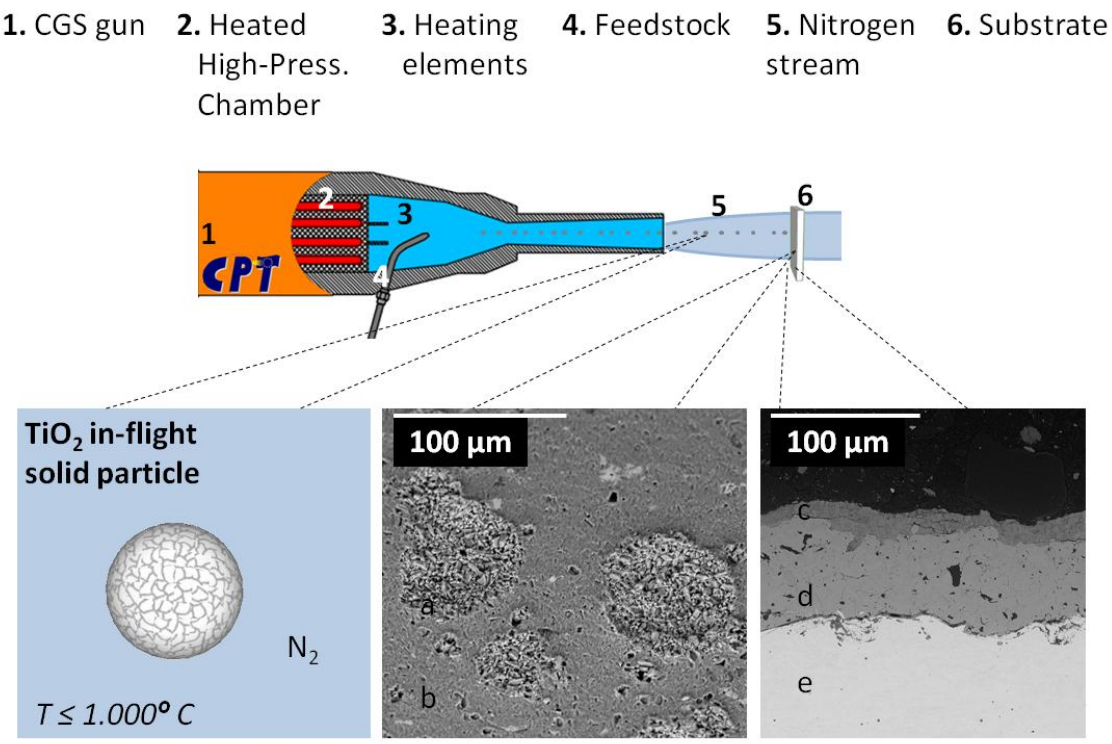

Figure 3. Scheme of a CGS gun [18]: interaction between TiO_2 particles and the nitrogen stream and representative obtained coatings. (a) TiO_2 inlaid particles, (b) aluminium, (c) TiO_2continuous layer, (d) APS TiO_{2-x} coating (e) steel.

An ineludible framework is created for starting a sufficiently justified debate concerning TS scientists and industrial professionals around synthesizing functional hard materials capable to be deposited by CGS throughout new approaches on how these powders must be designed. Having these concepts in mind, solid state anchoring of nano-TiO_2 particles by CGS onto a substrate may be achieved by mechanical embedment or possible chemical bonding among particles and between particles and the substrate when an appropriate synthesis route and spraying conditions are carried out. Figure 3 shows a scheme of the operation with agglomerated nanostructured anatase-TiO_2 particles in CGS process. First, scanning electron microscopy shows a tilted sample of TiO_2 embedded particles on an aluminium substrate. Then, a continuous CGS anatase coating is also shown.

3 Performance against competitors

With the aim of comprehending the competitiveness of functional TS TiO_2 coatings compared to major performances attained by different experimental procedures, it is essential to overview the corresponding outcomes. Therefore, the purpose of this section is to locate the most noteworthy results and significant variables in TS TiO_2 coatings for different active applications in front of available results obtained by other competitor coating technologies. A general scheme of the situation can be exposed although in certain applications is not so unproblematic to compare different TiO_2 coatings, especially when the information is obtained from different authors in separate works. Below is presented foremost data obtained by distinct processes in different surveys regarding the final application of the coatings ordered by charts.

a) Degradation of contaminants

Photodegradation efficiencies when removing pollutants may depend on the target substances and their involved mechanisms. Moreover, heterogeneous catalysis in gaseous and liquid phase diverges significantly and must be adequately differentiated. Table 1 presents available obtained results operating with organic contaminants such as phenol in liquid phase, which is concerning in chemical, petrochemical and pharmaceutical. Besides, Table 2 includes the results related to an inorganic contaminant in gaseous phase such as nitrogen oxides, which are especially controlled in urban atmospheres due to automotive emissions.

Table 1. Phenol degradation in gaseous phase. Most relevant data in various studies.

Deposition technique	Starting concentration	Radiation	Coating composition	Degradation	Bibliographic reference
HVOF	50 mg/L	UV-light, λ= 360 nm	57% anatase	90 % - 100 min	[66]
HVSFS*	50 ppm	UV-light, λ = 360 nm	100% rutile	100 % - 17 min	[96]
Sol-gel	21,6 ppm	UV-light, λ ≈ 335 nm	74% anatase	92 % - 60 min	[97]
Sol-gel TiO_2 fibers	50 mg/L	UV-light, λ = 365 nm	100 % anatase	87 % - 480 min	[98]

* The sprayed samples were annealed at 800 ºC during 30 minutes and complete transformation from anatase to rutile was found. XRD patterns revealed a considerable peak attributed to oxides of the substrate that could influence the interaction with hydrogen peroxide, which would boost the final performance of the coating.

Table 2. Nitrogen oxides degradation in gaseous phase. Most relevant data in various studies.

Deposition technique	Starting concentration	Radiation	Coating composition	Degradation	Bibliographic reference
SPS	2 ppm	UVA 30%, UVB 4%	100% anatase	50% NO, 30% NO_x - 45 min	[27]
CGS	1 ppm (50% humid.)	UV-light, λ = 365 nm	100% anatase	80 % NO - 60 min	[99]
Sol-gel	40 ppm	125 W, Hg-arc lamp	75 % anatase	67 % NO - 40 min	[100]

Incorp. into cement	20 ppmv (50% humid.)	UV-light, λ = 315-400 nm	100% rutile	60 % NO - 25 min	[101]

b) Biomedical applications

Substitute human tissue with biomaterials is a very attractive market of application due to global demand and important investments that are carried out in this field. TS TiO_2 coatings are commonly applied but is not the only industrial procedure for coating implants with this metal oxide. A wide heterogeneity in the exposure of the obtained results may be found in literature. Therefore, below is shown the evolution and proliferation of different cells on TiO_2 coatings obtained by distinct experimental techniques.

Table 3. Bioactivity on distinct TiO_2 coated substrates. Most relevant data in various studies.

Deposition technique	**Cell**	**Starting cell culture**	**Cell proliferation**	**Bibliographic reference**
HVOF	Human mesenchymal stem cell	$1{,}5 \cdot 10^6$ cells (day 0)	$7 \cdot 10^6$ cells (day 14)	[79,102]
TiO_2 nanowires (oxidation process)*****	Human osteosarcoma cells	$5 \cdot 10^4$ cells (day 0)	$9 \cdot 10^4$ cells (day 35)	[103]
Microarc oxidation**φ**	MG63 cell	$2{,}5 \cdot 10^4$ cells (day 5)	$9{,}5 \cdot 10^4$ cells (day 7)	[104]
Sol-gel	Human osteosarcoma cells	10^4 cells (day 0)	$2 \cdot 10^4$ cells (day 5)	[105]

* Obtained from a HVOF TiO2 coating that was gas heat treated (same study compared both coating materials and TiO2 nanowires improved HVOF samples).

φ The oxidation was developed on a TiO2-based coating containing P.

c) Conversion of solar energy

Despite DSSC are a relative new procedure for exploiting solar energy and some advances in materials and dyes are required, it is oddly the application less worked in terms of R+D+i in TS technologies. Thickness of the coatings is especially critical in this case and has a huge influence on the conversion efficiency. Therefore, it must be taken into account that the distinct collected values cannot be directly compared but give a perspective of the present situation.

Table 4 Conversion efficiency in DSSC. Most relevant data in various studies is presented.

Deposition technique	**Coating thickness**	**Radiation**	**Conversion Efficiency**	**Bibliographic reference**
VCS	15 µm	Xe lamp, 100 mW/cm^2	2,4 % - 4,9 %*	[94]
Spray Pyrolisis Deposition	6, 12, 20, 30 and 50 µm	AM-1.5, 100 mW/cm^2	5,1 %	[106]
Sol-gel	10 µm	Diffuse daylight	12 %	[107]
Doctor blade method	6-10 µm	AM-1.5, 100 mW/cm^2	7,9 %	[108]

* After annealing.

d) Disinfection of surfaces

Biomedical restrictions require surfaces free of bacteria in order to reach disinfected atmospheres. Therefore, bactericidal products may help to reach appropriate working environments and also can be applied as coatings onto surgical equipment. In addition, their application can be spread to other markets where sterilization of materials is required, which enhances the interest of deposit TS TiO_2 layers with success. Table 5 presents the data.

Table 5. Bactericidal coatings obtained by different techniques and most relevant data.

Deposition technique	**Bacteria**	**Radiation**	**Degradation**	**Bibliographic reference**
HVOF	P. Areuginosa	White light, λ = 380-750 nm	24 % - 120 min	[81]
CGS*	P. Areuginosa	UVA light, λ ≤ 385 nm	99,99 % - 5 min	[88]
Sol-Gel route*	P. Areuginosa	UV light, λ = 356 nm	99,99 % - 60 min	[109]
Jet Spray Screen Print.	P. Areuginosa	UV LED	99,99 % - 25 min	[110]

*It must be noted that both studies reported a limited performance due to the surfaces were not completely covered by the photocatalytic particles. This could be boosted by CGS applying nano-TiO2 powders synthesized for being deposited homogeneously creating chemical bonds with the substrate, which would lead to a complete covering.

4 Conclusions

The use of titanium dioxide as a ceramic material has not been limited to the protection of a substrate in surface manufacturing. Advances in surface engineering related to many different functional applications involving this metal oxide have not gone unnoticed for Thermal Spray technologies. Consequently, over more than a decade of toil has been fulfilled and interesting solutions are being reached, which can solve the scale-up of these coating products towards industrial development.

Chiefly, the ability of titanium dioxide to create an electron-hole pair when irradiating the solid with UV-light has pushed the interest of Thermal Spray to develop photocalytic layers able to degrade different contaminants and bacteria. Nonetheless, the heat entailed in the process supposes two main disadvantages: i) loss of anatase phase, which is presumed to be more active and; ii) increase of the grain size, which reduces the specific area of the solid. Despite this, reviewed literature suggests that pure anatase coatings are not the optimum material; a certain synergic effect is found when rutile is also present. Therefore, Atmospheric Plasma Spray fed by suspensions or solutions may overcome this issue. High Velocity Oxygen Fuel spray can work it out by adjusting the spraying conditions or even also using liquid feedstock. In this way, research groups and companies that operate with these processes may not reject to research and trade with this material with the aim of achieving photocatalytic applications because enough succeed has been reported and proved to report benefits. Notwithstanding, recent progress in Cold Gas Spray is demonstrating that is feasible to deposit homogeneous well-bonded nanostructured anatase coatings. More investigations on the powders are still required but an attractive trend could source and a new commercial coating technique and standard material could be established, which would unseat the rest of TS technologies and even competitor procedures.

As regards to bone implants, the addition of nano-TiO_2 to HA has improved the mechanical properties of TS coatings. Furthermore, nanostructure of the metal oxide can play a key role boosting protein adsorption, which leads to an enhanced cell adhesion. It is supposed that hydrophilic TiO_2 phases like anatase could help to induce this behavior but more research must be carried out for demonstrating this statement. Therefore, in spite of the involved temperature, Thermal Spray processes able to provide coatings with nanosized TiO_2 grains such as Suspension Plasma Spray and High Velocity Oxygen Fuel are facing an interesting business plan as well. Cold Gas Spray has not proved yet the possibility of developing implants basing its composition in nanostructured titanium dioxide, although its hatching does not seem far away.

Solar energy conversion and other different applications of nano-TiO_2 are demanding a major thrust from Thermal Spray in order to achieve successful efficiencies. More to the point, electrical resistivity of reduced stoichiometries of titanium dioxide together with their corrosion resistance may not be forgotten and interesting lines of research are open, which could contribute in many different devices especially related to electrochemistry.

5 Acknowledgements

The authors wish to thank the Generalitat de Catalunya for the financial support for this research project 2009 SGR 00390.

6 References

[1] J. J. Polidor. United States Patent 4.877.705.

[2] A. Makoto, N. Akio, M. Takashi. JP2004232035 (2004).

[3] M. Rosso, A. Scrivani, D. Ugues, S. Bertini. Corrosion resistance and properties of pump pistons coated with hard materials. International Journal of Refractory Metals and Hard Materials 19, 1 (2001) pp. 45.

[4] You Wang, Stephen Jiang, Meidong Wang, Shihe Wang, T.Danny Xiao, Peter R Strutt. Abrasive wear characteristics of plasma sprayed nanostructured alumina/titania coatings. Wear 237, 2 (2000) pp. 176.

[5] Yourong Liu, Traugott E. Fischera, Andrew Dent. Comparison of HVOF and plasma-sprayed alumina/titania coatings—microstructure, mechanical properties and abrasion behavior. Surface and Coatings Technology 167, 1 (2003) pp. 68.

[6] G. Barbezat, A.R. Nicol, A. Sickinger. Abrasion, erosion and scuffing resistance of carbide and oxide ceramic thermal sprayed coatings for different applications. Wear 162–164, Part A (1993) pp. 529.

[7] T.S. Sidhu, R.D. Agrawal, S. Prakash. Hot corrosion of some superalloys and role of high-velocity oxy-fuel spray coatings—a review. Surface and Coatings Technology 198, 1–3 (2005) pp. 441.

[8] K. A. Khor, Z. L. Dong, Y. W. Gu. Plasma sprayed functionally graded thermal barrier coatings. Materials Letters 38, 6 (1999) pp. 437.

[9] L. Wang, Y. Wang, X. G. Sun, J. Q. He, Z. Y. Pan, Y. Zhou, P. L. Wu. Influence of pores on the thermal insulation behavior of thermal barrier coatings prepared by atmospheric plasma spray. Materials & Design 32, 1 (2011) pp. 36.

[10] P. Ctibor, J. Sedláček, K. Neufuss. Influence of chemical composition on dielectric properties of Al_2O_3 and ZrO_2 plasma deposits. Ceramics International 29, 5 (2003) pp. 527.

[11] P. Ctibor, J. Sedláček, K. Neufuss, P. Chrásk. Dielectric relaxation in calcium titanate-containing ceramics prepared by plasma spraying. Ceramics International 29, 8 (2003) pp. 955.

[12]A. Joly, et al., Surf. Coat. Technol. (2013), http://dx.doi.org/10.1016/j.surfcoat.2012.12.020

[13] http://www.iluka.com/_uploads/documents/Briefing%20Material/ILU%20Mineral%20Sands%20Products%20Attributes%20and%20Applications.pdf (Accessed 12 march 2013).

[14] L. Pawłowski, Surf. Coat. Technol. (2012), doi:10.1016/j.surfcoat.2012.04.096

[15] U. Diebold. The surface science of titanium dioxide. Surface Science Reports 48 (2003) pp. 53.

[16] L. Pawlowski. The science and engineering of thermal spray coatings. Second Edition, John Wiley and Sons, Ltd (2008) ISBN 978-0-471-49049-4.

[17] A Ohmori, K.C. Park, M. Inuzuka, Y. Arata, K. Inoue, N. Iwamoto. Electrical conductivity of plasma-sprayed titanium oxide (rutile) coatings. Thin Solid Films 201, 1 (1991) pp. 1.

[18] M. Gardon, J. M. Guilemany. A review on fabrication, sensing mechanisms and performance of metal oxide gas sensors. J Mater Sci: Mater Electron DOI 10.1007/s10854-012-0974-4.

[19] M. Gardon, J. M. Guilemany. Inter. Therm. Spray Conf. Proc. (2012), Houston, USA.

[20] A. Fujishima, K. Honda. Electrochemical photolysis of water at a semiconductor electrode. Nature 238 (1972) pp. 37.

[21] A. Fujishima, , X. Zhang. Titanium dioxide photocatalysis: present situation and future approaches. Comptes Rendus Chimie 9, 5–6 (2006) pp. 750.

[22] B. Normand,V. Fervel, C. Coddet, V. Nikitine. Tribological properties of plasma sprayed alumina–titania coatings: role and control of the microstructure. Surface and Coatings Technology 123 (2000) pp. 278.

[23] M. Bounazef, S. Guessasma, G. Montavon, C. Coddet. Effect of APS process parameters on wear behaviour of alumina–titania coatings. Materials Letters 58 (2004) pp. 2451.

[24] G. Bertrand, N. Berger-Keller, C. Meunier, C. Coddet. Evaluation of metastable phase and microhardness on plasma sprayed titania coatings. Surface & Coatings Technology 200 (2006) pp. 5013.

[25] N. Berger-Keller, G. Bertrand, C. Filiatre, C. Meunier, C. Coddet. Microstructure of plasma-sprayed titania coatings deposited from spraydried powder. Surface and Coatings Technology 168 (2003) pp. 281.

[26] F. L. Toma, G. Bertrand, S. Begin, C. Meunier, O. Barres, D. Klein, C. Coddet. Microstructure and environmental functionalities of TiO_2-supported photocatalysts obtained by suspension plasma spraying. Applied Catalysis B: Environmental 68 (2006) pp. 74.

[27] F.-L. Toma, G. Bertrand, S. O. Chwa, C. Meunier, D. Klein, C. Coddet. Comparative study on the photocatalytic decomposition of nitrogen oxides using TiO_2 coatings prepared by conventional plasma spraying and suspension plasma spraying. Surface & Coatings Technology 200 (2006) pp. 5855.

[28] M.C. Bordes, M. Vicent, A. Moreno, R. Moreno, A. Borrell, M.D. Salvador, E. Sánchez. Microstructure and photocatalytic activity of APS coatings obtained from different TiO_2 nanopowders. Surf. Coat. Technol. (2012), http://dx.doi.org/10.1016/j.surfcoat.2012.08.059.

[29] M. Bozorgtabar, M. Rahimipour, M. Salehi, M. Jafarpour.Structure and photocatalytic activity of TiO2 coatings deposited by atmospheric plasma spraying. Surface & Coatings Technology 205 (2011) S229.

[30] T. Kanazawa, A. Ohmori. Behavior of TiO_2 coating formation on PET plate by plasma spraying and evaluation of coating's photocatalytic activity. Surface and Coatings Technology 197, 1 (2005) pp. 45.

[31] F.-L. Toma, G. Bertrand, D. Klein, C. Coddet, C. Meunier. Nanostructured Photocatalytic Titania Coatings Formed by Suspension Plasma Spraying. Journal of Thermal Spray Technology, 15,4 (2006) pp. 587.

[32] S. Kozerski, F.-L. Toma, L. Pawlowski, B. Leupolt, L. Latka, L.-M. Berger. Suspension plasma sprayed TiO2 coatings using different injectors and their photocatalytic properties. Surface & Coatings Technology 205 (2010) pp. 980.

[33] P. Ctibor, V. Stengl, I. Pís, T. Zahoranova, V. Nehasil. Plasma sprayed TiO2: The influence of power of an electric supply on relations among stoichiometry, surface state and photocatalytic decomposition of acetone. Ceramics International 38, 4 (2012) pp. 3453.

[34] E. Bannier, G. Darut, E. Sánchez, A. Denoirjean, M.C. Bordes, M.D. Salvador, E. Rayón, H. Ageorges. Microstructure and photocatalytic activity of suspension plasma sprayed TiO_2 coatings on steel and glass substrates. Surface & Coatings Technology 206 (2011) pp. 378.

[35] G. Mauer, A. Guignard, R. Vaßen. Surf. Coat. Technol. (2012), http://dx.doi.org/10.1016/j.surfcoat.2012.08.042.

[36] Y.-F. Lin, K.-L. Tung, Y.-S. Tzeng, J.-. Chen, K.-S. Chang. Rapid atmospheric plasma spray coating preparation and photocatalytic activity of macroporous titania nanocrystalline membranes. Journal of Membrane Science 389 (2012) pp. 83.

[37] V. Snapkauskiene, V. Valincius, V. Grigaitiene. Preparation and characterization of TiO_2-based plasma-sprayed coatings for NOx abatement. Catalysis Today 191 (2012) pp. 154.

[38] M. Vicent, E. Sánchez, A. Moreno, R. Moreno. Preparation of high solids content nano-titania suspensions to obtain spray-dried nanostructured powders for atmospheric plasma spraying. Journal of the European Ceramic Society 32, 1 (2012) pp. 185.

[39] Long M, Rack HJ. Titanium alloys in total joint replacement – a materials science perspective. Biomaterials. 19, 18 (19989 pp. 1621.

[40] Wu LN, Genge BR, Wuthier RE. Micropatterned TiO_2 effects on calcium phosphate mineralization. Mater Sci Eng C. 29, 8 (2009) pp. 2355.

[41] Karla S. Brammer, Seunghan Oh, Christine J. Frandsen and Sungho Jin (2011). Biomaterials and Biotechnology Schemes Utilizing TiO_2 Nanotube Arrays, Biomaterials Science and Engineering, Prof. Rosario Pignatello (Ed.), ISBN: 978-953-307-609-6, InTech, Available from:

http://www.intechopen.com/books/biomaterials-science-and-engineering/biomaterials-and-biotechnologyschemes-utilizing-tio2-nanotube-arrays (Accesed 18 march 2013).

[42] R.S. Lima, B.R. Marple. Thermal Spray Coatings Engineered from Nanostructured Ceramic Agglomerated Powders for Structural, Thermal Barrier and Biomedical Applications: A Review. Journal of Thermal Spray Technology 40, 16 (2007) pp. 40.

[43] J. He, W. Zhou, X. Zhou, X. Zhong, X. Zhang, P. Wan, B. Zhu, W. Chen. The anatase phase of nanotopography titania plays an important role on osteoblast cell morphology and proliferation. J Mater Sci: Mater Med, 19 (2008) pp. 3465.

[44] D. Yamamoto, K. Arii, K. Kuroda, R. Ichino, M. Okido, A. Seki. Osteoconductivity of Superhydrophilic Anodized TiO_2 Coatings on Ti Treated with Hydrothermal Processes.Journal of Biomaterials and Nanobiotechnology 4, 1 (2013) pp. 45.

[45] S. Rossi, N. Moritz, T. Tirri, T. Peltola, S. Areva, M. Jokinen, R.-P. Happonen, T. Närhi. Comparison between sol-gel-derived anatase- and rutile-structured TiO_2 coatings in soft-tissue environment. Journal of Biomedical Materials Research Part A, 82A, 4 (2007) pp. 965.

[46] X. B. Zheng, C. X. Ding. Characterization of plasma-sprayed hydroxyapatite/TiO_2 composite coatings. Journal of Thermal Spray Technology 9, 4 (2000) pp. 520-525.

[47] Y.-P. Lu, M.-S. Li, S.-T. Li, Z.-G. Wang, R.-F. Zhu. Plasma-sprayed hydroxyapatite+titania composite bond coat for hydroxyapatite coating on titanium substrate. Biomaterials 25, 18 (2004) pp. 4393.

[48] V. Cannillo, L. Lusvarghi, A. Sola. Production and characterization of plasma-sprayed TiO_2–hydroxyapatite functionally graded coatings. Journal of the European Ceramic Society 28, 11 (2008) pp. 2161.

[49] M.F. Morks. Plasma spraying of zirconia–titania–silica bio-ceramic composite coating for implant application. Materials Letters 64, 18 (2010) pp. 1968.

[50] X. Zhao, X. Liu, C. Ding, P. K. Chu. In vitro bioactivity of plasma-sprayed TiO_2 coating after sodium hydroxide treatment. Surface and Coatings Technology 200, 18–19 (2006) pp. 5487.

[51] D. Chen, E. H. Jordan, M. Gell, M. Wei. Apatite formation on alkaline-treated dense TiO_2 coatings deposited using the solution precursor plasma spray process. Acta Biomaterialia 4, 3 (2008) pp. 553.

[52] R. Lima, B. Marple, H. Li, K. A. Khor. United States Patent US2006199024 (2006).

[53] P. C. S. Hayfield, Development of a New Material: Monolithic Ti_4O_7 Ebonex® Ceramic. Royal Society of Chemistry, Cambridge (2002) ISBN 0-85404-984-3.

[54] L.M. Berger, Titanium Oxide—New Opportunities for an Established Coating Material, Thermal Spray Solutions: Advances in Technology and Application, May 10-12, 2004 (Osaka, Japan), DVS-Verlag, CDRom version.

[55] H. Hund, H. Schäfer, D. Bergner. Electrode for Electrolytic Processes. United States Patent US 4140813.

[56] A. Hill, K. Ellis. Method of applying conductive coating. WO 97/27344 (1997).

[57] S. Garcia-Segura, S. Dosta, J.M. Guilemany, E. Brillas. Solar photoelectrocatalytic degradation of Acid Orange 7 azo dye using a highly stable TiO_2 photoanode synthesized by atmospheric plasma spray. Applied Catalysis B: Environmental 132–133 (2013) pp. 142–150.

[58] W.W. Dai, C.X. Ding, J.F. Li, Y.F. Zhang, P.Y. Zhang. Wear Mechanism of Plasma-Sprayed TiO_2 Coating Against Stainless Steel. Wear 196, 1-2 (1996) pp 238.

[59] P. Ctibor, M. Hrabovsky. Plasma sprayed TiO_2: The influence of power of an electric supply on particle parameters in the flight and character of sprayed coating. Journal of the European Ceramic Society 30 (2010) pp. 3131.

[60] V. V. Sobolev, J. M. Guilemany, J. Nutting, S. Joshi, High Velocity Oxy-fuel Spraying: Theory, Structure-property Relationships and Applications, Maney Ed. London (2004) ISBN 1902653726

[61] R.S. Lima, B.R. Marple. From APS to HVOF spraying of conventional and nanostructured titania feedstock powders: a study on the enhancement of the mechanical properties. Surface & Coatings Technology 200 (2006) pp. 3428.

[62] A. Ibrahim, R.S. Lima, C.C. Berndt, B.R. Marple. Fatigue and mechanical properties of nanostructured and conventional titania (TiO2) thermal spray coatings. Surface & Coatings Technology 201 (2007) pp. 7589.

[63] L. Toma, N. Keller, G. Bertrand, D. Klein, C. Coddet. Elaboration and characterization of environmental properties of TiO_2 plasma sprayed coatings. International journal of photoenergy 5 (2003).

[64] F.-L. Toma, G. Bertrand, S. O. Chwa, D. Klein, H. Liao, C. Meunier, C. Coddet. Microstructure and photocatalytic properties of nanostructured TiO_2 and TiO_2–Al coatings elaborated by HVOF spraying for the nitrogen oxides removal. Materials Science and Engineering A 417 (2006) pp. 56.

[65] J. Colmenares-Angulo, S. Zhao, C. Young, A. Orlov. The effects of thermal spray technique and post-deposition treatment on the photocatalytic activity of TiO_2 coatings. Surface and Coatings Technology 203, 15 (2009) pp. 2150.

[66] G.-J. Yang, C.-J. Li, F. Han, A, Ohmori. Microstructure and photocatalytic performance of high velocity oxy-fuel sprayed TiO_2 coatings. Thin Solid Films 466 (2004) pp. 81.

[67] G.-J. Yang, C.-J. Li, Y.-Y. Wang, C.-X. Li. Dominant microstructural feature over photocatalytic activity of high velocity oxy-fuel sprayed TiO2 coating. Surface & Coatings Technology 202 (2007) pp. 63.

[68] K. Nakade, J. Yasuoka, A. Ohmori. The development of nano-photocatalytic TiO_2 coatings by thermal spraying. Novel Materials Processing by Advanced Electromagnetic Energy Sources (2005) pp. 407.

[69] R. Gadow, A. Killinger, M. Kuhn, and D. Lopez, Published patent application DE 10,2005,038,453 A1 (2007).

[70] R. Gadow, A. Killinger, J. Rauch. Introduction to High-Velocity Suspension Flame Spraying (HVSFS). Journal of Thermal Spray Technology 17, 5-6 (2008) pp. 655.

[71] G. Bolelli, V, Cannillo, R. Gadow, A. Killinger, L. Lusvarghi, J. Rauch. Properties of High Velocity Suspension Flame Sprayed (HVSFS) TiO_2 coatings. Surface and Coatings Technology 203, 12-15 (2009) pp. 1722.

[72] F.-L. Toma, L.-M. Berger, D. Jacquet, D. Wicky, I. Villaluenga, Y.R. de Miguel, J.S. Lindeløv. Comparative study on the photocatalytic behaviour of titanium oxide thermal sprayed coatings from powders and suspensions. Surface & Coatings Technology 203 (2009) pp. 2150.

[73] F.-L. Toma, L.-M. Berger, C. C. Stahr, T. Naumann, S. Langner.Microstructures and Functional Properties of Suspension-Sprayed Al_2O_3 and TiO_2 Coatings: An Overview. Journal of Thermal Spray Technology 19, 1-2 (2010) pp. 262.

[74] M. Gaona, R.S. Lima, B.R. Marple. Nanostructured titania/hydroxyapatite composite coatings deposited by high velocity oxy-fuel (HVOF) spraying. Materials Science and Engineering: A 458, 1-2 (2007) pp. 141.

[75] H. Melero, J. Fernández, S. Dosta, J. M. Guilemany. Caracterización de nuevos recubrimientos biocompatibles de hidroxiapatita-TiO_2 obtenidos mediante Proyección Térmica de Alta Velocidad. Boletín de la Sociedad Española de Cerámica y Vidrio, Vol 50, No 2 (2011) pp. 59-64. DOI:10.3989/cyv.082011

[76] H. Melero, J.Fernández, J.M. Guilemany. Recubrimientos biocompatibles de HAp y titania. Revista biomecánica, vol. 19 (2011).

[77] H. Li, K.A. Khor, P. Cheang. Titanium dioxide reinforced hydroxyapatite coatings deposited by high velocity oxy-fuel (HVOF) spray. Biomaterials 23 (2002) pp. 85–91.

[78] R. S. Lima, B. Marple, H. Li, K. A. Khor. Biocompatible Nanostructured High-Velocity Oxyfuel Sprayed Titania Coating: Deposition, Characterization, and Mechanical Properties. Intern. Thermal Spray Conf. proceed. (2006).

[79] R.S. Lima, S. Dimitrievska, M.N. Bureau, B.R. Marple, A. Petit, F. Mwale, J. Antoniou. HVOF-Sprayed Nano TiO_2-HA Coatings Exhibiting Enhanced Biocompatibility. Journal of Thermal Spray Technology 19, 12 (2010) pp. 363.

[80] A. Hill, K. Ellis. Method for applying conductive coatings. International Publication Patent: WO 97/27344 (1997).

[81] B. Jeffery, M. Peppler, R.S. Lima, A. McDonald. Bactericidal Effects of HVOF-Sprayed Nanostructured TiO_2 on Pseudomonas Aeruginosa. Journal of Thermal Spray Technology, 19, 1-2 (2010) pp. 344.

[82] V. Champagne. The Cold Spray Materials Deposition Process: Fundamentals and Applications. Woodhead Publishing in Materials (2007) ISBN: 1420066706.

[83] A. Papyrin. Cold Spray Technology. Elsevier Publications, 2007. ISBN-10: 0080451551.

[84] H. Gutzmann, S. Freese, F. Gärtner, T. Klassen. Layer formation of cold-sprayed ceramic titanium dioxide layers on metal surfaces. Intern. Thermal Spray Conf. proceed. (2010).

[85] G.J. Yang, C.J. Li, F. Han, W.Y. Li, A. Ohmori. Low temperature deposition and characterization of TiO_2 photocatalyitic film through cold spray. Applied Surface Science 254 (2008) pp. 3979.

[86] H. Gutzmann, S. Freese, F. Gärtner, T. Klassen. Cold Gas Spraying of ceramics using the example of titanium dioxide. Intern. Thermal Spray Conf. proceed. (2011).

[87] H. Gutzmann, J.-O. Kliemann, R. Albrecht, F. Gärtner, T. Klassen, F.-L. Toma, L.-M. Berger, B- Leupolt. Evaluation of the photocatalytic activity of TiO_2-coatings prepared by different thermal spray techniques. Intern. Thermal Spray Conf. proceed. (2010).

[88] K. J. –O. Kliemann, H. Gutzmann, F. Gärtner, T. Klassen, H. Gabriel. "Cold spraying for titanium dioxide coatings with high photocatalytic bactericidal activity". Intern. Thermal Spray Conf. proceed. (2010).

[89] M. Yamada, H. Isago, K. Shima, H. Nakano, M. Fukumoto. Deposition of TiO_2 ceramic particles on cold spray process. Intern. Thermal Spray Conf. proceed. (2010).

[90] N. Tjitra Salim, M. Yamada, H. Isago, K. Shima, H. Nakano, M. Fukumoto. The understanding on adhesion mechanism of cold sprayed TiO_2 coating. Intern. Thermal Spray Conf. proceed. (2011).

[91] N. Tjitra Salim, M. Yamada, H. Nakano, K. Shima, M. Fukumoto. The synthesis of titanium dioxide powders for cold spray. Intern. Thermal Spray Conf. proceed. (2011).

[92] S.-Q. Fan, G.-J. Yang, C.-J. Li, G.-J. Liu, C.-X. Li, L.-Z. Zhang. Characterization of Microstructure of Nano-TiO_2 Coating Deposited by Vacuum Cold Spraying. Journal of Thermal Spray Technology, 15, 4 (2006) pp. 513.

[93] S.-Q. Fan, C.-J. Li, C.-X. Li, G.-J. Liu, G.-J. Yang, L.-Z. Zhang. Preliminary Study of Performance of Dye-Sensitized Solar Cell of Nano-TiO_2 Coating Deposited by Vacuum Cold Spraying. Materials Transactions, 47, 7 (2006) pp. 1703.

[94] S.-Q. Fan, C.-J. Li, G.-J. Yang, L.-Z. Zhang, J.-C. Gao, Y.-X. Xi. Fabrication of Nano-TiO_2 Coating for Dye-Sensitized Solar Cell by Vacuum Cold Spraying at Room Temperature. Journal of Thermal Spray Technology 16, 5-6 (2007) pp. 893.

[95] http://www.metalfinishing.com/view/6310/current-trends-in-cold-spray-technology-looking-at-the-future/ (Accessed 12/04/2013).

[96] G.-J. Yang, C.-J. Li, F. Han, S.-F. Mao. Preparation of TiO_2 Photocatalyst by Thermal Spraying with Liquid Feedstock. International Thermal Spray Conference proceedings (2003).

[97] G. Goutailler, C. Guillard, S. Daniele, L. G. Hubert-Pfalzgraf. Low temperature and aqueous sol–gel deposit of photocatalytic active nanoparticulate TiO2. J. Mater. Chem. 13 (2003) pp. 342.

[98] S. Yao, Y. Zhang, Z. Shi, S. Wang. Physical Properties of Nano Titania Hollow Fibers and Their Photocatalytic Activity in the Decomposition of Phenol. Russian Journal of Physical Chemistry A, 87, 1 (2013) pp. 69.

[99] M. Yamada, H. Isago, H. Nakano, M. Fukumoto. Cold Spraying of TiO2 Photocatalyst Coating With Nitrogen Process Gas. Journal of Thermal Spray Technology 19, 6 (2010) pp. 1218.

[100] H. Wang, Z. Wu, W. Zhao, B. Guan. Photocatalytic oxidation of nitrogen oxides using TiO2 loading on woven glass fabric. Chemosphere 66, 1 (2007) pp. 185.

[101] J. V. S. de Melo, G. Trichês. Evaluation of the influence of environmental conditions on the efficiency of photocatalytic coatings in the degradation of nitrogen oxides (NOx). Building and Environment 49 (2012) pp. 117.

[102] S. Dimitrievska, M. N. Bureau, J. Antoniou, F. Mwale, A. Petit, R. S. Lima, B. R. Marple. Titania–hydroxyapatite nanocomposite coatings support human mesenchymal stem cells osteogenic differentiation. J. Biomed. Mater. Res. 98A, 5 (2011) pp. 576.

[103] B. Dinan, D. Gallego-Perez, H. Lee, D. Hansford, S.A. Akbar. Thermally grown TiO_2 nanowires to improve cell growth and proliferation on titanium based materials. Ceramics International 39, 5 (2013) pp. 5949.

[104] D. Wei, Y. Zhou. Preparation, biomimetic apatite induction and osteoblast proliferation test of TiO2-based coatings containing P with a graded structure. Ceramics International 35, 6 (2009) pp. 2343.

[105] H.-W. Kim, Y.-H. Koh, L.-H. Li, S. Lee, H.-E. Kim. Hydroxyapatite coating on titanium substrate with titania buffer layer processed by sol–gel method. Biomaterials 25, 13 (2004) pp. 2533.

[106] M. Okuya, K. Nakade, D. Osa, T. Nakano, G.R. A. Kumara, S. Kaneko. Fabrication of dye-sensitized solar cells by spray pyrolysis deposition (SPD) technique. Journal of Photochemistry and Photobiology A: Chemistry 164 (2004) pp. 167.

[107] B. O'Reagan, M. Grätzel. A low cost, high efficiency solar cell based in dye sensitized colloidal TiO2 films. Nature 353 (1991) pp. 737.

[108] T. Yamaguchi, N. Tobe, D. Matsumoto, T. Nagai, H. Arakawa.Highly efficient plastic-substrate dye-sensitized solar cells with validated conversion efficiency of 7,6%. Solar Energy Materials and Solar Cells 94, 5 (2010) pp. 812.

[109] K. P. Kühn, I. F. Chaberny, K. Massholder, M. Stickler, V. W. Benz, H.-G. Sonntag, L. Erdinger. Disinfection of surfaces by photocatalytic oxidation with titanium dioxide and UVA light. Chemosphere 53, 1 (2003) pp. 71.

[110] J.W. MacFarlane, H.F. Jenkinson, T.B. Scott. Sterilization of microorganisms on jet spray formed titanium dioxide surfaces. Applied Catalysis B: Environmental 106, 1–2 (2011) pp. 181.

4.2 Metal oxide gas sensors

As it was mentioned before, the initial aim of the thesis was to achieve good and reproducible responses in titanium dioxide gas sensors obtained by Atmospheric Plasma Spray. Previous contributions reported by other universities or research groups were not found. Therefore, understand the mechanisms that accomplish the performance of this actuators and their regular industrial production was determining for subsequently planning how thermal spray could contribute to this area. Along these lines, distinguish overall efficiencies in metal oxide gas sensors had to be carried out as well. Paper 2 compiles all this information and suggests the feasibility of operating with TS technologies for developing these active surfaces. Besides, the reader will notice that titanium dioxide surfaces with oxygen vacancies are specially highlighted related to the receptor function of sensing mechanisms.

4.2.1 Paper 2:

M. Gardon, J.M. Guilemany, A review on fabrication, sensing mechanisms and performance of metal oxide gas sensors, Journal of Materials Science: Materials in Electronics.

J Mater Sci: Mater Electron
DOI 10.1007/s10854-012-0974-4

REVIEW

A review on fabrication, sensing mechanisms and performance of metal oxide gas sensors

M. Gardon · J. M. Guilemany

Received: 18 September 2012 / Accepted: 1 November 2012

Abstract Processes for developing layers onto a substrate as the active component of metal oxide gas sensors are presented and other promising alternatives as thermal spraying are also proposed. In order to understand the electrochemical mechanisms involved, the relationship between surface reactions and the electrical signal is presented as determined by the influence of three main factors: the receptor function, the transducer function and the approachability. Distinct aspects for each key-step are discussed with the aim of achieving a better comprehension of the overall system. Performances of the most operated metal oxides and target-gases in distinct application markets are also reviewed.

1 Introduction

To control and record the air quality is required much for home facilities as for industry and urban atmosphere [1, 2]. Besides, the tightening each year of worldwide environmental regulations has developed an imperative need of industrial devices able to take over this task [3, 4]. As a global alarming situation, it is not a proper choice the fact of employing high-cost materials and equipment installation. Therefore, reliable and cheap gas sensors have grown as an important application within this field.

Among the different useful solid-state sensors, metal oxide gas sensors provide an excellent sensing response in front of a wide range of target gases by means of low cost materials and manufacturing [5]. Being first discovered at the middle of twentieth century [6, 7], many patents have been developed during the last decades [8–10] and by now it is a commercialized item by many international companies [11–13]. In addition, a considerable amount of research is being published in this line due to this technology is broadly interdisciplinary. A well-established market is found at present day and its main applications are combustible gas monitoring, humidity or oxygen sensing. However, several emerging markets are maturing in other fields like air cleaners equipped with an air-quality sensor for being installed in either car cabins or houses and more challenging ones as sensing toxic or hazardous gases [14].

The basic operating principle is the reversible change of the electrical conductivity caused by the interaction between the metal oxide and gaseous species in the environment before and afterwards that the latter ones are adsorbed. Thus, an electric output signal is generated once chemical reactions are initiated at the surface of the sensing layer. Although this procedure seems particularly simple, the understanding of the sensing mechanism and its control is not as precise as it is desired. Some drawbacks can be found during the operation of metal oxide gas sensors, whose main characteristics will be reviewed in this article. The sensor signal is strongly influenced by the pre-adsorbed species especially ionic adsorbed oxygen, which usually interacts directly with the target gas. Nevertheless, other species like hydroxyl groups or carbonates can handicap the adsorption of oxygen leading to a decrease in the sensing capacity of the active layer. This is also the case of humidity that is a significant shortcoming upon the scaling-up of the sensor from the laboratory to the industry. Therefore, is essential to approach as much as possible to the operation environment of the real application by means of an unfailing experimental atmosphere.

M. Gardon (✉) · J. M. Guilemany
Thermal Spray Centre, University of Barcelona,
Barcelona, Spain
e-mail: mgardon@cptub.eu

Published online: 09 November 2012

The electric overall response of a complex surface reactivity is recorded and measured by only the change of the resistance. Obviously, there is a missing of correlation between the adsorbed species and the electric response due to a lack of physical and chemical discrimination. In order to solve this, spectroscopic techniques should provide the wealth of data required. Unfortunately and similar than above, the spectroscopic information is not available when the sensor is operating at its optimal performance [15]. Although metal oxide layers are sensitive to many different gases or mixtures of gases, its yield is directly dependent on temperature. As long as the temperature increases, the adsorbed oxygen species, which react with the target-gas, are transformed towards more reactive ones, concretely from O_2 to O^-. Accordingly, the reactivity towards the target gas around 300 °C is boosted [6, 8]. Hence, if the sensing mechanism is activated partially by temperature, the device must contain a heater and could increase the complexity and cost of the sensor in some way.

Selectivity is generally a widely discussed issue in gas sensing and also in catalysis. As for metal oxide gas sensors, it has not been an easy task to assure an acceptable value for commercial applications. Certain metal oxides develop higher affinity towards certain target gases due to the physicochemical properties involved in these interactions. However, with the aim of enhancing selectivity is possible to apply filters on the sensing layer. Selective permeable ceramic coatings can be deposited by techniques like magnetron sputtering or chemical vapor deposition. Materials like silicon oxide and alumina can be employed as selectively gas barriers in gas sensors [16]. Detection limits are also deeply relevant. For example, ethanol gas sensors are specially produced for breath analysis. Therefore, this devices must detect at least 200 ppm, which corresponds to a concentration of 0.6 g alcohol/l in the blood [17].

The deposition of the active layer onto a substrate is a key step for the fabrication of the device. Depending on the energy supplied to the material during the process, structural changes can be reached or the grain size could be altered. The amount of grain boundaries play a key role in the sensing capability, as it will be discussed in further explanations. Variation of the grain size may have a direct influence in transport and concentration of charge carriers according to the target gas. Thenceforth, the different metal oxide deposition techniques must be thoroughly studied. Complication in achieving reliable sensing devices do not stop here, reproducibility must be also taken into account. Thus, the processes able to produce the layers are responsible to do it with the same properties and microstructure for distinct batches.

Despite metal oxide gas sensors state-of-the-art has been reviewed by many authors [15, 16, 18], in this paper the scope of the active layer deposition is given as well as the study of the most important oxides and the scope of their commercial exploitation. Furthermore, the sensing mechanism and the most influencing properties during the operation process are discussed.

2 Active layer deposition

The phenomenon of *chemical cause and electric response* that governs the behavior of a metal oxide gas sensor is a consequence of the material active nature. To build-up metal oxide layers onto a substrate requires supplying energy and heat is generated as a consequence. Therefore, structural changes induced by the different deposition processes can modify the surface reactivity and the electric response. Namely, the sensing performance of the device could be altered or even the ability to detect could be eliminated. From the most important processes that have been used for depositing metal oxides, sol–gel deposition, sputtering and thermal spraying as a promising technology in this field are highlighted.

2.1 Sol–gel techniques

A sol consists in a stable suspension of colloidal solid particles within a liquid whereas a gel is a porous 3-dimensionally interconnected solid network that expands in a stable fashion throughout a liquid medium. The gel is formed when the dispersion present in the initial suspension gets rigidified [19]. The chemistry related to the sol–gel processing attains two main methods: (1) gelation of colloidal powders solution and (2) alkoxide precursors, which are hydrolyzed and polycondensated, followed by a hypercritical drying or aging and drying under ambient atmospheres. Sol–gel processes can develop quite distinct coatings, from thicknesses of a few nanometers on microdevices to some tens of microns on very distinct substrates.

Firstly, a *mixing* phase is carried out. It can be developed by mechanical mixing of colloidal particles in water at a pH that avoids precipitation or by hydrolysis of a liquid alkoxide precursor, which follows the formula $M(OR)_x$ being R an hydrocarbon like CH_3 C_2H_5 or C_3H_7 and M the metallic compound. Anywise, the chance of using diversified routes, different chemical reagents or operational conditions [20–27] may develop a lack of common criteria for achieving successfully the desired sensing layer. At this point, the *gelation* step is followed unless a previous phase of *casting* should be prepared, whose goal is to cast the sol into a mold. During gelation colloidal particles condense and the viscosity increases sharply. To assure a proper formation of the gel, it is advisable a suitable *aging* according to the chemical components involved in the

system. It consists in a period of time, from hours to days, where the poly-condensation continues and the porosity decreases. This step must be conducted intelligently because a *drying* stage must be accomplished after the aging of the gel and it must resist cracking. Stresses can be developed while drying and it can cause catastrophic cracks unless the drying process is controlled by decreasing the liquid surface energy by means of adding surfactants or eliminating of pores [28]. A last step for sol–gel coatings must be carried out and it is known as *densification*. In this part of the process, the sensing material will be affected for a considerable amount of energy because high temperatures are required in order to eliminate porous and form the metal oxide coating. In other studies [29, 30], an increase of the grain size was reported as long as the calcination temperature was enhanced followed by an abrupt decrease in the sensing performance (See chapter 3.2 for this relation).

Sol–gel processes are widely understood and used for developing metal oxide layers in gas sensor devices. Moreover, it is very well adapted for thin film fabrication either by spin-coating or dip-coating, which are the two most common techniques for this layer deposition. In spin coating the precursor solution is placed on the surface substrate and then the piece is rotated at high speed spreading the solution by centrifugal force. Rotation must be controlled in order to achieve the desired thickness [31]. On the other hand, dip coating requires immersing the substrate piece in a tank of precursor solution. After remaining in contact with the liquid, the substrate is pulled up making possible the deposition of a thin layer. In this case, the withdrawal speed has a significant influence in the coating thickness [32]. As an inconvenience, the slow and careful manufacturing plus the high temperatures required for the post deposition treatment of the sol–gel processes do not seem straightforward drawbacks to deal with.

2.2 Sputtering

Sputtering is an extensive used technique for developing semiconductor thin films on specially silica substrates in integrated circuits. It is based in the interactions of incident particles with target surface atoms. The deposition process consists in the irradiation of energetic species, while other similar processes like chemical vapor deposition (CVD) use the decomposition of source materials [33]. As it has been introduced before, thermal activation is required for sensing gases because of the ionic adsorbed species that are formed with temperature. Thus, it is possible to deposit heaters, electrodes and the sensing layer using sputtering and CVD processes, particularly in micro-machined gas sensors. Unfortunately, it is complicate to fabricate reliable material constants for thin films. Although CVD and sputtering are not the same process, from a deposition point of view its main difference in comparison to sol–gel techniques is the layer thicknesses achieved. In this case, the thicknesses are ranged between 20 and 1,000 nm, which is especially an appropriate measure in micro-sensors [34].

2.3 Thermal spraying

Thermal spraying consists in deposit molten, semi-molten or solid particles on a substrate. Coatings are properly formed if the particles are able to deform plastically at the impact and it is just possible if these are molten or sufficiently rapid in case of being solid. The material to be deposited, which is generally powder, is accelerated by means of a high energetic stream. Different techniques have evolved depending on the stream generation methods. Traditionally, these technologies have not been strongly used in thick-film electronics or gas sensors. Nevertheless, during the last years it has been achieved an enhanced process control and monitoring, which eases its application. The chance of producing functional coatings is being approached by patents and publications, demonstrating that it is possible to reach the required response from the deposited material.

Among all the distinct technologies, particle acceleration systems, heat sources or guns; atmospheric plasma spray (APS), high-velocity-oxygen-fuel spray (HVOF) and cold gas spray (CGS) represent the three most significant milestones in thermal spraying according to molten, semi-molten and non-molten particles during the process. From a commercial application point of view, these three technologies are applied differently in order to supply more or less heat to the raw material and achieve a coating with a certain controlled composition. A diagram of each gun used in these three different techniques can be found in Fig. 1.

Sampath [35] exposed that thermal spraying offer several advantages in thick-film sensor and electronics manufacturing over other technologies. Its throughput manufacturing capability is higher. Moreover, there is an in situ application of different materials like metals, ceramics, polymers or any combinations of these. Just-in-time coatings are obtained and a wide variety of substrates and conformal shapes are allowed. Furthermore, high-reliability in reproduction of the as-obtained geometries is found due to it is used three-dimensional (3D) robotics during the manufacturing. On the other hand, it is a greener technology compared to plating, lithography or even sol–gel processes. Despite thermal spray fits in the need of depositing functional metal oxide layers, thermal decomposition could affect the initial powder. Techniques like HVOF or APS can reach flame and jet temperatures ranging from 1,000 to 20,000 °C, respectively [36, 37]. However, it has been possible to develop several

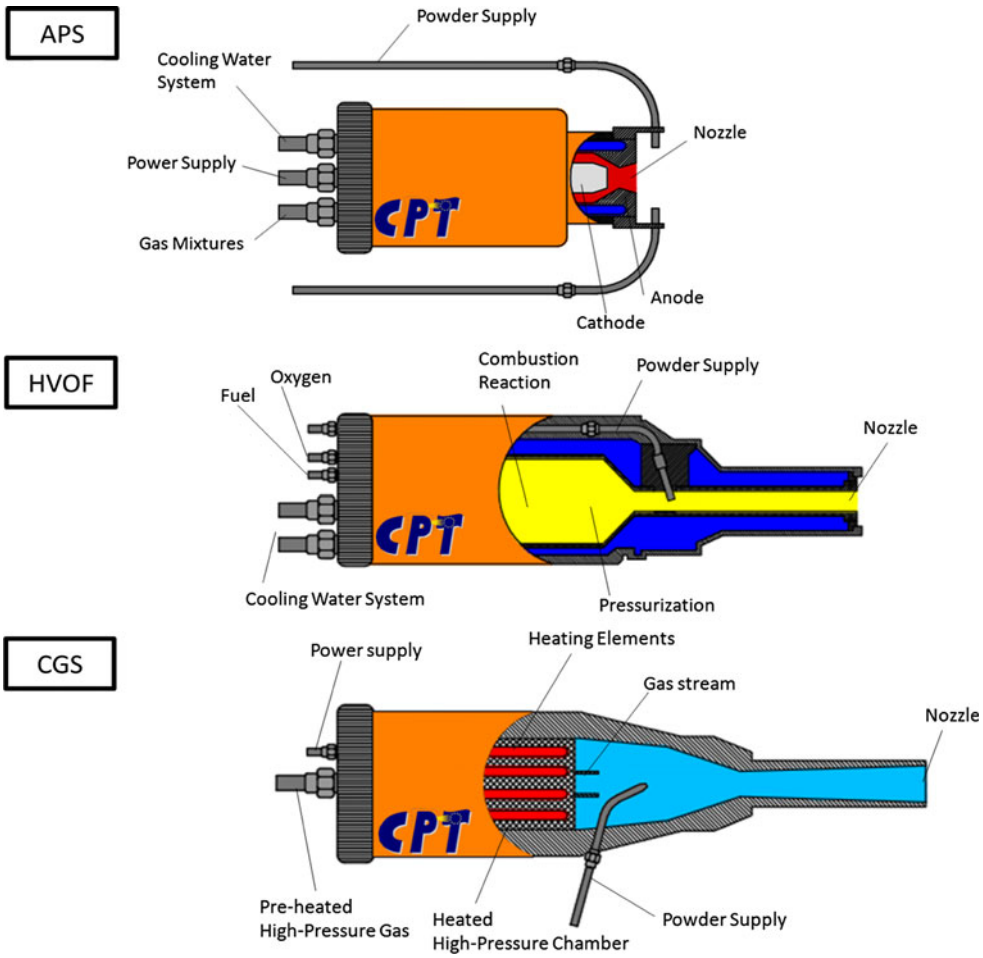

Fig. 1 Diagram of the cross-section and the main parts of APS, HVOF and CGS thermal spray guns respectively

patents related to the deposition of metal oxides by plasma spraying onto electrically insulating substrates for its use as a gas sensor [38]. Anyhow, the grain size could be affected by high temperatures during the process and species that are not desired could be formed, with a possible influence in the sensing activity. Consequently, APS or even HVOF seems to cause some inconveniences for the formation of the active layer. On the other hand, CGS operates at low temperatures and it does not provoke changes in the structure of the powder. Therefore, this technology appears as a very interesting technique for developing functional coatings without modifying the composition of the raw material. Besides, to produce ceramic coatings employing this technique is possible, even functional ceramic coatings whose physicochemical properties can be used in industrial applications [39–42].

3 Sensing mechanism basis

The sensing performance of the active layer is influenced by many different factors, which can be classified in three distinct groups. The physicochemical properties of the metal oxide on the surface determine how the target-gas is received by the first atomic layers. Therefore, the ability of the material to absorb the gas and interact with it leads to the Receptor function (Sect. 3.1) of the process. The structure of the solid like the grain size and the obtained carrier mobility are grouped in the Transducer function (Sect. 3.2), which consists in the capability of transforming the chemical interaction between the metal oxide and the gas to an electric output signal. Finally, other phenomena can influence inner grains accessibility for the gas. These concepts involve the pore size, diffusion depth or the film thickness and can be understood as the Approachability (Sect. 3.3) [14]. In this way, the gas sensing process is determined by the catalytic properties of the metal oxide and its behavior as a semiconductor.

3.1 Receptor function

The aptitude of any solid surface to adsorb gas molecules and decompose them is explained and determined by the physisorption and chemisorption capability. Firstly, weak physisorption is carried out determined by Van der Waals and dipole interactions. Afterwards, chemisorption is

achieved and a strong bond is formed developing charge transfer between the adsorbed species and the surface atoms. Physisorption is a fairly exothermic step; its coverage is decreased as long as temperature increases [43]. However, chemisorption requires certain activation energy for being reached. Its neat rate is given by Madou [44], where the activation energy is regarded as the difference in the electrochemical potential between the adsorbed oxygen and the semiconductor surface. Thus, as long as coverage increases, the activation energy is higher.

A wide accepted scheme for explaining the surface reactivity between the metal oxide and the reducing species to be detected implicates oxygen ionsorption. Liu et al. [45] explained the adsorption and reactivity of oxygen and its influence in a ZnO-sensor. O_2 (gas) is adsorbed onto the surface and different ionic forms of oxygen react with the current flow developing the following species (see Fig. 2):

$$O_2(\text{adsorbed}) + e^- \rightarrow O_2^- \quad \text{(a)}$$

$$O_2^- + e^- \rightarrow 2O^- \quad \text{(b)}$$

Above temperatures of 250 °C reaction (b) is activated instead of (a). This is one of the main reasons that sensing gases by means of metal oxides is a thermal-activated process. It is reported as well the reaction between CO gas and the ZnO surface covered by ionic oxygen species (see Fig. 3):

$$2CO + O_2^- \rightarrow 2CO_2 + e^- \quad \text{(c)}$$

$$CO + O^- \rightarrow CO_2 + e^- \quad \text{(d)}$$

$$CO + O^{2-} \rightarrow CO_2 + 2e^- \quad \text{(e)}$$

This possible reactivity is also supported by Dutta et al. [46], which studied the interaction of carbon monoxide and anatase surfaces at high temperature. Nevertheless, in this case carbon monoxide interacts with O^- instead of O^{2-}. This work purposes other alternative paths as well, where carbon monoxide reacts directly with titanium dioxide:

$$TiO_2 + CO(\text{adsorbed}) \rightarrow TiO_2(CO)_{ad} \quad \text{(f)}$$

$$TiO_2(CO)_{ad} \rightarrow TiO_x(\text{adsorbed intermediate}) \rightarrow TiO + CO_2 \quad \text{(g)}$$

$$Ti^{II} \rightarrow Ti^{IV} + 2e^- \quad \text{(h)}$$

$$TiO + 1/2O_2(g) \rightarrow TiO_2 \quad \text{(i)}$$

Therefore, it is clear how important is the concentration of gaseous oxygen in the sensor surrounding. As Ramamoorthy [47] reviewed for oxygen sensors, the electrical conductivity of semiconducting metal oxide gas sensors depend on the oxygen partial pressure, which is also affected by the type of the carrier (*n* or *p*) and the point defects (e.g. oxygen vacancies). However, there are n-type semiconductors like TiO_2 with a wide range of operation (PO_2:1–10^{-30} atm). Although the resistance of the sensor decreases with decreasing PO_2, for a given temperature the logarithmic variation of the senor resistance is found unaltered for the above mentioned oxygen concentration. For this reason, the TiO_2 based oxygen sensor is proposed for controlling the air-to-fuel ratio in combustion systems (lambda sensors).

In order to determine the influence of the acid–base properties of the sensing layer, Yamazoe [48] investigated the influence of adding Cs_2O, La_2O_3, Sm_2O_3, MnO_2 and WO_3 as basic and acid oxides to an SnO_2 active layer; ethanol was used as the target-gas. Ethanol gas undergoes two routes of decomposition reactions: dehydrogenation and dehydration, where CH_3CHO and C_2H_4 are obtained,

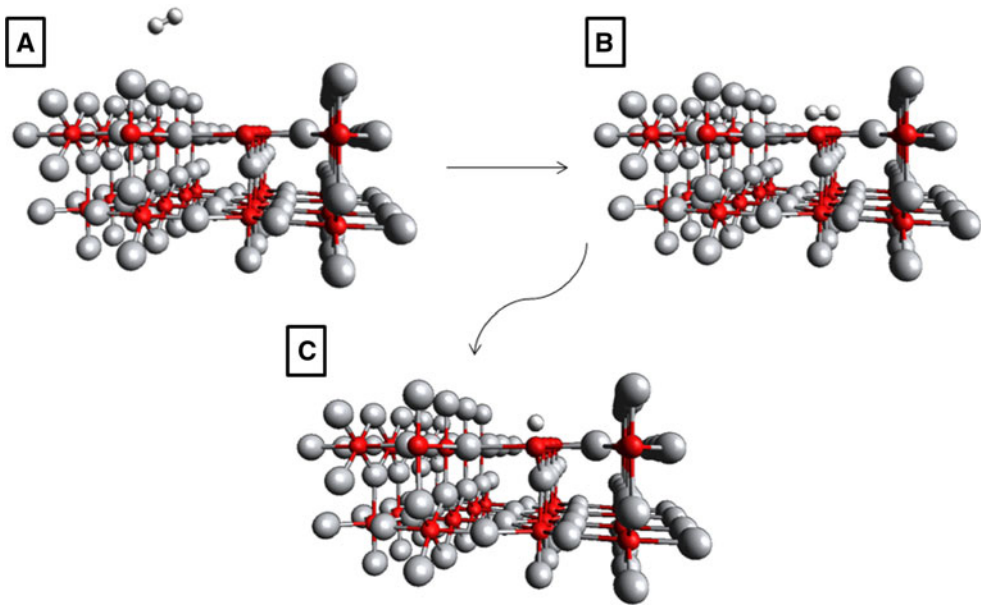

Fig. 2 Schematic model for the molecular O_2 adsorption at vacancy sites on TiO_2 (110) in a metal oxide gas sensing device: **a** Oxygen gas is directed towards a row of oxygen vacancies on the metal oxide surface. **b** Oxygen gas gets adsorbed on a vacancy site. **c** The oxygen gaseous adsorbed molecule is dissociated due to the interaction with the electric current of the sensing layer leading to the formation of adsorbed anionic species of oxygen and altering the electric output signal [see chemical reactions (a) and (b)] [51]

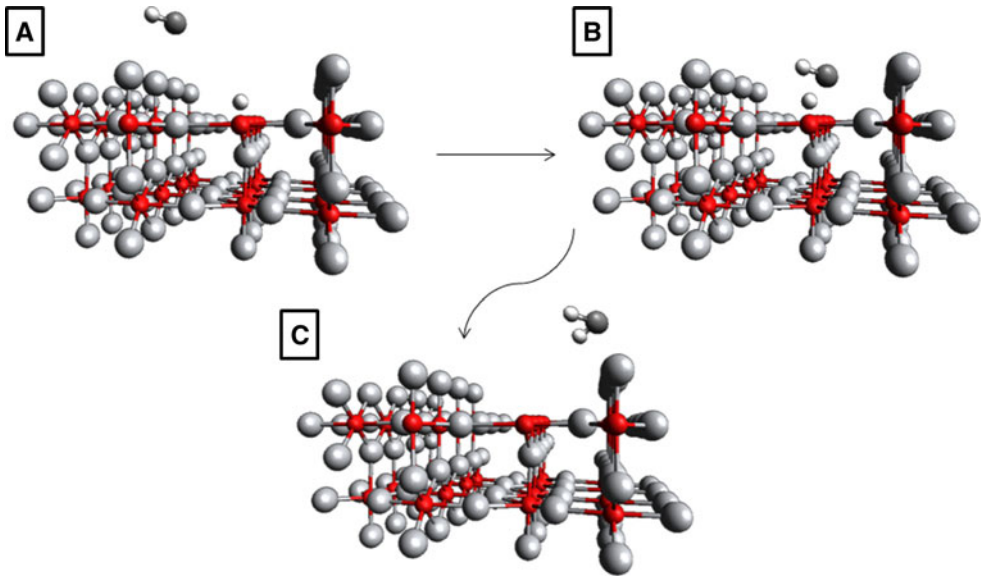

Fig. 3 Schematic model for the molecular CO adsorption on TiO_2 (110) in a metal oxide gas sensing device: **a** Carbon monoxide gas is directed towards a row of oxygen vacancies on the metal oxide surface where anionic oxygen is adsorbed. **b** Gaseous carbon monoxide reacts with the anionic adsorbed oxygen giving one electron to the metal oxide and altering the output signal [see chemical reactions (c), (d) and (e)]. **c** Carbon dioxide is formed because as the product of the step 1 and it gets desorbed [51]

respectively. It was found that as the electronegativity of the metal cation was higher, the dehydration reaction was promoted to detriment of the dehydrogenation reaction. Consecutive oxidations of the intermediate products towards CO_2 and H_2O were boosted when metal cations with lower electronegativity were employed. The highest increase in sensitivity was acquired adding La_2O_3 to SnO_2. Similar results were obtained by Rao [49], La_2O_3 was added again but in this case to ZnO. A better performance of the sensor in terms of sensitivity could be achieved by adding this basic oxide. Besides, it was possible to reduce the operating temperature. Rumyantseva et al. [50] studied the sensing properties of SnO_2/Fe_2O_3 nanocomposites towards CO, ethanol, H_2S and NO_2. It was concluded that an increase of Fe_2O_3 content generated a decrease of the acid sites on oxide surface and an enhancement of the oxidizing capability of SnO_2/Fe_2O_3 nanocomposites when using ethanol gas.

Following the model proposed above in the case of carbon monoxide detection [see reaction (d)] and using rutile as the sensing layer, it can be observed in Fig. 3 how the target-gas interacts with ionic adsorbed oxygen in order transfer electrons to the metal oxide coating, leading to change in the electric conductivity.

Obviously, the interaction of the gas and a certain metal oxide is not the same for all its crystal faces. In this way, the status of an oxide surface may be discussed by two main concepts:

Step 1 Tasker [52] introduced the stability of ionic surfaces by means of the most influencing electrostatic considerations. These involve three different types of surfaces: type 1, neutral surfaces with stoichiometric proportions of anions and cations in each plane (stable); type 2, charged surfaces with no dipole moment in the repeat unit perpendicular to the surface (stable as well) and; type 3, charged surfaces with dipole moment in the repeat unit perpendicular to the surface (unstable).
Step 2 The most stable surfaces are autocompensated. This means that the net result of cation- and anion-derived dangling bonds are either completely empty or completely full on stable surfaces.

Diebold [51] used these arguments for determining the structure stability of rutile (TiO_2) surface. It was found that the plane (1 1 0) − (1 × 1) is predicted to be the most stable. This plane consists of a type 2 surface, whose planes are charged, but there is not any dipole moment. Furthermore, the surface is autocompensated due to electrons from the dangling bonds on the Ti cations are transferred to the dangling bonds on the O anions, compensating the missing charge. SnO_2 planes were also reviewed by Batzill and Diebold [53]. In this work the surface energies of low index, which maintain the bulk composition, have been reviewed from the studies of different authors. It was concluded that the (1 1 0) surface has the lowest energy as the preferential termination of a SnO_2 single crystal due to this crystallographic plane is autocompensated, suggesting that a higher stability is reached.

With the purpose of improving the interaction of the gas on the surface of the metal oxide, to use noble metal particles like Pt, Pd, Au or Ag has been a decision widely carried out in many scientific papers in order to speed up surface reactions. A catalytic boost is achieved leading to an enhanced performance of the gas sensor and this contribution is due to the so-called *spillover effect*. Concretely, noble metal particles favour molecular oxygen adsorption and dissociation. Afterwards, the ionic oxygen species are

moved onto the metal oxide surface. Therefore, higher concentration of adsorbed ionic oxygen is reached at lower temperatures. It is possible to achieve this phenomenon replacing noble metal particles for another active metal oxide which behaves similarly as noble metals. Anyhow, either noble metal particles or active metal oxides must be supported closer to the grain boundaries where carrier transport takes place [17]. Moreover, it is believed as well that molecular oxygen resides briefly on the metal oxide surface and then moves onto the noble metal particles, this is known as the *back-spillover effect*.

As it has been mentioned above, there is a tremendous effect of the environment such as humidity in sensing gases. Bârsan [54] dealt with this previously by experimental measurements and calculations of CO sensing by Pd-doped SnO_2. By means of work function measurements and in order to characterize the influence of water (without CO), it was determined that as long as humidity increased, the resistance decreased and the electron affinity increased, which was attributed to a higher coverage of surface hydroxyl groups. Then, work function and resistance measurements were performed simultaneously for sensing CO in a humidified air and dry synthetic air. Contrary to zero humidity atmosphere, in the presence of water the electron affinity changed dramatically upon exposure to CO. Different mechanisms were explained with the aim of understanding the interaction of CO, Sn_{Sn}^{+}, OH^{-} and O_o. The decrease in the electric resistance was also observed by impedance spectroscopy measurements. It was suggested that CO sensing can occur via two pathways: (a) reaction with ionsorbed oxygen and; (b) reaction with hydroxyl groups. Finally, from DRIFT measurements and according also from the rest of analysis, it was concluded that the reaction between surface oxygen ions and CO is most probably responsible for the changes of the resistance in dry air. When operating in the presence of water, the sensor signal is increased because of the reaction between CO and hydroxyl groups that lead to hydrated protons.

Humidity sensors based in metal oxides with nanoscaled morphology were also studied by Varghese [55]. The selected systems were a highly uniform nanoporous Al_2O_3 for humidity sensing and TiO_2 nanotubes for hydrogen sensing. It was assumed that the sensitivity of the nanoporous alumina layer was caused by the certain amount of anions trapped within the pores as a result of the anodization process. The presence of these anions, even in a low-humidity atmosphere, provides a high charge density for easy physisorption of water molecules. On the other hand, titania nanotubes were found to be really sensitive to temperature when detecting hydrogen. An increase of the temperature led to a decrease in a response time and greater sensitivities. The authors believed that hydrogen sensitivity of TiO_2 nanotubes was due to hydrogen diffusion into the titania lattice, where they act as electron donors. Comini [56] also studied the influence of nanocrystalline metal oxides for gas sensing applications based in nanobelts or nanowires. The presented gas experiments show the feasibility of large scale manufacturing and good sensing properties in single crystal nanostructures. The larger surface-volume ratio, better stoichiometry and greater level of cristallinity make mono-dimensional metal oxide gas sensors a very promising field of research and application. However, a great control of the nanostructure growth must be reached in order to satisfy commercial standards.

3.2 Transducer function

The transducer function is governed by the semiconductor itself, the grain boundaries, the contacts between the metallic electrodes and the oxide and, finally, the electrochemical interaction that involves the metal oxide and the adsorbed species. As it has been explained before, oxygen plays a key role in the surface reactivity. Firstly, its adsorption and dissociation leads to a space charge region on the surface of each metal oxide grain. This surface volume is known as depleted zone, where the carrier concentration is smaller than its equilibrium value, developing certain decrease of the electric conductivity due to the existence of potential barriers formed at the inter-grain contacts, qV_s (the height of the Schottky barrier formed) and its corresponding band bending [57]. A widely accepted surface mechanism model of polycrystalline layers is represented in Fig. 4, where are included the physical, band and electronic model taken from bibliographic sources [58, 59].

The surface reaction carried out by O^{-} and the target gas, for example CO, transfers one electron to the bulk developing an increase in the electric conductivity [60], obtaining a decrease in the space charge region and the barrier height localized at the band bending is lowered as well. As a result, it is found the alteration of the output signal of the device, which diagnoses the presence of gaseous carbon monoxide.

The metal oxide sensitivity is directly influenced by the depth or thickness of the space charge layer (L) in relation to the grain diameter (D). Yamazoe [61] researched this relationship for SnO_2-based devices. It was found that the metal oxide particles were connected by necks. Nevertheless, this contact was occasionally done by grain boundaries, whose existence was considered to be the origin of the D-dependence of the gas sensitivity. As long as the grain size decreases, the depletion zone gets deeper into the grains, which is relatively less resistive than the depletion zone adjacent to the surface. Three distinct situations are reached according the correlation between D and L. For those grains with $D \gg 2L$, the crystallites are

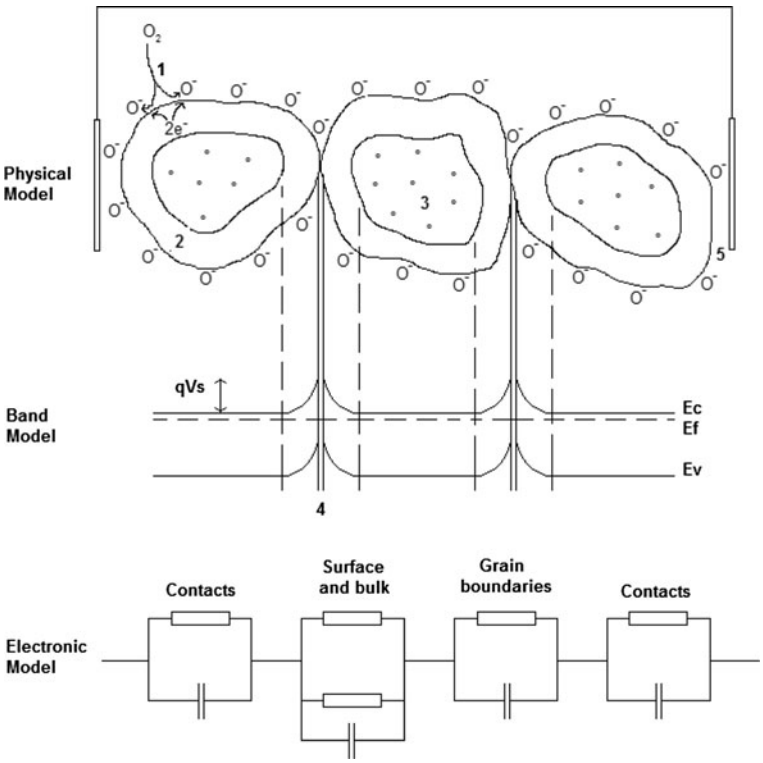

Fig. 4 Physical, band and electronic model of metal oxide grains when O^- is adsorbed. Parameters at the fig: *1* oxygen adsorption and dissociation to O^-, *2* space charge region or depleted zone, *3* conduction band electrons, *4* barrier at the grain boundary and the corresponding band bending and *5* the electric contacts

mostly unaffected by the surface interactions with the gas phase. In this case, the effect of the atmosphere induced by the interaction at the grain boundary barriers when the transport carriers are transferred from one grain to another predominates. Thus, the target gas alters the trapped charge density at the surface of the grains, modifying the overall electric conductivity value. It can be said that the sensing mechanism is controlled by the grain boundaries. For smaller grains, when $D \geq 2L$, the depletion zone surrounds each neck developing a constricted conduction channel. This fact makes that the effective cross section area of the electric current path through the grains is highly influenced by the depletion zone, namely, by the ambient gas. At this point, the metal oxide sensing mechanism is controlled by the grain diameter, as D decreases, it becomes more dependent. Finally, for those grains whose size is significantly smaller than the depletion zone, $D < 2L$, there is an almost complete lack of mobile charge carriers in the grain. Obviously, the resistivity considerably increases because of the conduction channels are mislaid. Since that, there are no significant barriers for the charge transport at the intergrains. Henceforth, the charge transport is fundamentally controlled by the grain conductivity. Rothschield [62] described the behaviour of $D < 2L$ nanosized grains by using computer simulations of the sensitivity in function of the grain size. It was demonstrated a steep decrease in the carrier concentration when the grains are fully depleted, namely, when the electrons are trapped at the surface of the grains. In this situation, significant changes in the effective carrier concentration leading to changes in the electrical conductivity were found even for very small variations ($\sim$1 ppm) of the environment.

3.3 Approachability

The last factor, approachability, means how much the inner grains are influenced by the target gas. Obviously, this fact must be seriously considered since the surface of each grain interacts directly with the gaseous species. Hence, several aspects related to this issue must be discussed.

Sensing layer thicknesses in metal oxide gas sensors range from nanometres (thin films) to even 100 μm (thick films), specially depending on the deposition method. Nevertheless, changes in the output signal are found when the distinct thicknesses of the active layer are used and the operational parameters have been constant during the sensing experiment. A common shortcoming of thick-film sensors is the necessity of using a higher level of heating compared to thin-films. On the other hand, thin-film devices are not very compatible with standard technologies for coating its substrates. Becker et al. [63] studied the gas sensing properties of thin- and thick-film tin-oxide coatings towards O_3, NO_2 (as oxidising gases) CO and CH_4 (as reducing gases). In their results, all the thin-film sensors reached their maximum sensitivity at higher values of operation temperature, compared to thick-film sensors. In order to explain this behaviour, the following mechanism

Table 1 Outline of the deposition technique for different metal oxide gas sensors and some of its sensing data towards NO_x detection

Active layer material	Deposition technique	Gas concentration	Operation temperature (°C)	Bibliographic references
Nanocomposites SnO_2:Fe_2O_3	Sol–gel route	50 ppb–10 ppm	T = 150–450	[50]
SnO_2	Sol–gel route	10 ppm	T = 100	[63]
WO_3	Atmospheric plasma spraying	0–450 ppb	T = 45–240	[68]
WO_3	Reactive magnetron sputtering	1 ppm	T = 200	[69]

was explained. Any target-gas molecule to be detected requires diffusing into the bulk of the active layer to develop the desired surface chemical reaction. In this way, the electric resistance of the metal oxide is done close to the reaction site. Of course, the more places where the detection reaction occurs, the greater the change in the value of the electric resistance is obtained. The authors calculated the gas penetration profile for both devices and it was found that at lower temperatures the gas penetration was higher for thick-devices, namely, the accessibility to the inner grains was higher and the change of the output signal was greater. The activation energy was also calculated and it was obtained higher values of this parameter for the thin-film layers. This is attributed to the heating of the gas molecules upon diffusion into the thick of the metal oxide. The numerous collisions of the molecules with the pore walls transfer thermal energy to the gaseous species and less activation energy is necessary for the detection reaction occurs. Contrary, such heating effects are less pronounced in thin-film devices. Other authors found a significant decrease of the sensing performance when increasing the thickness of the device [64]. However, it is not really an effect of the thickness. For the thicker layers in this study, the grain size was 390 nm and for the thinner ones 65 nm. Thus, the total surface area is greater for thin-film sensors and this leads to a larger adsorption and desorption sites. Moreover, as it has been seen in the Sect. 3.2, bellow certain sizes the grain is fully depleted of charge carriers and the change in the electric resistivity due to the surface reactions is raised.

If someone is interested in understanding the accessibility of the inner grains, porosity is noteworthy. In the case of porous layers, the active surface is much higher than in compact ones. Therefore, the interaction between the metal oxide and the environment is boosted. Nonetheless, porosity is not a simple factor to manage. An efficient diffusion is achieved if the pores are wide enough although as long as the pores are larger, the specific surface area is lower and the desired effect of porosity is missed. This phenomenon was discussed by Tiemann [65], who found deep dependences between the size of the porous and the diffusivity of the gas into the bulk of the metal oxide. For a layer that has mesopores ranged between 8 and 200 nm of diameter, a molecule is more likely to collide with a pore wall than with other molecules. As the gaseous species react and diffuse into the layer depth, a concentration gradient is formed along the bulk.

4 Application markets

The following section is not intended to discuss exhaustively all the available or commercial metal oxide gas sensors in each application market. However, a brief overview of the most relevant devices and environments are examined. A classification has been made in order to discern the different markets as a function of the most significant gases to detect [66, 67]. To achieve this, the information is presented in tables in order to outline the material of the sensing layer, its deposition technique and some sensing performance data in published research papers.

4.1 Automobile industry

A huge necessity of detecting gases has been developed in this field. Car ventilation control, filter control, gasoline vapour detection or alcohol breath tests are required to be monitored. Nevertheless, by-products from combustion in air like NO_x (NO_2, NO) are the most worrying due to the environment regulations. NO_x are produced also through combustion in chemical plants, these are toxic at low concentrations and NO_2 produces ground-level ozone. CO is an environmentally hazardous gas and it is emitted to the atmosphere due to incomplete combustion of fuels [50, 63, 68, 69]. Although amperometric gas sensors can be considered one of the primary methods for field detection of CO in air for industrial hygiene applications since the 1970s [70], metal oxide gas sensors have been also introduced in this area (Tables 1, 2).

4.2 Fuel gas

Methane is the main component of natural gas and it is used in many chemical processes. It may be transported as refrigerated (liquefied) and it has been broadly used in electric generation by its burning as a fuel in gas turbines or steam boilers. CH_4 emissions are severely regulated due to its powerful behavior as a green-house effect gas [72–75] (Table 3).

Table 2 Outline of the deposition technique for different metal oxide gas sensors and some of its sensing data towards CO detection

Active layer material	Deposition technique	Gas concentration (ppm)	Operation temperature (°C)	Bibliographic references
ZnO	Sol–gel route	250	T = 350	[22]
ZnO:Al	Reactive magnetron sputtering	1,000	T = 400	[71]
TiO_2	Reactive magnetron sputtering	40	T = 200	[69]
TiO_2:Va	Sol–gel route	100	T = 300–450	[25]

Table 3 Outline of the deposition technique for different metal oxide gas sensors and some of its sensing data towards CH_4 detection

Active layer material	Deposition technique	Gas concentration (ppm)	Operation temperature (°C)	Bibliographic references
TiO_2	Sol–gel route	75	T = 650	[72]
TiO_2	Sol–gel route	1,000	T = 350–550	[73]
InO_3:SnO_2:TiO_2	Sol–gel route, co-precipitation method	850	T = 100–350	[74]
ZnO:Sb	Sol–gel route	1,000	T = 360	[75]

Table 4 Outline of the deposition technique for different metal oxide gas sensors and some of its sensing data towards H_2S detection

Active layer material	Deposition technique	Gas concentration (ppm)	Operation temperature (°C)	Bibliographic references
WO_3:Au–Pt	RF sputtering	10–50	T = 220	[76]
Nanosized SnO_2:Fe	Sol–gel route	0–250	T = 0–350	[77]
SnO_2:CuO	Sol–gel route	100	T = 80	[78]
TiO_2:Al_2O_3	Sol–gel route	200–1,000	T = 225	[79]

4.3 Food industry

Hydrogen sulfide is present in crude petroleum and natural gas. Moreover, it is formed also due to bacterial breakdown of organic matter or wastes in food processing. At lower concentrations this gas has a characteristic rotten-egg smell but for greater concentrations may cause instant paralysis and death in an average adult. In situ detection and monitoring is highly important, especially in petrochemical and coal manufacturing industries [76–79] (Table 4).

4.4 Environmental control

Ammonia (NH_3) is produced in many sources as the animal manure decomposition. It is harmful due to it irritates the human eyes at low levels of concentration. Pharmaceutical processes use NH_3 commonly, but it must be exhaustively controlled due to it is hazardous [24, 80–83] (Table 5).

4.5 Industrial production

Sulfur dioxide (SO_2) gas is the main source of acid rain in the global atmosphere. Henceforth, the control mechanisms of SO_2 emissions are a concerning matter of discussion. In the view of these environment and safety concerns, the development of sulfur dioxide sensor is very urgent and important. SO_2 is especially very controlled in the petroleum industry by means of the Claus process [83–86] (Table 6).

5 Conclusions

In this paper, the main processes for depositing the active layer of metal oxide gas sensors have been reviewed. In order to link its capacity of high manufacturing with brief or long times required, it has been concluded that thermal spraying is a promising alternative for developing metal oxide gas sensors and electronic devices. Besides, this technique permits the whole fabrication of the device, including the heating layers or the electrodes.

The sensing mechanisms have been sub-divided in three major steps whose existence is necessary for achieving a fine response of the device. Henceforth, the guidelines for acquiring materials with better performances towards different target gases are given. To understand the physico-chemical properties of the surface is essential for recognizing

Table 5 Outline of the deposition technique for different metal oxide gas sensors and some of its sensing data towards NH_3 detection

Active layer material	Deposition technique	Gas concentration	Operation temperature (°C)	Bibliographic references
SiO_2:SnO_x:AgO_y	Sol–gel route	500 ppm	T = 250	[24]
TiO_2	Reactive magnetron sputtering	500 ppm	T = 250	[80]
Carbon nanotubes:TiO_2	Sol–gel route	1 Vol.%	T = 27	[81]
Nanosized WO_3	Photolithography	2,5 ppb	T = 300	[82]

Table 6 Outline of the deposition technique for different metal oxide gas sensors and some of its sensing data towards SO_2 detection

Active layer material	Deposition technique	Gas concentration (ppm)	Operation temperature (°C)	Bibliographic references
WO_3	Sol–gel route	200–800	T = 100–800	[83]
NASICON:$ZnSnO_3$	Sol–gel route	5–50	T = 360–390	[84]
NASICON:V_2O_5:TiO_2	Sol–gel route	1–50	T = 200–400	[85]
SnO_2:Ni	Sol–gel route	0–150	T = 300	[86]

whether the interaction with the gas to detect will be appreciated. The structure of the metal oxide must be controlled. Especially the grain size, which is in command of deplete completely the charge carriers when anionic oxygen is adsorbed. The accessibility of the inner grains cannot stay poorly explained, its interaction guarantee an enhanced output signal. Consequently, to ease the adsorption of the gas will be determining.

More markets and the support of more professionals and technologies are concerned in ensuring safety environments. Thus, it has been briefly overviewed some application markets, the most worrying target-gases and the operation conditions of different metal oxide sensing layers. It has been concluded that the challenge of developing a unique model for sensing gases using metal oxides seems to be quite unrealistic. On the other hand, to understand the electrochemical interactions in each surrounding will necessary lead to different devices and materials that perform satisfactorily.

Acknowledgments The authors wish to thank the Generalitat de Catalunya for the financial support for this research project 2009 SGR 00390.

References

1. T. Nakahara, in *Proceedings of 38th Chemistry Sensors Symposium* (2004)
2. H. Akimoto, Science **5**, 302 (2003)
3. http://eur-lex.europa.eu/LexUriServ/LexUriServ.do?uri=OJ:L:2008:152:0001:0044:EN:PDF. Accessed 12 Feb 2012
4. http://unfccc.int/resource/docs/convkp/kpeng.pdf. Accessed 5 March 2012
5. T. Hirai, S.I. Hirano, Y. Takeda. The basic science division. Ceram. Soc. Jpn. **145**, 145 (1996)
6. A. Bielanski, J. Deren, J. Haber, Electr. Nature **179**, 668–669 (1957)
7. T. Seiyama, A. Kato, K. Fujiishi, Ma. Nagatani, Anal. Chem. **34**, 11 (1962)
8. S. Sakai. Patent number: 4535315 (1985)
9. S. Yagawara, W. Ohta, Patent number: 5250170 (1993)
10. M.J. Donelon, P. Kikuchi, M.E. Nottingham, Patent number: 6585872 B2 (2003)
11. http://www.ipm.fraunhofer.de/fhg/ipm_en/solutions_services/processmonitoring/sensors/index.jsp. Accessed 15 Feb 2012
12. http://www.fisinc.co.jp./en/products/basic.html. Accessed 21 Feb 2012
13. http://www.figarosensor.com/products/common(1104).pdf. Accessed 21 Feb 2012
14. N. Yamazoe, Sens. Actuat. B **108**, 2–14 (2005)
15. N. Barsan, U. Weimar, Sens. Actuat. B **121**, 18–35 (2007)
16. C.A. Papadopoulos, D.S. Vlachos, J.N. Avaritsiotis, Sens. Actuat. **32**, 61–69 (1996)
17. C. Garzella, E. Comini, E. Tempesti, C. Frigeri, G. Sberveglieri, Sens. Actuat. B **68**, 189–196 (2000)
18. Comini, G. Faglia, G. Sberveglieri. *Solid State Gas Sensing* (Ed. Springer, 2009). ISBN: 978-0-387-09664-3
19. A.C. Pierre, *Introduction to Sol–Gel Processing*, (Kluwer, Massachussets, 1998) ISBN-10: 0792381211
20. R. Rella, A. Serra, P. Siciliano, L. Vasanelli, A. Licciulli, A. Quirini, Sens. Actuat. B **44**, 462–467 (1997)
21. L. Francioso, M. Russo, A.M. Taurino, P. Siciliano, Sens. Actuat. B **119**, 159–166 (2006)
22. H.W. Ryu, B.S. Park, S.A. Akbar, W.S. Lee, K.J. Hong, Y.J. Seo, D.C. Shin, J.S. Park, G.P. Choi, Sens. Actuat. B **96**, 717–722 (2003)
23. T. Ivanova, A. Harizanova, T. Koutzarova, B. Vertruyen, Mater. Lett. **64**, 1147–1149 (2010)
24. V.V. Petrov, T.N. Nazarova, A.N. Korolev, N.F. Kopilova, Sens. Actuat. B **133**, 291–295 (2008)
25. M.C. Carotta, M. Ferroni, S. Gherardi, V. Guidi, C. Malagù, G. Martinelli, M. Sacerdoti, M.L. Di Vona, S. Licoccia, E. Traversa, J. Eur. Ceram. Soc. **24**, 1409–1413 (2004)
26. F. Morazzoni, C. Canevali, N. Chiodini, C. Mari, R. Ruffo, R. Scotti, L. Armelao, E. Tondello, L.E. Depero, E. Bontempi, Chem. Mat **13**, 4355–4361 (2001)

27. J. Shieh, H.M. Feng, M.H. Hon, H.Y. Juang, Sens. Actuat. B **86**, 75–80 (2002)
28. L.L. Hench, J.K. West, Chem. Rev. **90**, 33–72 (1990)
29. E. Traversa, M.L. Di Vona, S. Licoccia, M. Sacherdoti, M.C. Carotta, L. Crema, G. Martinelli, J. Sol. Gel Sci. Technol. **22**, 167–179 (2001)
30. A. Cabot, J. Arbiol, J.R. Morante, U. Weimar, N. Bârsan, W. Göpel, Sens. Actuat. B **70**, 87–100 (2000)
31. R. Capan, N.B. Chaure, A.K. Hassan, A.K. Ray, Semicond. Sci. Technol. **19**, 198–202 (2004)
32. L.E. Scriven, Better Ceram. Chem. **III**, 121 (2008)
33. K. Wasa, M. Kitabatake, H. Adachi, *Thin Film Materials Technology: Sputtering of Compound Materials*, (William Andrew Inc. Norwich, NY, 2005). ISBN-10: 0815514832
34. I. Simon, N. Bârsan, M. Bauer, U. Weimar, Sens. Actuat. B **73**, 1–26 (2001)
35. S. Sampath, J. Therm. Spray Technol. **19**, 5 (2010)
36. L. Pawlowski, *The Science and Engineering of Thermal Spray Coatings*, 2nd edn. (Wiley, Chichester, 2008). ISBN: 978-0-471-49049-4
37. V.V. Sobolev, J.M. Guilemany, J. Nutting, S. Joshi, *High Velocity Oxy-fuel spraying: Theory, Structure–Property Relationships and Applications*, (Maney Ed. London, 2004). ISBN 1902653726
38. A. Sunano, K. Asahi, K. Toshio, Patent number: 4713646 (1985)
39. M. Gardon, J.M. Guilemany, *Intern* (Therm. Spray Conf. Proc. Houston, USA, 2012)
40. J.-O. Kliemann, H. Gutzmann, F. Gärtner, H. Hübner, C. Borchers, T. Klassen, J. Therm. Spray Technol. **20**, 1–2 (2010)
41. G.J. Yang, C.J. Li, F. Han, W.Y. Li, A. Ohmori, Appl. Surf. Sci. **254**, 3979–3982 (2008)
42. M. Yamada, H. Isago, K. Shima, H. Nakano, M. Fukumoto, *Intern* (Therm. Spray Conf. Proc, Singapore, 2010)
43. J.E. Lennard-Jones, Trans. Faraday Soc. **28**, 333–359 (1932)
44. M.J. Madou, S.R. Morrison, *Chemical Sensing with Solid State Devices*, (Academic Press Inc. London, 1989). ISBN-10: 0124649653
45. C.Y. Liu, C.F. Chen, J.P. Leu, J. Electrochem. Soc. **156**, 16–19 (2009)
46. P.K. Dutta, A. Ginwalla, B. Hogg, B.R. Patton, B. Chwieroth, Z. Liang, P. Gouma, M. Mills, S. Akbar, J. Phys. Chem. B **103**, 4412–4422 (1999)
47. R. Ramamoorthy, P.K. Dutta, J. Mat. Sci. **38**, 4271–4282 (2003)
48. T. Jinkawa, G. Sakai, J. Tamaki, N. Miura, N. Yamazoe, J. Mol. Catal. A: Chem. **155**, 193–200 (2000)
49. B.B. Rao, Mat. Chem. Phys. **64**, 62–65 (2002)
50. M. Rumyantseva, V. Kovalenko, A. Gaskov, E. Makshina, V. Yuschenko, I. Ivanova, A. Ponzoni, G. Faglia, E. Comini, Sens. Actuat. B **118**, 1–2 (2006)
51. U. Diebold, Surf. Sci. Rep. **48**, 53–229 (2003)
52. P.W. Tasker, Sol. State Phys. **22**, 4977–4984 (1979)
53. M. Batzill, U. Diebold, Prog. Surf. Sci. **79** (2005)
54. N. Bârsan, U. Weimar, J. Phys. Condens. Matter **15**, R813–R819 (2003)
55. O.K. Varghese, C.A. Grimes, J. Nanosci. Nanotechnol. **3**, 4 (2003)
56. E. Comini, Analytica Chimica Acta **568**, 28–40 (2006)
57. W. Göpel, K.D. Schierbaum, Sens. Actuat. B **26**(1–3), 26–27 (1995)
58. N. Barsan, U. Weimar, J. Electroceram. **7**, 143–167 (2001)
59. J. Tamaki, Z. Zhang, K. Fujimori, M. Akiyama, T. Harada, N. Miura, J. Electrochem. Soc. **141**, 8 (1994)
60. K.D. Schierbaum, U. Weimar, W. Göpel, Conductance, work function and catalytic activity of SnO_2-based gas sensors. Sens. Actuat. B: Chem. **3**, 205–214 (1991)
61. C. Xu, J. Tamaki, N. Miura, N. Yamazoe, Sens. Actuat. B **3**, 2 (1991)
62. A. Rothschild, Y. Komem, J. Appl. Phys. **95**, 11 (2004)
63. T. Becker, S. Ahlers, C. Bosch-v.Braunmühl, G. Müller, O. Kiesewetter, Sens. Actuat. B **77**, 55–61 (2001)
64. J.F. Chang, H.H. Kuo, I.C. Leu, M.H. Hon, Sens. Actuat. B **84**, 258–264 (2002)
65. M. Tiemann, Chem. Eur. J. **13**, 30 (2007)
66. S. Capone, A. Forleo, L. Francioso, R. Rella, P. Siciliano, J. Spadavecchia, D.S. Presicce, A.M. Taurino, J. Optoelectr, Adv. Mat. **5**, 5 (2003)
67. K. Wetchakun, T. Samerjai, N. Tamaekong, C. Liewhiran, C. Siriwong, V. Kruefu, A. Wisitsoraat, A. Tuantranont, S. Phanichphant, Sens. Actuat. B **160**, 1 (2011)
68. C. Zhang, M. Debliquy, A. Boudiba, H. Liao, C. Coddet, Sens. Actuat. B **144**, 280–288 (2010)
69. Y. Shen, T. Yamazaki, Z. Liu, D. Meng, T. Kikuta, N. Nakatani, Thin Solid Films **517**, 2069–2072 (2009)
70. J.R. Setter, J. Li, Chem. Rev. **108**, 352–366 (2008)
71. I.A. Al-Homoudi, J.S. Thakur, R. Naik, G.W. Auner, G. Newaz, Appl. Surf. Sci. **253**, 8607–8614 (2007)
72. L. Francioso, D.S. Presicce, M. Epifani, P. Siciliano, A. Ficarella, Sens. Actuat. B **107**, 563–571 (2005)
73. M.C. Carotta, S. Gherardi, C. Malagù, M. Nagliati, B. Vendemiati, G. Martinelli, M. Sacerdoti, I.G. Lesci, Thin Solid Films **515**, 23 (2007)
74. A. Chena, S. Baia, B. Shia, Z. Liua, D. Lia, C.C. Liu, Sens. Actuat. B **135**, 1 (2008)
75. N.J. Dayan, S.R. Sainkar, R.N. Karekar, R.C. Aiyer, Thin Solid Films **325**, 254–258 (1998)
76. W.H. Tao, C.H. Tsai, Sens. Actuat. B **81**, 2–3 (2002)
77. M.V. Vaishampayan, R.G. Deshmukh, P. Walke, I.S. Mulla, Mat. Chem. Phys. **109**, 2–3 (2008)
78. S.V. Manoramaa, C.V. Gopal Reddya, V.J. Rao, Nanostruct. Mater **11**, 5 (1999)
79. G.N. Chaudhari, D.R. Bambole, A.B. Bodade, P.R. Padole, J. Mat. Sci. **41**, 15 (2005)
80. B. Karunagarana, P. Uthirakumara, S.J. Chunga, S. Velumanib, E.-K. Suh, Mater. Charact. **58**, 8–9 (2007)
81. M. Sánchez, M.E. Rincón, Sens. Actuat. B **140**, 17–23 (2009)
82. D.V. Dao, K. Shibuya, T. Thanh Bui, S. Sugiyama, Proc. Eng. **25**, 1149–1152 (2011)
83. Y. Shimizu, N. Matsunaga, T. Hyodo, M. Egashira, Sens. Actuat. B **77**, 1–2 (2001)
84. T. Zhong, B. Quan, X. Liang, F. Liu, B. Wang, Mater. Sci. Eng. B **151**, 2 (2008)
85. X. Liang, T. Zhong, B. Quan, B. Wang, H. Guan, Sens. Actuat. B **134**, 1 (2008)
86. P. Hidalgo, R.H.R. Castro, A.C.V. Coelho, D. Gouveâ, Chem. Mater **17**, 16 (2005)

5 Experimental procedures

5.1 Technologies

Atmospheric Plasma Spray and Cold Gas Spray were used for building-up the coatings. The aim of this section is determine the influence of operational parameters analysed during the experiments. Concretely: temperature of APS plasma jet and velocity of CGS N_2 stream.

5.1.1 Atmospheric Plasma Spray

Thermal spray equipment based on APS A-3000S system with an F4 plasma torch (Sulzer Metco, Germany) was used. Atmospheric Plasma Spray propels powder particles to a substrate by means of a plasma jet, which is formed because of the flow of Ar + H_2 mixture through an electric arc. Coatings are built-up due to particles are molten and solidified on the substrate surface. This technology permits to easily deposit any material. Unfortunately, undesired microstructural and compositional changes are often obtained. Coating procedure is commanded by the energetic conditions of the plasma jet, which in turn supplies velocity and heat to the particles. Commonly, arc intensity increases the specific enthalpy of the plasma and it leads to greater particle temperatures. The equipment provides necessary data such as: cooling water flow, water temperatures, electric intensity and voltage. Therefore, some calculations can be carried out in order to estimate plasma enthalpy:

P: power

P_c: cooling power

P_p: plasma power

q: water flow

q_m: molar flow

C_p: specific heat of water

T_1: inlet temperature (water cooling)

T_2: outlet temperature (water cooling)

H_p: plasma enthalpy

$$P\ [W] = I \cdot V \qquad \text{Eq. 1}$$

$$P_c\ [W] = q \cdot C_p \cdot (T_2 - T_1) \qquad \text{Eq. 2}$$

$$P_p\ [W] = P \cdot -P_c \qquad \text{Eq. 3}$$

$$q_m\ [mol/s] = qAr + qH_2 \qquad \text{Eq. 4}$$

$$H_p[kJ/mol] = P_p/q_m \qquad \text{Eq. 5}$$

Henceforth, distinct routes can be used for calculating plasma temperature as a function of plasma composition. In this case, graphic procedure has been selected as a semi-quantitative method [6]. Figure 3 shows plasma temperature dependence with composition and enthalpy. From this, it can be found an approximate value related to the energetic conditions of the plasma with which that is operating.

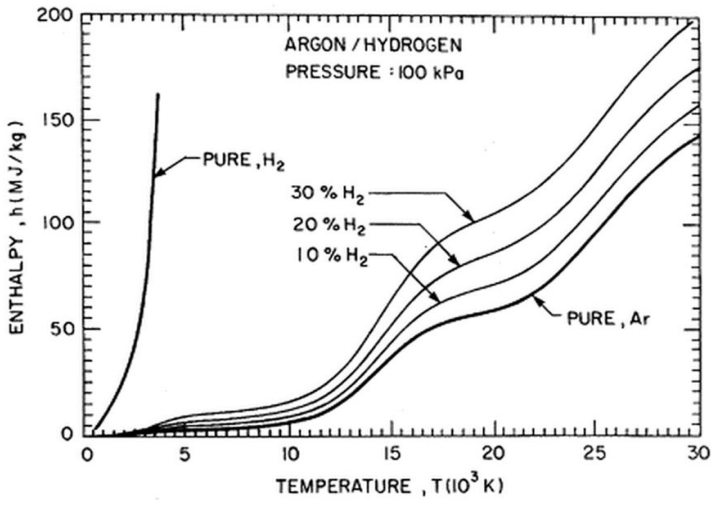

Figure 3. Plasma enthalpy for different compositions and their temperature.

Anyhow, hydrogen and argon contribute in a different way to the feedstock in terms of energy. In spite of argon has a higher plasma temperature compared to hydrogen for a given enthalpy, argon plasma has a lower capacity of transferring heat to the powder due to its lower thermal convection coefficient (figure 4). On the other hand, argon disposes a greater capacity of propelling the particles. Therefore, spraying parameters must be adequately balanced with the aim of achieving the required level of acceleration and fusion.

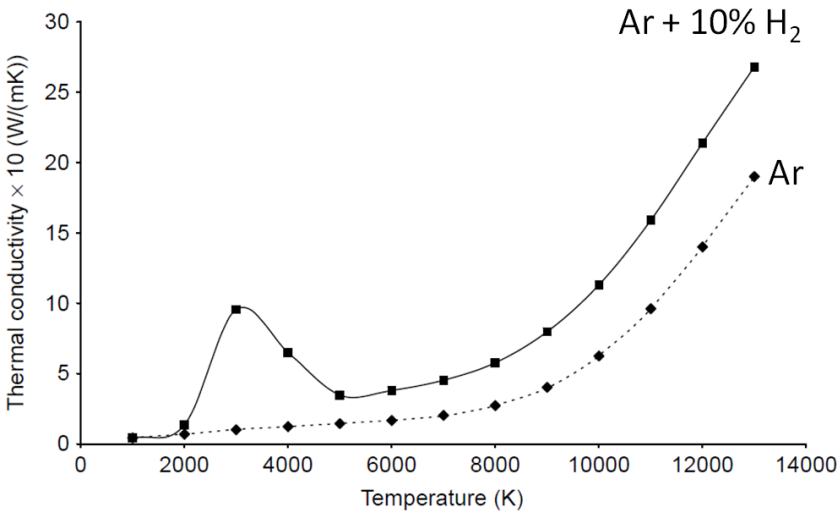

Figure 4. Thermal conductivity of pure Ar plasma and Ar plasma with 10% of H2 [7].

5.1.2 Cold Gas Spray

The CGS equipment was a KINETICS® 4000 (Cold Gas Technology, Ampfing, Germany), with a maximum operating pressure of 40 bar, temperature of 800 °C and it used nitrogen as the propellant gas. In addition, KINETICS® 4000 had the possibility of using a pre-chamber of 120 mm in length connected to the nozzle of the gun where powders are heated up for a longer time.

Main parameters studied in CGS during this thesis were temperature and pressure. Convergent-divergent design of the nozzle is able to propel powder particles to high velocities. Then, these are plastically deformed and anchored onto the substrate. Inlet temperature is in command to accelerate N_2 to supersonic regime and may favour the deformation of feedstock due to certain thermal softening. Pressure provides more energy to the in-flight particles at the outlet in order to achieve a proper bonding onto the substrate.

Some authors have adjusted fluid mechanics to CGS equipment so as to understand the influence of starting pressure and temperature [8]. The flow is considered uniform, adiabatic and isentropic. Control-volume is defined and non-deformable. The problem is solved in steady-state without losses. Here, main equations are included:

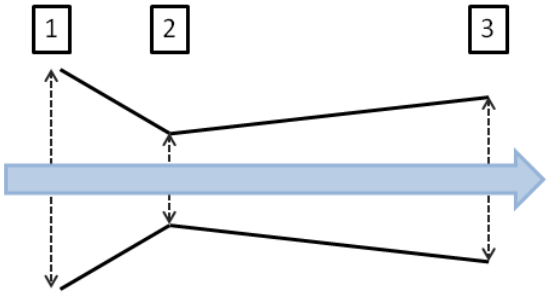

Figure 5. CGS nozzle diagram:1/ inlet, 2/ throat and 3/ outlet.

r: radius

A: area

R_{N2}: ideal gas constant

γ: adiabatic parameter

T: temperature

P: pressure

ρ: density

M: mach

v: velocity

T_0,P_0, ρ_0: stagnation values

Table 2. Known data in CGS system.

r_1 [m]	r_2 [m]	r_3 [m]	γ	R_{N_2} [J/K·Kg]	T_1 [K]	P_1 [Pa]
0,009	0,0015	0,003	1,4	297	*input*	*input*

Figure 5 shows a diagram of the nozzle with its studied points. Data can be found in table 2. From relation between areas, it is possible to calculate Mach number at point 1. Then, velocity and mass-flow may be directly estimated because T, P and ρ are known.

Mach number:

$$\frac{A_1}{A*} = \frac{1}{M_1}\left[\left(\frac{2}{\gamma+1}\right)\left(1+\left(\frac{\gamma-1}{2}\right)M_1^2\right)\right]^{\frac{\gamma+1}{2(\gamma-1)}} \quad \text{Eq. 6}$$

$$-\frac{5}{6}M_1^{-1/3} - \frac{1}{6}M_1^{5/3} + \sqrt[3]{\frac{A_1}{A*}} = 0 \quad \text{Eq. 7}$$

Density:

$$\rho_1 = \frac{P_1}{R \cdot T_1} \quad \text{Eq. 8}$$

Velocity:

$$v_1 = M_1\sqrt{R \cdot \gamma \cdot T_1} \quad \text{Eq. 9}$$

Mass-flow:

$$m_1 = v_1 \cdot S_1 \cdot \rho_1 \qquad \text{Eq. 10}$$

Before going to point 2, stagnation temperature, pressure and density must be calculated. Stagnation values are constant and may be useful for calculating temperature, pressure and density at any point of the nozzle if Mach number is known.

Stagnation temperature:

$$T_0 = T_1 \cdot \left(1 + \frac{(\gamma-1)}{2} M_1^2\right) \qquad \text{Eq. 11}$$

Stagnation pressure:

$$P_0 = P_1 \cdot \left(1 + \frac{(\gamma-1)}{2} M_1^2\right)^{\frac{\gamma}{\gamma-1}} \qquad \text{Eq. 12}$$

Stagnation density:

$$\rho_0 = \rho_1 \cdot \left(1 + \frac{(\gamma-1)}{2} M_1^2\right)^{\frac{1}{\gamma-1}} \qquad \text{Eq. 13}$$

T, P and ρ at point 2 are calculated according stagnation values. Note that Mach number may not be estimated because its value is 1 at the throat.

Temperature:

$$T_2 = \frac{T_0}{\left(1+\frac{(\gamma-1)}{2} M_2^2\right)} \qquad \text{Eq. 14}$$

Pressure:

$$P_2 = \frac{P_0}{\left(1+\frac{(\gamma-1)}{2}M_2^2\right)^{\frac{\gamma}{\gamma-1}}} \quad \text{Eq. 15}$$

Density:

$$\rho_2 = \frac{\rho_0}{\left(1+\frac{(\gamma-1)}{2}M_2^2\right)^{\frac{1}{\gamma-1}}} \quad \text{Eq. 16}$$

Velocity:

$$v_2 = M_2\sqrt{R \cdot \gamma \cdot T_2} \quad \text{Eq. 17}$$

Mass-flow:

$$m_2 = v_2 \cdot S_2 \cdot \rho_2 \quad \text{Eq. 18}$$

Parameters at point 3 may be calculated as a combination of the equations in points 1 and 2. First, M number is determined and then T, P and ρ are estimated as a function of stagnation parameters.

Mach number:

$$\frac{A_3}{A*} = \frac{1}{M_3}\left[\left(\frac{2}{\gamma+1}\right)\left(1+\left(\frac{\gamma-1}{2}\right)M_3^2\right)\right]^{\frac{\gamma+1}{2(\gamma-1)}} \quad \text{Eq. 19}$$

$$-\frac{5}{6}M_3^{-1/3} - \frac{1}{6}M_3^{5/3} + \sqrt[3]{\frac{A_3}{A*}} = 0 \quad \text{Eq. 20}$$

Temperature:

$$T_3 = \frac{T_0}{\left(1+\frac{(\gamma-1)}{2}M_3^2\right)} \quad \text{Eq. 21}$$

Pressure:

$$P_3 = \frac{P_0}{\left(1+\frac{(\gamma-1)}{2}M_3^2\right)^{\frac{\gamma}{\gamma-1}}} \quad \text{Eq. 22}$$

Density:

$$\rho_3 = \frac{\rho_0}{\left(1+\frac{(\gamma-1)}{2}M_3^2\right)^{\frac{1}{\gamma-1}}} \quad \text{Eq. 23}$$

Velocity:

$$v_3 = M_3\sqrt{R \cdot \gamma \cdot T_3} \quad \text{Eq. 24}$$

Mass-flow:

$$m_3 = v_3 \cdot S_3 \cdot \rho_3 \quad \text{Eq. 25}$$

5.2 Characterization techniques

5.2.1 Characterization of powders and coatings

Microscopy: Optical Microscopy (DMI-M Leica), Scanning Electron Microscopy (JSM-5310, Jeol – ProX, Phenom) and Field-Emission Scanning Electron Microscopy (401s, Hitachi) were used for the observation of feedstock powders, substrates and coated pieces. Previous metallographic preparation was done following the standard ASTM E3-95.

- Energy Dispersive Spectroscopy (EDS): Common point and scanning analysis (Xflash detector X5010, Bruker) were carried out in powders and coatings.

- Diferential Scanning Calorimeter: was used for determining the re-oxidation of oxygen vacancies in the crystal lattice of rutile (DSC Perkin-Elmer DSC-7).

- X-Ray Diffraction (XRD): crystalline composition of different powders, substrates and coatings was analyzed by means of a diffractometer (X'Pert PRO MPD, PANalytical).

- X-ray Photoelectron Spectroscopy (XPS): attempts for measuring the amount of oxygen vacancies in titanium dioxide powders and coatings were performed in a PHI 5500 Multitechnique System (Physical Electronics).

- Micro-Raman Spectroscopy: Surface composition of metal oxides and some polymers is accurately analyzed by Raman spectroscopy (Labram HR800, Horiba).

- Laser Scattering (LS): particle size distribution must be specially controlled and it was carried out using a Laser Diffraction Particle Size Analyser Beckman Coulter LS 13320.

- Hardness: this parameter has been evaluated by means of a Matsuzawa MTX-α Vickers equipment according to the ASTM E384-99 standard.

- Tensile Strength: coating adhesion has been evaluated following the ASTM C-633 standard (SERVOSIS ME-402/10).

- Roughness: roughness of the substrate must be especially controlled in TS processes and it was conducted in this study using a rugosimeter SJ-210 (Mitutoyo).

- Grit-Blasting: corundum particles were propelled to substrates using a stream of compressed air (MAB-4, Mab Industrial, S.A.).

5.2.2 Factorial design of experiments

Large amount of influencing parameters in Thermal Spray processes obligue to plan detailed experimental procedures so as to understand the effect of each variable. Thus, factorial design of experiments has been commonly selected as a tool for achieving coherent results. Plasma intensity, Ar/H_2 ratio, stand-off distance, flow rate and cooling system have been standard studied

parameters in APS. On the other hand, N_2 pressure, N_2 temperature, stand-off distance, flow rate and substrate surface were analyzed factors in CGS. Number of levels depended on materials involved and starting hypothesis.

5.2.3 Analysis of functional coatings

Techniques and equipments related to electrodes, gas sensors, photocatalysts and bone implants are available in the reports presented in this thesis (Papers 4-8,10). As regards to measurements of radiation sensors, UV measurements were made with a xenon lamp, model LC8 with a maximum power of 4500 mW/cm^2 at 365 nm wavelength, with a dispersion of 220 nm to 580 nm. Visible light LEDs were used as commercial lighting KA-8070QB10Z1S with peak emission at 453 nm and KA-8070ZG10Z1S with peak emission at 530 nm.

6. Results and partial discussion

6.1 Atmospheric Plasma Spray

6.1.1 Detailed background

a) Irreversible transformations

As it has been reviewed before, high temperatures and chemical composition in the plasma jet may alter the starting feedstock. First trials were carried out using a non-commercial powder supplied by Degussa®. As it can be observed in figure 6, powder was spherical and had a wide particle size distribution. Common spraying conditions in APS for metal oxides and steel substrates were used with different stand-off distances (summarized in Appendix – Table 1).

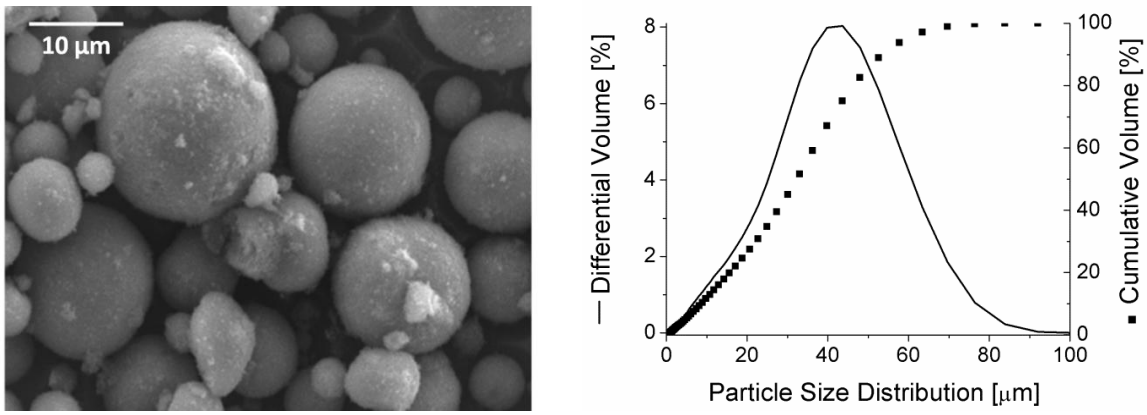

Figure 6. Left: Scanning electron micrograph of the powder. Right: particle size distribution.

At first glance, it was effortless to identify that uncontrolled phenomena could be happening by simply observation of the coatings. Figure 7 shows a macrography of the feedstock and a coated sample. There is a change in the colour from a typical white of titanium dioxide, which has led this material to be one of the most used pigments [9], towards blue-black.

Figure 7. Image of TiO_2 feedstock powder and a coated sample.

Publications reported by other authors attribute this colour transformation to partial deoxidation of titanium dioxide and incorporation of oxygen vacancies into the crystal lattice of rutile [10]. XRD analysis was carried out to starting powder and APS coating (figure 8). As regards to the amount of metastable anatase phase, a clear decrease is observed when comparing its peaks. It is possible to estimate the fraction of anatase compared rutile using equation 6 and taking into account the intensity associated to crystallographic plane (1 1 0) of rutile and (1 0 1) of anatase respectively found at 27,5° and 25,5° [11]. Thus, initial amount of 83% in anatase was decreased to final 11%. This loss is in agreement with all the literature reviewed in Paper 1 (3.1 State-of-the-art). It could be possible to readjust the spraying conditions for developing a less energetic plasma stream and supply cooling by N_2 to the substrates during the coating process in order

to preserve the amount of anatase in the coating. However, competitive values are out of reach.

$$Y_r = \frac{1}{[1+0{,}8\cdot\left(\frac{I_a}{I_r}\right)]} \qquad \text{Eq. 26}$$

Y_r= fraction of rutile

I_a= intensity of peak (1 0 1) in anatase

I_r= intensity of peak (1 1 0) in rutile

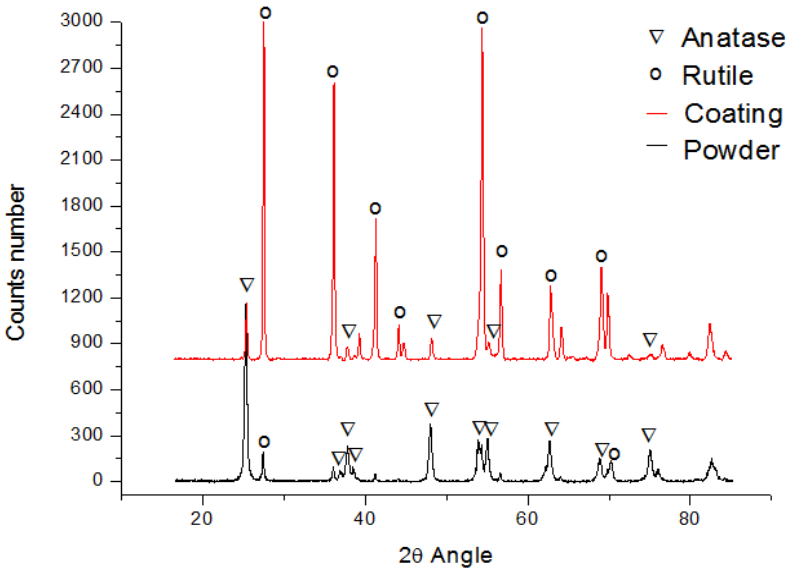

Figure 8. XRD of starting powder and characteristic APS titanium dioxide coating.

b) Titanium sub-oxide coatings

The supposed different oxidation degree of powder and coating was not properly represented by X-Ray Diffraction. XRD determines the structure of a

crystal by means of an X-ray beam that diffract to specific directions. Therefore, if same elements and crystal is studied, it makes difficult to analyze their differences. Crystalline structure of non-stoichiometric TiO_{2-x} ($x \leq 10^{-2}$) and Magnéli phases (Ti_nO_{2n-1} n=4-10) is the same than rutile, having the latter some characteristic crystallographic shear planes [5]. Thus, its discrimination by XRD technique may be almost impossible due to a quasi-complete overlapping of their peaks [12].

Micro-Raman Spectroscopy was also used for comparing the nature of the surface of distinct titanium oxides. It was obtained a significant differentiation in the spectra, shown in Paper 5. Oxidation degree could be correlated to the position of a flattened peak at 550 cm^{-1}, which differed when comparing starting feedstock with titanium sub-oxide coating. Nevertheless, this data is just related to the surface and may not be representative.

Previous studies have reported that Ti^{3+} peaks in X-Ray Photoemission Spectroscopy spectra of TiO_2 could be linked with the concentration of oxygen vacancies [13]. Actually, removal of a neutral oxygen atom leaves behind two electrons, which lead to the formation of Ti^{3+} states [14]. XPS provides spectra as a function of the binding energy of these electrons. Thus, high resolution using X-ray Photoelectron Spectroscopy in the area around the corresponding contribution provided more information related to oxygen vacancies. Then, curves were normalized using solver equation in Excel (Microsoft®) data sheet fitting the total area under the spectra with different Gaussian curves associated to Ti^{4+} and Ti^{3+} orbitals. Figure 9 represents XPS spectra of Ti-O system of a powder with large amount of oxygen vacancies, commercially acquired from Ebonex®, where corresponding curves of TiO_2 and TiO_{2-x} are also shown.

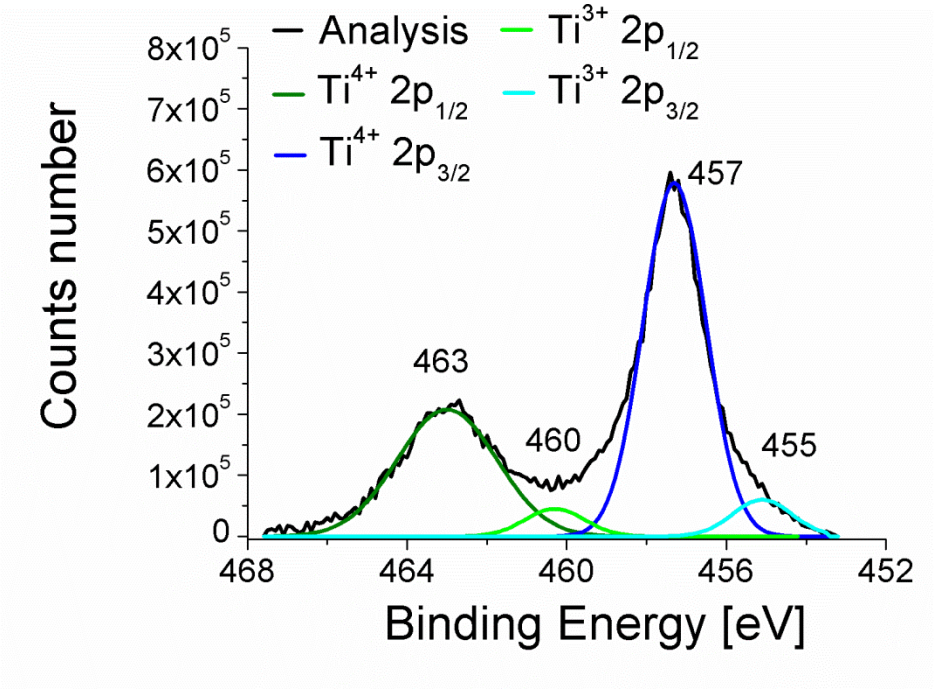

Figure 9. High Resolution XPS around Ti^{4+} and Ti^{3+}.

Following the same procedure than above, it was compared a powder based on Magnéli Phases (Ti_4O_7, Ti_5O_9), APS TiO_{2-x} coating obtained from previous section and pure rutile powder (Sulzer Metco®). Table 3 and 4 compiles binding energies associated to electrons and each corresponding area of Ti^{3+}, which lead to the amount of oxygen vacancies in the solid.

Table 3. Binding energies of Ti^{4+} and Ti^{3+} orbitals measured by XPS.

Ti^{4+} $2p_{1/2}$	Ti^{4+} $2p_{3/2}$	Ti^{3+} $2p_{1/2}$	Ti^{3+} $2p_{3/2}$
462,9 eV	457,3 eV	460,5 eV	455,4 eV

Table 4. Area associated to Ti^{3+}.

TiO_2	APS TiO_{2-x} coating	Ti_nO_{2n-1}
18,3%	23,2%	29,9%

Despite observing in this example an expected increase in the area associated to Ti^{3+}, namely oxygen vacancies, XPS may not provide the desired accurate measures that would discriminate Ti^{3+} values among different coatings. Various repetitions gave significantly different results, which even led to some contradictions when comparing APS coatings. This was attributed to slight changes in the experimental conditions applied during the XPS analysis. In front of these difficulties, best way for understanding the oxidation degree of titanium dioxide was XRD analysis together with electrical resistivity of the samples measured experimentally.

6.1.2 Electrodes

Having in mind the formation of oxygen vacancies during the spraying process starting from pure TiO_2 and the high interest of titanium sub-oxides as electroceramics; it was sprayed again onto non-conducting ceramic tile for measuring the electric resistivity of the samples. Already reduced titanium dioxide powder was selected as feedstock in order to reach higher electrical conductivities (characterization included in Paper 3, 4). Ar/H_2 ratio was studied so as to understand the influence of hydrogen in the reduction of titanium dioxide towards reduced stoichiometries. Furthermore, hydrogen is in command to transfer more energy to the particles. Coefficient of Thermal Expansion (CTE) mismatch could be enhanced and should be controlled as well. Stand-off distances would also be an interesting parameter for being studied. Spraying conditions are included in Appendix.

a) Paper 3:

M. Gardon, J. M. Guilemany. The influence of titanium sub-oxides in thermal sprayed coatings, Int. Thermal Spray Conf. proceedings 2012.

The following report summarizes starting findings related to APS titanium dioxide coatings onto ceramic tiles. Main concerns were based on achieving a proper bonding without delamination between layers. Different APS parameters were studied and correlated with coating microstructure and electrical resistivity.

Thermal Spray 2012: Proceedings from the International Thermal Spray Conference and Exposition
May 21–24, 2012, Houston, Texas, USA
R.S. Lima, A. Agarwal, M.M. Hyland, Y.-C. Lau, C.-J. Li, A. McDonald, F.-L. Toma, editors

The Influence of Titanium Sub-Oxides in Thermal Sprayed Coatings

M. Gardon, J. M. Guilemany*
Thermal Spray Centre, University of Barcelona, Barcelona, Spain
**E-mail: jmguilemany@ub.edu*

Abstract

Plasma spray process has been used for achieving titanium oxide coatings under the current stoichiometry of titania and titanium suboxides. It was used a feedstock powder based in: Magnéli phases Ti_nO_{2n-1}, slightly reduced titania TiO_{2-x} and rutile. A factorial design of experiments is included in this study for a better understanding of the influence that the operational parameters have in the coating quality, the electric resistivity and the oxidation degree of titanium oxide during the spraying. Firstly, arc current intensity and stand-off distance were studied finding deep correlations between particle temperatures and the electric resistivity of the coating. Then, different plasma compositions were used in order to understand the influence of hydrogen in the formation of titanium sub-oxides. The hardness of the most significant coatings was analyzed.

Introduction

Among the different metal oxides used for industrial applications, titanium oxide is a well-known material with a wide range of final purposes. A considerable amount of research has been focused in titanium dioxide thermal sprayed coatings in order to improve the catalytic performance of different organic compounds degradation (Ref 1, Ref 2). Nevertheless, reduced stoichiometries of titanium dioxide have been studied and used in thermal spraying processes as well. These reduced forms are known as Magnéli phases (Ti_nO_{2n-1}, n= 4-10) and have reached a great interest in research and industrial applications due to its optimal lubricant performance and low electrical resistivity in comparison with rutile, anatase or brookite (Ref 3, Ref 4).

As has been published before (Ref 5), the gas composition used for the plasma generation is a determining variable in the formation of oxygen vacancies in the crystal lattice. A flame reach in hydrogen has a reducing effect in titanium dioxide powders. In addition, different electric arc intensities alter the plasma temperature and, as a consequence, the transferred energy from the plasma to the particle. Henceforth, particle temperature and velocity are affected.

The aim of this work is based in achieving functional coatings by thermal spray for different industrial applications.

Experimental

Materials

A commercially available powder was used (Metco 102, Sulzer Metco) and it contained a mixture of TiO_2 (rutile), Ti_8O_{15} and Ti_9O_{17}, Fig. 1 shows its X-Ray diffractogram. The powder particle size range was -55, +10 µm. As it can be observed in Fig. 2, it has an angular geometry. The substrates were ceramic plates (40x40x5mm) commonly used in decorative construction based on a mixture of clays, silica, dyes and other materials. Before spraying, all substrates were grit-blasted and cleaned with ultrasounds and acetone.

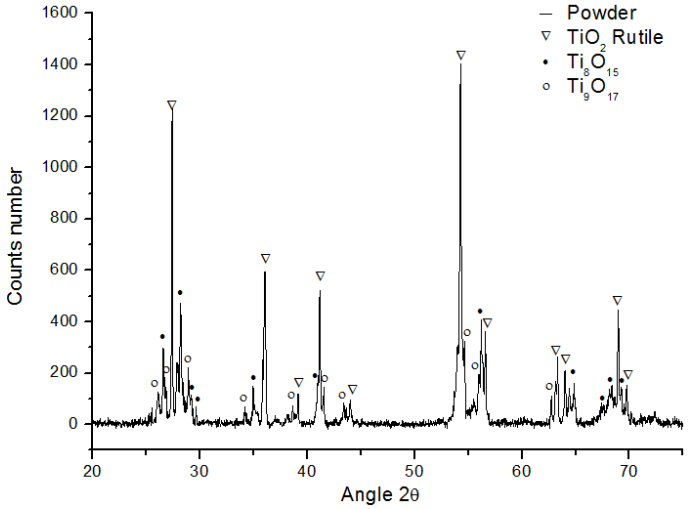

Figure 1: X-ray spraying powder diffractogram.

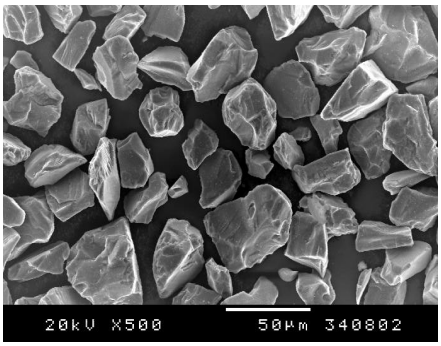

Figure 2: Powder morphology. Micrograph taken through Scanning Electron Microscopy.

Equipment

The feedstock powder was sprayed using an Atmospheric Plasma Spray (APS) A-3000S system with an F4 plasma torch (Sulzer Metco, Germany). Velocity and temperature of the in-flight particles were measured using the Spraywatch system (Oseir, Tampere, Finland). Concretely, particle temperature was measured using two-color pyrometry. In the case of particle velocity, a CCD camera determined the length traveled by the particles in the capture time. The mechanical characterization was carried out on the cross-section of the coatings by means of Nanoindenter XP (MTS, USA). A four-point probe test was developed employing a Multimeter 3478A (Hewlett-Packard, USA) for determining the value of the electric resistivity in each coating. Cross-section area of the coatings was studied by Optical Microscopy, OM (DMI 5000M, Leica) and Scanning Electron Micrsocopy, SEM (JSM-5310, Jeol).

Factorial Design of Experiments

Arc current Intensity and stand-off distance were the analyzed factors for the factorial design of experiments. Concretely, the studied levels where: i) four equidistant levels for the distance (in ascending order: 1A, 1B, 1C and 1D) and; ii) three equidistant levels in the case of electric intensity (in ascending order: 2A, 2B and 2C). In this way, it was sprayed $3^2 + 3^1$ conditions. Figure 3 shows a diagram of this factorial design of experiments. Other parameters like the spraying angle, feeding rate and Ar/H_2 flow were not altered in order to understand the interaction of the chosen factors. In the Table 1 are collected different and constant parameters of the spraying system.

Table 1: Values of the spraying parameters used.

Ar/H_2 flow	40-55 L/min
Feeding rate (carrier gas)	3-4,5 L/min
Spraying angle	90º
Gun speed in each pass	100-500 mm/s
Number of cycles	4
Stand-off Distance	80-150 mm
Arc current intensity	350-650 A

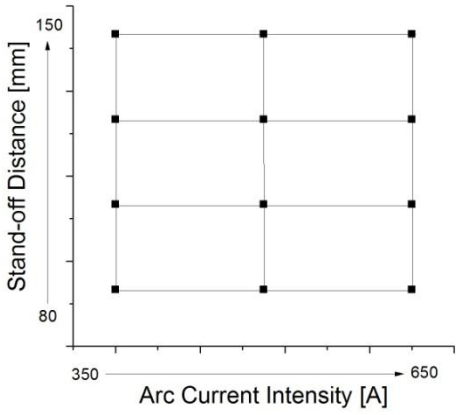

Figure 3: Factorial design of experiments. Stand-off distance versus arc current intensity.

In order to understand how the hydrogen influences the oxidation grade of titanium oxide thermal sprayed coatings, the quality of its microstructure and the value of the electric resistivity other sprayings were done. This was achieved by reducing the amount of H_2 in a 50%, 75% and 100% of its starting Ar/H_2 mix. The arc current intensity and the spraying distances were taken from the coating that showed higher mechanical properties. A determining variable was the cracking number, which consists in the amount of cracks starting from the coating surface and ending at the substrate on the cross-section area of each coating. The number of these cracks was studied for all the samples observing the cross-section area by OM and SEM. Henceforth, the chosen condition for the hydrogen experience was accordingly to the coating that had less cracks in its cross-section area and that had better adhesion.

Results and Discussion

All coatings showed a lamellar structure because of the different oxidation degree of the titanium-oxygen system. This phenomenon is caused by the interaction of the powder and the flame in each passing of the gun. Although the porosity was almost constant for all the samples, a clear tendency was observed when the spraying distance was increased; the cracking number was abruptly reduced. In addition, this decrease was absolutely regardless of the arc current intensity. The value of the cracking number and the particle temperature are shown in Fig. 4.

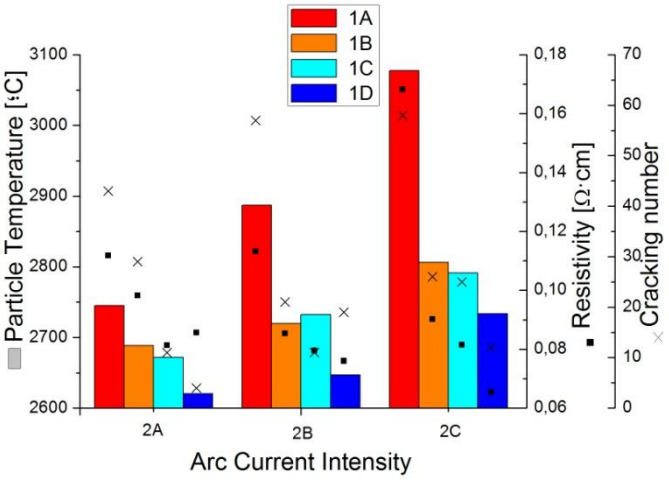

Figure 4: Evolution of particle temperature and cracking number of the coatings for the different operation conditions.

As stand-off distance decreased and the arc current intensity increased, the particle temperature was enhanced. This may be the main reason why the cracking number is lower for higher distances. Deformation as a result of thermal expansion is greater. Finally, greater residual stresses are found in the coatings leading to more cracks and a poorer quality of these. The particle velocity follows the same trend than the particle temperature. It is reduced as the stand-off distances increases (Fig. 5).

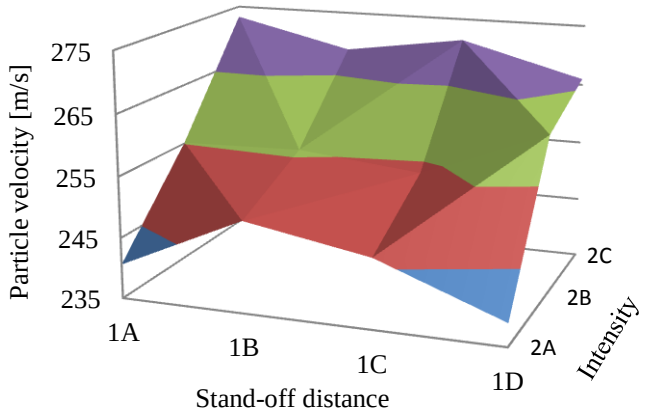

Figure 5: Evolution of particle velocity for the different operation conditions.

The best quality of the samples was determined by Optical and Scanning Electron Microscopy observation. Almost no cracks were found when spraying at the largest distance (1D) and the lowest arc current intensity (2A). The cross-section of this coating can be observed in Fig. 6 and its composition is showed by means of an X-ray diffractogram in Fig. 7.

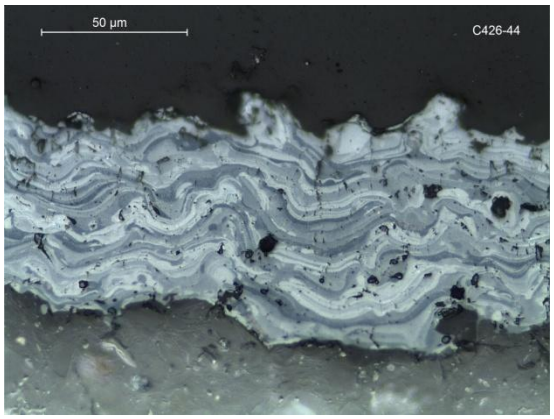

Figure 6: Optical micrograph of the coating which showed less number of cracks in its cross-section area and better adhesion.

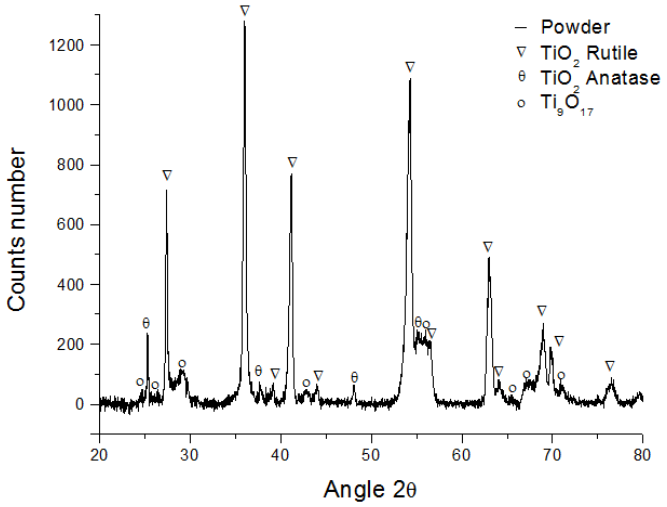

Figure 7: X-ray diffractogram of the coating showed in Fig. 6.

These conditions were used for the study of the influence of hydrogen in the oxidation degree of titanium oxide coatings. Although X-Ray Diffraction is a common tool used for determining the phase composition of raw materials and coatings in thermal spraying, it is not a proper way for measuring the oxidation degree in titanium sub-oxides due to the overlapping of the peaks corresponding to Magnéli phases and rutile (Ref 6). However, it is possible to understand the oxidation degree by means of the electric resistance of the coating. As the value of the resistivity increases, the oxidation degree grows. Thus, as it can be observed in Fig. 8, for those spraying conditions with less hydrogen, the electric output signal shows higher resistivity. Moreover, it is also noteworthy that the cracking number for the conditions with hydrogen is increased. Samples sprayed with no hydrogen have less electric resistivity although they have more cracks, which act as a barrier for electron mobility. Concretely, 0.06 Ω·cm when using the starting mixture of Ar/H_2 and 0.33 Ω·cm when H_2 was completely removed from the mix. This

fact can also be explained by the same reason than above. Argon plasma has a higher temperature than hydrogen plasma (Ref 7). However, the heat convection coefficient for argon is much lower than in the case of hydrogen. Therefore, an Ar/H_2 plasma mix which has lower amount of hydrogen will develop higher flame temperatures but lower capacity of transfer heat from the flame to the particle, which was also ratified by means of using Spraywatch and it is included in the Fig. 8. This confirms that reduced stoichiometries of titanium oxide may be assured by the use of hydrogen during the spraying process, as it has been published by other authors in the past (Ref 5).

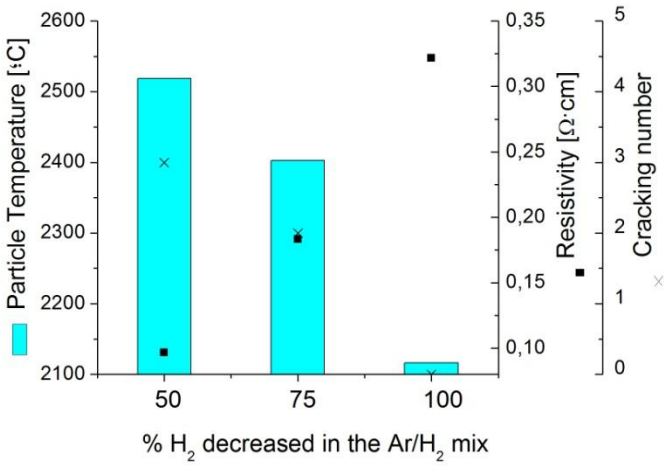

Figure 8: Evolution of particle temperature, cracking number and electric resistivity of the coatings for the different operation conditions.

The characteristics of the selected coatings for analyzing its hardness are summarized in the Table 2. It was a key step to observe each indentation one-by-one. Thereafter, defective values were rejected because of the existence of microcracks or porous on the surface.

Table 2. Spraying conditions of the selected coatings for studying its hardness.

Coating	Ar/H_2 mixture	Stand-off distance
C426-A	Starting mix	1D
C426-B	Starting mix	1A
C426-C	Decrease of 50% H_2	1D
C426-D	Decrease of 100% H_2	1D

5 matrices of 10x3 indentations were done for each coating using loads of 500 mN. In order to avoid the influence of one indentation towards the others, a minimum space of 1500 micrometers was applied between the matrices and 20 micrometers of separation was used among the indentations. The results show similar values for the different coatings. In the case of coatings with reduced oxides, the hardness is lower. This could be due to the presence of several layers of different sub-oxides that develop a lamellar structure. Thus, the coatings that have been obtained with little or no quantity of hydrogen may have not the same incidence of interlamellar cracking phenomena.

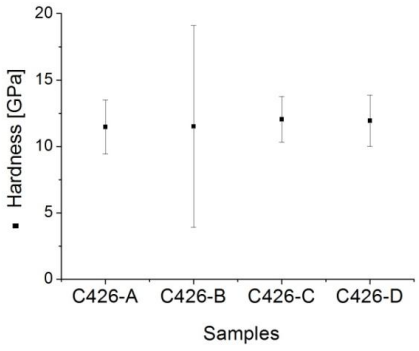

Figure 9: Hardness of the coatings C426-A,B (reduced oxides from the factorial design of experiments) and C426-C,D (sprayed with less or without H_2 in the plasma mixture).

The sample that showed highest standard deviation is the one with worst quality in the experimental design. The rising in the amount of cracks (Fig. 4) in these spraying conditions may be the cause of the increase in the standard deviation. The hardness values for the studied coatings can be observed in Fig. 9.

Conclusions

Titanium sub-oxides with distinct levels of oxidation induced by the operational conditions of plasma spraying and different levels of quality related to its microstructure have been deposited as coatings of ceramic substrates. The main conclusions of this study are:

- A decrease in the value of the electric resistivity was found as long as the spray distance was larger. This may be because of the particle temperature is higher at lower stand-off distances and the effect of the difference in the thermal expansion coefficient between the powder and the substrate is emphasized. For this reason, more residual stress is accumulated and more cracks are formed, especially for the most energetic conditions (1A, 2C).
- The value of the resistivity is decreased when the cracking number increases due to each crack acts as a barrier-resistance for the electric current, with the exception of those sprayings in which the amount of hydrogen decreases (Fig. 8).
- To reduce the amount of hydrogen in the mixture of Ar/H_2 for the forming plasma-gas leads to a flame with a lower capability of transferring energy to the particles and less cracks are formed in the coating.

However, flames with a lower amount of hydrogen do not have the capability of reducing titanium dioxide towards titanium sub-oxides/magnéli phases. Thus, the electric conductivity of the coating decreases.

- It is possible to yield titanium sub-oxide plasma sprayed coatings without cracks in its structure and with an electric resistance bellow 0,33 Ω·cm.

Acknowledgments.

The authors wish to thank the Generalitat de Catalunya for the financial support for this research project 2009 SGR 00390.

References

1. F. L. Toma, D. Sokolov, G. Bertrand, D. Klein, C. Coddet, and C. Meunier, Comparison of the Photocatalytic Behavior of TiO_2 Coatings Elaborated by Different Thermal Spraying Processes, *J. Therm. Spray Technol*., 2006, **15**(4), p 576-581
2. S. Kozerski, F.L. Toma, L. Pawlowski, B. Leupolt, L. Latka, L. M. Berger, Suspension Plasma Sprayed TiO_2 Coatings Using Different Injectors and Their Photocatalytic Properties, *Surf. Coat. Tech*., 2010, **205**(4), p 980-986
3. A. Skopp, N. Kelling, M. Woydt, L.-M. Berger, Thermally Sprayed Titanium Suboxide Coatings for Piston Ring/Cylinder Liners under Mixed Lubrication and Dry-Running Conditions, *Wear*, 2007, **262** (9-10), p 1061-1070
4. R. G. A. Wills, F. C. Walsh, The Continuing Development of Magnéli Phase Titanium Sub-Oxides and Ebonex® Electrodes, *Electrochim. Acta*, 2010, **55** (22), p 6342-6351
5. L.M. Berger, Titanium Oxide—New Opportunities for an Established Coating Material, *Thermal Spray Solutions: Advances in Technology and Application*, May 10-12, 2004 (Osaka, Japan), DVS-Verlag, CDRom version
6. P. C. S. Hayfield, *Development of a New Material: Monolithic Ti_4O_7 Ebonex® Ceramic*, Royal Society of Chemistry, Cambridge, U.K., 2001
7. L. Pawlowski, *The Science and Engineering of Thermal Spray Coatings*, John Wiley & Sons, Chichester, U.K., 1995.

b) Paper 4:

M. Gardon, S. Dosta, J. M. Guilemany, M. Kourasi, B. Mellor, R. G. A. Wills. Improved, high conductivity titanium sub-oxide coated electrodes obtained by Atmospheric Plasma Spray, Journal of Power Sources.

After certain approaches in the optimization of the electric resistivity in APS TiO_{2-x} coatings on ceramic tiles (paper 3); stainless steel substrates were coated for their application as electrodes in simulated batteries in paper 4. Again CTE mismatch could be especially influenced due to the increased difference between TiO_2 and steel. Moreover, dependence of mechanical properties as a function of thickness had to be analysed as well. From a functional point of view, This report presented first performances of APS TiO_{2-x} coating materials as electrodes in simulated batteries.

Journal of Power Sources 238 (2013) 430–434

Contents lists available at SciVerse ScienceDirect

Journal of Power Sources

journal homepage: www.elsevier.com/locate/jpowsour

Short communication

Improved, high conductivity titanium sub-oxide coated electrodes obtained by Atmospheric Plasma Spray

M. Gardon [a,*], S. Dosta [a], J.M. Guilemany [a], M. Kourasi [b], B. Mellor [b], R. Wills [b]

[a] Thermal Spray Centre, CPT, University of Barcelona, Martí i Franquès, 1, 08028 Barcelona, Spain
[b] Research Institute for Industry Faculty of Engineering & the Environment, University of Southampton, SO17 1BJ Southampton, United Kingdom

HIGHLIGHTS

- Titanium sub-oxide coatings were obtained by Atmospheric Plasma Spray.
- Coated samples exhibited good mechanical properties.
- Coated samples showed an increased range of operation than uncoated electrodes.
- Coated samples had higher electrical conductivity compared to standard electrodes.

ARTICLE INFO

Article history:
Received 27 February 2013
Received in revised form
7 April 2013
Accepted 15 April 2013
Available online 20 April 2013

Keywords:
Electrodes
Bipolar batteries
Redox flow batteries
Thermal spray
Titanium sub-oxides
Coatings

ABSTRACT

Coatings based on reduced stoichiometries of titanium dioxide obtained by Atmospheric Plasma Spray are presented for their application as electrodes in devices such as lead acid batteries, redox flow batteries and electrochemical reactors. A study of their microstructure, composition and mechanical properties is first presented in this paper to show that the layers are compact, free of cracking and well adhered to the substrate. The presence of Magnéli phase oxides, particularly Ti_8O_{15} was identified in the coatings, which enhances their electrical conductivity. In order to understand the behaviour of this material as an electrode, an electrochemical analysis of the coatings was also done. The coated samples showed higher oxygen and hydrogen evolution overpotentials and lower electrochemical corrosion compared to typically used commercial stainless steel and carbon–polymer composite electrodes.

1. Introduction

Bipolar lead acid batteries have attracted attention because of potential improvements in active mass utilization, uniform current distribution and lighter-weight construction (higher energy density) in comparison to conventional batteries that contain lead grids [1]. Furthermore, bipolar electrodes are typically used for redox flow batteries, fuel cells and electrochemical reactors. In these electrochemical devices, a stack of bipoles are arranged such that the current passes orthogonally and the stack is capped by two endplates (monopoles). Bipolar electrodes for such applications must be electrically conductive but chemically inert; the operating environment is often highly acidic or alkali and highly positive and negative electrode potentials are desirable. Currently the material of choice is often carbon or carbon composites. These can suffer from degradation over time and are limited in electrical conductivity. Metallic plates have considerably higher electrical conductivity, are lower cost and easier to manufacture but are not stable in the electrolytes or at the operational potentials required. If low cost metallic substrates could be coated with an electrically conductive, chemically robust layer, they would have significant commercial potential. From a cost-effectiveness point of view, processes that can provide the active components in these devices like electrodes, bipolar walls or even insulating layers in a rapid manufacturing process would be highly beneficial. Thermal spray technologies provide a very interesting solution that can fit in this necessity. Atmospheric Plasma Spray (APS) builds-up coatings by the impact onto a substrate of powder particles that are propelled by a plasma jet, which is formed via a typical gaseous mixture of Ar/H_2 that flows through an electric arc [2]. APS has been extensively used for

* Corresponding author. Tel.: +34 634538544.
E-mail address: mgardon@cptub.eu (M. Gardon).

0378-7753/$ – see front matter © 2013 Elsevier B.V. All rights reserved.
http://dx.doi.org/10.1016/j.jpowsour.2013.04.078

producing passive surfaces that work against wear and corrosion phenomena. Nevertheless, it is also possible to develop functional active surfaces by this technique [3].

In this paper, titanium sub-oxide (TiO_{2-x}) coatings obtained by APS onto stainless steel substrates are presented as low cost, chemically inert electrodes principally for batteries but also potentially for many aqueous electrochemical devices. Optimized spraying conditions starting from previous studies have been selected and the mechanical properties of the obtained samples are included. The electrochemical characterization of the thermal spray coatings has been also carried out with the aim of forecasting its performance as electrodes and the results were compared with commercial standard materials.

2. Experimental

A feedstock powder based on rutile TiO_2 and Magnéli phases (Ti_8O_{15} and Ti_9O_{17})was sprayed using an APS A-3000S system with an F4 plasma torch (Sulzer Metco, Germany). The particle size distribution was measured by Laser Scattering using the LS Beckman Coulter equipment. Powder and cross-section area of the coatings was studied by Scanning Electron Microscopy, SEM (JSM-5310, Jeol). The phase composition powder and coating was analyzed by a X'Pert PRO MPD diffractometer (PANalytical). Coated samples were cut and mounted in a conductive phenolic resin (Konductomet, Buehler) followed by the metallographic preparation. The hardness of the coatings was analyzed by a MXT-α microhardness tester (Matsuzawa) following the UNE 7-423/2 standard. In order to determine the bonding strengths of the sprayed samples, adhesion tests were performed on each selected coating following the ASTM F1147 (2005) standard. A testing apparatus SERVOSIS ME-402/10 model was used with a cross-head velocity of 0.02 mm s^{-1}, which was controlled by under displacement. Electrolytes for electrochemical characterization of the electrodes were made using deionized water obtained from a Purite water purifier. KOH and H_2SO_4 were used as received from Sigma Aldrich. Electrochemical measurements were taken in a standard two-compartment glass electrochemical cell using an Autolab potentiostat/galvanostat operating with GPES acquisition software. Potentials were measured against a saturated calomel reference electrode (SCE) and a platinum counter electrode was used. Measurements were taken at 20 °C electrolytes were de-oxygenated using a vigorous stream of N_2 gas.

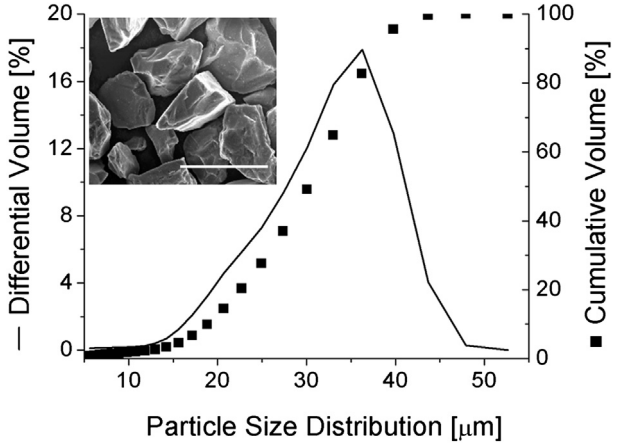

Fig. 1. Particle size distribution of the sprayed powder. A scanning electron micrograph of the feedstock (the scale bar represents 50 microns) is also given.

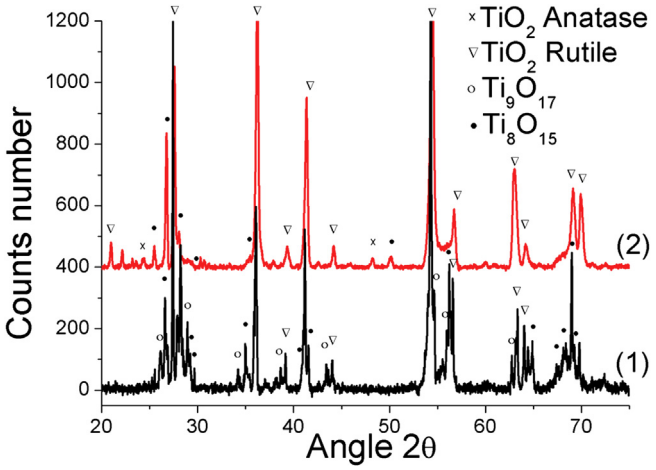

Fig. 2. Comparison between the XRD of the starting powder (1) and the obtained coating (2).

3. Results and discussion

The spraying conditions were optimized in a previous work, which focused on arc current intensity, stand-off distance and the influence of H_2 in the plasma power [4]. A strong correlation between particle temperature and the number of cracks in the coating cross-section was found. The particle size distribution of the powder and a micrograph can be observed in Fig. 1. The feed rate of the powder into the plasma jet and especially the gun velocity were also varied leading finally to a sample with a resistivity of 0.05 Ω cm. Fig. 2 shows the X-Ray Diffraction (XRD) analysis of the feedstock powder and the optimized coating. A certain loss of the percentage of Magnéli phases was found when spraying the powder. A low flow rate of hydrogen was used in these spraying conditions in order to decrease the temperature of the particles due to hydrogen plasma has a higher heat convection coefficient. However, it was noted that lower rates of hydrogen and higher rates of argon may partially re-oxidize the reduced stoichiometries towards titanium dioxide. Although XRD analysis of the coating shows mainly titanium dioxide in its rutile phase, it may be a lack of information related to the oxygen vacancies, which are the responsible for the electric conductivity. P.C.S. Hayfield reported the

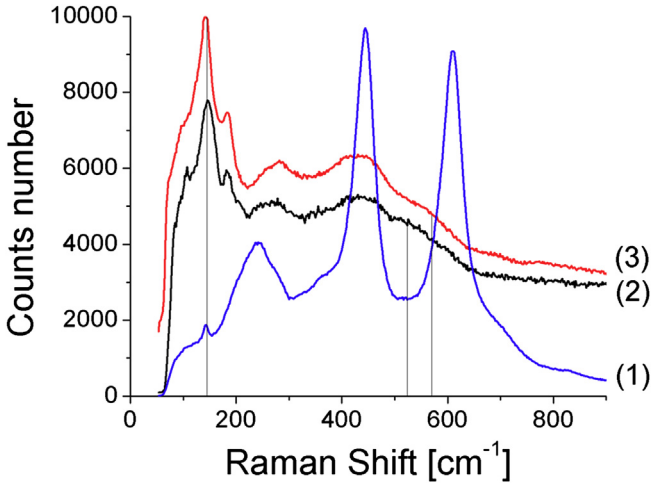

Fig. 3. Raman spectroscopy of a commercially available rutile powder (1), the feedstock powder (2) and the APS coating (3).

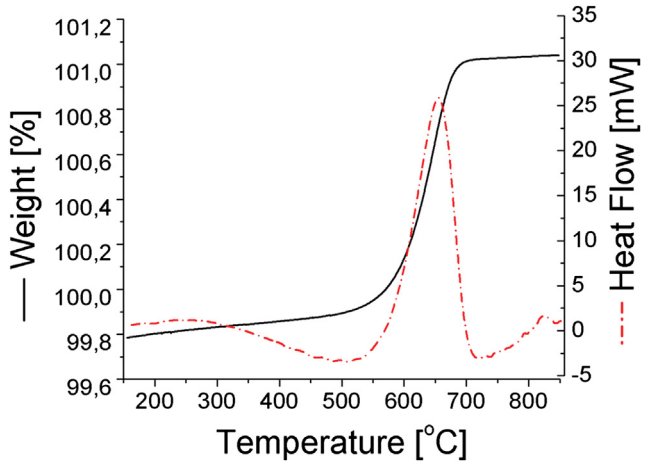

Fig. 4. DSC of the starting powder.

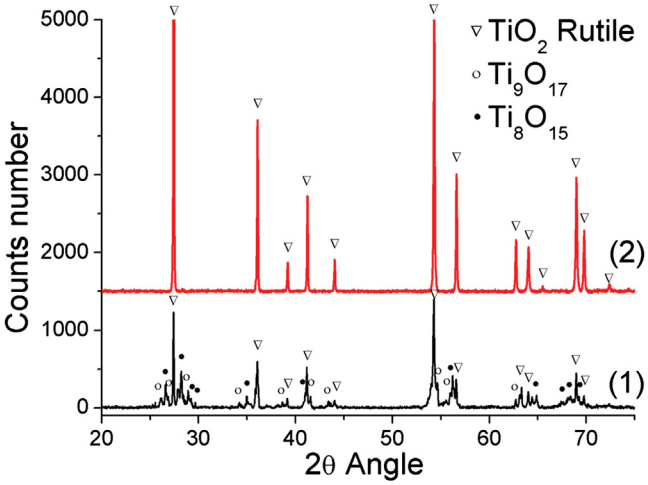

Fig. 5. Comparison between the XRD of the starting powder (1) and heated powder up to a complete oxidation (2).

overlapping of rutile XRD peaks with reduced stoichiometries of titanium oxide [5]. Raman spectroscopy can supply more information about the nature of titanium sub-oxide in its surface. It is possible to observe in Fig. 3 a comparison between the Raman spectra of a commercially available rutile powder, the feedstock powder used in this experiments and a typical spectrum of the obtained coating. As L.M. Berger et al. found previously [6], below 200 cm^{-1} the intensities of Raman peaks are attributed to reduced stoichiometries of titanium dioxide, which are not so visible for commercial rutile powder. The flattened peak above 550 cm^{-1} has been shifted to a higher wavelength when comparing the powder with the coating. This may indicate a higher amount of oxygen in the coating because of the thermal spray process.

The conductor behaviour of titanium sub-oxides is based in the existence of oxygen vacancies. A Differential Scanning Calorimetry (DSC) analysis was carried out in order to quantify the limit of the operation temperature when the coating is applied as an electrode (Fig. 4). At 500 °C an exothermic peak is found, which is characteristic of an oxidation. There is also an increase of the weight due to the complete oxidation from titanium sub-oxides towards titanium dioxide, especially in oxygen-containing surroundings. Therefore, this material should not be processed in conditions above 500 °C or its stoichiometry will change. This is corroborated by the XRD of the powder before and after the calorimetry (Fig. 5).

With the aim of studying the influence of the thickness in the mechanical and electrochemical properties of the samples, the number of spraying cycles was varied to obtain the following thickness: 47 μm (C146), 97 μm (C147), 155 μm (C148), 202 μm (C149) and 256 μm (C150). Fig. 6 shows SEM micrographs of the cross-section area. It is possible to observe some sub-surface porosity, typical of APS coatings, but which does not contain inter-pore linkage and so the overall coating is non-porous. The samples had a good adherence and no cracks were found in their cross-section area.

The long-term performance of an electrode in a device will be determined by a combination of its mechanical properties and chemical properties. Vickers hardness and bonding strength of the coatings were assessed as a measure of the mechanical properties. The hardness measured increases when the coating thickness is greater (Fig. 7). This suggests that the hardness measured for thin coatings is affected by the mounting resin and the substrate. This effect is reduced as coating thickness increases and therefore leads to an increase of microhardness value. As regards the tensile strength, the glue used in the test has a strength of approximately 57 MPa. The coating with lowest thickness has a bonding strength above this value. However, with increasing coating thickness a decrease to approximately 40 MPa was found. For samples C147 and C148 a cohesive rupture was observed, which implies some delamination between layers due to the increase in the number of cycles. In the case of the samples C149 and C150 an adhesive rupture was obtained and this could be due to a lower adhesion of the coating. Increasing the number of cycles (coating thickness) could boost the residual stress in the coating-substrate system which would favour decohesion between substrate and coating.

After observing the cross-section area and analyzing the mechanical properties of the different coatings, spraying conditions were selected to prepare sample C148 for building-up the TiO_{2-x} coatings and studying the electrochemical performance. Fig. 8 shows the cyclic voltammograms obtained at the APS TiO_{2-x} stainless steel coated electrode and at an uncoated stainless steel electrode. Experiments were performed at 20 °C in an aqueous electrolyte solution contained 4.0 mol dm^{-3} KOH with a potential sweep rate of 50 mV s^{-1}. The uncoated stainless steel electrodes show a significant oxidation at potentials more positive than 0.5 V *vs.* SCE. Hydrogen evolution occurs at potentials more negative than −1.5 V *vs.* SCE. At the TiO_{2-x} coated electrode, an irreversible oxidation peak at circa 0.75 V *vs.* SCE following which, oxygen evolution occurs at potentials more positive than 1.0 V *vs.* SCE.

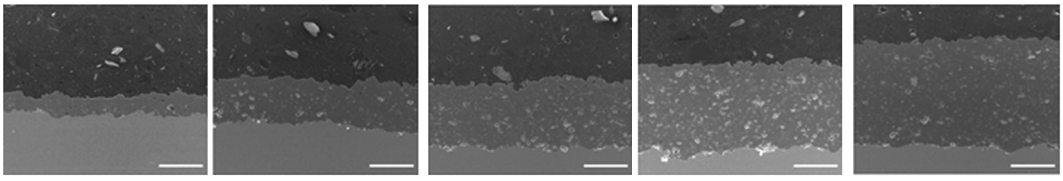

Fig. 6. Comparison of the increasing thickness of each sample by scanning electron microscopy. From left to right: C146, C147, C148, C149 and C150 (the scale bar represents 100 μm).

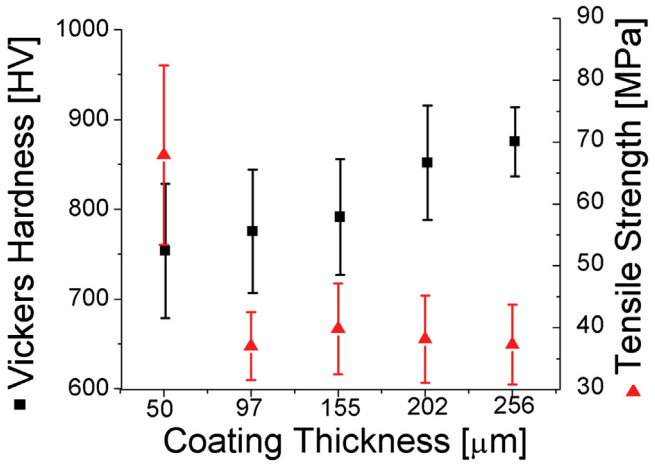

Fig. 7. Vickers hardness and tensile strength values as a function of coating thicknesses.

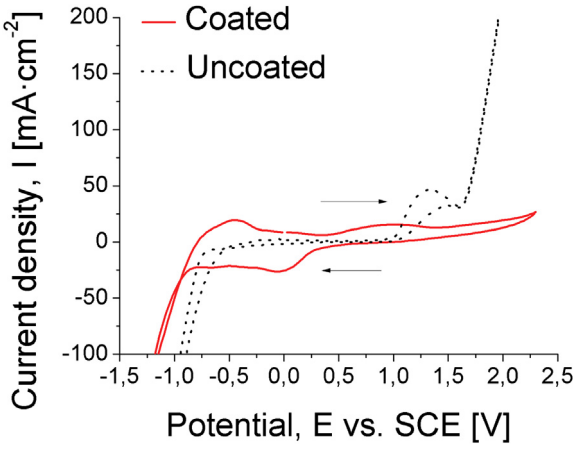

Fig. 9. Cyclic voltammograms obtained in an aqueous electrolyte solution 1.0 mol dm^{-3} H_2SO_4. APS TiO_{2-x} coating onto stainless steel electrode (line) compared to uncoated stainless steel substrate (dots).

At negative potentials, there is also a semi-reversible reduction wave at −1.0 V *vs.* SCE with hydrogen evolution at potentials more negative than −1.5 V. This electrochemical response is typical of the Magnéli phase components of the coating.

A similar set of cyclic voltammograms was recorded at the coated sample and at an uncoated stainless steel substrate using an aqueous electrolyte solution contained 1.0 mol dm^{-3} H_2SO_4. The temperature was again 20 °C with a potential sweep rate of 50 mV s^{-1}. Fig. 9 shows the obtained results. In acid media, there is also significant oxidation of the stainless steel samples at potentials higher than 1.0 V *vs.* SCE. Hydrogen evolution occurs at potentials more negative than −0.75 V. In contrast, the coated sample exhibits little electrochemical activity at positive potentials before the onset of oxygen evolution at circa 2.4 V *vs.* SCE. At negative potentials, there are a number of redox processes between 0 and −1.0 V *vs.* SCE with hydrogen evolution at potentials more negative than −1.0 V.

In acid and alkali environments, the overpotentials for oxygen and hydrogen evolution are larger for the coated electrodes than for the substrate stainless steel. This provides the coated electrodes of a wider potential operation window. In particular, the coating significantly suppresses the oxidation and bulk oxygen evolution of the stainless steel at positive potentials.

Additional cyclic voltammograms were also carried out and are shown in Fig. 10. In this characterization, the aqueous electrolyte solution contained 1.0 mol dm^{-3} CH_3SO_3H and once again the potential sweep rate was of 50 mV s^{-1}. The stainless steel substrate exhibits hydrogen evolution commencing at approximately −0.6 V *vs.* SCE and oxygen evolution/corrosion commencing at approximately 1.6 V *vs.* SCE. In addition an anodic peak can be seen at approximately 1.2 V *vs.* SCE, which is probably due to oxidation of one of the stainless steel components. As in sulphuric acid, the APS TiO_{2-x} electrode demonstrates suppressed hydrogen and oxygen evolution by comparison.

Methanesulphonic acid is the electrolyte of choice for the soluble lead flow battery. In this battery, solid lead and lead dioxide deposits are plated respectively at the negative and positive electrodes during charge and then dissolved back into the electrolyte as Pb^{2+} ions during discharge. The deposition and dissolution of Pb from an aqueous electrolyte solution initially containing 1.5 mol dm^{-3} Pb^{2+} and 1.0 mol dm^{-3} CH_3SO_3H was studied to show the coated stainless steel electrodes are suitable for such an application. The results of the coated samples were compared to the performance of a carbon–polymer composite electrode, typically used for the soluble lead flow battery, with equivalent dimensions (Fig. 11). The experiment

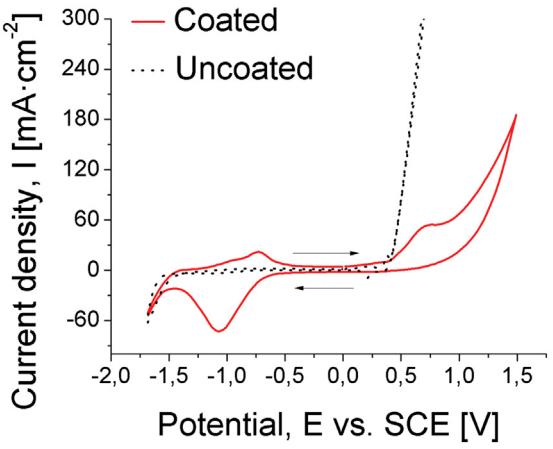

Fig. 8. Cyclic voltammograms obtained in an aqueous electrolyte solution 4.0 mol dm^{-3} KOH. APS TiO_{2-x} onto stainless steel electrode (lines) compared to uncoated stainless steel substrate (dots).

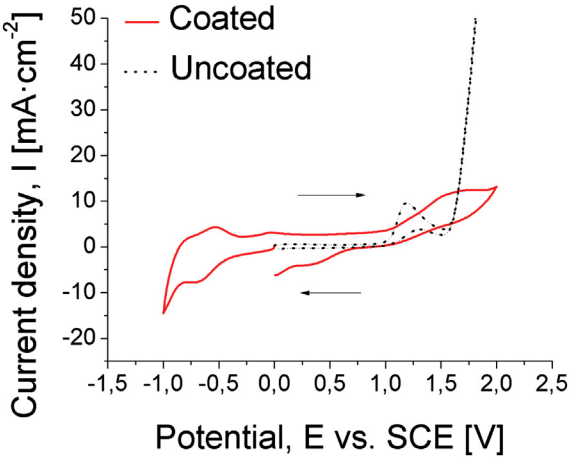

Fig. 10. Cyclic voltammograms obtained in aqueous electrolyte solution 1.0 mol dm^{-3} CH_3SO_3H. APS TiO_{2-x} coating onto stainless steel electrode (line) compared to uncoated stainless steel substrate (dots).

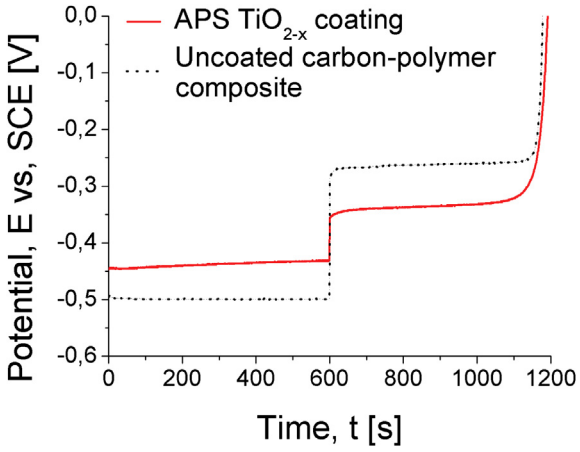

Fig. 11. Voltage *vs.* time plot for the deposition and dissolution of Pb from an aqueous electrolyte solution containing 1.5 mol dm^{-3} Pb^{2+} and 1.0 mol dm^{-3} CH_3SO_3H (APS TiO_{2-x} coating: line, uncoated carbon composite: dots).

consisted of two periods of constant current being applied to the cell while the cell potential was monitored as a function of time. The first 600 s correspond to Pb deposition and the last 600 s correspond to Pb dissolution. The applied current density was 50 mA cm^{-2} throughout. The deposition and dissolution of Pb corresponds to the charge and discharge reactions respectively of the soluble lead acid flow battery. The lower voltage difference between deposition and dissolution reactions for the APS TiO_{2-x} electrode compared to the carbon composite are likely due to the better electrical conductivity of the former compared to the latter. Therefore, compared to the carbon–polymer electrodes, the coated ones have much better electrical conductivity and hence lower overpotential for the electrodeposition and dissolution of the electrode deposits.

4. Conclusions

Below are presented the main conclusions referred to the APS titanium sub-oxide coatings development, its mechanical properties and its suitability as electrodes:

- It is feasible to coat stainless steel with titanium sub-oxide by means of Atmospheric Plasma Spraying achieving a satisfactory electric resistivity of the coating.
- The end-use of the electrode must not exceed the 300 °C in order to avoid re-oxidation of the reduced stoichiometries towards TiO_2.
- The cross-section area of the samples showed good coating-substrate adhesion and no vertical or interlayer cracks in its cross-section area.
- As long as thickness increases, the bonding strength is decreased due to the delamination between layers and decohesion between the substrate and the coating. Moreover, the Vickers hardness increases because the influence of the resin and the substrate decreases when the samples are indented.
- In both acid and alkali environments, APS TiO_{2-x} coated samples showed an increased potential range of operation than the uncoated stainless steel electrodes.
- APS TiO_{2-x} coated samples showed a higher electrical conductivity in a simulated lead flow battery compared to the most commonly used carbon–polymer electrodes. This led to a decrease in the overpotential for the electrodeposition and dissolution in these devices. It should be noted that the coated electrodes are also likely to have a slightly higher surface area compared to the carbon composite electrodes, which would give an effectively lower current density per geometrical area but may also provide better adhesion of the deposit to the surface.

Acknowledgements

The authors wish to thank the Generalitat de Catalunya for the financial support for this research project 2009 SGR 00390.

References

[1] K. Ellis, A. Hill, J. Hill, A. Loyns, T. Partington, J. Power Sources 136 (2004) 336–371.
[2] L. Pawlowski, Science and Engineering of Thermal Spray Coatings, John Wiley & Sons, Chichester, U.K., 1995.
[3] M. Gardon, J.M. Guilemany, J. Mater. Sci. Mater. Electron. (2012), http://dx.doi.org/10.1007/s10854-012-0974-4.
[4] M. Gardon, J.M. Guilemany, Proc. Int. Therm. Spray Conf. (2012). Houston, USA.
[5] P.C.S. Hayfield, Development of a New Material - Monolithic Ti4O7 Ebonex Ceramic, Royal Society of Chemistry, Cambridge, U.K., 2001.
[6] A. Skopp, N. Kelling, M. Woydt, L.-M. Berger, Wear 262 (2007) 1061–1070.

c) Paper 5:

M. Gardon, S. Dosta, J. M. Guilemany, M. Kourasi, B. Mellor, R. G. A. Wills. Enhanced performance of common electrode materials by means of thermal spray coatings.

More efforts were encouraged in this line of research. Standard electrode materials commonly applied in different batteries such as: i) thin steel film; ii) thin aluminium film; iii) carbon-polymer composite and; iv) nickel foams were selected as substrates. Starting hypothesis was based on reaching less aggressive conditions by means of modifying the spraying parameters in order to reduce CTE mismatch for metallic thin films and avoid degradation of the carbon-polymer composites and nickel foams. Surface roughness of the substrate was of special concern in this study.

Enhanced performance of common electrode materials by means of Thermal Spray coatings

M. Gardon [1], S. Dosta [1], J.M.Guilemany [1]

M. Kourasi [2], B. Mellor [2], R. Wills [2]

[1] Thermal Spray Centre, CPT, University of Barcelona. Martí i Franquès, 1 08028, Barcelona, Spain. Contact details: mgardon@cptub.eu - (0034) 634538544

[2] Research Institute for Industry Faculty of Engineering & the Environment, University of Southampton. SO17 1BJ, Southampton, United Kingdom.

Abstract

Atmospheric Plasma Spray has been used to obtain titanium sub-oxide coatings on steel film, aluminium film, carbon-polymer composite and nickel foam substrates for application as electrodes. Substrate roughness had to be increased for boosting the adhesion of the coating on the smooth electrodes, which was especially critical for the fragile carbon-polymer composite. High energetic conditions increased coefficient of thermal expansion mismatch for coating steel and aluminium thin sheets and degraded carbon-polymer composite and nickel foam. Therefore, it was necessary to adjust the spraying parameters towards lower energetic conditions in order to achieve well-bonded and homogeneous coatings on all four different substrates without the presence of cracks in their cross-sectional area.

Keywords: titanium sub-oxide, atmospheric plasma spray, electrodes, coatings.

Highlights

- CET mismatch can be effectively controlled for Al and Steel thin sheets.
- Fragile carbon-polymer composites and delicate Ni foams were properly coated.
- Same low energetic spraying conditions successfully coated all electrode materials.

1 Introduction

Rise in fuel prices and permanent increase in greenhouse emissions are the chief dominant forces moving the industry towards a more effective use of energy. Among distinct established lines for solving this scenario, energy storage could assist the transition between suppliers and demanders. This leads to a looked-for independency from resource intermittency, energy distribution or daily fluctuations in consumption [1]. Bi-polar batteries and redox flow batteries are becoming extensively used in systems of electrochemical energy storage and conversion. However, their efficiency is strongly subject to bulk resistivity of electrodes, bipolar plates and the contact resistance between them. Cost-effective and rapid manufacturing processes able to coat these materials with electrical conductive and corrosion resistant materials are expected to improve their overall performance. In this way, Atmospheric Plasma Spray (APS) that propels molten particles towards a substrate by means of a plasma jet could be a suitable procedure for carrying it out [2]. As a result, metallic, ceramic or polymeric well-bonded homogeneous coatings are built-up onto a wide variety of pieces in a brief fabrication and it can also be applied as a technique for achieving functional materials [3].

Despite the lack of published articles related to the application of thermal spray processes for the development of battery components, several intellectual properties may be found involving many different electrode materials. M. William et al. in the early 90s patented a stacked cell array bipolar battery with a thermal sprayed lithium alloy and FeS_2 resistant ceramic layer as a container and cell

seal [4]. A similar design was purposed by G. Barlow *et al.* [5]. However, in this case it was not hermetically sealed. The migration of the electrolyte around the bipolar wall and a further formation of ionically conducting paths were prevented by means of a non-wettable material strategically placed around the cells at the periphery of the bipolar walls. A method for fabricating an electrochemical capacitor was developed by L. Bai *et al*. [6]. The device used bipolar plates made of cobalt, iron or nickel alloys which acted as both the cathode and the substrate upon which the anodes were formed. In one embodiment, this layer could be formed by a bismuth/antimony alloy and deposited by thermal spray with a thickness between 0,001 and 100 micrometers. A similar patent was filed by B. C. Muffoletto et al. but a more detailed description of the APS operation conditions was given [7]. H. Ye *et al*. mentioned that the patent designed by Muffoletto et al. could have significant drawbacks [8]. The thermal instability of certain electrochemically active materials must be taken into account. Particularly, iron disulfide decomposes to FeS at about 550ºC, which is much cooler than the flame temperatures of APS. The undesired decomposition of the active raw material was also handled by J. Dai *et al*. [9]. In their work, the feedstock was a mixture comprising an effective quantity of a source of a thermally protective salt, LiCl or LiBr, and nano- or microstructured active materials like sulfides. This mixture was sprayed onto 304 stainless steel and graphite. It was believed that the thermally protective salt prevented the decomposition of the active material by providing cooling *via* the heat of fusion. The energy associated with the fusion of the salt acts to cool the active material particles and thus prevent their thermal dissociation. Sulfur is a good choice for preventing the powder degradation due to it being a poor heat conductor and slowing the heating of the pyrite particles as other authors previously reported. However, J. Dai *et al.* assure that thermally protective salt has a number of advantages over sulfur: the combination of the salt with the active material avoids leaching with flammable carbon disulfide; the amount of salt may be adjusted to control final porosity of the coating and the salt can function as an electrolyte, which is useful from an electrochemical performance standpoint. Nonetheless, same authors also added sulfur in the elemental feedstock in a following patent with the same purpose [10]. More

recently, D. Batson designed a bipolar battery electrode structure and the sealed bipolar battery assembly [11]. In this case, electrode substrates and bipolar walls were configured as circular areas. A thermoplastic layer material was applied by thermal spray with the purpose of electrically insulating the outer surface of the battery. However, in this case the active components of the device were not obtained as coatings by any process related to thermal spray technologies.

Thermal spray processes have been also widely used as a technique for developing electrode materials in Solid Oxide Fuel Cells (SOFC) and many scientific contributions were published. In these devices, an electrochemical conversion is carried out producing electricity directly from oxidizing a fuel, in addition a solid oxide or a ceramic are used as electrolytes. Despite the materials involved do not perform in the same environment than those electrodes in standard, bi-polar or mobile batteries, is worthy to review some of the chosen experimental procedures during the last years. H. Nie *et al.* produced strontium-doped $LaMnO_3$ perovskites (LSM) as cathodes for SOFC [12]. A certain decrease in the electric conductivity was found due to the porous structure of the APS coating when compared to the LSM bulk sample. However, at 800ºC it met the conductivity requirements of the cathode for high temperature SOFC. Moreover, this porosity favored air/O_2 transportation to reaction sites and lowered the cathodic polarization. It was finally concluded that APS appeared as a plausible technique for obtaining porous LSM cathodes with good performances. On the other hand, anode layers for SOFC built-up by APS using different feedstocks were studied by D. Hathiramani *et al.* [13]. To end up with a high electrochemical activity, NiO and Y_2O_3-stabilized zirconia were milled to a particle size bellow 1 micron and then agglomerated below 80 microns. This manufacturing method provided powders with very good properties but with lower flowabilities. Then, feedstock was mixed with commercial available materials. The results showed no difference between the submicron-sized powders and those NiO and YSZ with larger grain sizes but it was observed a better thermal cycle resistance when the anodes were produced by separately injecting NiO and YSZ powder into the plasma plume. O.

Kwon *et al.* also worked in this line [14]. It was compared spraydried nano- and microsized NiO and YSZ powders spraying at different Ar/H_2 ratios. The mechanical properties and electrical conductivity of the coatings were strongly dependent on the nature of the powder feedstock. Those coatings built-up from spraydried powders contained a nanosized phase distribution and more three-phase boundaries, which lead to a higher electrical conductivity due to the more uniform distribution of the phases throughout the coatings when compared to the microsized feedstock. An increase of hydrogen in the plasma jet must be also taken into account because it had the capacity of lowering the electrical conductivity of the anode. More recently, J. M. Guilemany *et al.* used APS to produce all the components of a SOFC: Anode (YSZ-NiO), Cathode (LSM) and Electrolyte (YSZ) [15]. The three layers were properly assembled and adhered due to an on-time gradual transition of the materials during the spraying.

It should be noted that these previous examples of the use of thermal spray technologies in energy storage devices are limited to the application of non-conductive seals or for the application of active materials in a morphologically attractive form. Reduced stoichiometries of titanium dioxide (TiO_{2-x}) are well known due to its characteristics and properties. The electrical conductivity in combination with the chemical resistance of this material is of interest for many applications in electrochemistry [16]. In this work, different substrates such as steel, aluminium, carbon polymer composite and nickel foam commonly applied as electrodes in batteries have been coated by reduced stoichiometries of titanium dioxide using Atmospheric Plasma Spray. Electrochemical performances of each coated piece have been compared with the original commercial uncoated samples.

2 Materials

Feedstock powder based in TiO_2 rutile and certain amount of Magnéli phases Ti_8O_{15} and Ti_9O_{17} (Sulzer Metco) was sprayed using an APS A-3000S system with an F4 plasma torch (Sulzer Metco,

Germany). Particle size distribution was measured by Laser Scattering (LS Beckman Coulter). Substrate materials were: i) steel film (thickness 0,5 mm), ii) aluminum film (thickness: 1 mm) iii) carbon-polymer composite (thickness: 4 mm) and iv) nickel foam (thickness: 1 mm, diameter of Ni network: 80 microns). Substrates were cleaned before the spraying process by means of an ultrasonic equipment (Ultrasons-HD, J.P. Selecta) and acetone (Panreac) and their roughness was measured by a profilometer (SJ-210, Mitutoyo). Cross-section area of the coatings was studied by Scanning Electron Microscopy, SEM (ProX Phenom). Coated samples were cut and mounted in a conductive phenolic resin (Konductomet, Buehler) followed by the metallographic preparation. Electrolytes for electrochemical characterization of the electrodes were made using deionized water obtained from a Purite water purifier. KOH and H_2SO_4 were used as received from Sigma Aldrich. Electrochemical measurements were taken in a standard two-compartment glass electrochemical cell using an Autolab potentiostat/galvanostat operating with GPES acquisition software. Potentials were measured against a saturated calomel reference electrode (SCE) and a platinum counter electrode was used. Measurements were taken at 20ºC electrolytes were de-oxygenated using a vigorous stream of N_2 gas.

3 Results and Discussion

3.1 Coating development

In a previous work, the authors presented APS manufactured TiO_{2-x} coatings as a novel method for preparing electrode surfaces [17]. Coated samples exhibited good mechanical properties regarding their microhardness and adhesion to steel substrates. In both acid and alkali environments it was found an increased potential range of operation compared to uncoated stainless steel electrodes. Besides this, coated samples showed higher electrical conductivity in a simulated lead flow battery compared to the most commonly used carbon-polymer electrodes as commercial standard material. Atmospheric Plasma Spray involves high temperatures up to 15.000 ºC [2]. Therefore, the

interaction of each different substrate material with the molten particles and the plasma jet may carry out very distinct results. This is especially emphasized in the coefficient of thermal expansion (CTE) mismatch during the spraying. In this way, operation conditions may be adjusted to provide a satisfactory performance of the obtained coating. Besides this, as it has been reported before [18], the composition of the plasma causes a different degree of oxidation to TiO_2 coating, namely, the formation of distinct amounts of oxygen vacancies in its crystal lattice, which leads to a range of electric resistivities. Thus, neither Ar/H_2 ratios nor plasma intensity were altered in this study and the composition of the coating was remained constant based on TiO_2 rutile and Magnéli phase Ti_8O_{15}. Figure 1 shows the XRD results of each substrate material. The previously prepared APS coatings used a relatively heavy-duty steel substrate, having a thickness of 6 mm [17]. Although this was sufficient to prove the concept of electrode manufacture, it is not practical to use such substantial substrates for many battery applications. The results presented in this paper focus on optimising the coating process to enable truly lightweight, corrosion resistant electrode materials. In this regard, four further substrates were investigated. It is essential that for these materials the spray coating process does not perforate or deform the substrate from a planar geometry. Furthermore, for the nickel foam, a coating covering all surfaces throughout the porous structure is required.

3.1.1 Steel substrates

In this survey, the starting powder was based on TiO_2 rutile and certain amount of Magnéli phases Ti_8O_{15} and Ti_9O_{17}. The particles had an irregular morphology and their size distribution range was -45 +15 µm. Thin steel films were used as electrodes due to its general application, especially as relatively low cost materials. Substrates were subjected to ultrasonic cleaning with acetone during 10 min in order to remove dirt and impurities present on the surface. Then, the metallic pieces were sprayed using operation conditions from the formerly mentioned work and can be understood in this

study as high energetic conditions (HEC). However, the coatings were not properly bonded, which was attributed to the smooth surface of the electrode materials. Molten particles did not find anchoring points at the impact, which difficult its adhesion during the re-solidification of the particle. Therefore, the metallic pieces were homogeneously grit-blasted by a stream of 5 bar of compressed air containing alumina particles with an approximate particle diameter of 700 µm. Surface roughness (R_a) was increased from 0,47 µm to 6,87 µm. Subsequently, the samples were cleaned and sprayed following same above procedure. Coatings were successfully built-up and their cross-section area was studied by SEM (figure 2a). In spite of having TiO_{2-x} deposited onto the substrate, the coating exhibited an almost complete decohesion from steel surface. Moreover, a considerable number of vertical cracks was also found. CTE mismatch between metal oxide coating and metallic substrate may be leading to considerable accumulation of residual stress, which develops either cracks or lack of attachment. Two actions were carried out with the purpose of avoiding this outcome. First, it was used nitrogen in order to refrigerate the metallic substrates. Then, starting stand-off distance (D0) was increased in a 40, 60 and 80% (D1, D2, D3 respectively). Significant differences were obtained as long as the spraying distance was enlarged. Concretely, samples sprayed at D2 and D3 distances were properly bonded without the presence of cracks or decohesion between layers. A slight proportional decrease in thickness was also observed from D0 to D3. Both consequences could be based on the temperature of the particles, which is reduced for larger in-flight times and distances. Therefore, particles at lower temperature impacting onto steel, together with N_2 cooling, contribute to avoid CTE mismatch leading to less residual stress and cracking. Decrease in thickness could be attributed to lower deposition efficiency when spraying the metal oxide particle at lower temperatures. These spraying conditions can be considered as low energetic conditions (LEC). Figure 2b shows a proper bonded APS TiO_{2-x} coating using LEC.

3.1.2 Aluminium substrates

Deposit an APS TiO_{2-x} coating on aluminium provides a functional and corrosion resistant layer for lightweight electrodes. In this case, substrates were also grit-blasted to a R_a of 6,23 µm and again the samples were adequately cleaned before the coating process. Comparable CTE made to spray directly with LEC instead of beginning with HEC [19]. After characterizing cross-section area of the coatings, it was observed that the samples did not exhibit cracks and were well bonded to the metal film (figure 3).

3.1.3 Carbon-polymer composite substrates

Electrodes based on carbon-polymer composites are attractive due to its moderate corrosion resistance and low weight. This material is composed by a blend of different polymers with conductive carbon black. Bulk electrodes can be obtained by isostatic pressing. Therefore, develop enough roughness on smooth composite material was critical because of its fragile inner granular structure (figure 4). Grit-blasting broke the substrate at high (standard) pressures. Thus, it was decreased down to 2 bar with the purpose of preventing that the substrate could break again. Impacting alumina particles did not deform plastically the composite, but removed very quickly polymer and carbon material. Finally, R_a of 5,69 µm was obtained and damages in the overall substrate structure were not found. Due to the novelty of this composite in thermal spray technologies, both HEC and LEC were tested. Firstly, energetic conditions were carried out and the metal oxide coating was successfully built-up. However, stress accumulated in the contact between the composite and the metallic support while thermal spraying, led to localized fissures in the substrate and eventually fragmented the sample. Thus, LEC were selected and APS metal oxide layers were properly bonded lacking fractures where the composite piece was fixed. Coating material was well-bonded onto the composite without presence of vertical or horizontal cracks.

3.1.4 Ni foam

Ni foams have also drawn considerable attention because of its lightweight and pore size, which leads to high specific surface areas. Despite the internal complexity of the net, APS technology may be used for coating non-planar pieces, namely, 3D-geometries such as foams. No alteration of the substrate surfaces was done due to the impossibility to increase roughness to this material by means of grit-blasting process. Consequently, samples were directly sprayed after ultrasonic cleaning with acetone. HEC dramatically damaged the filaments of the foams and the structure was practically useless for the final application. On the other hand, LEC homogeneously coated the Ni foam. Figure 5a and 5b show uncoated and coated foam respectively. Besides this, cross-section of APS TiO_{2-x} coatings did not show cracks and were well-bonded onto the nickel surface. However, filaments were just coated on one side. Therefore, both sides of the Ni foam were coated and a complete layer of TiO_{2-x} rounded the material (figures 5c and 5d).

3.2 Electrochemical performance

Cyclic voltammetry was used to assess the potentials over which the electrode performed adequately. The voltammetry was performed in sulphuric acid and potassium hydroxide electrolytes to simulate conditions within typical battery environments (e.g. lead acid and NiMH). Each of the coated substrates displayed similar electrochemical responses. The voltammograms obtained for the aluminium and coated aluminium are presented in Figure 6. The coated aluminium shows a voltammetric response typical for Magneli phase materials. Towards positive potentials, oxygen evolution commences at circa 2.0 V vs. SCE. Towards negative potentials, hydrogen evolution commences at circa -1.0 V vs. SCE. Between -1.0 and -0.2 V vs. SCE some reversible redox activity of the titanium sub-oxides can be seen. This is in agreement with previous literature studies [20]. Repeated voltammograms on the same electrode did not show any shift in the electrochemical

response. The voltammogram suggests that the electrode would be stable in this acid electrolyte between voltages of -1 and +2 V vs. SCE. The uncoated, aluminium plate showed significant oxidation currents on the initial scan towards positive potentials, corresponding to the formation of an oxide layer. Further cycling did not result in additional dissolution. Figure 7 presents the cyclic voltammograms obtained at the coated aluminium (Fig 7a) and uncoated aluminium substrate (Fig 7b) obtained in the KOH electrolyte. In this media, the aluminium substrate showed considerable oxidation and dissolution at potentials more positive than -1.0 V vs. SCE. The coated aluminium, however, displayed the expected response for titanium sub-oxides in an alkaline electrolyte [20] and demonstrates that the coating substantially protects the underlying aluminium from corrosion.

4 **Conclusions**

Atmospheric Plasma Spray (APS) can be used for coating different electrode substrate materials such as steel film, aluminium film, carbon-polymer composite and nickel foam characterized by its low-cost, lightweight, corrosion resistance and 3D-geometry with high specific surface respectively. Smooth metallic films must be mechanically treated in order to increase their roughness with the aim of easing the adhesion of the molten particles. This step must be especially careful in the case of carbon-polymer composite because of its fragile granular structure. High and Low Energetic Conditions (HEC and LEC) were tested. Mismatch in coefficient of thermal expansion was considerably influenced when spraying on steel using HEC and dramatically damaged carbon-polymer composite and nickel foam leading to partial or total rupture of the substrates. LEC deposited well-bonded homogeneous TiO_{2-x} layers on steel and aluminium sheets, carbon-polymer composite and also rounded completely Ni foam filaments when spraying from both sides. Thus, LEC could be used for properly coating four considerably different electrode materials with a titanium sub-oxide thick and homogeneous layer. This highlights the versatility of APS technology and how fits in the scale-up of these products. APS TiO_{2-x} coated aluminium films were stable

between -1.0 and +2.0 V. vs SCE in sulphuric acid and uncoated piece showed oxidation on initial scan towards positive potentials. In potassium hydroxide electrolyte, coated electrodes avoided oxidation and dissolution found in uncoated pieces at potentials more positive than -1.0 V vs. SCE.

5 Acknowledgments.

The authors wish to thank the Generalitat de Catalunya for the financial support for this research project 2009 SGR 00390.

6 References

[1] M. Semadeni. Storage of Energy, Overview. Encyclopedia of Energy (2004) pp. 719.

[2] L. Pawlowski. Science and Engineering of Thermal Spray Coatings. John Wiley & Sons, Chichester, U.K., 1995.

[3] M. Gardon, J M. Guilemany. J. Mat. Sci.: Mat. Elec. (2012) DOI: 10.1007/s10854-012-0974-4.

[4] M. T. Williams, J. D. Briscoe, S. M. Oweis. United States Patent 5.254.415 (1993).

[5] G. Barlow, S. J. Specht. United States Patent 5.411.818 (1995).

[6] L. Bai, J. G. Kincs, M. Chason. United States Patent 5.568.353 (1996).

[7] B. C. Muffoletto, W. M. Paulot, J. E. Spaulding. United States Patent 5.716.422 (1998).

[8] H. Ye, C. Strock, T. Xiao, P. R. Strutt, D. E. Resiner. International Patent WO 99/64641 (1999).

[9] J. Dai, R. A. Guidotti, T. D. Xiao, D. E. Reisner. United States Patent 6.794.086 B2 (2004).

[10] R. A. Guidotti, H. Ye, T. D. Xiao, D. E. Reisner, D. H. Doughty. United States Patent 6.926.997 B2 (2005).

[11] D. Batson. United States Patent US2008/0090146 A1 (2008).

[12] H. Nie, W. Huang, T. Wen, H. Tu, Z. Zhan. J. Mat. Sci. Let. 21 (2002) 1951-1953.

[13] D. Hathiramani, R. Vaben, D. Stöver, R. J. Damani. J. Therm. Spray Tech. 15, 4 (2006) 593-597.

[14] O. Kwon, S. Kumar, S. Park, C. Lee. J Pow. Sour. 171 (2007) 441-447.

[15] J. M. Guilemany, M. Torrell, I. G. Cano, J. Fernández. Inter. Therm. Spray Conf. proc. (2012) Houston, USA.

[16] S. Andersson, B. Collen, U. Kuylenstierna, A. Magnéli Acta Chem. Scand, 11 (1957), p. 5.

[17] M. Gardon, S. Dosta, J. M. Guilemany, M. Kourasi, B. Mellor, R. Wills. J Pow. Sour. 238 (2013) pp. 430-434.

[18] M. Gardon, J. M. Guilemany. Inter. Therm. Spray Conf. proc. (2012) Houston, USA.

[19] http://www.matweb.com/ (accessed 07/04/2013).

[20] R.G.A.Wills, F.C. Walsh. Electrochim. Acta. 55 (2010), 6342.

List of figure captions

List of figures

Fig. 1

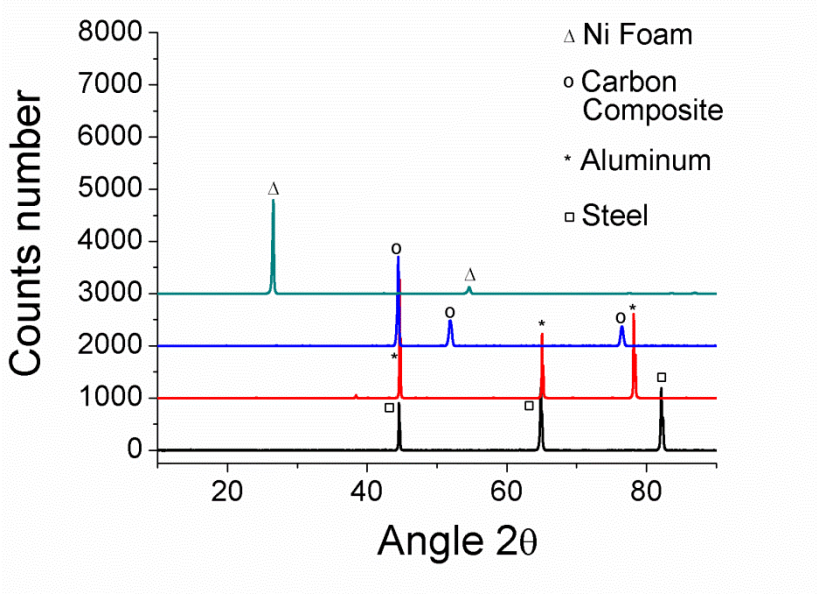

Fig. 2

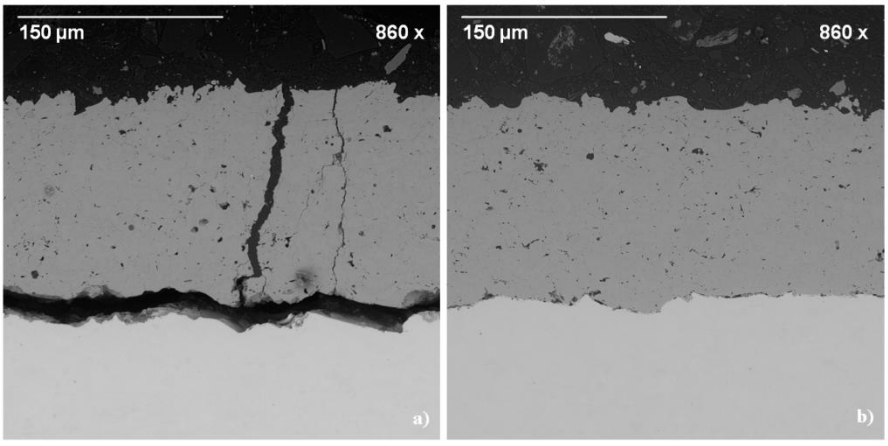

Fig. 3

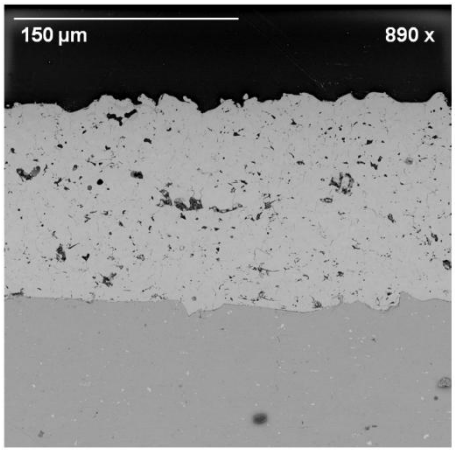

Fig. 4

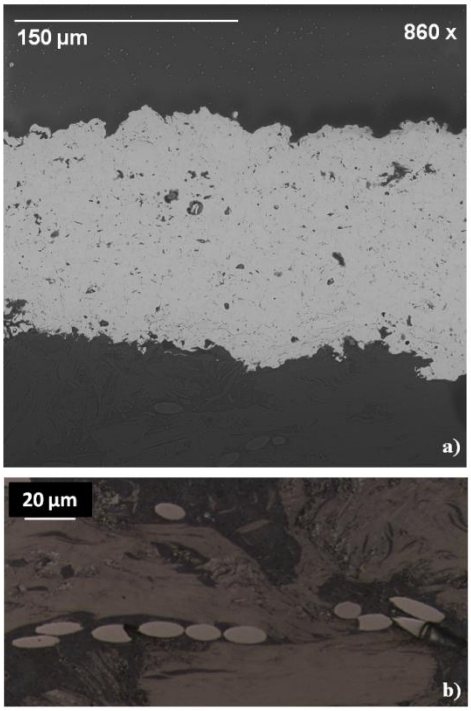

Fig. 5

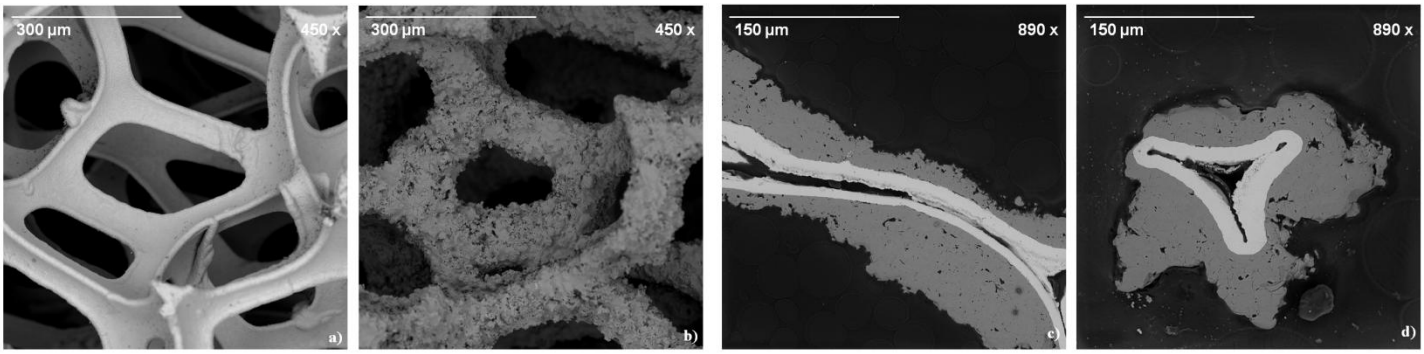
300 µm
450 x
a)
300 µm
450 x
b)
150 µm
890 x
c)
150 µm
890 x
d)

Fig. 6

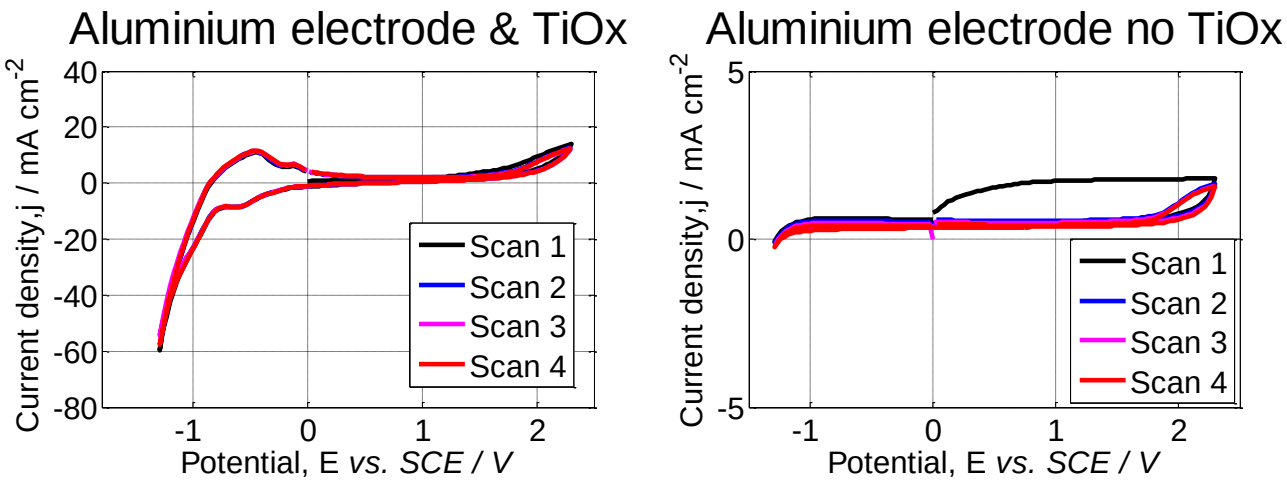
Aluminium electrode & TiOx
Current density,j / mA cm-2
40
20
0
-20
-40
-60
-80
-1
0
1
2
Potential, E vs. SCE / V
Scan 1
Scan 2
Scan 3
Scan 4
Aluminium electrode no TiOx
Current density,j / mA cm-2
5
0
-5
-1
0
1
2
Potential, E vs. SCE / V
Scan 1
Scan 2
Scan 3
Scan 4

Fig. 7

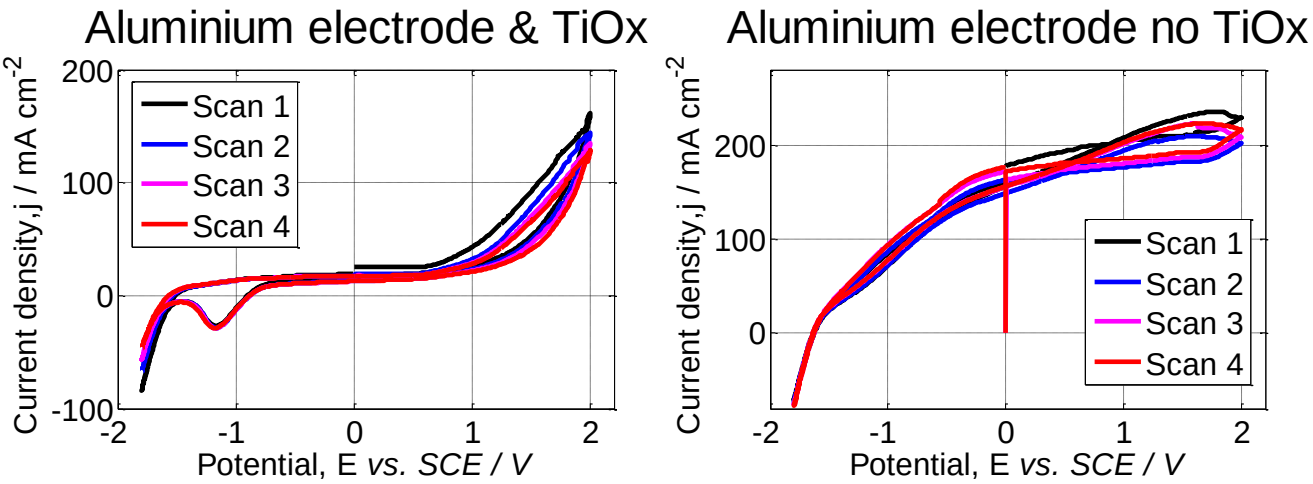
Aluminium electrode & TiOx
Aluminium electrode no TiOx
Current density,j / mA cm-2
Potential, E vs. SCE / V
Scan 1
Scan 2
Scan 3
Scan 4
200
100
0
-100
-2
-1
0
1
2

6.1.3. Gas sensors

Flexible gas sensors have an especial application in smart clothing market, where large demand of coated area is required and TS processes may offer an appealing coating procedure. The possibility of constant monitoring human atmosphere is of great interest for industrial and urban environments. Typically, sol-gel processes and chemical vapour deposition have been used for building-up these layers. However, it is quite complex to deposit well-bonded active metal oxide layers on a flexible polymer. Besides this, ceramic materials cannot deform the way polymeric films do; complete decohesion of the functional coating was found when flexing the substrate. Although Thermal Spray may be used as coating method in this application, it has not been reported any contribution to this field.

Before starting with the experiments, four critical steps may be identified: i) deposit a coating with a capacity of sensing a gas, ii) avoid thermal degradation of the polymeric substrate due to the temperatures involved in the plasma jet; iii) deposit well-bonded APS TiO_{2-x} coating on the polymeric film Kapton® and provide electric contact between the electrodes; and iv) deposit a coating geometry that could provide certain flexibility without leading to partial- or total-rupture. Paper 6 deals with these concepts.

a) Paper 6:

M. Gardon, O. Monereo, S. Dosta, G. Vescio, A. Cirera, J. M. Guilemany. New procedures for building-up the active layer of gas sensors on flexible polymers.

Literature reports that the plane (1 1 0) of rutile-TiO_2 has a high surface stability, which makes it suitable for sensing gases due to its capacity of adsorbing highly reactive gaseous species. Starting hypothesis here considered that oxygen vacancies present at the top surface of the coating could act as adsorbing centres and favouring the interaction with the reactive gases and target gas, boosting the Receptor Function. Moreover, porous microstructure of APS TiO_{2-x} coating should enlarge the specific surface area enhancing the Approachability of the system. On the topic of stability of the substrate, it will be necessary to reach less energetic conditions. Regarding flexibility of the device, coating geometry may play a key role and it had to be studied.

New procedures for building-up the active layer of gas sensors on flexible polymers

M. Gardon [1], O. Monereo [2], S. Dosta [1], G. Vescio [2], A. Cirera [2], J. M. Guilemany [1]

[1] Thermal Spray Centre, CPT, University of Barcelona. Martí i franquès 1, 08028, Barcelona, Spain. Contact details: mgardon@cptub.eu - (0034) 634538544

[2] MIND. Department of Electronics, University of Barcelona. Martí i franquès 1, 08028, Barcelona, Spain.

Abstract

The development of an active metal oxide layer by Atmospheric Plasma Spray in a gas sensor consisting of a flexible polymeric thin film was the target of the research. A factorial design of experiments was carried out in order to find out the operation conditions that could avoid the thermal degradation of the polymer due to the heat involved in the plasma spraying process. $NH_{3(g)}$ was used in a range of concentrations for ratifying the gas sensing capability of the device.

Keywords: Gas sensor, flexible electronics, thermal spray, titanium sub-oxide, coating.

Highlights

- TiO_{2-x} coatings were deposited on a flexible polymer by Atmospheric Plasma Spray.
- The flexible polymer film was not degraded during the coating process.
- The device showed positive and reproducible response in front of $NH_{3\,(g)}$.
- Oxygen vacancies and inner porosity enhance the sensitivity of the active layer.

1 Introduction

Enhanced control of the pollutants in the environment by means of metal oxide gas sensors is increasing because of the upward contamination in urban atmospheres. Furthermore, wearable flexible sensors have become an important market of application among smart clothes, medical status monitoring and industrial or military field [1]. Thus, cost-effective and rapid manufacturing processes able to deposit active layers used in the detection of harmful gaseous species are openly expected. Typically, thin film technologies like sol-gel or PVD have been usually applied as coating techniques in this field. However, Thermal Spray (TS) processes can also be used as an attractive technology for depositing the active layer of a metal oxide gas sensor with the aim of providing competitive results [2]. Among the very distinct spraying techniques in this field, Atmospheric Plasma Spray (APS) has been deeply used for achieving metal oxide coatings as passive-protecting layers [3,4]. Nevertheless, developing functional surfaces is also feasible with this technology. APS propels powder particles in its melted state towards a substrate by means of a plasma jet in order to build-up the coating. By controlling the plasma composition, which is typically an Ar/H_2 mixture, it is possible to take over the energy of the jet. Although the plasma temperatures may achieve 15.000ºC [5], substrates that are not so thermally resistant can also be used in APS. Therefore, this process seems to be a very interesting procedure to carry out the scale-up of active layers for these actuators.

The basic principle of operation metal oxide gas sensors is the change of the electrical resistance depending on the gas surrounding due to the chemical reactions that are developed on the metal oxide surface. Nonetheless, the involved sensing mechanisms that assure a proper performance of the device are not simple. Its performance may depend on three key-steps: i) receptor function, which determines the adsorption of the gas on the metal oxide surface, ii) transducer function, which is in command to transform the chemical interaction towards an output signal and iii) approachability, that eases the access of the gas into the inner grains of the solid.

The applications in electronics and sensors of coatings obtained by TS technologies have been reviewed before [6]. TS may offer new opportunities for hybrid thick-film electronics and thick-film sensors. This explanaition is based on the advantages associated to these processes: high manufacturing capability, in situ application of different types of materials and geometries, readily available system for customizing special electronics and sensor systems (i.e., prototyping) and it is a greener technology compared to plating, lithography, and so forth. The possibility of developing metal oxide gas sensors by APS has been patented by other authors in the past [7]. Besides this, C. Coddet et al. contributed scientifically with a publication related to tungsten oxide (WO_3) sensitive layers onto an alumina plate by means of APS technology for controlling gaseous NO_2 [8]. In this work, the reducing atmosphere in Ar/H_2 plasma developed a certain amount of WO_{3-x} composition, which made difficult to obtain a stable resistivity. For this reason, the samples were heat-treated in order to recover the oxygen deficiency. However, no significant differences were observed in the response time and sensitivity when comparing those samples obtained in a reduced and non-reduced atmosphere. It was proved that APS could be successfully used a technique for achieving satisfactory results in the fabrication and performance of the active layer of gas sensors.

Despite temperature of either melted particles or plasma jet may be especially critical for thin polymeric substrates; the spraying conditions can be adjusted in order to avoid its thermal degradation. This opens the possibility of coating flexible polymers that are being used in electronic systems. Titanium dioxide is a widely used material in the field of sensors and actuators. Its chemical stability and realtive low cost make it attractive for its industrial application and has been extensively selected as feedstock in APS. Therefore, the fabrication of titanium sub-oxide (TiO_{2-x}) coatings by means of Atmospheric Plasma Spray onto the flexible polymer Kapton® is studied in this paper and its application as the active layer of metal oxide gas sensors is presented. The performance of the device has been tested using $NH_{3(g)}$ at different concentrations.

2 Experimental details

A commercially available powder containing a mixture of TiO_2 (rutile), Ti_8O_{15} and Ti_9O_{17} was used (Metco 102, Sulzer Metco). The coatings were built-up onto the flexible polymeric film Kapton® with a thickness of 50 microns. In a few samples, Ag electrodes and a heater were previously printed over and below the substrate respectively with an inkjet technique in order to perform gas sensing experiments. The feedstock powder was sprayed using an Atmospheric Plasma Spray (APS) A-3000S system with an F4 plasma torch (Sulzer Metco, Germany). Temperature of the in-flight particles was measured using the Spraywatch system (Oseir, Tampere, Finland). Particularly, particle temperature was measured using a two-color pyrometer. The sensing experiments were performed in a test chamber with 15 ml in volume maintaining constant gas flow at 200 ml/min with a gas mixer controller (MGP-2, Gometrics S.L., Spain). Gaseous environments were obtained by mixing calibrated bottles of dry synthetic air (SA, which contains 21% of O_2 and 79% of N_2) and $NH_{3(g)}$ (100 ppm diluted in SA). Water vapour was introduced in the gas mixture bubbling dry synthetic air through a vase containing deionized water at room temperature (25°C). A Source-Measurement double unit (2602A, Keithley) was used to measure the electrical signal of the sensor and power of an integrated heater. The response of the sensor to gas (Response [%]) was defined as the difference between the measured resistance when there is a change in the atmosphere composition (R) and the initial resistance value (R_0) normalized to R_0.

3 Results and discussion

3.1 Coating development

Particle size range of the feedstock was -55 +10 µm and had an angular shape. Besides, its average crystallite size was well above nanoscaled materials commonly used as the active layer of metal oxide gas sensors (figure 1). In a previous work, it was studied the influence of

different percentages of hydrogen in the plasma jet [9]. Hydrogen present in the plasma jet could reduce Ti^{4+} to Ti^{3+}, which led to large accumulation of oxygen vacancies in the coating. As a result, titanium sub-oxide (TiO_{2-x}) coatings with very low electric resistivity were obtained and their performance as electrodes in simulated lead batteries was later studied as well [10]. Same spraying conditions were selected in this study. Particle temperature was approximately 2050ºC. Thus, substrate degradation was of special concern. Glass transition temperature of the polymer was theoretically espected between 380 and 410 ºC and melting temperature above 500ºC [11]. In this way, starting trials were carried out in order to modify the power of the plasma jet by means of altering the plasma intensity and hydrogen/argon rates. Although it was possible to considerably decrease the temperature of the particles, which reduced the thermal effect on the polymer, the coating was not properly built-up due to feedstock material was not sufficiently molten for being adequately deposited.

Therefore, it was decided to fix operation parameters such as spraying angle, feeding rate, plasma intensity and Ar/H_2 rates from above mentioned previous reports. Number of cycles and stand-off distance were the analyzed factors for carrying out a factorial design of experiments. Concretely, the studied levels were: i) five equidistant number of cycles (in ascending order: 1A, 1B, 1C, 1D, 1E) and; ii) five equidistant stand-off distances (in ascending order: 2A, 2B, 2C, 2D, 2E). Table 1 compiles the operation ranges. It was observed that as long as the stand-off distance was enlarged, temperature of the plasma jet decreased, which was in agreement with previous findings and the work published by other authors [5,9]. Although plasma jet may be cool enough for preventing damage of the substrate, particles were still arriving at high temperatures. At spraying distances 2A, 2B and 2C, polymer degradation was produced independently of the number of cycles. Just those samples obtained above 2C distance were satisfactorily obtained without substrate degradation. Thus, heat provided to the substrate by impacting molten particles that were being solidified was low enough for avoiding the alteration of the starting nature of the polymer. Number of cycles had not critical effects on the system; increased values did not thermally degrade the substrate for appropiate stand-off distances (2D

and 2E). However, proper electric contact was not achieved for the lowest number of cycles, which was attributed to uncoated spots. As long as the number of cycles increased, it was found that the resistance decreased between the printed electrodes from 1,05 to 0,05 Ω caused by an improved connection between the electrodes. Coating porosity was not influenced by this spraying parameter and remained constant.

Figure 2 shows a characteristic cross-section area of the coated polymer. It can be observed that the coating was properly bonded onto the polymeric film. Mismatch in the coefficient of thermal expansion (CTE) between the substrate and the coating is usually a worrying phenomenom in APS. Nevertheless, in this study it was not observed delamination or vertical cracks caused by accumulated stress induced by distinct expansion and contraction of the coating-substrate system. Besides, it is noteworthy to mention that nitrogen cooling was not required, which is commonly applied in APS when working with delicate substrates. As regards to their surface composition, micro-Raman spectra of a coating compared to pure rutile can be observed in figure 3. Shift and intensity of the peaks observed when comparing oxygen-defective APS TiO_{2-x} with completely oxidized rutile powder is caused by the different Ti/O ratios contained in each material [12].

Polymer film was sprayed using a mask that made possible to build-up the coating on a circular area with a diameter of 8 mm, where the electrodes were previously printed by inkjet printing (figure 4).

3.2 Sensor performance

$NH_{3(g)}$ gas experiments were conducted with the purpose of testing the sensing performance of the samples that had: i) electric contact among the splats and; ii) a flexible behavior (spraying conditions: 1C,D-2C). The expected behaviour of the reduced surface could be explained by the large amount of oxygen vacancies that were present on the APS TiO_{2-x} coating. Each vacancy

could act as an active centre for the adsorption of $O_{2(g)}$. Then, the interaction of the adsorbed $O_{2(g)}$ with the electric current led to anionic oxygen species, which are highly reactive towards $NH_{3(g)}$. In this way, the receptor function was boosted due to a possible increase in the affinity of the metal oxide surface and the desired sensing reactivity. A scheme of plane (1 1 0) of rutile with a certain amount of oxygen vacancies and the involved gaseous species is shown in figure 5. The chemical reactions developed on the surface of the metal oxide are shown below [13]:

$$O_{2(g)} + e^- \rightarrow O^{2-}_{(ads)} \quad (1)$$

$$O^{2-}_{(ads)} + e^- \rightarrow 2O^-_{(ads)} \quad (2)$$

$$2NH_3 + 3O^-_{(ads)} \rightarrow N_2 + 3H_2O + 3e^- \quad (3)$$

Feedstock powder was microstructured (figure 1); according to transducer function, these materials are not very sensitive to surface reactions. Adsorbtion and dissociation of O^2 and O^{2-} (reactions 1 and 2) leads to a space charge region on the surface of each metal oxide grain due to the transfer of the electrons from the bulk to adsorbed oxygen species [2]. This region also known as depleted zone determines the sensitivity of the device if its thickness is comparable to crystallite size. Nonetheless, microstructured materials are supposed to have a grain size much bigger than the space charge region. Then, overall electric resistivity is not so affected by surface reactivity, which decreases the transducer funciton of the sensor. On the other hand, an approximate 5-8% of porosity was measured. Besides, the access of the inner grains could be enhanced, which can also help in providing acceptable levels of sensitivity in front of the target gas. In this way, TiO_{2-x} active layer provided by APS may have poor capacity of transforming chemical reactions at the top surface of the coating to a monitored output signal due to its microsized crystallites. However, proper sensitivity of the system may be assured by means of: i) coating enhanced capacity of adsorbing gaseous species because of the presence of oxygen vacancies at the metal oxide surface and ii) presence of porosity which may favour the interaction between solid and target gas.

Figure 6 shows the change in the electric resistivity of the active layer respect to different $NH_{3,(g)}$ concentrations (100-50-25-12,5 ppm). Although this demonstrated that it made difficult to monitor gas exposures as long as the concentration decreased, satisfactory output down to 12,5 ppm was observed, which makes it suitable for monitoring hazardous human environments or pollution control [14]. Then, it was tested the performance of the sensor when exposing the active layer to intervals of the target gas in a constant concentration. The results showed that the device performs with reproducibility, indicating its suitability from an industrial point of view. In both cases, an average response and recovery times of 2 and 8 minutes were determined respectively. Almost linear response trend of the sensor against different $NH_{3,(g)}$ concentrations was observed. For higher concentrations like 100 ppm, a response of 7% in the active layer was reached. The output signal of the MOX sensor for concentrations around 12,5 ppm was approximately 1,30%. The obtained results matched with data available in different publications, especially related to the sensing response [15,16].

4 Conclusions

A metal oxide gas sensor has been feasibly produced by Atmospheric Plasma Spray (APS) onto a flexible polymeric thin film. Despite the high temperatures involved in APS, the polymer was not degraded during the process, obtaining a well-bonded titanium sub-oxide coating. Stand-off distance was in command to provide adequate particle temperature for avoiding damage of the polymer. The sensing behavior of the metal oxide layer was tested by means of $NH_{3,(g)}$ proving positive results ranging from 100 to 10 ppm. This could be attributed to the high amount of oxygen vacancies present on the top surface of the coating material and the porosity contained in the thickness of the active layer, which respectively increase adsorption capacity and enlarge surface of interaction.

5 Acknowledgments.

The authors wish to thank the Generalitat de Catalunya for the financial support for this research project 2009 SGR 00390.

6 References

[1] M. Suh, K. Carroll, N. Cassill. J. Text. App. Tech. Manag. 6, 4 (2010).

[2] M. Gardon, J. M. Guilemany. J. Mat. Sc.: Mat. Elec. 24, 5 (2013) pp. 1410-1421.

[3] L. L. Shaw, D. Goberman, R. Ren, M. Gell, S. Jiang, Y. Wang, T. D. Xiao, P. R. Strutt. Surf. Coat. Tech. 130 (2000) pp. 1-8.

[4] H.M. Hawthorne, L.C. Erickson, D. Ross, H. Tai, T. Troczynski. Wear 203–204 (1997) pp. 709.

[5] L. Pawlowski. John Wiley & Sons, Chichester, U.K., 1995.

[6] S. Sampath. J. Therm. Spray Tech. 19, 5 (2010) pp. 921-949.

[7] A. Iwata. United States Patent US2004/0074072 A1.

[8] C. Zhanga, M. Debliquya, A. Boudiba, H. Liaob, C. Coddet. Sens. Actuators B-Chem.,144 (2010) pp. 280.

[9] M. Gardon, J. M. Guilemany. Intern. Therm. Spray Conf. proc. 2012, Houston, USA. CD-Rom, Paper number: 29746, page 34.

[10] M. Gardon, S. Dosta, J. M. Guilemany, M. Kourasi, B. Mellor, R. Wills. J. Pow. Sour. 238 (2013) pp. 430-434.

[11] http://www2.dupont.com/Kapton/en_US/assets/ downloads/pdf/HN_datasheet.pdf . Accessed 19/12/2012.

[12] J. C. Parker, R. W. Siegel. Appl. Phys. Lett. 57 (1990) pp. 943-945.

[13] C. W. Lin, H. I. Chen, T.Y. Chen,C. C. Huang, C. S. Hsu, R. C. Liu, W. C. Liu. Sens. Actuators B-Chem., 160, 1 (2011) pp. 1481-1484.

[14] C. S. Rout, M. Hegde, A. Govindaraj, C. N. RRao. Nanotechn. 18 (2007) pp. 205504. 12.http://gestis-en.itrust.de/nxt/gateway.dll?f=templates&fn=default.htm&vid=gestiseng:sdbeng. Accessed 04/02/2013.

[15] B. Timmer, W. Olthuis, A. Van den Berg. Sens. Actuators B-Chem.,107, 2 (2005) pp. 666.

[16] S. Claramunt, O. Monereo, M. Boix, R. Leghrib, J.D. Prades, A. Cornet, P. Merino, C. Merino, A. Cirera. Sens. Actuators B-Chem. (2012) Doi:10.1016/j.snb.2012.12.093.

List of tables

Ar/H_2 flow ratio	3-7
Feeding rate (carrier gas)	2-4 L/min
Spraying angle	90º
Gun speed in each pass	100-500 mm/s
Stand-off Distance	50-250 mm
Plasma intensity	450-550 A
Coating thickness	20-90 µm

List of figure captions

List of figures

Fig. 1

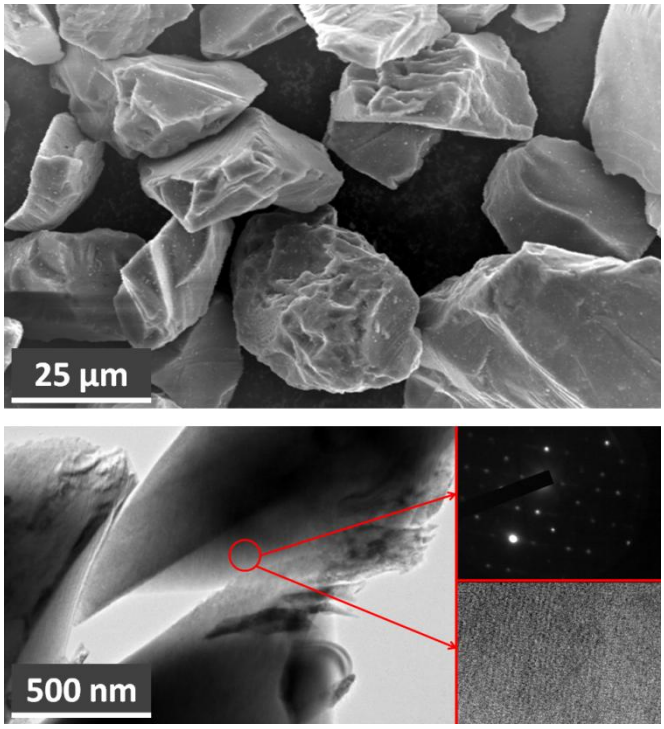

Fig. 2

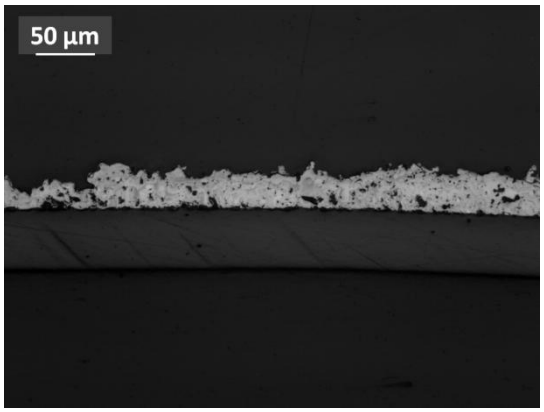

Fig. 3

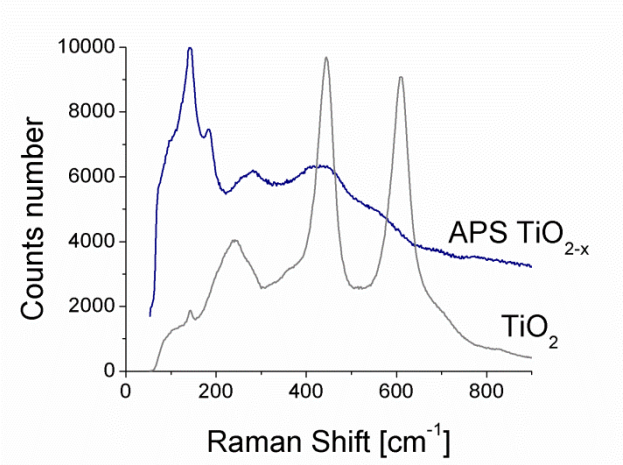
10000
8000
6000
4000
2000
0
Counts number
0
200
400
600
800
Raman Shift [cm-1]
APS TiO2-x
TiO2

Fig. 4

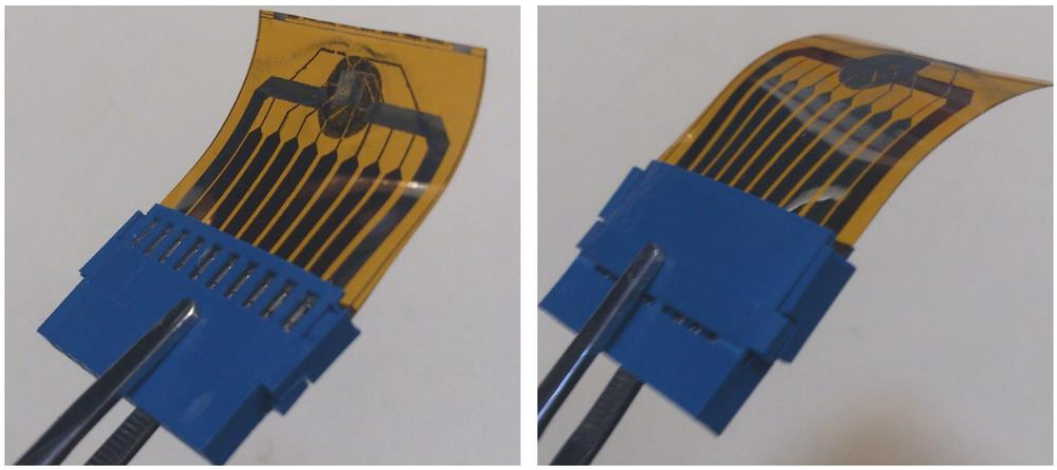

Fig. 5

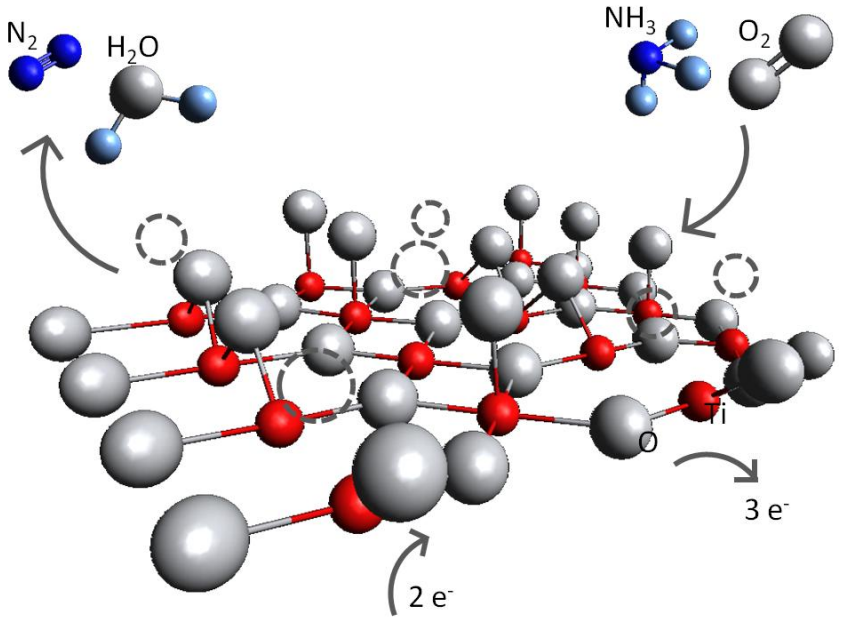
N2
H2O
NH3
O2
Ti
O
3 e-
2 e-

Fig. 6

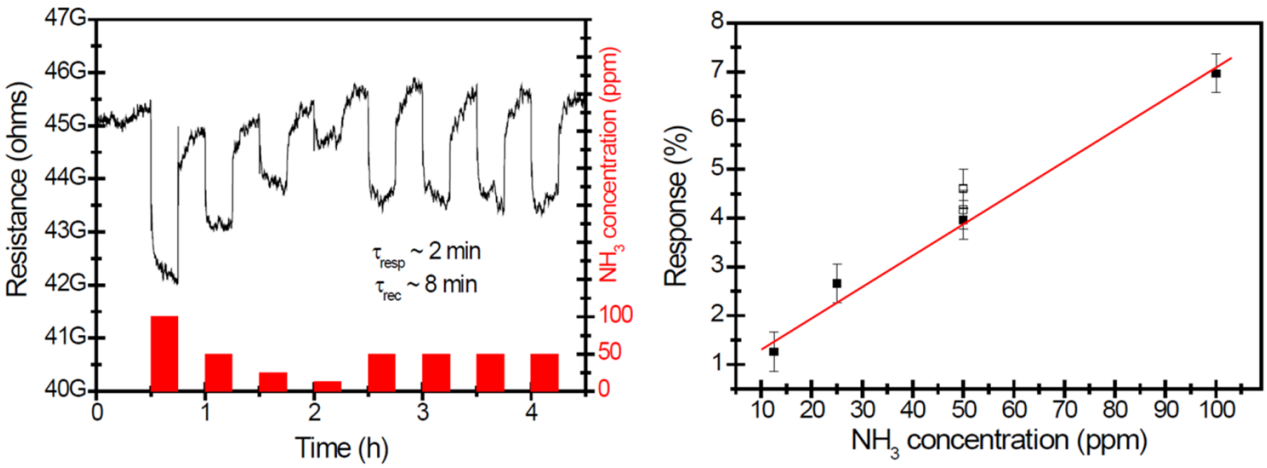
Resistance (ohms)
47G
46G
45G
44G
43G
42G
41G
40G
0
1
2
3
4
Time (h)
τresp ~ 2 min
τrec ~ 8 min
NH3 concentration (ppm)
100
50
0
Response (%)
8
7
6
5
4
3
2
1
10
20
30
40
50
60
70
80
90
100
NH3 concentration (ppm)

Additional experimental trials were carried out in order to test the response of the active layer in front of radiation. Figure 10, 11 and 12 provide the data related to sensibility to UV light, LED blue light and LED red light.

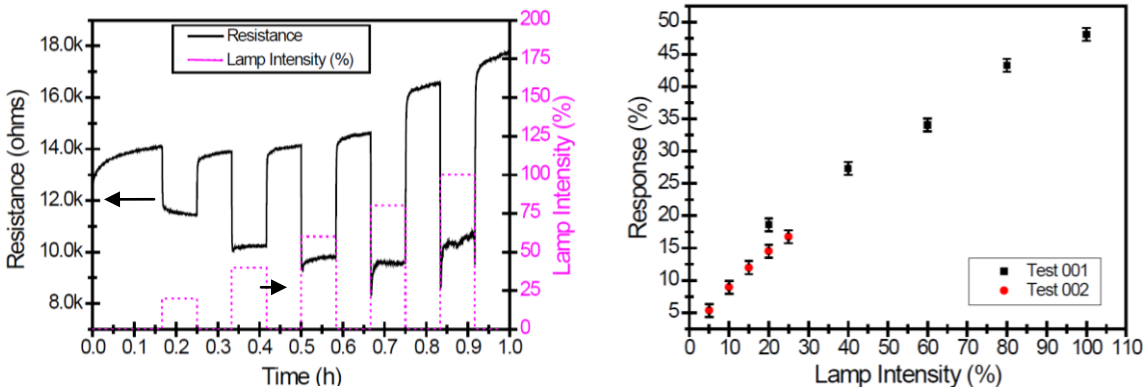

Figure 10. Left: Response of the sensor in front of UV light (λ = 365 nm) using different intensities. Right: Response of the sensor as a function of the intensity.

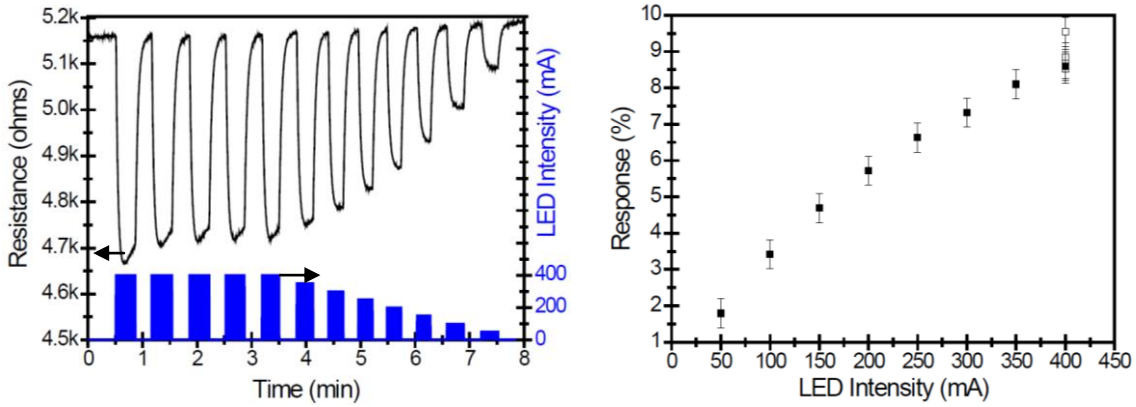

Figure 11. Left: Response of the sensor in front of LED blue light (λ = 453 nm) using different intensities. Right: Response of the sensor as a function of the intensity.

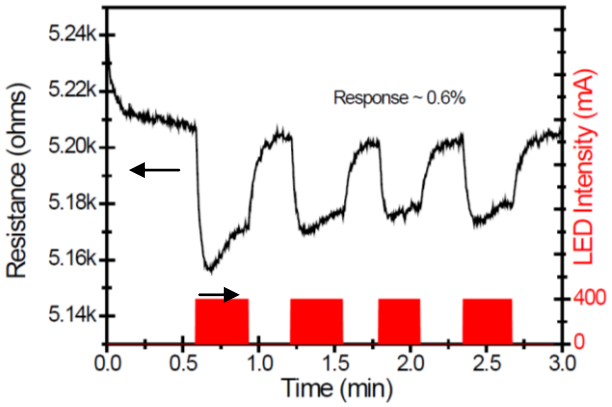

Figure 12: Response of the sensor in front of LED yellow light (λ= 530 nm).

Sensing performance of APS TiO_{2-x} coatings in front of different radiation gave positive and reproducible results. UV-light and LED blue light had the same tendency; sensing response increased as long as radiation intensity was enhanced. In the case of UV-light, an approximate shift of 6% in the resistance of the active layer was measured as output for lamp intensities down to 5%. Regarding LED blue light satisfactory sensing output was monitored using intensities of 50 mA. Lower sensibility was detected when irradiating the solid with LED yellow light. However, approximate response of 0,6% was measured using an intensity of 400 mA.

6.2 Cold Gas Spray

6.2.1 Detailed background

a) Starting scenario in CGS nano-TiO_2 coatings

Reviewed literature in Paper 1 suggested that main interest in TiO_2 surfaces obtained by Thermal Spray was the development of nanostructured photocatalytic anatase layers obtained by CGS. Nevertheless, a chief shortcoming was found when CGS technology was selected for depositing anatase surfaces; ceramic TiO_2 particles may not deform plastically. As it has been explained before, it is possible to solve this by means of embedding particles onto a ductile surface substrate. However, it leads to other two drawbacks: i) it is experimentally unfeasible to completely coat the substrate and; ii) particles can detach from the surface because of an inappropriate anchoring.

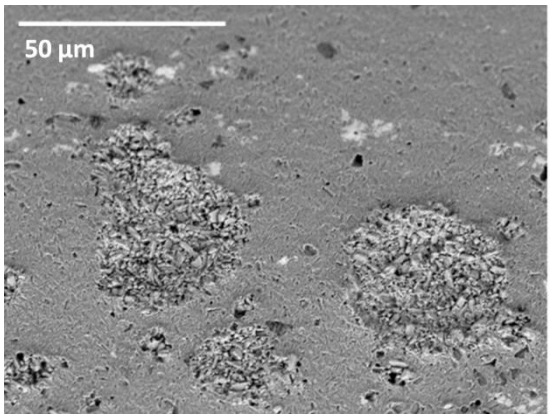

Figure 13. SEM micrograph: Titanium dioxide particles embedded on an Al surface, tilted sample.

Anyhow, it was used high-energetic spraying conditions in order to try to achieve well-bonded TiO_2 layers onto aluminium. Spraying conditions can be found in table 9 - Appendix. As it can be seen in figure 13, particles were embedded onto the ductile substrate. However, heterogeneities were commonly found and it was relatively simple to detach particles.

Paper 1 revised new nanostructured anatase powders designed for being used in CGS. These are supposed to be able to create chemical bonds with the substrate and among particles at the impact in order to build-up the coating. During the thesis, it was possible to a deal with the corresponding manufacturer and acquiring certain amount of this feedstock (C426-D). Paper 7 exhibits a micrograph of the powder, its nanostructure and particle size distribution. First trials provided confidence and for instants a quick and simple success seemed to come. Nonetheless, a sudden stop in the feeding flow was observed.

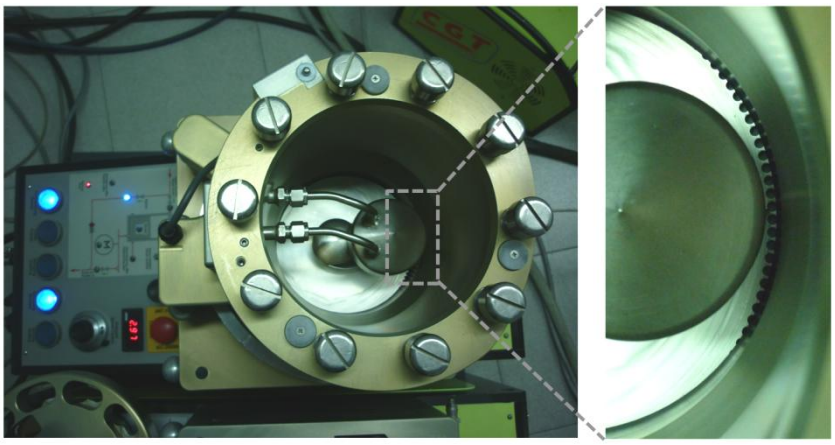

Figure 14. Top view of CGS feeding system

CGS feeding system uses a rotating feeder with a circular plate that contains holes in its edge (figure 14). The powder falls through these pits and is propelled by N_2 gas to an inlet pipe that is directed to the gun. After using the powder C426-D during approximately 2 minutes the system was clogged. Figure 15

shows the obturation of the holes in the circular plate and the clogged entrance of the pipeline. Thus, the authors could use highly photocatalytic nanostructured anatase powder able to be deposited by CGS, but without enough flowability for being transported from the feeding to the gun.

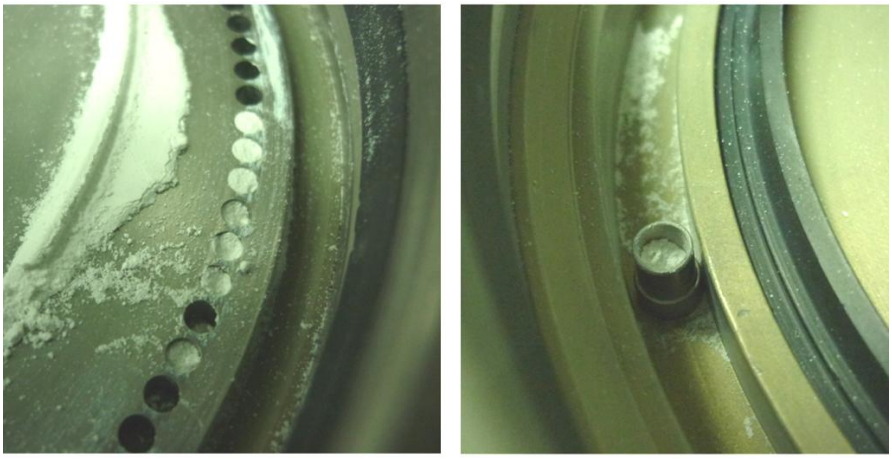

Figure 15. Clogging of the feeding system.

b)TiO_2-based feedstock blends

With the purpose of improving the flowability of C426-D, different blends with powders that flowed appropriately (PFA) were prepared so as to avoid the clogging of the feeder. This is not a standard procedure in thermal spraying and the hypothesis was supported on the thrust of PFA particles. Therefore, two different powders were selected as PFA: i) copper powder and ii) microstructured anatase powder. Table 5 compiles the percentages of blended powders:

Table 5. Selected blend percentages:

Blends	C426-D [% in vol.]	Copper [% in vol.]	Micro-TiO_2 [% in vol.]
A	50	50	---
B	70	30	---
C	50	---	50
D	70	---	30

6.2.2 Photocatalysts

After solving main inconveniences found in the development of CGS nano-anatase coatings, this section provides the obtained results and the application of the coatings as photocatalysts. The active surfaces were applied for the degradation of contaminants in gaseous and liquid phase (Paper 7 and 8).

a) Paper 7:

M. Gardon, C. Fernandez, M. Torrell, S. Dosta, J. M. Guilemany. Developing photocatalytic Copper/nano-Anatase coatings by Cold Gas Spray.

Copper was not selected just for its high flowability, it could also play different key roles. This material is widely used in Cold Gas Spray due to its easiness for being plastically deformed. Thus, it could act as a ductile matrix for improving the adhesion of hard TiO_2 particles. Moreover, Paper 2 reviewed the effect of metallic clusters on functional metal oxides during the interaction with gaseous species. The so-called spill-over effect may occur. Paper 7 presents the obtained results and the application of the composite coating as a photocatalyst in gaseous phase.

Developing photocatalytic Copper/nano-Anatase coatings by Cold Gas Spray

M. Gardon[1], C. Fernández-Rodríguez[2], M.R. Espino Estévez[2], M. Torrell[1], S. Dosta[1], J. M. Guilemany[1]

[1] Thermal Spray Centre, CPT, University of Barcelona. Martí i Franquès, 1. 08028 Barcelona, Spain. Contact details: mgardon@cptub.eu - (0034) 634538544

[2] Grupo de Fotocatálisis y Espectroscopía Aplicada al Medioambiente-FEAM (Unidad Asociada al ICMSE-C.S.I.C.), CIDIA-Dpto. de Química, Universidad de Las Palmas de Gran Canaria, Parque científico-tecnológico, Campus universitario de Tafira, 35017 Las Palmas, Spain.

Abstract

Coatings based in copper and nanostructured anatase were deposited by Cold Gas Spray onto stainless steel tubular substrates using different starting feedstock mixtures and distinct spraying conditions. It was observed that copper particles were bonded onto the substrate and titanium dioxide was adhered afterwards. This fact made possible to have the desired photocatalyitic effect at the top of the coating surface. Low temperatures involved in Cold Gas Spray assured that deposited-TiO_2 consisted in nanostructured anatase, which was also ratified by means of the sample characterization. The photocatalytic performance of the obtained coatings was tested by degradation of toluene in gaseous phase.

Keywords: Cold Gas Spray, anatase, photocatalysis, toluene.

Highlights

- Copper/nano-anatase coatings were successfully deposited by Cold Gas Spray.
- Up to 70% of the coating top surface was covered by the photocatalytic material.
- Toluene was completely degraded by irradiating the photocatalyst with UV-light.

1 Introduction

Nanostructured anatase coatings with copper clusters have been used in photocatalysis and a certain synergetic outcome of both materials was found, where the final efficiency was boosted. Distinct techniques have been applied for achieving Cu/nano-TiO_2 layers such as magnetron sputtering, chemical vapour deposition or sol-gel process [1-3]. Despite its success in many photocatalytic applications, the scale-up towards industrial exploitation may be not so direct. In this way, coating processes able to deposit in a quick single step large photocatalytic surfaces in a cost-effective procedure are highly demanded.

Thermal Spray (TS) techniques accelerate powder particles in molten, semi-molten or solid state towards a substrate in order to build-up a coating in a rapid manufacturing method. The distinct TS techniques can be classified according how the particles are propelled. A wide research has been carried out during the last decade in order to achieve satisfactory photocatalytic TiO_2 layers by TS. However, those coatings obtained by means of TS technologies activated by temperature led to: a decrease in the content of metastable anatase phase and; a certain loss in the nanosized starting metal oxide grains, which decreased the efficiency of the samples. T. Klassen *et al.* studied the photocatalytic degradation of dichloroacetic acid using anatase-TiO_2 coatings produced by Atmospheric Plasma Spray (APS), High-Velocity-Oxygen-Fuel spray (HVOF) and Cold Gas Spray (CGS) [4]. APS and HVOF make use of a plasma jet and combustion flame for accelerating the

particles in a molten and semi-molten state respectively. On the other hand, CGS does not need high temperatures for building-up coatings due to the particles are bonded because of its plastic deformation at the impact [5]. The authors found that the photocatalytic performance of those coatings obtained by thermally non-agressive techniques like CGS was at least three times higher than High-Velocity-Oxygen-Fuel (HVOF) spraying or Atmospheric Plasma Spraying (APS), which flame and jet temperatures are above the melting point. It was concluded that spraying processes that higher temperatures involved converted anatase phase to rutile, whose photoactivity is lower. Moreover, an increase in the grain size may happen, which would lead to a decrease in the specific surface. Other studies had also reported lower efficiencies when using TS techniques that operate with high temperatures for building-up photocatalytic titanium dioxide coatings [6,7].

CGS meets the requirements as a process for yielding photocatalytic coatings on an industrial scale while maintaining the structure and composition of nanostructured anatase. In this work, we have mixed copper and nanostructured anatase powder in order to obtain a threefold effect: i) develop a ductile matrix for easing the deposition of the ceramic particles, ii) boost the adhesion of the ceramic particles and iii) equalize or enhance the photocatalytic behaviour of the obtained samples. Despite copper has been commonly used in CGS technology, it has never been reported Cu/nano-TiO_2 as feedstock for building-up photocatalytic coatings onto steel cylinders.

2 Materials

2.1 Coating preparation and characterization

Nanostructured TiO_2 powder based in anatase phase (Tayca, Japan) and Cu powder (Sulzer, Germany) were used as feedstock; two different mixtures were prepared using a stirring tank (SD-1 Laboratory Attritor, Union Process). The CGS equipment utilized for obtaining the coatings was a KINETICS® 4000 (Cold Gas Technology, Ampfing, Germany), with a maximum operating pressure

of 40 bar, temperature of 800 °C and it uses nitrogen as the propellant gas. In addition, KINETICS® 4000 has the possibility of using a pre-chamber of 120 mm in length connected to the nozzle of the gun where powders are heated up for a longer time. Phase composition of powders was analyzed by a X'Pert PRO MPD diffractometer (PANalytical). Powder and coating cross-section area were observed by Optical Microscopy (DMI-M Leica), Scanning Electron Microscopy (JSM-5310 Jeol) and Field-Emission Scanning Electron Microscopy FESEM (Hitachi 401s, Japan). Grain size of the metal oxide powder was studied by Transmission Electron Microscopy TEM (Hitachi H7100). Composition of the coatings was analyzed by Energy Dispersive Spectroscopy EDS (Xflash detector X5010, Bruker) and micro-Raman technique (Labram HR800, Horiba). Two different spraying conditions and two powders with a distinct anatase/copper ratio were studied, which developed a 2^2 factorial design of experiments. Stainless steel tubular substrates were used for producing the coatings. The coated cyilinders were mounted in tubular glass reactors for its application as photocatalysts in the degradation of toluene in gaseous phase using UV-light.

2.2 Photocatalytic experimental set-up

The reactor consisted of a cylindrical inner tube made of stainless steel (300x20x10 mm) in a pyrex glass reactor, 32 mm in diameter, between which the reactant mixture was passing through. The light source were commercial 15 W UVA-light (spectral peak centred around 365 nm) located outside of the reactor. The toluene inlet concentration was set at 25 ppmv in air and the inlet flow was 10 mL/min. Before switching on the UVA light, the catalyst was first exposed to the polluted air stream until dark-adsorption equilibrium was reached. On-line detection and quantification of toluene and CO_2 were performed by gas chromatography with a mass spectrometry detector. The experimental setup is summarized in figure 1.

3 Results and discussion

3.1 Coating development

Copper and nano-anatase powders were analyzed by X-Ray Diffraction (XRD) and it was determined that the materials were crystalline without the presence of other phases (figure 2). TiO_2 powder had a particle diameter almost three times below Cu and contained a considerable amount of fines. Figure 3 shows a FE-SEM micrograph of both spherical powders and their particle size distribution. In order to increase the specific area of the photoactive material, nanostructured anatase was used. Figure 4 shows the size of the metal oxide grains by means of a TEM micrograph. Several measures were carried out and a value between 30 and 100 nm was obtained.

Four different experiments were done taking into account two operation spraying conditions for two blended powders obtained through a process protected by a trade secret. Previously, a wider range of spraying conditions was analyzed for finally focusing on the selected design of experiments. Pressure and temperature are commonly studied CGS parameters in order to: a) increase in-flight velocity of the particles in the nitrogen stream and; b) provide certain softening activated by temperature to the material with the purpose of supplying plastic deformation. From this preliminary study, it was observed that as long as the pressure and temperature increased only copper was able to get adhered onto the substrate without the presence of anatase. This was attributed to the hard but fragile characteristics of metal oxides. Thus, when operating at higher kinetic conditions ceramic particles achieved enough velocity for eroding the substrate and were broken at the impact and a thick Cu coating was obtained but useless for the final application of the product. On the other hand, when operating with lower pressures and temperatures, deposition efficiency of copper was drastically reduced because of the insufficient velocities reached by the metallic particles, which cannot deform plastically. In this case, titanium dioxide particles were heterogeneously mechanically embedded onto the substrate surface but in a very heterogeneous mode. However,

the presence of coated areas was not truly convincing for applying directly this disposition as a photocatalyst. More cycles were carried out with the purpose of increasing the amount of single TiO_2 particles incrusted into the metallic substrate. However, it was not possible to bond more particles because it was obtained a similar effect than grit-blasting. A second pass of the gun torn off the particles embedded in the previous cycle and it was not observed a clear increase of titanium dioxide on the substrate surface. Therefore, the experiments were designed with the purpose of studying the region located between the above mentioned upper and lower conditions. Table 1 compiles the nomenclature and Cu-TiO_2 ratios implemented for the factorial design of experiments. The values are given in ratios of pressure (P)/stand-off distance (d) and temperature (T)/stand-off distance (d).

Gun velocity, feeding rate, spraying angle and stand-off distance were all remained constant. Figure 4 shows the cross-section area of the obtained samples. Although it seems that the coatings consist mainly in copper, it can be observed that TiO_2 is adhered at the top surface of the coating. This fact is beyond doubt determining due to anatase is the responsible material for carrying out the photocatalytic process. Therefore, to have deposited anatase particles at the top of the coating surface, where the interaction between the photocatalyst and the species to be degraded is achieved, will make possible that the coating perform satisfactorily. Copper particles have a larger particle size distribution and also greater density. In the studied operation conditions become more accelerated and impact first onto the substrate. Immediately after that, titanium dioxide particles impact onto the copper, where plastic deformation can be easily reached. The most energetic conditions were able to bond a higher amount of material. Besides this, more anatase was bonded onto the metallic particles due to a higher TiO_2/Cu ratio in the sample C293.

Anatase content at the top of the coating surface was determined by EDS. SEM micrographs of the top surface of the coatings are presented in figure 6 as well as the detection of Ti, Cu and O. Both

mappings showed a TiO_2-based surface where some clusters of copper could be found. In the case of C293, the amount of metallic clusters was slightly reduced presenting larger areas without copper. Anyhow, the amount of anatase was determined at the top of the coating for samples C291 and C293. It was obtained a covered area of 50-60% and 60-70% respectively. Presence of anatase and copper on the surface was also ratified by means of Raman spectroscopy (Figure 7).

3.2 Photocatalytic performance

In order to prove the photocatalytic behaviour of the coatings, a steel cylinder was coated using the spraying conditions of the sample C293 and it was introduced into the glass reactor. Figure 8 plots the normalized concentration of toluene and carbon dioxide as function of time and UV light. During the first hour of experiment, despite UVA-light remained turned off it was observed a decrease of toluene concentration, but CO_2 did not increase. Thus, there was no degradation of toluene, but adsorption of the gas onto the CGS coating. Nevertheless, once the UV light was switchturned on, concentration of toluene drastically decreased almost to zero in just 30 minutes, obtaining a complete degradation in less than 60 minutes. This could not be explained by gas adsorption due to the concentration of CO2 increased caused by a complete mineralization of toluene. Since the production of undesirable intermediates and by-products is a problem in the photocatalytic oxidation of VOCs, such as toluene, the preparation of coatings with high selectivity for total mineralization (i.e. CO_2 and H_2O) is of outmost importance. TiO_2 with very low particle size was used as photocatalysts in order to increase the selectivity to complete toluene photo-oxidation since TiO_2 with smaller particle size showed less by-products when were used as photocatalyst [8]. In fact, any intermediates were detected in the outlet stream of the reactor after the photo-oxidation of toluene over CGS coating.

Figure 9 shows a scheme of the possible situations that may happen as regards to the interaction among: UV-light, nanostructured titanium dioxide particles, copper particles and the gaseous species. It includes the following steps: [A] adsorption of toluene and oxygen, [B] excited electron and hole due to UV-light (reaction 1), [C] trapping photogenerated electrons by Cu^{2+} ions (reaction 4), [D] surface reaction between oxygen and excited electrons (reaction 3), [E] surface reaction between toluene and hydroxyl radicals (reaction 9), [F] degradation of toluene and [G] oxidation of Cu^{+} or Cu^{0} by O_2 (reaction 5). According to Xu and Schoonen [9] the conduction (CB) and valence (VB) band edges of TiO_2 and CuO are -0.29, 0.46 and 2.91, 2.16 eV vs. NHE, respectively. Since conduction band of CuO is situated below the CB of TiO_2, the electrons might be transferred from TiO_2 to CuO deposits close to TiO_2. Copper ions can act as e^{-} traps to reduce the recombination rate of h^{+}/e^{-} pairs photo-generated and hence enhance the efficiency of the process. Furthermore, highly reactive species are obtained from this interaction. The reactions that lead to the formation of radicals are shown below:

$$TiO_2\ (hv) \rightarrow TiO_2\ (e^{-}_{cb};\ h^{+}_{vb}) \quad (1)$$

$$OH^{-}\ (ads) + h^{+}_{vb} \rightarrow \bullet OH\ (ads) \quad (2)$$

$$O_2\ (ads) + e^{-}_{cb} + H^{+} \rightarrow HO_2\bullet^{-} \quad (3)$$

$$Cu^{2+} + e^{-}_{cb} \rightarrow Cu^{+} \quad (4)$$

$$Cu^{+} + O_2\ (\text{or other oxidants}) \rightarrow Cu^{2+} \quad (5)$$

$$2\ HO_2\bullet^{-} \rightarrow H_2O_2 + O_2 \quad (6)$$

$$H_2O_2 + O_2\bullet \rightarrow \bullet OH + O_2 + OH^{-} \quad (7)$$

$$H_2O_2 + e^{-}_{cb} \rightarrow \bullet OH + OH^{-} \quad (8)$$

$$\bullet OH\ (ads)\ \text{or}\ \bullet OH + C_7H_8\ (ads) \rightarrow C_7H_8\ (oxid) \quad (9)$$

The appearance of •OH and $HO_2\bullet^{-}$ may directly (or partially) lead to many distinct routes of toluene degradation and a considerable amount of intermediate products may take place in a complex reaction system [10].

CGS is limited by the hardness of certain materials such as functional metal oxides. They are very attractive for a wide range of application and may be potentially used combined with ductile materials that can provide plastic deformation at the impact and active behaviour when running in the desired conditions of operation. This could be achieved by mixing the powders or also by a milling process where hard metal oxide particles are inlaid in ductile active components. In this way, novel cermet powders would be designed for being deposited by CGS, which could open a new line of research in this field.

4 **Conclusions**

Cold Gas Spray can be used for building-up photocatalytic copper/nanostructured-anatase layers onto steel cylinders. Adding copper particles to titanium dioxide powder provides enough plastic deformation at the impact for easing the adhesion of the metal oxide particles. The spraying conditions were adjusted in order to assure that the photocatalyst is at the top of the coating surface, making feasible the final application of the material. Photocatalytic behaviour of the coating was proved by means of the complete degradation of 25 ppm of toluene in less than 60 minutes.

5 Acknowledgments.

The authors wish to thank the Generalitat de Catalunya for the financial support for this research project 2009 SGR 00390.

6 References

[1] S. Xu, J. Ng, X. Zhang, H. Bai, D. D. Sun. Inter. J. Hydr. Energy, 35 (2010) 5245.

[2] J. Araña, A. P. Alonso, J.M. Doña Rodríguez, J.A. Herrera Melián, O. G. Díaz, J. P. Peña. Appl. Cat. B: Env. 78 (2008) 355.

[3] H.A. Foster, D.W. Sheel, P. Sheel, P. Evans, S. Varghese, N. Rutschke, H.M. Yates. J. Photochem. Photobio. A 216, 2-3 (2010) 283.

[4] H. Gutzmann, J.-O. Kliemann, R. Albrecht, F. Gärtner, T. Klassen, F.-L. Toma, L.-M. Berger, B-Leupolt. Inter. Therm. Spray Conf. proceed. 2010.

[5] L. Pawlowski, Science and Engineering of Thermal Spray Coatings, John Wiley & Sons, Chichester, U.K., 1995.

[6] F.-L. Toma, G. Bertrand, S. O. Chwa, D. Klein, H. Liao, C. Meunier, C. Coddet. Mat. Sci. Eng. A 417 (2006) 56.

[7] J. Colmenares-Angulo, S. Zhao, C. Young, A. Orlov. Surf. Coat. Tech. 203, 15 (2009) .2150.

[8] A.J. Maira, K.L. Yeung, J. Soria, J.M. Coronado, C. Belver, C.Y. Lee, V. Augugliaro. Applied Catalysis B: Environmental 29 (2001) pp. 327.

[9] Y. Xu, M.A.A. Schoonen Am. Miner., 85 (2000) pp. 543.

[10] J. Mo, Y. Zhang, Q. Xu, Y. Zhu, J. J. Lamson, R. Zhao. Applied Catalysis B: Environmental 89 (2009) pp. 570.

List of tables

Table 1. Nomenclature of the obtained samples for the factorial design of experiments and its corresponding ratios:

		P/T [bar/ ºC]	
		25-35	**15-25**
TiO_2/Cu [ml/ml]	**0,8-1,2**	C290	C291
	1,4-1,8	C292	C293

List of figure captions

List of figures

Fig. 1

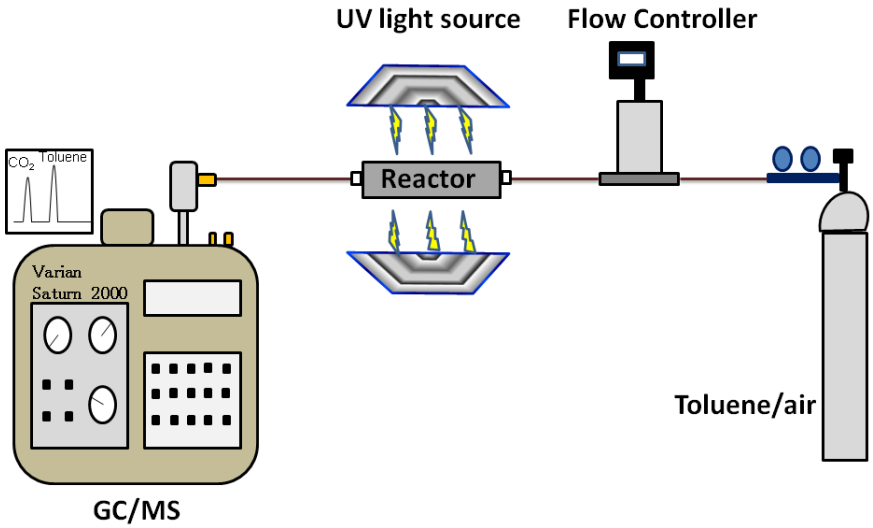

Fig. 2

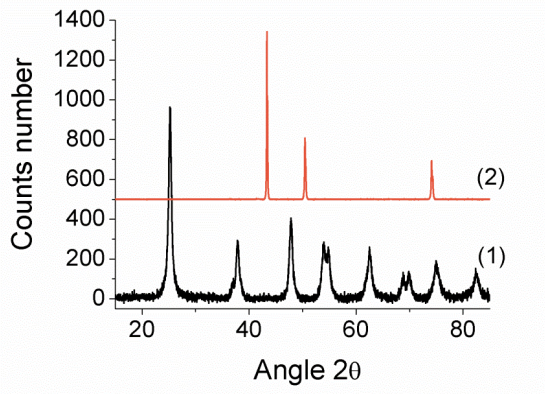

Fig. 3

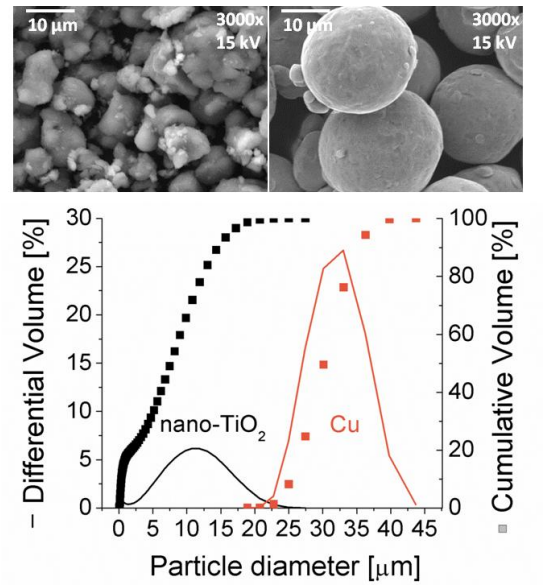
10 µm
3000x
15 kV
10 µm
3000x
15 kV
Differential Volume [%]
Cumulative Volume [%]
nano-TiO2
Cu
Particle diameter [µm]

Fig. 4

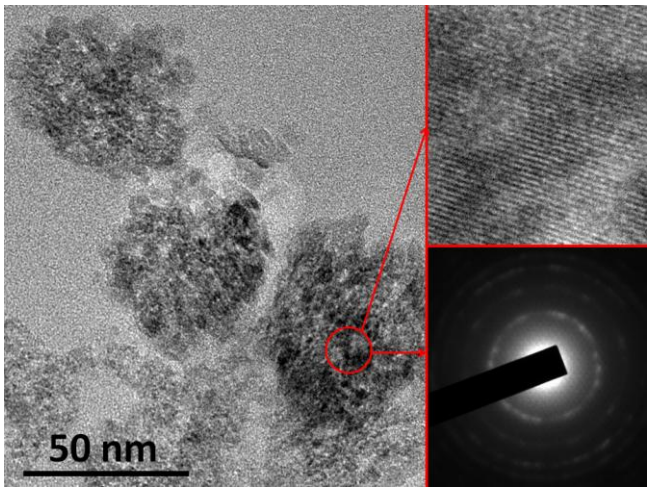
50 nm

Fig. 5

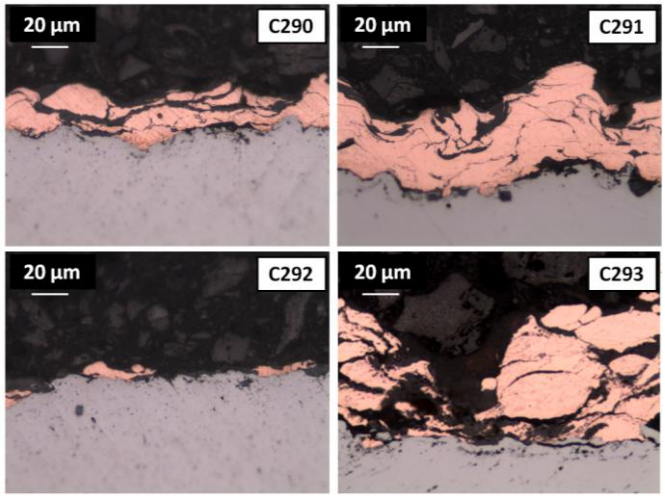
20 µm
C290
20 µm
C291
20 µm
C292
20 µm
C293

Fig. 6

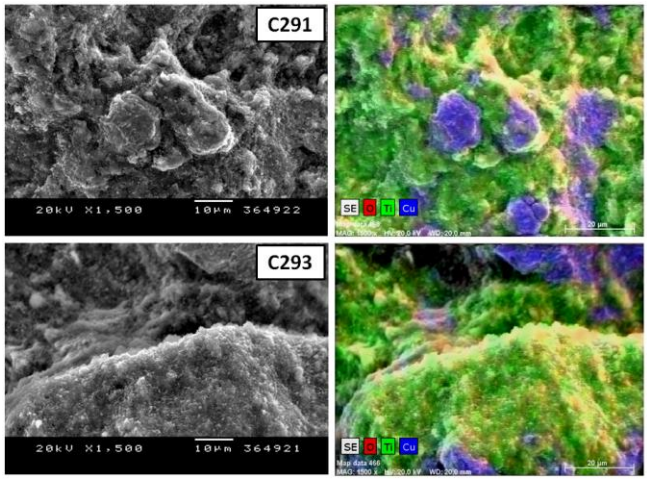
C291
20kV X1,500 10µm 364922
SE O Ti Cu
C293
20kV X1,500 10µm 364921
SE O Ti Cu

Fig. 7

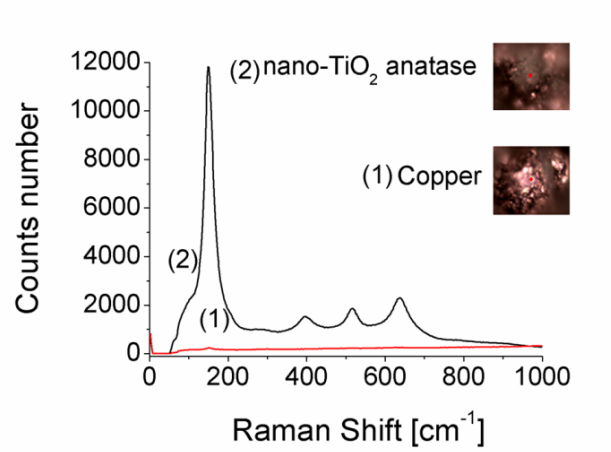
12000
10000
8000
6000
4000
2000
0
Counts number
(2) nano-TiO2 anatase
(1) Copper
(2)
(1)
0
200
400
600
800
1000
Raman Shift [cm-1]

Fig. 8

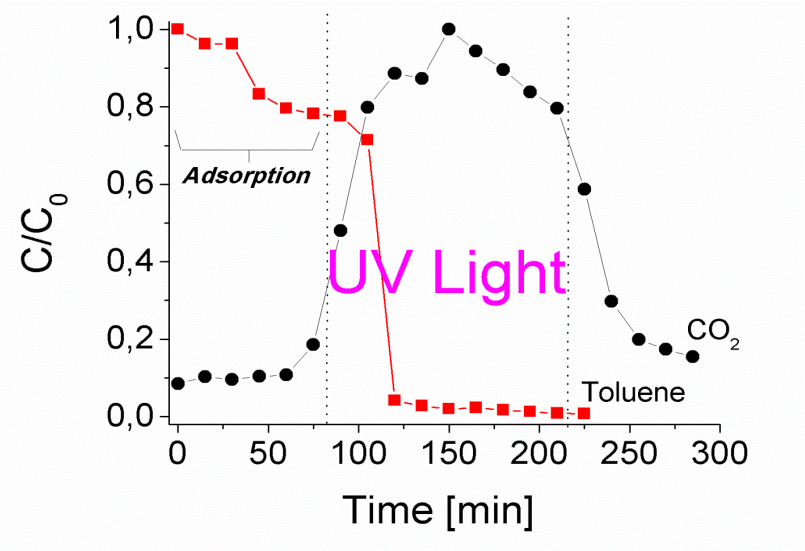
1,0
0,8
0,6
0,4
0,2
0,0
C/C0
Adsorption
UV Light
CO2
Toluene
0
50
100
150
200
250
300
Time [min]

Fig. 9

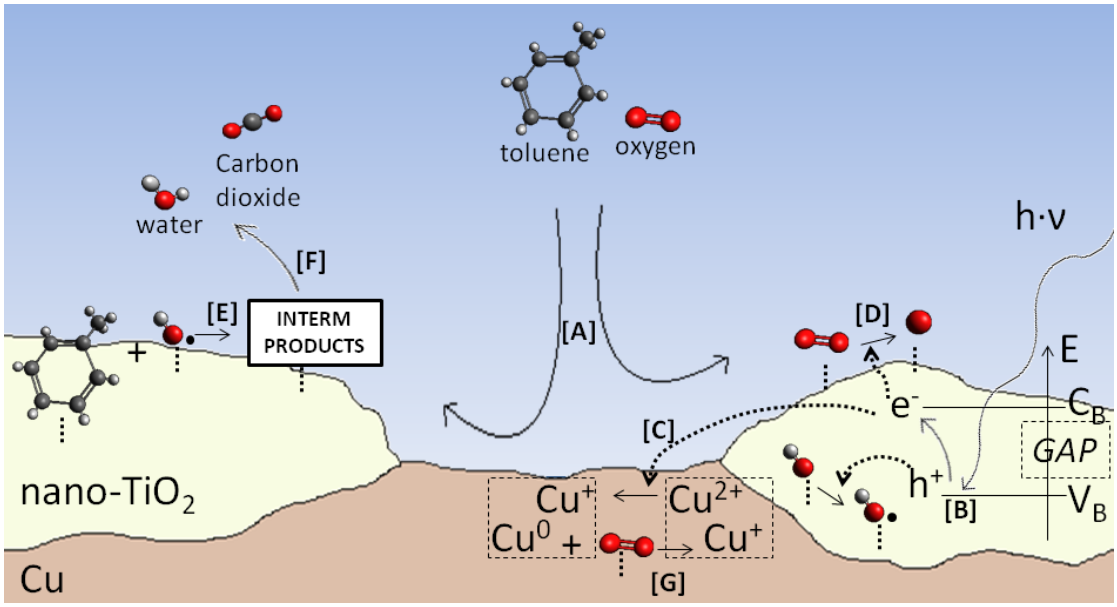
toluene
oxygen
Carbon dioxide
water
[F]
[E]
INTERM PRODUCTS
[A]
h·ν
[D]
E
e^-
C_B
[C]
GAP
nano-TiO_2
h^+
[B]
V_B
Cu^+
Cu^{2+}
Cu^0 +
Cu^+
[G]
Cu

b) Paper 8:

M. Gardon, C. Fernández, M. Torrell, S. Dosta, J. M. Guilemany. Improved photocatalytic nanostructured anatase coatings obtained by Cold Gas Spray.

Copper/nano-anatase coatings were also used for degrading species in liquid phase. However, there were found small concentrations of copper in the outlet of the reactor, which may be of special concern due to environmental regulations on this field.

Thus, building-up pure anatase coatings was an important objective to be completed. Paper 8 explains how nano-TiO_2 particles can be adhered onto a substrate by means of a bond coat. Its functional application is also reported.

Improved photocatalytic nanostructured anatase coatings obtained by Cold Gas Spray

M. Gardon [1], C. Fernández-Rodríguez[2], M.R. Espino Estévez[2], S. Dosta[1], J. M. Guilemany[1]

[1] Thermal Spray Centre, CPT, University of Barcelona. Martí i Franquès, 1. 08028 Barcelona, Spain. Contact details: mgardon@cptub.eu - (0034) 634538544.

[2] Grupo de Fotocatálisis y Espectroscopía Aplicada al Medioambiente-FEAM (Unidad Asociada al ICMSE-C.S.I.C.), CIDIA-Dpto. de Química, Universidad de Las Palmas de Gran Canaria, Parque científico-tecnológico, Campus universitario de Tafira, 35017 Las Palmas, Spain.

Abstract

The present survey describes a photocatalytic nanostructured anatase coating deposited by Cold Gas Spray supported on titanium sub-oxide layers obtained by Atmospheric Plasma Spray onto stainless steel cylinders. The photocatalytic coating was homogeneous and preserved composition and nanostructure of starting powder. Inner titanium sub-oxide layer favored the deposition of anatase particles in solid state and improved mobility of charge carriers due to its low electrical resistivity. Photocatalytic activity was measured by degrading phenol and formic acid in aqueous phase and was compared to sol-gel coatings based on commercial standard P25®. Obtained results showed improved efficiencies when using CGS nano-TiO_2 photocatalysts both for phenol and formic acid degradation.

Keywords: Cold Gas Spray, nanostructure, P25®, phenol, formic acid.

1 Introduction

A reduction of pollutants in the environment has drawn attention on a global framework of different disciplines of research. Development of materials and technologies capable to assure non-harmful surroundings is challenging a wide range of professionals in either scientific or industrial world. In this line, photocatalysis seems to become a chief tool in order to achieve acceptable levels of depollution. Besides, this process has some advantages towards its competitors: it does not need oxidation agents and; temperature is not required for its operation, which reduces the cost of the technology. Nanostructured TiO_2-anatase coatings are being applied as the flagship functional material in this field due to its high photoactivity, chemical stability, relatively low cost and large active surface [1]. Furthermore, the global market for nanotechnology products was estimated at about $15.7 billion in 2010, with an approximate average compound annual growth rate of 11.1%, which included well-established commercial applications in nanomaterials such the one presented in this work [2]. Together with the increase in contamination of air and water; industrial and domestic claim may request large surfaces covered by these compounds as from coating processes that can provide balanced performances among cost, yield capacity, operation times and a satisfactory behavior of the final product.

Adequate efficiencies in heterogeneous photocatalysis are commonly reached by applying the active material as coatings. Nonetheless, to coat large surfaces with nanostructured TiO_2 is not so simple. Nowadays, sol-gel processes are commonly used for depositing the coatings in this application. However, the slow and careful manufacturing plus the high temperatures required for the post deposition treatment difficult the scale-up of the manufactured goods [3]. As an alternative, Thermal Spray (TS) can be applied faster and cost-effectively to achieve photocatalytic TiO_2 coatings as a rapid and cost-effective method. A considerable amount of scientific reports based on conventional TS processes have been published and the intention of global TS industry to stay in this synergy has been clearly demonstrated. However,

temperatures involved in the plasma jet of Atmospheric Plasma Spray (APS) or in the flame of High-Velocity-Oxygen-Fuel Spray (HVOF) increase the grain size of the starting powder and transform anatase to rutile (both TiO_2 phases, being anatase the corresponding metastable phase), which is photocatalytically less active. As a consequence, the effectiveness of the obtained samples decreased [4-6].

Alternatively, Cold Gas Spray (CGS) does not require melting the material to be deposited. Therefore, it could be able to avoid undesired phase transformations and growth in the grain size among TS processes. A high kinetic nitrogen stream propels powder particles, which are plastically deformed at the impact with the substrate. Metallic layers have been successfully built-up due to the ductility of these materials. Nonetheless, ceramic particles cannot mechanically behave in this way and it makes difficult to coat a substrate. Anyhow, interesting applications have been reported. P. Heinrich et al. embedded anatase particles by CGS onto a plastic surface for its application as a photocatalyst [7]. The particles penetrated in the polymer providing certain area of the metal oxide on the surface, which was supposed to make possible the photocatalytic degradation of the contaminants. Later on, T. Klassen et al. purposed the disclosure of the manufacturing of metallic objects with a photocatalytic coating by Cold Gas Spray, where the starting photocatalytic metal oxide powder was mixed with a ductile metallic powder that provided plastic deformation at the impact of the particles onto the substrate surface [8]. The top surface was preferably covered between 30 and 80% of metal oxide particles, which may limit the final performance of the photocatalyst.

Surfaces completely covered by nanostructured anatase particles using CGS were reported by M. Fukumoto et al. obtaining a thickness of more than one hundred microns [9]. Possible chemical bonding was suggested because the particles were not embedded onto the substrate surface. Transmission Electron Microscopy (TEM) revealed that the metal oxide particles were connected as a single crystal. In a further work, the same authors attributed this possibility to a

unique chemical route for synthesizing and agglomerating nanostructured anatase crystallites [10].

In the present work, homogeneous nanostructured anatase coatings have been obtained by Cold Gas Spray starting from a home-made powder. The photocalytic activity of CGS nano-TiO_2 coatings was tested in the degradation of phenol in liquid phase and was compared to standard sol-gel P25 (Degussa®) coating as a commonly-used commercial photocatalyst.

2 Materials

2.1 Coating preparation and characterization

Nanostructured TiO_2 powder based in anatase phase was used as feedstock for developing the photoactive coating and reduced TiO_2-rutile was sprayed onto steel as support for the catalytic layer using an APS A-3000S system with an F4 plasma torch (Sulzer Metco, Germany). The CGS equipment utilized was a KINETICS® 4000 (Cold Gas Technology, Ampfing, Germany), with a maximum operating pressure of 40 bar, temperature of 800 °C and it uses nitrogen as the propellant gas. In addition, KINETICS® 4000 has the possibility of using a pre-chamber of 120 mm in length connected to the nozzle of the gun where powders are heated up for a longer time. Powder and coating cross-section area were observed by Scanning Electron Microscopy (Phenom). Grain size of the metal oxide powder was studied by Transmission Electron Microscopy TEM (Hitachi H7100). Composition of the coatings was analyzed by micro-Raman technique (Labram HR800, Horiba). Stainless steel tubular substrates were used for producing the coatings. Roughness was analyzed using a rugosimeter SJ-210 (Mitutoyo).

2.2 Photocatalytic experimental set-up

Coated cylinders were mounted in tubular glass reactors for its application as photocatalysts in the degradation of phenol in liquid phase using UV-light. The reactor consisted of a cylindrical

inner tube made of stainless steel (300x20x10 mm) in a Pyrex glass reactor, 32 mm in diameter, between which the reactant mixture was passing through. The light source were commercial 15 W UVA-light (spectral peak centered approximately on 365 nm) located outside of the reactor. Both phenol and formic acid inlet concentration were set at 10 mg/L in water and the inlet flow was 10 ml/min. Before switching on the UVA light, the catalyst was first exposed to a polluted air stream until dark-adsorption equilibrium was reached. On-line detection and quantification of toluene and CO_2 were performed by gas chromatography with a mass spectrometry detector.

3 Results and Discussion

3.1 Coating development

Nanostructured particles were agglomerated obtaining a particle size distribution of -30 +10 µm with a considerable amount of fines (figure 1). Starting powder was based in pure crystalline anatase and its grain size was ranged between 20 and 100 nm. Preliminary trials were carried out spraying nano-anatase onto smooth stainless steel and ceramic tiles in a range of spraying conditions from low pressure and temperature to higher values in order to study the influence of the particle velocity in the deposition behaviour. Despite the difference in the operation parameters, the coatings were not built-up in any of both materials. Provide roughness to a substrate surface is a usual step for improving the adhesion of the particles in thermal spray processes. Therefore, the pieces were grit-blasted at 6 bar pressure. Average final roughness of stainless steel and ceramic tiles was 6,7 µm and 7,2 µm respectively. Then, same spraying conditions were repeated. Again, stainless steel was not coated in spite of altering the operation conditions of the process. Ceramic tiles were eroded when operating at higher energetic parameters. However, it was observed a certain deposition at low spraying conditions where some of the anatase particles were adhered, although it was in a very low efficiency and homogeneity. Some findings could be drawn: i) the roughness of the substrate was significant; ii) substrate composition could be providing chemical affinities in the interaction of the particles

at the impact and; iii) hardness of the substrate material may be required for easing this interaction.

As it has been reviewed in many scientific contributions, CGS coatings are formed due to plastic deformation of the sprayed particles during impact [11,12]. In this case, nano-TiO_2 cannot deform plastically but other mechanisms can occur. A. Ohmori et al. reported that nanostructured TiO_2 particles could deform during impact in certain operation conditions [13]. Moreover, chemical bonding between particles and substrate or among particles may offer the possibility that the substrate would be playing a key role in terms of hardness and chemical composition when nanostructured anatase particles are being adhered by CGS. Therefore, it was decided to previously coat stainless steel with titanium sub-oxide (TiO_{2-x}) by Atmospheric Plasma Spray. This new coated surface could provide enough hardness for developing the breakdown/deformation of nano-TiO_2 particles and its composition may ease the formation of chemical bonds boosting the adhesion of the coating. Moreover, the top surface of an APS metal oxide coating presents certain roughness, which was observed to be a key factor during the first trials. The spraying conditions were adjusted in order to have enough particle velocity for activating the bonding mechanisms but not so much for eroding the APS TiO_{2-x} coating.

Figure 2 shows the cross-section area of an obtained multilayered sample. It is possible to observe that nanostructured anatase coating was homogeneously deposited onto APS TiO_{2-x} layer. Thus, a complete coverage of the surface by the active particles may offer higher performances when degrading contaminants. A detailed observation of the interface between both coatings is shown in figure 3, no cracks were found and good adhesion was obtained. As regards to the composition of the coatings, inner layer was based in reduced stoichiometries of titanium dioxide; corresponding spraying conditions were reported in previous surveys [14,15]. Main features of this coating material were based on its outstanding behaviour as electrode in simulated lead batteries. Top surface of the coating was based on anatase phase, which is in command to accomplish the photocatalytic process (figure 4).

In order to explain the building-up of the coating, the following mechanism is described. Roughness at the top surface of the APS TiO_{2-x} coating contained certain holes or valleys. This microtexture supplied a profile that favored the anchoring of nanostructured anatase. CGS nitrogen stream propelled highly reactive fine TiO_2 particles, which filled the above mentioned gaps (clearly visible in figure 3). Energy released when compressing the particles into TiO_{2-x} hollows could be enough for creating chemical bonds between particles and substrate. Then, nano-TiO_2 particles were bonded among them increasing the thickness of the coating. Although roughness may not be found for easing the adhesion regarding coarser anatase particles that arrived to the substrate after the finest ones were deposited, its affinity could be enough for creating the required linkage. Figure 5 represents each step of the process. Microhardness of the nanostructured anatase layer was tested obtaining a mean value of 132±32 HV, which is much lower than bulk TiO_2. This could be explained due to the CGS anatase coating is behaving as a ceramic green preform before sintering the material. Spraying process has developed necks among the particles but the overall structure is not as consistent as the bulk titanium dioxide (in agreement with other authors [16]).

3.2 Photocatalytic performance

Photocatalytic performance of the TS multilayered samples was tested by means of coated stainless steel cylinders. Phenol and formic acid were selected as contaminants in aqueous phase starting from a composition of 10 mg/L. Starting trials related to phenol showed little difference between CGS and sol-gel coating. Therefore, it was decided to carry out three experiments and the amount of phenol at the reactor outlet was analyzed in intervals of 30 minutes. Obtained results were compared with the performance of a sol-gel coating composed by commercially available nanosized anatase powder (P25, Degussa®). As it is shown in figure 6(a), CGS nano-TiO_2 coating had slightly improved efficiency compared to sol-gel P25®, especially after 1 hour of experiment. Starting concentration of the contaminant was

proportionally reduced and deviation among repetitions was low. After 90 minutes CGS nano-TiO_2 photocatalyst deposited by CGS had slightly superior performance. As regards to formic acid removal, starting experiments showed significant differences among repetitions related to CGS coating. Moreover, constant disturbances made difficult to stabilize initial concentration. Therefore, concentration of the contaminant was measured each 15 minutes with the aim of having an accurate monitoring of the degradation. Evolution of formic acid concentration with time when irradiating with UV light is plotted in figure 6(b). In this case, sol-gel P25® reached maximum degradation rate after 60 minutes. Once again, CGS nano-TiO_2 photocatalyst had superior performance in the last measure (75 minutes). This may be attributed to the difference in the composition of both photocatalysts. P25® is based on 75% of anatase and 25% of rutile. Many authors have reported that a combination of these titanium dioxide phases can have certain synergetic effect when degrading contaminants. Besides this, role of crystallite size may be also determining. Nevertheless, enhanced performance of P25® was overcomed by the outstanding photocatalytic behaviour of nanostructured anatase coating deposited by CGS. Deviation among repetitions increased considerably in both cases, which was especially observed for CGS photocatalyst.

It is worthy to mention that only 5 minutes were required for coating a cylinder with a length and diameter of 30 cm and 2 cm respectively using Cold Spray equipment. On the other hand, an overall time above 240 minutes was spent when depositing the sol-gel layer on the same steel piece. Therefore, CGS competitiveness in nano-TiO_2 photocatalysts is not just based on their operational times needed for manufacturing the coatings, but in the fact that equalizes or even improves the obtained values when using commonly standard sol-gel P25® coatings.

Lower layer based on titanium sub-oxide may be not only favoring the deposition of CGS nano-TiO_2 particles; it could be also acting as a current collector due to its low electric resistivity (0,33 Ω·cm [14]). In this way, photogenerated electrons would be distributed more homogeneously to the photoactive surface, which could boost the degradation of either phenol or formic acid.

Figure 7 represents an example of possible interactions that would be carried out in the degradation of phenol, although reactive species and overall mechanism are considered to be the same for formic acid: [A] adsorption of phenol, water and oxygen onto titanium dioxide surface, [B] photogeneration of the electron-hole pair (reaction 1), [C] transport of excited electrons along the photocatalyst, [D] interaction between holes and adsorbed dissociated water at the surface (reaction 2), [E] possible reactivity between electrons and adsorbed oxygen in water (reaction 3), [F] distinct degradation routes of phenol and [G] desorption of intermediate compounds after their complete mineralization.

$$TiO_2\ (hv) \rightarrow TiO_2\ (e^-_{cb};\ h^+_{vb}) \quad (1)$$

$$OH^-\ (\text{water on surface}) + h^+_{vb} \rightarrow \cdot OH\ (\text{ads}) \quad (2)$$

$$O_2\ (\text{ads}) + e^-_{cb} \rightarrow O_2^-\ (\text{ads}) \quad (3)$$

4 Conclusions

Cold Gas Spray nano-anatase coatings were deposited onto steel cylinders previously coated with titanium sub-oxide layers obtained by Atmospheric Plasma Spray. The photocatalytic coating preserved its composition and nanostructure. Titanium sub-oxide coating provided a necessary surface geometry and composition that favored the deposition of anatase particles, which were not plastically deformed at the impact but bonded by chemical interactions with the substrate. Phenol in aqueous phase was degraded obtaining improved results compared to sol-gel anatase coatings based on P25®. Different repetitions exhibited almost the same results, with very low deviations. Formic acid was successfully degraded after 75 minutes increasing again the performance of sol-gel coatings. TiO_{2-x} undercoat could act as current collector, distributing homogeneously photogenerated electrons to the photocatalyst.

5 Ackowledgements

The authors wish to thank the Generalitat de Catalunya for the financial support for this research project 2009 SGR 00390.

6 References

[1] A. Fujishima, X. Zhang.. Comptes Rendus Chimie 9, 5–6 (2006) pp. 750.

[2] L.A. Dobrzanski, M. Pawlyta, A. Hudescki. Journal of Achievements in Materials and Manufacturing Engineering 49, 2(2011) pp. 550.

[3] M. Gardon, J M. Guilemany. J. Mat. Sci.: Mat. Elec. (2012) DOI: 10.1007/s10854-012-0974-4.

[4] N. Berger-Keller, G. Bertrand, C. Filiatre, C. Meunier, C. Coddet. Surface and Coatings Technology 168 (2003) pp. 281.

[5] F. L. Toma, G. Bertrand, S. Begin, C. Meunier, O. Barres, D. Klein, C. Coddet. Applied Catalysis B: Environmental 68 (2006) pp. 74.

[6] F.-L. Toma, G. Bertrand, S. O. Chwa, C. Meunier, D. Klein, C. Coddet. Surface & Coatings Technology 200 (2006) pp. 5855.

[7] Heinrich, H. Kreye, T. Schmidt, F. Gaertner. German Patent Document Nº DE10 2004 038795 (2004).

[8] T. Klassen, J. A. Kliemann. United States Patent US2007148363A1 (2007).

[9] M. Yamada, H. Isago, K. Shima, H. Nakano, M. Fukumoto. Intern. Thermal Spray Conf. proceed (2010).

[10] N. Tjitra Salim, M. Yamada, H. Nakano, K. Shima, M. Fukumoto. Intern. Thermal Spray Conf. proceed (2011).

[11] V. Champagne. Woodhead Publishing in Materials (2007) ISBN-10: 1420066706.

[12] A. Papyrin. Elsevier Publications (2007) ISBN-10: 0080451551.

[13] G.J. Yang, C.J. Li, F. Han, W.Y. Li, A. Ohmori. Applied Surface Science 254 (2008) pp. 3979.

[14] M. Gardon, J. M. Guilemany. Intern. Thermal Spray Conf. proceed (2011).

[15] M. Gardon, S. Dosta, J. M. Guilemany, M. Kourasi, B. Mellor, R. Wills. Journal of Power Sources 238 (2013) pp. 430.

[16] S.-Q. Fan, G.-J. Yang, C.-J. Li, G.-J. Liu, C.-X. Li, L.-Z. Zhang. Journal of Thermal Spray Technology, 15, 4 (2006) pp. 513.

List of figure captions

List of figures

Fig. 1

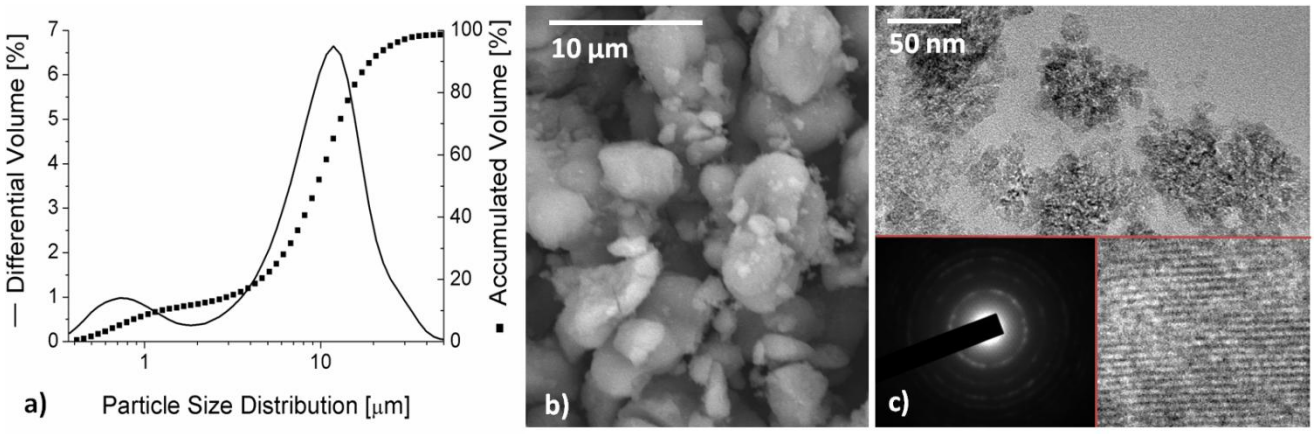

Fig. 2

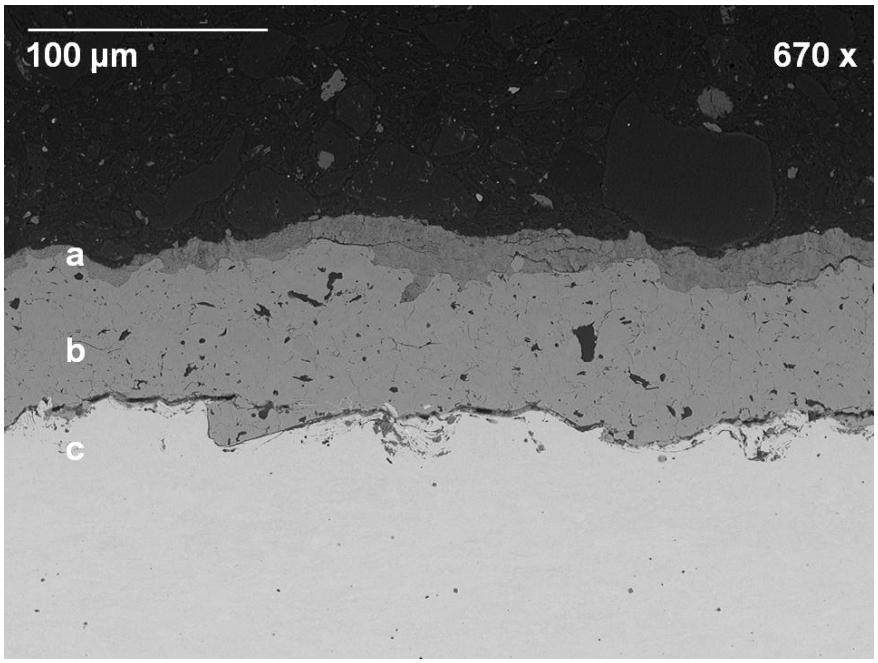

Fig. 3

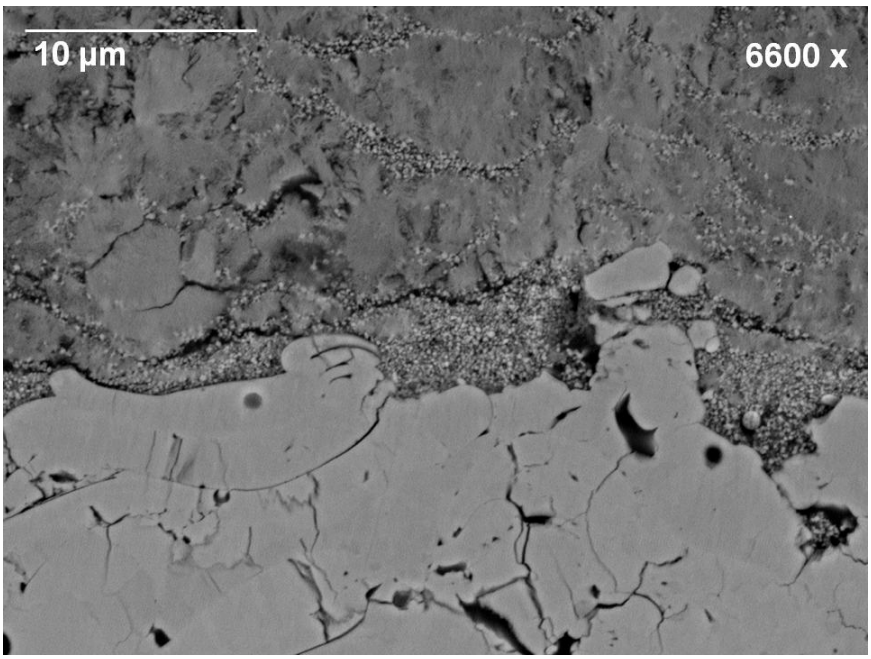
10 µm
6600 x

Fig. 4

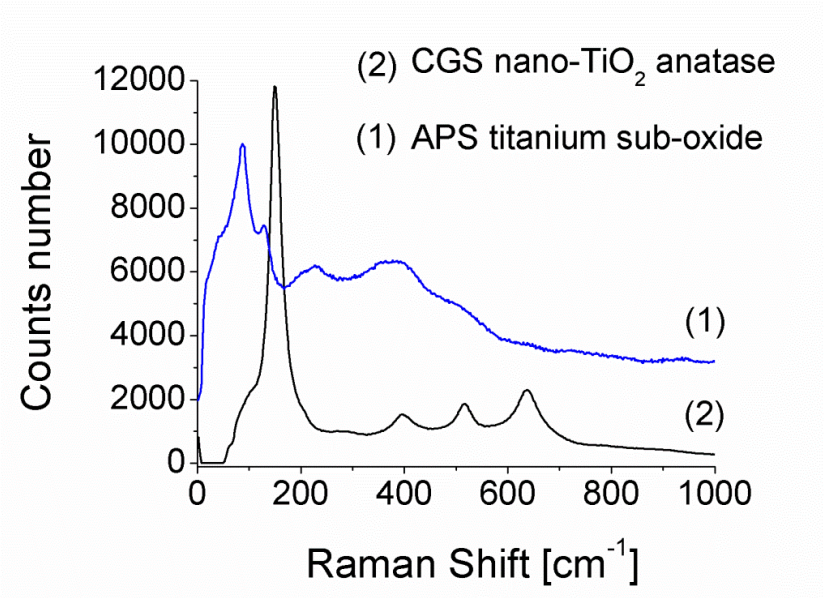
(2) CGS nano-TiO2 anatase
(1) APS titanium sub-oxide
Counts number
12000
10000
8000
6000
4000
2000
0
0
200
400
600
800
1000
Raman Shift [cm-1]
(1)
(2)

Fig. 5

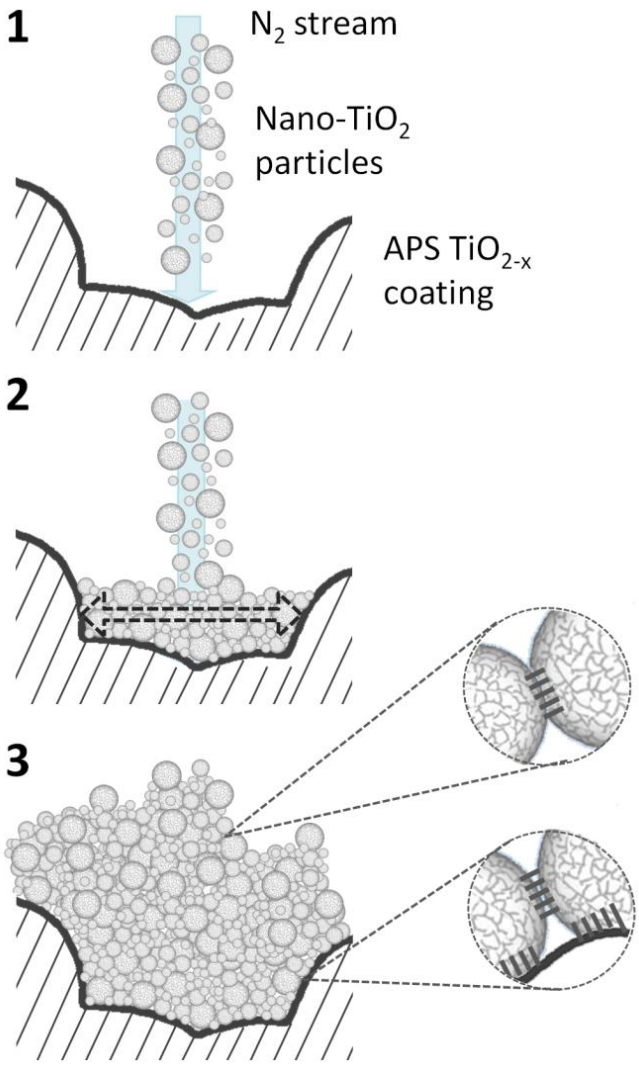

Fig. 6

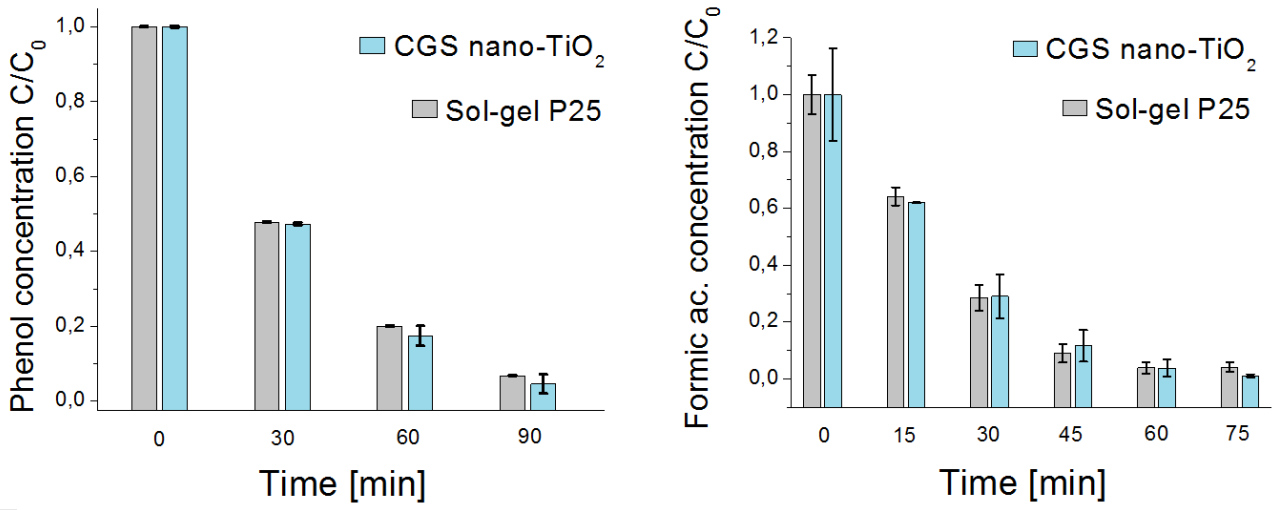
Phenol concentration C/C0
1,0
0,8
0,6
0,4
0,2
0,0
CGS nano-TiO2
Sol-gel P25
0
30
60
90
Time [min]
Formic ac. concentration C/C0
1,2
1,0
0,8
0,6
0,4
0,2
0,0
CGS nano-TiO2
Sol-gel P25
0
15
30
45
60
75
Time [min]

Fig. 7

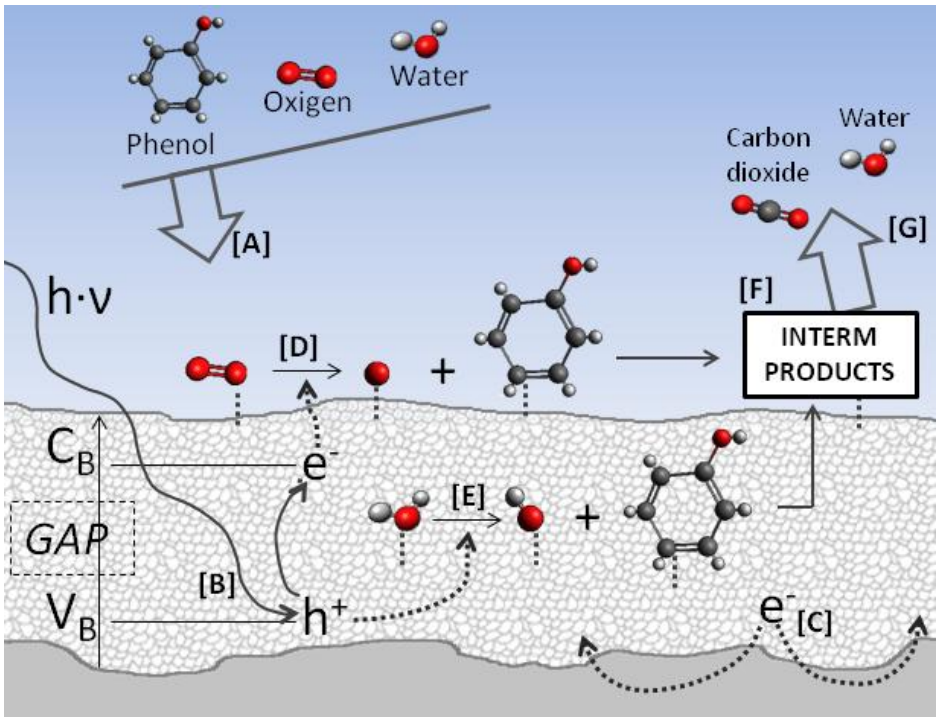
Phenol
Oxigen
Water
[A]
h·ν
[D]
+
Carbon dioxide
Water
[G]
[F]
INTERM PRODUCTS
CB
e-
GAP
[E]
+
[B]
h+
VB
e-
[C]

6.2.3 Biomedical applications

Findings related to feasible deposition of nanostructured anatase coatings by Cold Gas Spray in Paper 8 gave the idea of using these surfaces in biomedical applications. As it was reviewed in Paper 1, Thermal Spray has been constantly contributing to the state-of-the-art of bone tissue substitutes. Therefore, it was decided to apply CGS nano-TiO_2 coatings onto implants.

Once again and similarly to the situation with metal oxide gas sensors, it would have been worthless and little enriching from a scientific standpoint to coat standard substrates and continue the available research in literature without cutting-edge inputs. Thus, a biocompatible polymer based on Polyetheretherketone (PEEK) was selected as implant material in spite of all the starting inconveniences that could be found.

a) Paper 9:

M. Gardon, A.Latorre, M. Torrell, S. Dosta, J. Fernández, J. M. Guilemany. Cold Gas Spray Titanium coatings onto a biocompatible polymer, Materials Letters.

The authors did not successfully deposit nanostructured TiO_2 directly onto PEEK. Therefore, it was decided to repeat a similar strategy as in Paper 8; develop a bond coat that could ease the adhesion of nanostructured anatase particles. In this case, this lower layer was based on Ti. Paper 9 shows its fabrication and the discussion of the results.

Materials Letters 106 (2013) 97–99

Contents lists available at SciVerse ScienceDirect

Materials Letters

journal homepage: www.elsevier.com/locate/matlet

Cold gas spray titanium coatings onto a biocompatible polymer

M. Gardon*, A. Latorre, M. Torrell, S. Dosta, J. Fernández, J.M. Guilemany

Thermal Spray Centre, CPT, University of Barcelona. Martí i Franquès 1, 08028 Barcelona, Spain

ARTICLE INFO

Article history:
Received 21 February 2013
Accepted 30 April 2013
Available online 10 May 2013

Keywords:
Cold Gas Spray
Coating
Titanium
Polymer
Implant

ABSTRACT

Titanium particles were deposited onto Polyetheretherketone substrates using Cold Gas Spray technology and a factorial number of experiments were designed in order to study different spraying conditions. The starting powder and the obtained coatings were characterized with the aim of linking the results with the coating process. By means of micro-Raman analysis, it was observed that the polymer was not degraded during the process in spite of the conditions of the nitrogen gas stream. X-Ray Diffraction analysis also confirms that the composition of the metallic particles was not affected. The results show that it is possible to coat biocompatible polymer implants with titanium leading to thick, homogeneous and well-adhered coatings.

1. Introduction

Polyetheretherketone (PEEK) polymer is known to be bioinert in hard and soft tissues when present as a bulk implant. Although it is not a bioactive material, direct bone contact has been previously reported [1]. In order to enhance the application of PEEK implants assuring a long-lasting life of the material, an improvement of its bioactivity is imperative. Therefore, processes able to coat the polymeric bulk without modifying its composition and boosting its performance are becoming required for carrying out the scaling-up of this product.

Cold Gas Spray (CGS) is a technique for developing coatings by means of accelerating powder particles towards a substrate using a gas stream. These layers are built-up due to the plastic deformation of the particles at the impact. Mainly, CGS attractiveness is based in its direct manufacturing and the possibility of coating large areas in brief periods of time combined with the low temperatures involved, which avoid the thermal degradation of the particle/substrate system. CGS has been widely used for fabricating coatings onto metallic substrates. Nevertheless, it is also feasible to develop metallic layers onto polymer substrates. R. Lupoi et al. studied the deposition of Co, Al and Sn powders on polyamide 6, polystyrene, polypropylene and polycarbonate-ABS blend [2]. Copper particles led to an excessive stress that predominantly eroded the polymer. Aluminum, due to its low specific weight, did not bring any considerable damage to the surface; however it was not possible to reach enough velocity for bonding the particles with the equipment that have been used in these experiments. On the other hand, tin coatings were successfully produced. Better results were obtained by Zhou et al. when spraying Al/Cu on the surface of carbon fiber-reinforced polymer matrix composite (PMC) for its use in the aerospace industry [3]. It was observed that the substrates softened to a minimal degree when exposed to the process gas, which enabled the Al particles to penetrate the polymer and form a mechanical bond. Later, Ganesan et al. effectively fabricated thick copper coatings (1000 μm) on polyvinyl chloride (PVC) polymeric substrate [4]. The results showed that the deposition efficiency was highly sensitive to the glass transition temperature of the substrate, irrespective of the process gas pressure. More recently, Jahedi et al. have dealt with the deposition of Cu particles on several polymers [5]. It was presented a very useful and complete study based in how the particles are mechanically embedded into the substrates depending on the spraying conditions and the nature of the polymer. Other authors have worked with the deposition of non-metallic powders on polymer substrates using CGS technology. Burlacov et al. deposited TiO_2 thin films on different types of thermoplastic polysulfone (PSU) [6]. The particles were mechanically fixed onto PSU and it was suggested that the polymeric material squeezed out of the surface after the particle impact, which would likely act as particle binder. Despite there is a lack of published data related to PEEK used in CGS technology, Sanpo et al. studied the antibacterial property of cold-sprayed HA-Ag/PEEK powders onto glass slides [7]. The study demonstrated the ability of depositing the composite powder and building-up the coating, which retained its inherent antibacterial property as clearly verified from the bacterial assays.

With the aim of enhancing the biocompatibility of PEEK implants, different CGS operation conditions of titanium powder on the polymer have been carried out. The scope of this study is based on the analysis of the selected spraying conditions and the characterization of the materials involved with the purpose of

* Corresponding author. Tel.: +34 63 453 85 44; fax: +34 93 402 16 38.
E-mail address: mgardon@cptub.eu (M. Gardon).

0167-577X/$ - see front matter © 2013 Elsevier B.V. All rights reserved.
http://dx.doi.org/10.1016/j.matlet.2013.04.115

bringing certain criteria related to the interaction of Ti particles and PEEK substrates when operating with CGS systems.

2. Material and methods

A titanium powder obtained from a fused and crushed process was used as feedstock. The powder was quite angular and its particle size distribution was ranged between 20 and 90 μm. The CGS equipment used for obtaining the coatings was a KINETICS® 4000 (Cold Gas Technology, Ampfing, Germany), with a maximum operating pressure of 40 bar, temperature of 800 °C and it operated with nitrogen as the propellant gas. In addition, KINETICS® 4000 had the possibility of using a pre-chamber of 120 mm in length connected to the nozzle of the gun where powders are heated up for a longer time. The powder and the cross-section area of the samples were observed by Scanning Electron Microscopy, SEM (ProX Phenom). The particle size distribution was measured by laser diffraction and the substrate composition was determined by micro-Raman (Labram HR800, Horiba) with the purpose of determining if the polymer had been degraded during the spraying process. The phase composition of the powder and coatings was analyzed by a X'Pert PRO MPD diffractometer (PANalytical).

3. Results and discussion

A factorial design of experiments 2^2 was developed in order to determine the influence of temperature, pressure and the stand-off distance of the samples. Table 1 compiles the nomenclature and the distinct conditions of each spraying. The values are given in ratios of pressure (P)/stand-off distance (d) and temperature (T)/stand-off distance (d). The quality of the coatings differed sharply depending on the spraying conditions. In the case of the samples C295, C298 and C300 it was not possible to form the coating. The particles were mechanically embedded into the softened plastic substrate without the possibility of building-up the titanium layers. However, in the case of the sample C297, the coating was properly obtained showing a homogeneous thickness and a well-adhered structure free of cracks.

Table 1
Nomenclature of the obtained samples for the factorial design of experiments and its corresponding ratios.

		P/d [bar/mm]	
		1,5–2	**2–2,5**
T/d [°C/mm]	**20–35**	C297	C300
	30–35	C298	C295

In Fig. 1a and b it is possible to observe the cross-section area of the most significant coatings. Caused by the polymer softening because of the nitrogen stream, those samples sprayed with more energetic conditions led to a certain amount of titanium particles anchored into the PEEK substrate but without building-up the coating. This may be caused since the polymer cannot provide enough hardness in these spraying conditions for easing the plastic deformation of the particles at the impact. Previous to this experiments it was studied the variation of the gun velocity, which alters the period of time that the substrate is in contact with the gas stream. Thus, spraying with rapid gun velocities may not greatly affect the polymer. In any case, it was not observed the formation of the coating when comparing the distinct stand-off distances of those conditions with higher pressures (C295 and C300). On the other hand, reducing these variables would avoid the softening of the polymer, which leads to an increase in the plastic deformation of the titanium particles at the impact. Therefore, the sample C297 that was obtained by the lower-energetic spraying conditions was satisfactorily adhered to the substrate reaching thicknesses above 1000 μm. It is also possible to observe that the superior part of the coating has certain porosity, whereas closer to PEEK the coating is denser. This is caused by the peening effect of the impacting particles in CGS. Nevertheless, when using higher temperatures and maintaining fixed this pressure, it was not possible to achieve the same thickness.

The top surface areas of both the C297 sample and the PEEK substrate are presented in Fig. 1c and d. The polymer shows a flattened surface with no irregularities. On the other hand, the CGS coating provides great roughnesses to the top layer as the last particles that reached the substrate were not so drastically deformed. This can also be checked when observing its cross-section area in Fig. 1a. Anyhow, to achieve a rough biocompatible surface is a key-point for the final application of the material because this texture enhances the biocompatibility of the implant [8].

Raman spectroscopy was used in order to determine if the PEEK localized at the area closer to the first adhered particles was affected in some way by the heat of the gas stream or by the heat of the particles (Fig. 2). Other authors have reported the PEEK Raman band as a function of its plastic deformation. It was found a shift of the peaks during the tensile deformation [9]. Although is referenced in literature and also checked in this study that the polymer PEEK typically produces a spectra dominated by fluorescence [10], this was solved using Raman radiation with a wavelength of 1060 nm. The comparison of both spectra shows no differences, which suggests that the polymer was not severely affected in the coating process. Fig. 3 was carried out on the top

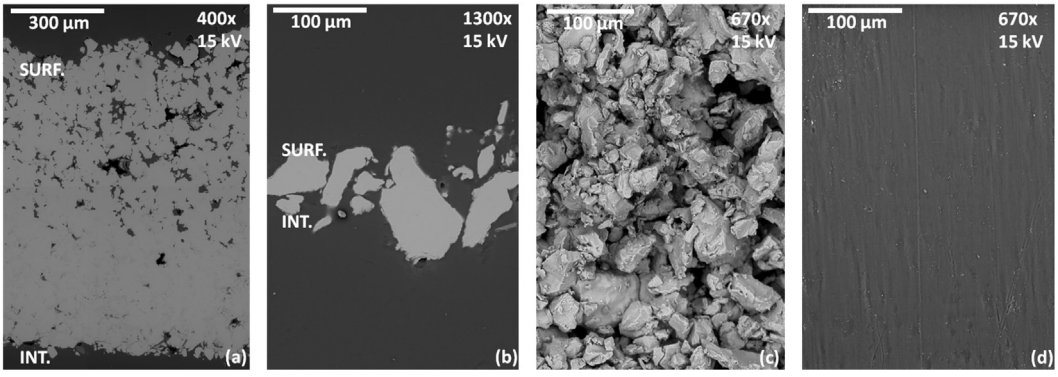

Fig. 1. SEM micrographs. Cross-section area of the samples: (a) C297 and (b) C295. Top surface area of the samples: (c) C295 and (d) PEEK polymer. Surface of the coating and interface are also detailed in samples C297 and C295 (1(a) and (b)).

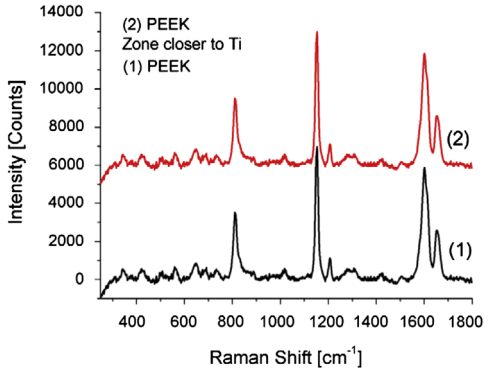

Fig. 2. Raman spectra obtained from PEEK (bulk) and a zone of PEEK substrate close to the Ti particles at the substrate boundary (CGS sample).

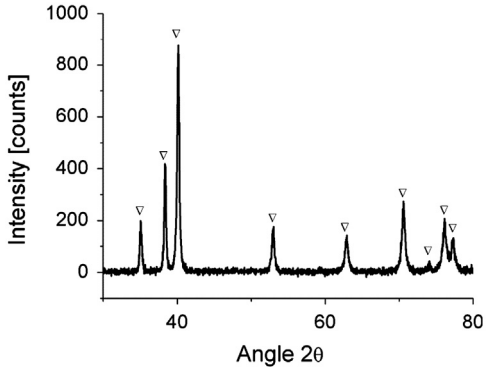

Fig. 3. XRD pattern of the sample C297.

surface of the coating and it was found that its composition consists in crystalline metallic Ti without presence of other species/undesired phases [11].

4. Conclusions

Thick, homogeneous and well-adhered titanium coatings were deposited on Polyetheretherketone (PEEK) polymer by Cold Gas Spray. From the proposed factorial design of experiments, it is concluded that the heat supplied by the gas stream softens the substrate. This fact critically influences the deposition of the metallic particles and the formation of the coating. However, it is possible to reach a balance between thermal softening of the polymer material and plastic deformation of the titanium particles at the impact in order to build-up the coating. It was not observed a shift in the Raman spectrum of the PEEK bulk compared to a PEEK area closer to the first adhered particles, which suggests that the starting polymer has not been degraded. Furthermore, composition of the metallic powder was not affected.

Acknowledgments

The authors wish to thank the Generalitat de Catalunya for the financial support for this Research Project 2009 SGR 00390.

References

[1] Toth JM. Biocompatibility of polyaryletheretherketone polymers. In: Kurtz SM, editor. PEEK biomaterials handbook. William Andrew, Waltham, USA; 2011. p. 81.
[2] Lupoi R, O'Neill W. Surface and Coatings Technology 2010;205:2173.
[3] Zhou XL, Chen AF, Liu JC, Wu XK, Zhang JS. Surface and Coatings Technology 2011;206:136.
[4] Ganesan A, Affi J, Yamada M, Fukumoto. M. Surface and Coatings Technology 2012;207:269.
[5] King PC, Poole AJ, Horne S, de Nys R, Gulizia S, Jahedi MZ. Surface and Coatings Technology 2012. http://dx.doi.org/10.1016/j.surfcoat.2012.11.023.
[6] Burlacov I, Jirkovsky J, Kavan L, Ballhorn R, Heimann RB. Surface and Coatings Technology 2012;207:269.
[7] Sanpo N, Tan ML, Cheang P, Khor. KA. Journal of Thermal Spray Technology 2009;18:10.
[8] Hossain MM, Gao W. Trends in Biomaterials and Artificial Organs 2008;22 (3):144.
[9] Kong K, Davies RJ, Young RJ, Eichhorn SJ. Macromolecules 2008;41:7519.
[10] Young RJ, Day RJ, Zakikhani M, Robinson IM. Composites Science and Technology 1989;34:243.
[11] Wood RM. Proceedings of the Physical Society 1962;80:783.

b) Paper 10:

M. Gardon, H. Melero, S. Dosta, J. M. Guilemany. Enhancing the biocactivity of polymeric implants by means of Cold Gas Spray coatings.

The deposition of nano-TiO_2 by CGS on PEEK is explained in this study. Besides, biological performance of PEEK, CGS Ti layers and CGS nano-TiO_2 coatings is also reported; assays of cell adhesion, proliferation and differentiation were carried out.

Enhancing the bioactivity of polymeric implants by means of Cold Gas Spray coatings

M. Gardon[1], H. Melero[1, 2], N. Garcia-Giralt[2], S. Dosta[1], J. Fernández[1], J.M.Guilemany[1]

[1]Thermal Spray Centre, CPT, University of Barcelona. Martí i Franquès, 1, 08028 Barcelona, Spain. Contact details: mgardon@cptub.eu - (0034) 634538544

[2]URFOA, IMIM (Institut Hospital del Mar d'Investigacions Mèdiques), RETICEF. Doctor Aiguader, 80, 08003 Barcelona, Spain

Abstract

Nanostructured anatase coatings were built-up on biocompatible Polyetheretherketone (PEEK) by means of Cold Gas Spray. Titanium layer was previously desposited, which acted as bond coat between PEEK and metal oxide. Semi-crystalline polymer was not degraded during the spraying process and starting composition of titanium dioxide was not affected. TiO_2 was homogeneously obtained onto CGS Ti layer and completely covered the piece. Primary human osteoblasts were seeded onto biomaterials and *in vitro* cell experiments provided evidence to confirm that nanostructured anatase coatings deposited by Cold Gas Spray improve the performance of PEEK implants.

Keywords: Cold Gas Spray, Nanostructure, Titanium Dioxide, Titanium, Polymer, Implant.

1 Introduction

Mechanical properties of Polyetheretherketone (PEEK) provide enough bone-like stiffness, fatigue and chemical resistance for being an excellent choice as bone tissue substitute in the biomedical field [1,2]. Therefore, it has gained much attention in those orthopedic applications where severe load-bearing behaviour is imperative [3-5]. Nevertheless, it is also attributed limited bioactivity to this material; harsh opposition to allow protein adsorption or promote cell adhesion has been found [6,7].

Attempts for improving its bioactivity have been carried out by many authors through distinct routes and materials [8-10]. Rapid manufacturing processes that could enhance the biological response of PEEK surfaces are urgently welcomed and promoted. In this line, Thermal Spray techniques have been historically contributing to the state-of-the-art offering high-performance coatings by means of titanium dioxide feedstock. Initial works involved hydroxiapatite (HA) + TiO_2 layers which were obtained by Atmospheric Plasma Spray (APS) and High-Velocity-Oxygen-Fuel Spray (HVOF) [11-14]. In these cases, plasma jet and combustion flame propelled ceramic particles towards a substrate and were bonded due its total or partial melting. Obtained results in both technologies demonstrated superior mechanical properties. TiO_2 decreased mismatch of thermal expansion between coating and substrate. Besides, it acted as obstacle for micro-cracking propagation induced by stress. Conversely, HA was in command to favour the biocompatibility of the system. In a further work, nanostructured titanium dioxide layers were successfully deposited using HVOF and applied as implants [15]. Enlarge the specific surface of titanium dioxide by means of nanostructured grains improves protein adsorption, which leads to increased adhesion of the osteoblasts. Thus, satisfactory results related to cell proliferation were attributed to nanoroughness of the metal oxide. At this point titanium dioxide was not behaving anymore as passive material being attractive because of the contribution of its mechanical properties, but was playing a

functional task due to its role in the interaction with proteins. In any case, temperature involved in above mentioned processes could increase the grain size of TiO_2 and would reduce specific surface of the solid for finally decreasing adsorption of organic molecules on the implant surface.

On the other hand, Cold Gas Spray (CGS) accelerates feedstock powder by means of nitrogen stream and does not require temperature for building-up the coatings, which could assure a higher amount of low-sized TiO_2 grains [16]. Thus, deposit homogeneous nanostructured TiO_2 layers by CGS would improve the final performance of PEEK implants. Nevertheless, it is not so straightforward to develop a continuous layer of hard and fragile TiO_2 due to the impossibility of ceramic particles to deform plastically at the impact, which is the main bonding mechanism in CGS for building-up metallic coatings. With the purpose of solving this issue, it was used anatase powder in this work designed to create chemical bonds with the substrate and among particles at the impact easing the development of the coating [17].

2 Material and methods

2.1 Coating development and characterization

Titanium powder obtained from a fused and crushed process was used as feedstock. The CGS equipment used for obtaining the coatings was a KINETICS® 4000 (Cold Gas Technology, Ampfing, Germany), with a maximum operating pressure of 40 bar, temperature of 800 °C and it operated with nitrogen as the propellant gas. In addition, KINETICS® 4000 had the possibility of using a pre-chamber of 120 mm in length connected to the nozzle of the gun where powders are heated up for a longer time. Powder and cross-section area of the samples were observed by Scanning Electron Microscopy, SEM (ProX Phenom). The phase composition of the substrate and coatings was analyzed by a X'Pert PRO MPD diffractometer (PANalytical). Roughness was analyzed using a profilometer SJ-210 (Mitutoyo).

2.2 Cell culture

Human Osteoblastic cells were obtained from trabecular bone dissected after knee replacement according to the protocol described by M. Nacher et al. [18]. The study was conducted in accordance with the 1975 Declaration of Helsinki, as revised in 1983, and approved by our local Ethics Committee. All patients submitted written informed consent before their inclusion in the study. Tested samples were placed on a 24-well polystyrene culture plate (Nunc A/S) containing Dulbecco's modified Eagle's medium (DMEM) containing 4.5 g/L glucose and supplemented with 10% FBS, pyruvate (1 mM), glutamine (2 mM), penicillin (100 UI/mL), streptomycin (100 UI/mL) and ascorbic acid (100 mg/ml) (Invitrogen), and seeded with 10000 cells/sample for viability and proliferation studies and 20000 cells/sample for differentiation studies. Three materials were tested: i) PEEK; ii) CGS Ti coating and; iii) CGS nano-TiO_2 coating. Next day after seeding, specimens were changed to a new well in order to discard non-adhered cells. Cell assays were carried out for 7 samples per case after 1, 3 and 7 days of culture. Seeded surfaces were also observed by SEM at different times of culture after cell fixation by glutaraldehyde diluted in cacodylate buffer, then critical point drying. Negative controls (materials without cells) and positive controls (cells seeded directly on PS) were employed.

2.3 Cell adhesion and viability assay

Live cells reduce water-soluble yellow coloured 3-(4,5-dimethylthiazol-2-yl)-2,5-diphenyltetrazoliumbromide (MTT) to a water-insoluble purple coloured formazan product [19]. To analyze cell viability following this principle, a MTT colorimetric assay kit (Roche Diagnostics GmbH) was employed, which solubilises the crystals before the measurement in a scanning multi-well spectrophotometer (ELISA reader) at 550 nm (reference wavelength > 650nm).

2.4 Cell proliferation assay

The 5-bromo-2'-deoxyuridine (BrdU) incorporated into cellular DNA during cell proliferation is detected using a peroxidase-conjugated anti-BrdU antibody A BrdU colorimetric immunoassay kit (Roche Diagnostics GmbH) was employed according to the manufacturer instructions. The reaction product was quantified by measuring the absorbance using a scanning multi-well spectrophotometer (ELISA reader) at 450 nm (reference wavelength of 690 nm).

2.5 Cell differentiation

Differentiated osteoblasts secrete alkaline phosphatase (ALP), which catalyses the hydrolysis of p-nitrophenyl phosphate liberating p-nitrophenol and phosphate developing a characteristic yellow color. ALP activity was measured using an Abcam's Alkaline Phosphatase Assay Kit, and the resulting absorbance was also measured using a scanning multi-well spectrophotometer, at 405nm.

2.6 Statistical analyses

Wilcoxon test was used in order to compare MTT, BrdU and ALP results among tested specimens. Significant p values <0.05 are considered significant.

3 Results and Discussion

3.1 Coating development

Cold Gas Spray may be used for embedding bioactive ceramic particles on a polymeric substrate for its application as implant [20]. However, it is quite complex to develop homogeneous covering

based on this kind of feedstock. Breakdown of the fragile particles at the impact leads to considerable difficulties for building-up of the coating. Recent endeavour provided by TS professionals have led to metal oxide powders able to be deposited by CGS due to its capacity of interacting chemically with the substrate. Therefore, anatase powder designed with this purpose was used in this survey. Figure 1 and 2 show its particle size distribution and also details TEM micrographs; average crystallite size was ranged between 20 and 100 nm. Different spraying conditions were tested in order to study the influence of particle velocity and temperature with the polymer through variation of pressure and temperature of nitrogen stream. Nevertheless, unsatisfactory results were obtained. When operating under less energetic conditions, nanostructured anatase particles did not reach enough velocity for embedding mechanically onto the ductile surface of PEEK. Although ease plastic deformation of the substrate by means of thermal softening is a common procedure selected in CGS, the authors did not provide temperature to the polymer in order to avoid changes in the chemical composition of PEEK. Higher energetic conditions were also tested via increasing gradually pressure and temperature of the propelling gas. Nonetheless, TiO_2 particles were slightly introduced into the surface with low anchoring and poor adhesion.

In a previous work, CGS Ti coatings were successfully deposited onto PEEK [21]. Metallic layers were properly bonded obtaining thickness above 1,2 millimeters. Besides, micro-Raman spectroscopy confirmed that the polymer was not degraded during the process due to the low temperatures involved. In this study, it was used this Ti layer as bond coat for depositing nanostructured anatase by means of Ti particles ranging -90+20 µm (figure 1). Metallic lower coating could provide hardness, surface geometry and chemical composition for easing the adhesion of nano-TiO_2 particles [22]. In this case, 2^2 factorial design of experiments was purposed in order to study the influence of gun velocity (v_g)/stand-off distance (d_s) and pressure/temperature ratio. Table 1 summarizes the spraying conditions.

Certain operation parameters provided the adequate balance for adhering nanostructured particles onto titanium (Conditions C353). Neither temperature nor stand-off distance had a deep effect on the coating development in the studied range. On the other hand, pressure critically influenced the deposition of the particles. First, it was possible to observe during the spraying that nano-TiO_2 was getting adhered as long as the gun advanced. However, higher pressures gave counterproductive results; previously bonded particles were detached when the nozzle sprayed material closer to an already coated area. Similar consequence was obtained when altering gun velocity. Slower gun velocities increased the number of impacting particles in a given time, which results to initial adhesion of TiO_2 and its immediate posterior detachment because of the eroding effect caused by *secondary* impinging particles. Finally, either pressure or gun velocity were adjusted for effectively bonding anatase. Figure 3 shows cross-section micrographs of both coatings (3.a, 3.c), each interface is detailed (3.b, 3.d); both layers are homogeneous and well bonded. Nanotexture of anatase coating adhered onto irregular titanium, where nanostructured metal oxide particles are properly bonded on the rough surface of the CGS Ti layer. It was found a complete coverage of valleys and holes developed by non-dramatically deformed titanium particles impigning at the top surface of the bond coat. Both rough surfaces are shown in figure 4. As regards to surface was almost completely flat, presenting a roughness value of 0,5±0,1 µm. CGS Ti layers presented an irregular surface with sharp peaks whose rougness was 22,6±3,6 µm and CGS nano-TiO_2 eased off the pointed profile of the metallic coating leading to a value of 17,9±1,0 µm.

Figure 5 represents phase composition (XRD) of PEEK substrate, CGS Ti layer and CGS nano-TiO_2 coating. It is possible to observe that all materials did not have the presence of impurities or undesired phase transformations.

3.2 Biological response

3.2.1 Cell viability

Results at the first day of culture regarding cell adhesion showed the same performance either for bulk polymer or both CGS coating materials (Figure 6). However, titanium layer and nanostructured titanium dioxide coating doubled cell viability of PEEK after 7 days. No significant differences could be observed when comparing metal and metal oxide. Capacity of cells to get adhered on a surface is determined by the adsorption of proteins that are present on the extracellular matrix (ECM) [23]. Surface stability provided by crystallographic planes of TiO_2, commonly used in catalysis, may provide an ideal scenario for boosting desired pre-adsorption of organic molecules. Nevertheless, cell adhesion in nanostructured anatase did not increase compared to titanium. Some authors have reported that Ti biocompatibility is given by thin titanium dioxide layer formed at the top surface of metallic grains [24,25]. Therefore, lack of difference observed between CGS coatings in this assay may be determined by co-existence of the above mentioned metal oxide monolayer in both materials, which would be in charge of equalizing the adsorption of proteins. The increase of MTT results at 7 days of CGS Ti and CGS nano-TiO_2 are attributed to increased proliferation in this specimens compared to PEEK but it not reach to control results.

3.2.2 Cell proliferation

Nanostructured TiO_2 coatings had a slight proliferation increase on day 1 and 3 (Figure 7). As MTT results, both titanium and titanium dioxide showed superior performance on the seventh day compared to PEEK but less than control samples. Proliferation may be stimulated up to a certain value as long as roughness increases in Ti surfaces [26]. Thus, differences in surface geometry between titanium and anatase could explain our results both cell adhesion/viability and proliferation. These results corroborate the MTT measurements suggesting clearly a high performance of Ti materials.

3.2.2 Cell differentiation

Alcaline phosphatase is highly expressed in differentiated osteoblasts and is currenly used as a marker of differentiation status. CGS nano-TiO_2 showed a superior capacity of differentiating cells from third day of culture (figure 8) compared to other materials tested. At 7 days of culture, TiO_2 coatings had similar behaviour than control cultures. In contrast, titanium layers showed the worsts results. Last analysis revealed that nanostructured metal oxide coating had an excellent ability in cell differentiation, obtaining one order of magnitude above the value of PEEK.

These results give evidence that surface roughness provided by nanostructured scaffolds may also have a crucial role in the interaction between cells and solid substrates [27]. Nanotextures at the surface of the coating resembled the nanoarchitecture of natural ECM, which may facilitate differentiation. Besides, other authors have reported that TiO2 coatings with nanometer thickness enhance the biological response of microroughened titanium surfaces in terms of cell differentiation [28]. In this study, roughness of titanium and titanium dioxide coatings built-up by CGS were not quite dissimilar (measured values are shown in section 3.2.1). Nevertheless, it is worthy to understand the distinctiveness between microroughness and nanoroughness. Thus, superficial features of nano-TiO2 would be in charge of developing successful results in cell differentiation.

3.2.2 Cell observation

Geometry and aspect of the cells on PEEK and coating materials was studied after 1, 3 and 7 days of culture. Figure 9 shows top surface micrographs of polymer, CGS Ti and CGS nano-TiO_2 with corresponding adhered cells. In all cases, typical osteoblastic shape was observed with similar spreading among materials tested. In spite of differences in parameters such as cell adhesion, proliferation or differentiation, it was unfeasible to correlate the obtained values with scanning electron micrographs. Punctual covering was spread on the polymer, coating metal and metal oxide

without noteworthy divergences. In our materials, SEM methology is not able to detect minimal changes in cell conformation and focal adhesions between samples. However, these results corroborate that three materials are biocompatible and allow osteoblast culture.

4 Conclusions

Homogeneous nanostructured anatase coatings were applied onto biocompatible polyetheretherketone (PEEK) by Cold Gas Spray (CGS). TiO_2 particles were weakly embedded on the polymer. CGS Titanium layers were used as bond coat for for easing the adhesion of ceramic particles, which could provide a surface able to ease chemical bonding with anatase particles. CGS spraying conditions were adequately adjusted in order to improve the adhesion of nanostructured metal oxide on Ti bond coat. The polymer was not degraded during the coating process, crystalline structure of titanium was unaffected and titanium dioxide preserved its nanostructure. Biological response of the Ti surfaces was significantly better than PEEK from 3 days of culture regarding cell viability and proliferation. However, in terms of osteoblast differentiation, polymer coated with nanostructured titanium dioxide showed optimal results. Surface micro- and nanoroughness may be a significant parameter to be controlled during CGS process so as to optimize the bioactivity of these coating materials.

5 Acknowledgments.

The authors wish to thank the Generalitat de Catalunya for the financial support for this research project 2009 SGR 00390.

6 References

[1] U. Spetzger, V. Vougioukas, J. Schipper. Materials and techniques for osseous skull reconstruction. Minimally Invasive Therapy 19 (2010) pp. 110.

[2] http://www.invibio.com/ (Acessed 08/02/2013).

[3] R. K. Ponnappan, H. Serhan, B. Zarda, R. Patel, T. Albert, A. R. Vaccaro. Biomechanical evaluation and comparison of polyetheretherketone rod system to traditional titanium rod fixation. The Spine Journal 9 (2009) pp. 263.

[4] S.M. Kurtz, J.N. Devine. PEEK biomaterials in trauma, orthopedic, and spinal implants. Biomaterials 28 (2007) pp. 4845.

[5] J. M. Toth, M. Wang, B. T. Estes, J. L. Scifert, H.B. Seim III, A. S. Turner. Polyetheretherketone as a biomaterial for spinal applications. Biomaterials 27, 3 (2006) pp. 324.

[6] O. Noiset, C. Henneuse, Y.-J. Schneider, J. Marchand-Brynaert. Surface Reduction of Poly(aryl ether ether ketone) Film: UV Spectrophotometric, 3H Radiochemical, and X-ray Photoelectron Spectroscopic Assays of the Hydroxyl Functions. Macromolecules 30 (1997) pp. 540.

[7] O. Noiset, C. Henneuse, Y.-J. Schneider, J. Marchand-Brynaert. Fibronectin adsorption or/and covalent grafting on chemically modified PEEK film surfaces. Journal of Biomaterials Science, Polymer Edition, 10:6 (1999) pp. 657.

[8] M.S. Abu Bakar, M.H.W. Cheng, S.M. Tang, S.C. Yu, K. Liao, C.T. Tan, K.A. Khor, P. Chean. Tensile properties, tension–tension fatigue and biological response of polyetheretherketone–hydroxyapatite composites for load-bearing orthopedic implants. Biomaterials 24 (2003) pp. 2245.

[9] S. Ramakrishna, J. Mayer, E. Wintermantel, K. W. Leong. Biomedical applications of polymer-composite materials: a review. Composites Science and Technology 61 (2001) pp. 1189.

[10] G.L. Converse, W. Yue, R. K. Roede. Processing and tensile properties of hydroxyapatite-whisker-reinforced polyetheretherketone. Biomaterials 28, 6 (2007) pp. 927

[11] X. B. Zheng, C. X. Ding. Characterization of plasma-sprayed hydroxyapatite/TiO_2 composite coatings. Journal of Thermal Spray Technology 9, 4 (2000) pp. 520.

[12] Y.-P. Lu, M.-S. Li, S.-T. Li, Z.-G. Wang, R.-F. Zhu. Plasma-sprayed hydroxyapatite+titania composite bond coat for hydroxyapatite coating on titanium substrate. Biomaterials 25, 18 (2004) pp. 4393.

[13] M. Gaona, R.S. Lima, B.R. Marple. Nanostructured titania/hydroxyapatite composite coatings deposited by high velocity oxy-fuel (HVOF) spraying. Materials Science and Engineering: A 458, 1-2 (2007) pp. 141.

[14] H. Li, K.A. Khor, P. Cheang. Titanium dioxide reinforced hydroxyapatite coatings deposited by high velocity oxy-fuel (HVOF) spray. Biomaterials 23 (2002) pp. 85.

[15] M. Gaona, R.S. Lima, B.R. Marple. Nanostructured titania/hydroxyapatite composite coatings deposited by high velocity oxy-fuel (HVOF) spraying. Materials Science and Engineering: A 458, 1-2 (2007) pp. 141.

[16] V. Champagne. The Cold Spray Materials Deposition Process: Fundamentals and Applications. Woodhead Publishing in Materials, 2007. ISBN-10: 1420066706.

[17] M. Yamada, H. Isago, K. Shima, H. Nakano, M. Fukumoto. Deposition of TiO_2 ceramic particles on cold spray process. Intern. Thermal Spray Conf. Proceed. (2010).

[18] M. Nacher, J. Aubia, S. Serrano, M.L. Marinoso, J. Hernandez, J. Bosch, A. Diez, J.M. Puig, J. Lloveras. Effect of cyclosporine A on normal human osteoblasts in vitro. Bone Miner. 26 (1994) pp. 231.

[19] A. M. Sieuwerts, J. G. M. Klijn, H. A. Peters, J. A. Foekens. The MTT Tetrazolium Salt Assay Scrutinized: How to Use this Assay Reliably to Measure Metabolic Activity of Cell Cultures in vitro for the Assessment of Growth Characteristics, IC50-Values and Cell Survival. Eur. J. Clin. Chem. Clin. Biochem. 33 (1995) pp. 813.

[20] J. H. Lee, H. L. Jang, K. M. Lee, H.-R. Baek, K. Jin, K. S. Hong, J. H. Noh, H.-K. Lee. In vitro and in vivo evaluation of the bioactivity of hydroxyapatitecoated polyetheretherketone biocomposites created by cold spray technology. Acta Biomaterialia 9 (2013) pp. 6177.

[21] M. Gardon, A. Latorre, M. Torrell, S. Dosta, J. Fernández, J.M. Guilemany. Cold Gas Spray Titanium coatings onto a biocompatible polymer. Materials Letters (2013) DOI: 10.1016/j.matlet.2013.04.115.

[22] M. Gardon, C. Fernández-Rodríguez, M.R. Espino Estévez, S. Dosta, J. M. Guilemany. Photocatalytic nanostructured anatase coatings obtained by Cold Gas Spray. *To be published.*

[23] B. M. Gumbiner. Cell Adhesion: The Molecular Basis of Tissue Architecture and Morphogenesis. Cells 84, 3 (1996) pp. 345.

[24] Long M, Rack HJ. Titanium alloys in total joint replacement – a materials science perspective. Biomaterials 19, 18 (1998) pp.1621.

[25] Wu LN, Genge BR, Wuthier RE. Micropatterned TiO_2 effects on calcium phosphate mineralization. Mater Sci. Eng. C 29, 8 (2009) pp. 2355.

[26] K. Mustafa, A. Wennerberg, J. Wroblewski, K. Hultenby, B. S. Lopez, K. Arvidson. Determining optimal surface roughness of TiO_2 blasted titanium implant material for attachment, proliferation and differentiation of cells derived from human mandibular alveolar bone. Clin. Oral Impl. Res. 12 (2001) pp. 515.

[27] C. Zhao, A. Tan, G. Pastorin, H. K. Ho. Nanomaterial scaffolds for stem cell proliferation and differentiation in tissue engineering. Biotechnology Advances (2012) DOI: http://dx.doi.org/10.1016/j.biotechadv.2012.08.001.

[28] Y. Sugita, K. Ishizaki, F. Iwasa, T. Ueno, H. Minamikawa, M. Yamada, T. Suzuki, T. Ogawa. Effects of pico-to-nanometer-thin TiO_2 coating on the biological properties of microroughened titanium. Biomaterials 32 (2011) pp. 8374.

List of tables

Table 1. Nomenclature of the spraying conditions for the factorial design of experiments and its corresponding ratios:

		T [ºC] / P [bar]	
		15-25	**25-35**
v_g [mm/s]/ d_s [mm]	**4-8**	C350	C351
	8-12	C352	C353

List of figure captions

List of figures

Fig. 1

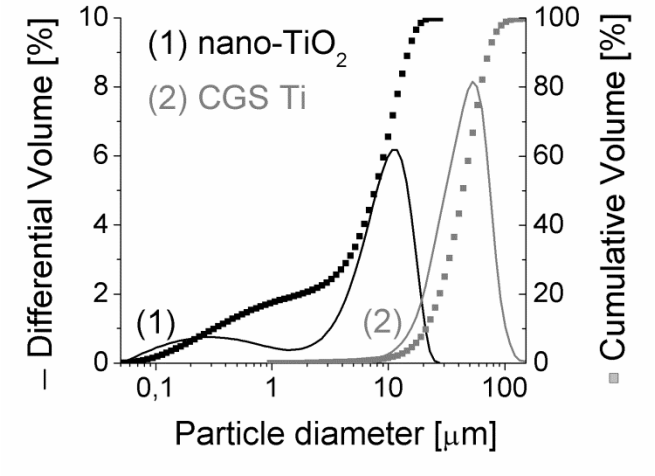

Fig. 2

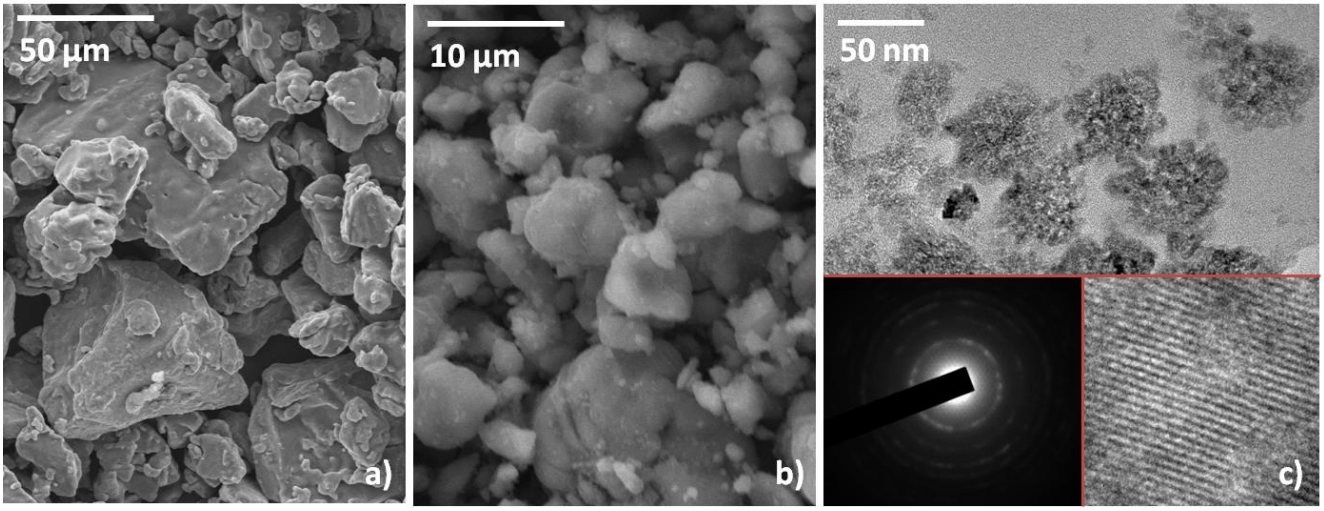

Fig. 3

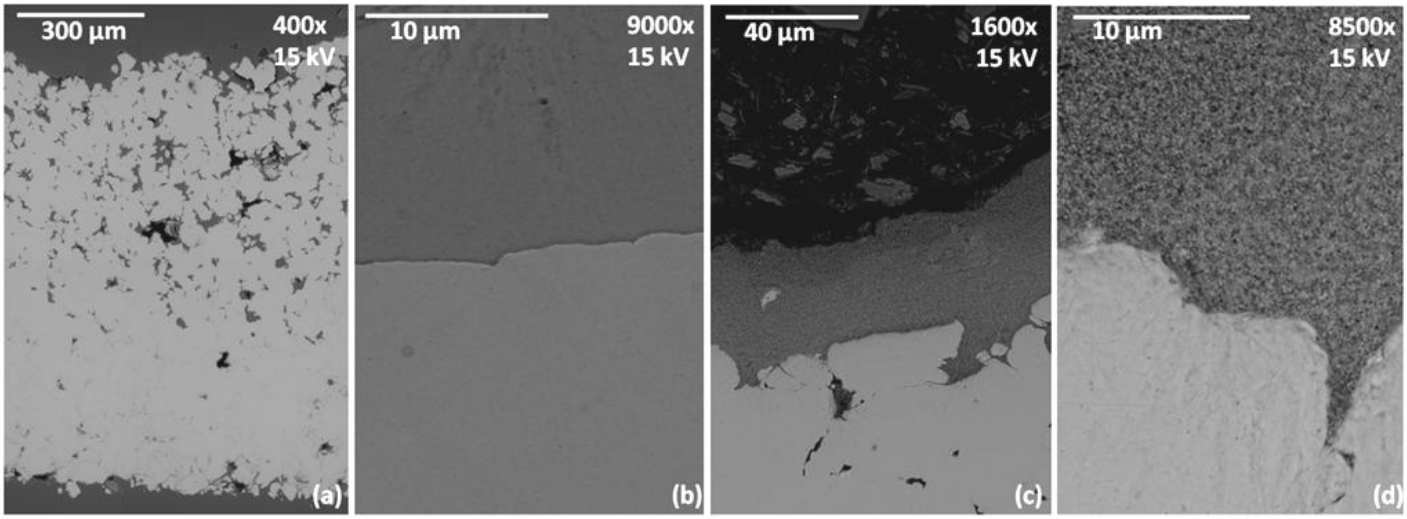
300 µm
400x
15 kV
(a)
10 µm
9000x
15 kV
(b)
40 µm
1600x
15 kV
(c)
10 µm
8500x
15 kV
(d)

Fig. 4

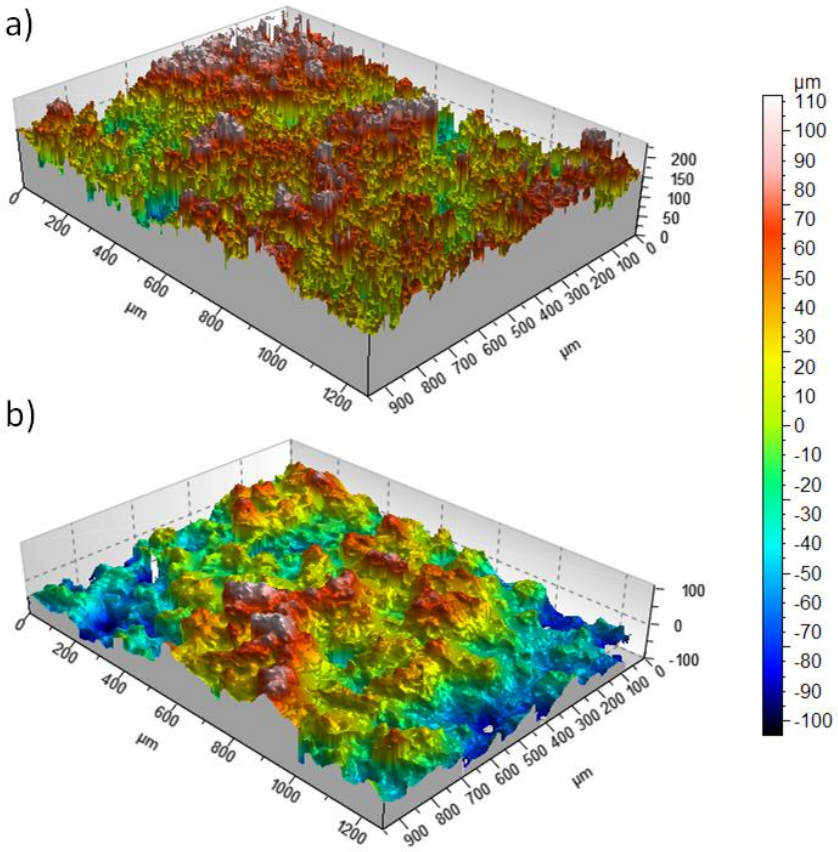
a)
b)
µm
110
100
90
80
70
60
50
40
30
20
10
0
-10
-20
-30
-40
-50
-60
-70
-80
-90
-100
200
150
100
50
0
µm
100
0
-100
µm

Fig. 5

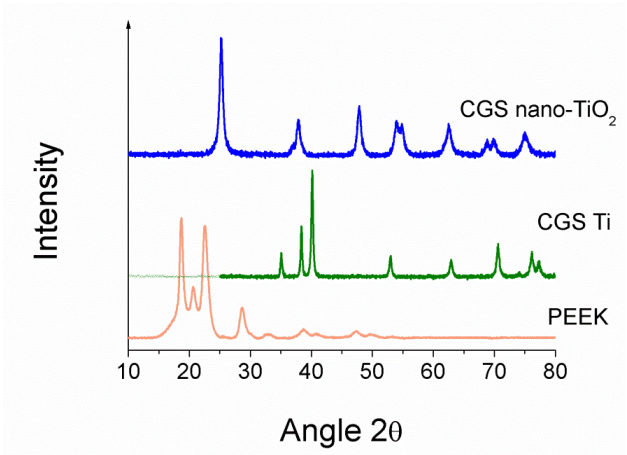
CGS nano-TiO2
CGS Ti
PEEK
Intensity
10
20
30
40
50
60
70
80
Angle 2θ

Fig. 6

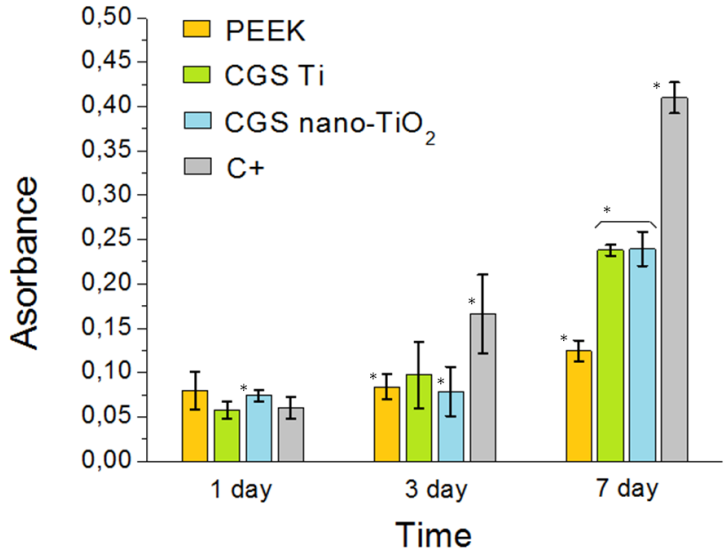
0,50
0,45
0,40
0,35
0,30
0,25
0,20
0,15
0,10
0,05
0,00
Asorbance
PEEK
CGS Ti
CGS nano-TiO2
C+
1 day
3 day
7 day
Time

Fig. 7

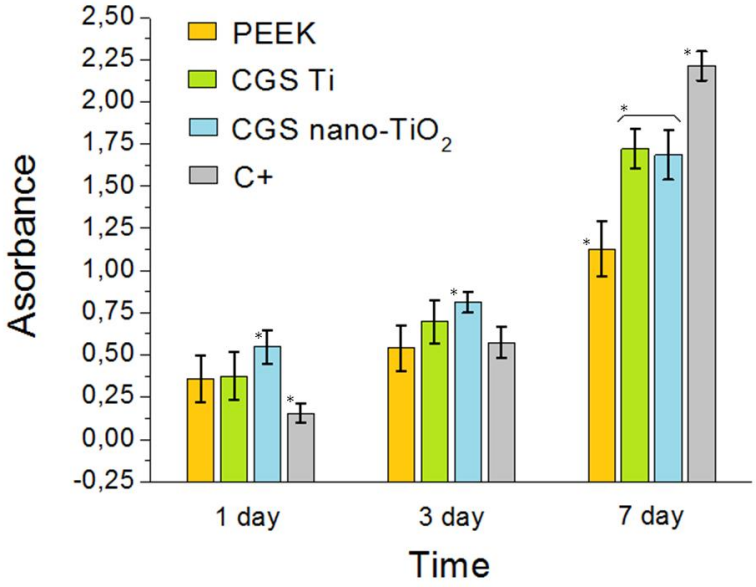
2,50
2,25
2,00
1,75
1,50
1,25
1,00
0,75
0,50
0,25
0,00
-0,25
Asorbance
PEEK
CGS Ti
CGS nano-TiO2
C+
1 day
3 day
7 day
Time

Fig. 8

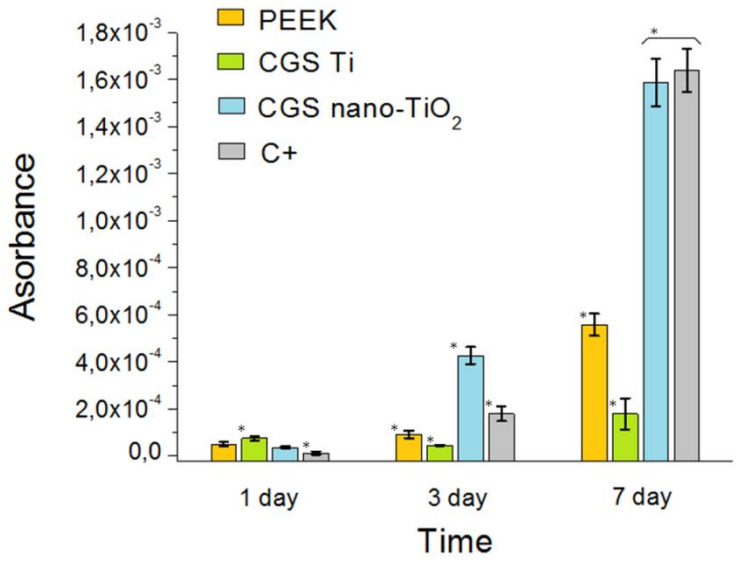
PEEK
CGS Ti
CGS nano-TiO2
C+
Asorbance
1,8x10-3
1,6x10-3
1,4x10-3
1,2x10-3
1,0x10-3
8,0x10-4
6,0x10-4
4,0x10-4
2,0x10-4
0,0
1 day
3 day
7 day
Time

Fig. 9

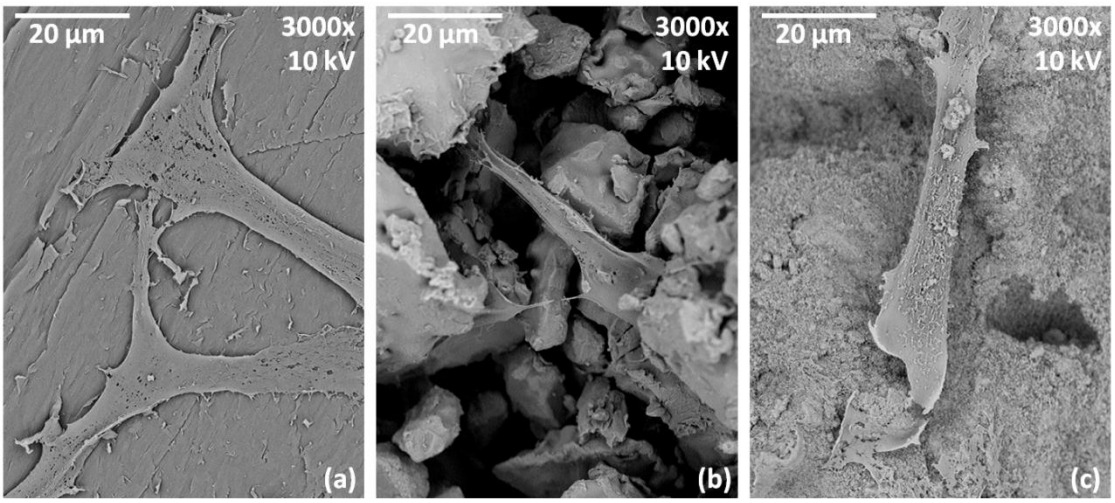
20 µm
3000x
10 kV
(a)
20 µm
3000x
10 kV
(b)
20 µm
3000x
10 kV
(c)

7. Overall discussion

The previous chapter presented the results compiled in scientific papers regarding Atmospheric Plasma Spray and Cold Gas Spray coatings using different TiO_2 feedstock. This chapter does not repeat above examined topics again in a detailed way, but looks at all the obtained coatings and tackles most relevant points and some gaps that were not properly explained in the articles. Punctual results that have not been showed before are presented here so as to support the discussion.

7.1 Starting considerations

From the general overview in Paper 1, it could be highlighted that the chief attractive of TS titanium dioxide surfaces is based on building-up photocatalytic anatase layers with large specific surfaces, which are provided by means of nanostructured feedstock. Then, make use of these layers for degrading contaminants in heterogeneous photochemical reactions. Furthermore, same material can be used as bactericide or in Dye-Sensitized-Solar-Cells. However, many disadvantages were found in its fabrication. Heat involved in conventional plasma jets and combustion flames (APS and HVOF) develops undesired phase transformations and growth in the grain size that reduces the effectiveness of the devices. On the other hand, CGS is in command to establish a new procedure for achieving large areas coated by this material. For the interests of the authors, it should be carried out more research related to the design of the powders able to be deposited by CGS and study their adhesion phenomena. Findings on this area could provide enough control for a realistic fabrication of homogeneous nanostructured anatase coatings.

*Paper 1: Milestones in functional titanium dioxide thermal spray coatings.

As regards to biomedical applications, titanium dioxide has been mainly used as a substitute of bone tissue due to its mechanical properties. Nevertheless, chemical stability and specific surface of nanostructured TiO_2 could enhance protein adsorption and cell adhesion. Therefore, new interesting lines of research could appear based on obtaining titanium dioxide coatings with low-sized grains.

Besides, oxygen vacancies in APS TiO_{2-x} coatings, which are commonly undesired, lead to layers with low electric resistivity. Electrical conducting and corrosion resistant surfaces obtained by means of low-cost process may be applied in many different devices used in electrochemistry. This property is of high significance and was decided to be exploited as well by the authors.

As regards to operation temperature, intermediate TS processes such as HVOF are not motivating because of the heat produced in the flame. Therefore, it is more appealing to work directly with CGS in spite of the controversy that rounds powder synthesis in ceramics. Anyhow, professionals/researchers in HVOF may not discard developing functional TiO_2 coatings because of enough success has been reported after appropriately adjusting spraying parameters or even feeding the system by suspensions. HVOF may also be interesting for reaching reduced stoichiometries of titanium dioxide by means of flames powered by chemical reaction between hydrogen and oxygen. However, it seems more feasible to achieve it by APS, especially after noting the lack of publications.

Fabrication, sensing mechanisms and performance of metal oxide gas sensors were also studied. These devices are controlled by three main mechanisms: i) receptor function; ii) transducer function and iii) approachability. After analyzing these concepts it may be assured that TS technologies can supply coating materials that: i) adsorb target gas and enhance its interaction; ii) provide an adequate output signal and; iii) assure the access of the inner grains. Thus, preliminary theoretical approach confirmed that TS processes can be successfully used for depositing the active layer of metal oxide gas sensors

Nevertheless, a huge question rises from the overviewed references in this article: is it really interesting to base a PhD on the development of TiO_2 active layers for its application as gas sensors by means of Thermal Spray? If the key point of TS technologies is the capacity of coating large areas in a rapid

manufacturing procedure with a low cost associated, does this topic take profit of it if small areas should be coated? Here, it is not being questioned that if successful it would contribute to the state-of-the-art and even commercially compete with established standards when a considerable number of devices must be fabricated, but if functional TS TiO_2 coatings have its best application as gas sensors instead of other interesting possibilities that could be reached during the way. In this sense, investigate other feasible applications became accepted. Thus, the thesis was open to other interesting paths and goals such as electrodes, photocatalysts and implants and its development would depend on the obtained results.

7.2 Atmospheric Plasma Spray

7.2.1 Electrodes

a) Coating development

- Ceramic tile substrates:

Reduced stoichiometries of Ti-O system are industrially obtained by means of heating titanium dioxide in a reducing atmosphere granted by the presence of gaseous H_2 , which partially transform Ti^{4+} to Ti^{3+} under reaction 1 [12]:

$4TiO_2 + H_2 \leftrightarrow Ti_4O_7 + H_2O$ Reac. 1

Consequently, it does seem reasonable to get profit of H_2 involved in the plasma jet of APS for reaching titanium sub-oxides and Magnéli phases as coatings (Paper 3).

*Paper 3: The influence of titanium sub-oxides in thermal sprayed coatings.

However, before trying to understand the correlation of hydrogen and titanium dioxide during the coating process, it must be explained if the coating can be deposited without cracks and delamination. First, ceramic tiles were used as substrates. Despite CTE mismatch among ceramics should not be very pointed, it was a worrying parameter. Each gun pass provided enough thermal effect for developing certain expansion and contraction to solid materials, which was also powered when various cycles were carried out. Besides, as long as the spraying process advanced and thickness increased, difference in the expansion and contraction between tile and APS TiO_{2-x} coating was enhanced, which led to higher residual stress accumulated. Then, this energy was freed in form of cracks. Thus, any experimental procedure in APS that could contribute in minimizing the accumulation of stress was gratefully accepted.

It was found in literature that a standard plasma mixture can decrease from 10.000º C in the electric arc (where the plasma is formed) to 2.000º C in 100 mm [7]. Plasma species are recombined forming gaseous species and rapidly lose energy, namely, temperature decreases. Then, samples were placed at larger stand-off distances. Transfer of energy from the plasma towards the feedstock was lower and temperature of TiO_2 in-flight particles decreased. In this sense, enlarge stand-off distances decreased particle temperatures, which was correlated by means of its accurate measurement using Spraywatch® equipment.

Large stand-off distances led to not-so-aggressive thermal cycles and CTE mismatch gradually decreased. This was clearly visible when studying the number of vertical cracks in the cross-section area of the coatings. Besides this, poor adhesion and even total decohesion was also mitigated. XRD was used for analyzing phase composition of two samples obtained by means of same spraying parameters (Appendix – Table 1) but with different stand-off distances. It was expected that the considerable amount of hydrogen used in this conditions could favour the formation of oxygen vacancies when increasing the residence of TiO_2 particles in the reducing atmosphere. However, exactly the same composition was found. From this, it could be understood that, at least in these range of operation, it was not possible to increase the amount of oxygen

vacancies in titanium dioxide coatings by means of enlarging stand-off distances.

With the purpose of providing less temperature to the substrate, it was necessary to find some other path in APS that could reduce the energetic conditions of the process. Figures 3, 4 and equations 1-5 (section 4.1.1) correlate plasma temperature with: i) arc current intensity (Ar/H_2) and; ii) composition of the starting mixture. Equations and graphics helped to deduce that an increase in the plasma intensity (amperage) would boost the power of plasma. Then, if specific enthalpy of the formed plasma was enhanced, the temperature of the jet would have increased. Following this statement it was decided to reduce plasma intensity in order to develop lower energetic conditions, which could lead to coatings with less stress, less cracks and lower electric resistivity. It was found that number of cracks and resistivity decreased when plasma intensity was reduced, proving the importance of specific enthalpy of the plasma.

The effect of the mixture of argon and hydrogen was also studied. It was carried out a stepped decrease in the amount of hydrogen maintaining constant argon flow. Table 4 in Appendix shows the jet temperatures associated to this experiment. It was possible to observe that plasma temperature increased as long as hydrogen decreased. This could be highly undesirable due to it would be counterproductive. However, argon has a lower coefficient of thermal convection compared to hydrogen. Thus, plasma with higher temperature was obtained but also had lower capacity of transferring this energy to the particles. Measurements of particle temperature revealed that this value was reduced significantly. Besides, number of vertical cracks in its cross-section area of the coatings was also reduced to zero. Nevertheless, electric resistivity increased. This was attributed to certain loss of oxygen vacancies caused by jet flame with lower amount of reducing hydrogen. XRD analyses were carried out to both samples obtained with different Ar/H_2 ratio. However, this technique did not provide differences between both samples. Lack of information related to oxygen vacancies became present and techniques such as XPS, DRX or EDS may not provide accurate measurements for discriminating differences in APS TiO_{2-x} coatings.

Micro-hardness of these coating materials was around 11,5 GPa. No significant differences were observed when comparing hardness of samples obtained by distinct spraying conditions. However, large standard deviation was obtained for thermally-aggressive conditions. This could be attributed to combination of denser areas (particles more molten) that provided harder values and spots in presence of cracks, which reduced the hardness.

- Stainless steel substrates:

Metallic electrodes such as stainless steel are commonly used in batteries. For this reason, it was necessary to transfer all the findings previously explained to these substrates (Paper 4). In this case, CTE mismatch was much more worrying. Transfer of heat to crystal lattice of steel increases the distance among atoms due to its vibration movement, which leads to a considerable expansion of the material. Covalent or ionic bonding in ceramics does not permit same vibration, namely expansion, than the one occurred in metals and excessive energy leads to cracks because of non-accumulated stress. Therefore, different expansion and contraction by part of distinct materials in the interface is the source of crack propagation and decohesion of the coating.

In order to solve this, it was decided to use nitrogen cooling. Although this procedure could be selected from the beginning of the study, it was preferred not to use this solution in order to avoid rise in the cost of the experimental procedure. Samples were placed on a circular plate, which turned during the coating process. Stream of cold N_2 gas was directed to the substrates so as to avoid interacting with the plasma jet. The final result consisted on maintaining the steel substrate to a lower constant temperature, which reduced its expansion and contraction. In addition, feed rate was increased. It was supposed that the *load effect* reduced heat transfer from the hot plasma to the particles [7]; larger quantities of particles may cool down the jet. After applying these two actions, APS TiO_{2-x} coatings were successfully achieved on stainless steel substrates of 50x20x5mm without showing cracks or partial decohesion.

*Paper 4: Improved, high conductivity titanium sub-oxide coated electrodes obtained by Atmospheric Plasma Spray.

Performance of an electrode is highly dependent on its mechanical properties. Hardness value was increased from 7,50 to 8,70 GPa as long as thickness rose from 49 to 247 microns. Indentations were carried out on the cross-section area of the coating. Thus, obtained values could be influenced by mounting resin when coatings with lower thickness were studied. Besides, these values are slightly below than the obtained on ceramic tiles. Present spraying conditions were supposed to reduce particle temperature. Then, some non-melted micro-zones could coexist in the coating and generation of these heterogeneities may affect to overall microhardness value. Bonding strength had a maximum value for the thinnest film, which was attributed to weaker cohesion between layers when thickness was increased; stress and microcracks could increase when number of cycles was higher.

- Common electrode materials as substrates:

Thin stainless steel and aluminium films, carbon-polymer composites and nickel foams have more interest because are usually applied in these devices. Thus, the efforts were focused on achieving electrical conducting and well-bonded APS TiO_{2-x} coatings onto the distinct electrode materials (Paper 5). Starting trials were focused on 1 mm-thick stainless steel films. Spraying conditions were acquired from parameters used in stainless steel thick substrates but without nitrogen in order to save this resource. First trials built-up the coating but completely detached the layer from the substrate surface, which was attributed to lack of roughness. Smooth surfaces have less anchoring points for favouring adhesion of impacting molten particles. Therefore, surface roughness was increased by means of grit-blasting process and was determining for easing the adhesion of TiO_2 particles. Spraying process was repeated and visually the coating was adhered. Nonetheless, once again heat supplied by plasma jet and impacting particles was excessive and led to vertical cracks and partial decohesion.

*Paper 5: Enhanced performance of common electrode materials by means of Thermal Spray coatings.

It was decided to enlarge more the stand-off distance of the samples. Table 6 in Appendix summarizes the data. Besides, cooling nitrogen was used again. In this case, coatings were properly built-up but their thickness was slightly decreased. This dropping may not be significant at first sight, but it was informing of a decrease in the efficiency of the process. Particles were arriving less melted; its capacity of damaging the already formed coating was reduced, which led to well-bonded and free-of-crack layers. Nevertheless, fewer particles were getting adhered. Although detailed economical considerations are not considered in this thesis, the idea of reaching cost-effective products has been always present and non-profitable industrial applications were not being considered during the research. In this way, increase stand-off distance so as to reduce CTE mismatch may be carefully selected as the standard procedure because part of the powder is being lost in the process. Same conditions were applied to aluminium films and coatings were also adequately obtained.

Carbon-polymer composites had a granular structure with relative poor compaction due to the process of fabrication, which made truly difficult to increase their roughness by erosion of impinging alumina particles (figure 16). Substrates were broken during grit-blasting and it was necessary to reduce the pressure of the air stream and separate as much as possible the piece from the nozzle. Besides, the composites were tilted so as to avoid the accumulation of stress. It must be said that substrates must be cautiously fixed on the supports. Its fragility is so pronounced that the pieces were easily broken if the washers were hardly squeezed. As regards to coating development, starting high energetic conditions completely damaged the substrate. Molten particles eroded the composite and the accumulated stress on the squeezed area broken the sample. As long as stand-off distance increased, the erosion was reduced and proper adhesion of the particles was observed. For larger distances, substrate was not broken in the subjected area closer to the washers and coating was successfully deposited. Again, low energetic conditions appropriately coated the substrates.

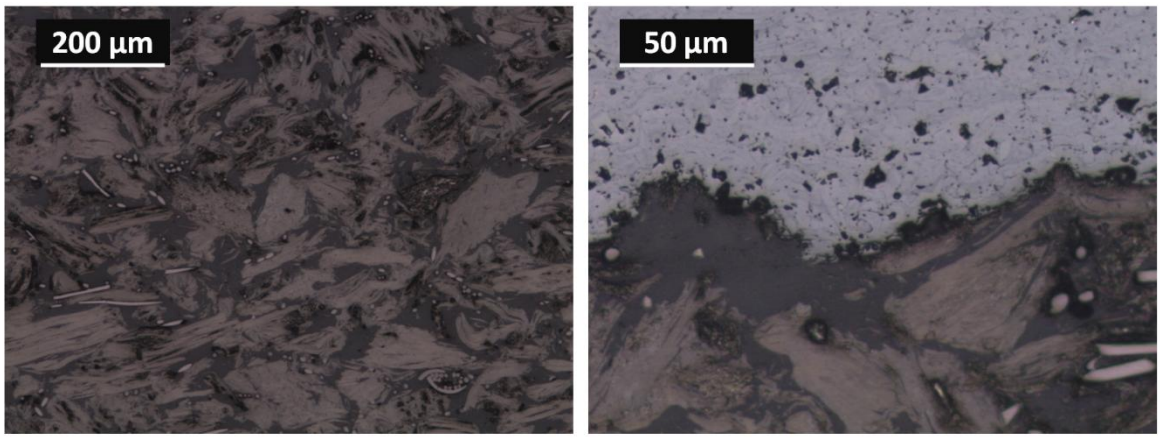

Figure 16. Left: granular structure of carbon-polymer composite. Right: interface coating/substrate.

Ni foams were directly sprayed without any previous surface treatment, except standard ultrasonic cleaning with acetone. When washers used in the subjection were too tightened during the coating process, foams were also damaged due to its delicate nature (figure 17). Therefore, it was required to squeeze the washers sufficiently for having an adequate subjection but not enough for damaging the foam. High energetic starting conditions completely destroyed the substrate. Again, stand-off distance diminished thermal effect of jet and particles leading to well-bonded coatings on the foam. It was supposed that melted particles shocked against the filaments and could be divided in smaller droplets and deviated in many directions. Then, smaller droplets would solidify on the lateral walls of the filaments. This made possible to coat both sides of the filament that were parallel to the starting trajectory of the particles. After that, semi-coated foam was turned in order to coat the backside of the substrate. Finally, complete 3-dimension covering was obtained.

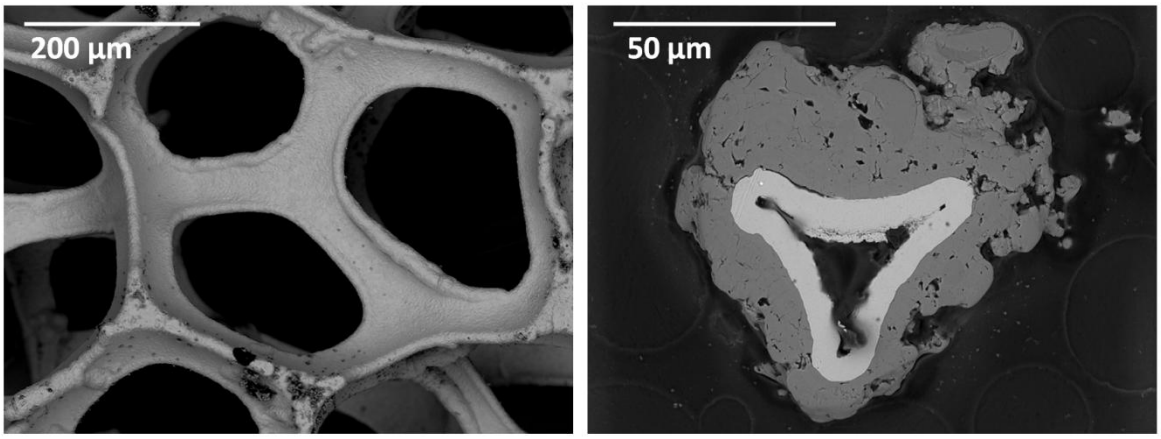

Figure 17. Left: thin filaments of Ni foam network. Right: 3-dimensionally coated filaments.

b) Key-properties evaluation

The interest of APS TiO_{2-x} coatings in electrochemical applications is their intrinsic chemical stability and low electric resistance. Then, electrical resistivity was of special concern. This value was continuously studied and optimized with the aim of enhancing the electrochemical process where the material would be functionally applied. In this way, electric resistivity of the coatings deposited onto the different substrates studied from Paper 3, 4 and 5 is summarized in figure 18. It may be taken into account that decrease of the resistivity when comparing coated materials was not entirely attributed to physical and microstructural features of the coatings (e.g. oxygen vacancies, cracks, porosity). Resistivity was enhanced depending on the electrical properties of the substrate.

*Paper 3: The influence of titanium sub-oxides in thermal sprayed coatings.
Paper 4: Improved, high conductivity titanium sub-oxide coated electrodes obtained by Atmospheric Plasma Spray.
Paper 5: Enhanced performance of common electrode materials by means of Thermal Spray coatings.

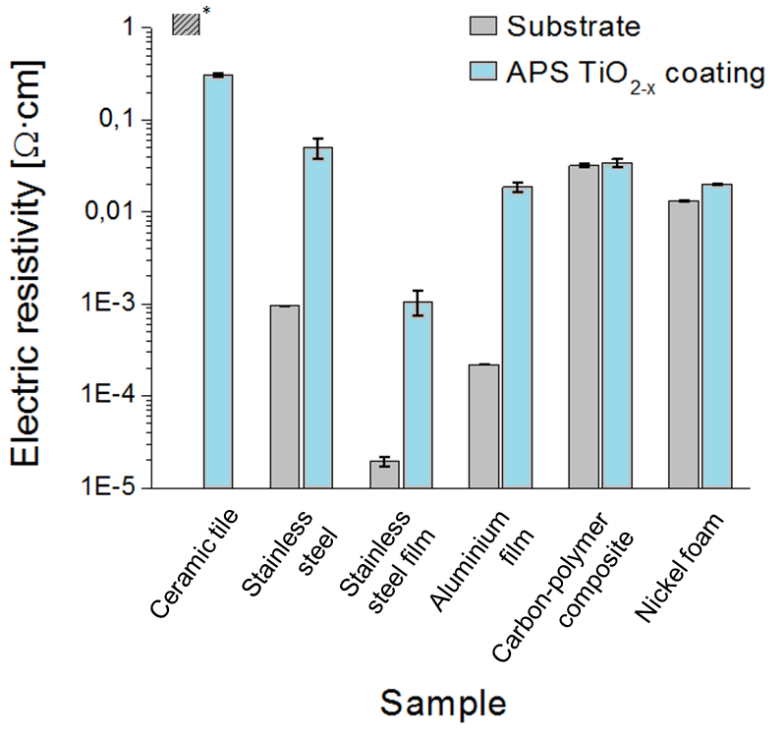

Figure 18. Electric resistivity of different electrode materials and APS TiO_{2-x} coatings (*resistivity of ceramic tile was out of range).

Within the studied ranges of operation, it can be stated that electrical resistivity of APS TiO_{2-x} coatings was decreased when plasma intensity and particle temperature were reduced. Furthermore, larger stand-off distances and feed rates had also the capacity of achieving samples with lower electrical resistivity. This general behaviour was attributed to the fact of achieving lower energetic conditions. When this situation was reached, stress accumulated in the coating-substrate system was lower and generation of nano- or micro-cracks in the coating was lesser. Then, charge carriers found minus opposition while moving through the active layer.

c) Functional application

Cyclic voltammograms were conducted for analyzing the performance of coated and uncoated samples as working electrodes. In addition to the data presented in Paper 4, it must be explained that in this technique potential was applied between working electrode and electrode of reference (Standard Calomelans Electrode, SCE). Then, intensity was measured between working electrode and platinum counter-electrode (figures 8-10, Paper 4). The target of these measurements was observing hydrogen (descending peak at the cathode, left side of the diagram) and oxygen evolution (ascending peak at the anode, right side of the diagram), which are usually undesired electrochemical processes because they limit the applied voltage.

Regarding thicker stainless steel substrates, different acid electrolytes were used. Results in sulphuric acid related to uncoated pieces were limited to positive potentials of 1.0 V vs. SCE, which means that oxygen evolution occurred when increasing this threshold voltage between working electrode and electrode of reference as it is shown in reaction 2. Therefore, amperage suddenly increased which restricted reaching higher potentials. On the other hand, negative potential was limited below -1.0 V vs. SCE, which was caused by hydrogen evolution (reaction 3).

$2H_2O \leftrightarrow O_2 + 4H^+ + 4e^-$ Reac. 2

$2H^+ + 2e^- \leftrightarrow H_2$ Reac. 3

*Paper 4: Improved, high conductivity titanium sub-oxide coated electrodes obtained by Atmospheric Plasma Spray.

Coated samples showed little electrochemical activity in positive potentials before the onset of oxygen evolution. At negative potentials it can be found some activity between 0 and -1 E vs. SCE with hydrogen evolution at potentials below -1 E vs. SCE. Then, it can be understood that when stainless steel is coated with APS $TiO_{2-x,}$ potential can be increased compared to uncoated pieces retarding hydrogen and oxygen evolution. This is determining because the fact of providing higher potentials permits to enlarge operation window, which increases the power supply.

Methanesulfonic acid was also tested as electrolyte. The use of this compound has increased in redox flow batteries due to it is benign and materials friendly [15]. Also in this case, coated samples suppressed hydrogen and oxygen evolution in comparison to uncoated substrates, which showed electrochemical activity at lower potentials.

In addition, tests under alkaline environment also carried out successful results. In negative potentials, both APS TiO_{2-x} coating and stainless steel exhibited hydrogen evolution circa -1,5 V vs. SCE. On the other hand, oxygen evolution was increased from 0,5 to 1,5 V vs. SCE.

After ratifying that titanium sub-oxide coatings on stainless steel substrates obtained by APS enhanced the performance of uncoated electrodes, it was studied their behaviour in the dissolution and deposition of lead in methanesulfonic acid in a simulated battery, results were compared with uncoated carbon-polymer composite electrode. In this experiment, first 600 seconds are used for the charge and next 600 seconds for the discharge (reaction 4 and 5).

Negative electrode (Reac. 4):

DISCHARGE $Pb^{2+} + 2e^{-} \leftrightarrow Pb$ *CHARGE*

Positive electrode (Reac. 5):

DISCHARGE $Pb^{2+} + 2H_2O - 2e^{-} \leftrightarrow PbO_2$ *CHARGE*

It was observed lower voltage difference between lead deposition and dissolution reactions for coated stainless steel compared to uncoated composite. This was attributed to lower electric resistance of coated samples. Electrodeposition of PbO_2 was supposed to develop certain resistance when changing the applied voltage from charge to discharge. APS TiO_{2-x} coating may reduce this effect. Moreover, specific surface area could be also playing an important role. Despite no measurements of this parameter were carried out, average porosity of 5-7% was found in APS TiO_{2-x} coatings obtained on the distinct substrates, which suggests that the area interacting with the medium was larger.

Spraying parameters selected in the deposition of titanium sub-oxide coatings and its performance as electrodes was protected by a Trade Secret (Protected on 10th January, 2013).

7.2.2 Flexible sensors

a) Coating development

Regarding gas sensor development, main concern was focused on avoiding thermal degradation of Kapton®. This material is a polyimide film with 50 micron of thickness. From the know-how gained when spraying titanium dioxide onto delicate materials such as nickel foam, it was decided to use large and unusual stand-off distances for Atmospheric Plasma Spray. Besides, gun velocity was considerably increased in order to minimize the effect of heat of the plasma jet and melted particles on the thin polymeric film. In this way, APS TiO_{2-x} coatings were properly built-up onto Kapton® without substrate degradation.

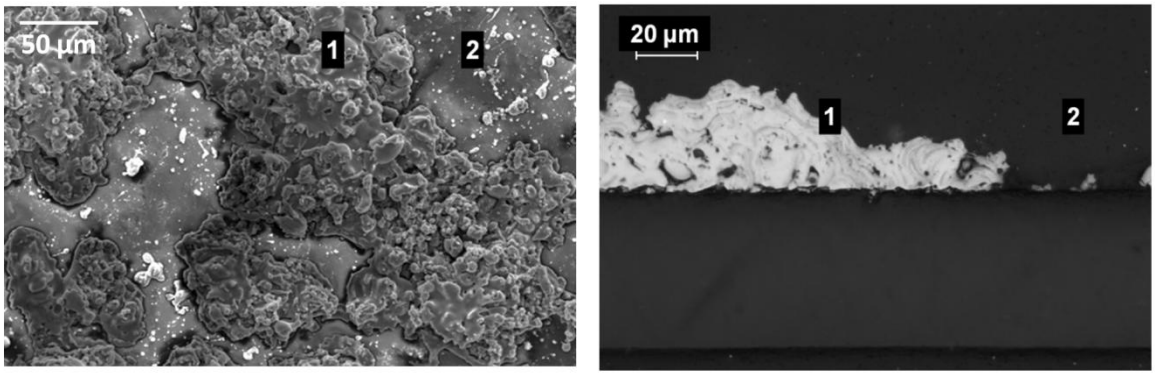

Figure 19. Left: top surface of the coated polymer, SEM micrograph. Right: cross-section area of the coating, OM micrograph.

Number of cycles was the key point for achieving titanium dioxide coatings on the polymer film that provided certain flexibility to the system. As long as the gun-pass increased, the amount of melted particles impacting onto the substrate increased and also the thickness of the layer. Lower number of cycles did not coat enough polymeric area so as to supply proper electric contact between the electrodes of the sensor. Thus, the device did not work. Higher number of cycles presented complete coverage of the substrate, which led to a proper electric contact between electrodes. However, thicker APS TiO_{2-x} layers were broken when flexing the coated polymer and even total decohesion could be obtained.

On the other hand, satisfactory results were attained when intermediate number of cycles was studied (see table 8, Appendix). It was possible to reach non-continuous coating with some coated areas and uncoated spots. This structure supplied electric contact between both electrodes, assuring the operation of the device and permitted to have certain flexibility without decohesion or rupture of the active layer. Figure 19 shows the top surface area of the APS TiO_{2-x} coated

polymer (SEM) and its cross-section area (OM). Note that uncoated areas are shown and also the connection among coated spots.

b) Key-properties evaluation

Electrical resistivity, porosity and surface composition were critically evaluated. These variables were considered determining for achieving successful performance of APS TiO_{2-x} coatings as the active layer of metal oxide gas sensors (figure 20).

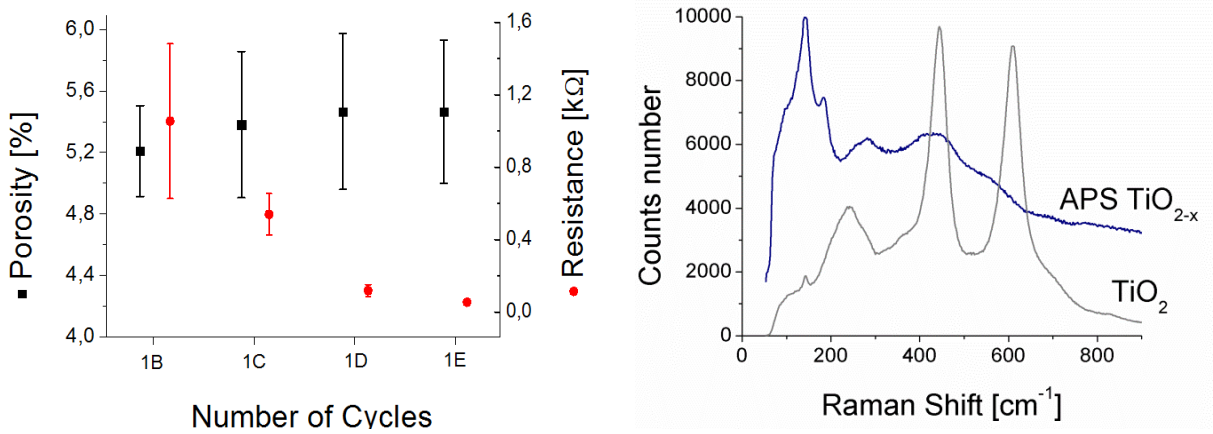

Figure 20. Left: porosity and resistance as a function of the number of cycles. Right: Raman spectra of APS TiO_{2-x} coating and pure rutile.

Resistivity of the samples decreased as long as the number of cycles was higher. For lower cycles, the amount of uncoated spots was predominant. Then, resistance between electrodes printed on the polymer was higher and even led to open circuit. Porosity may also be controlled due to it increased the specific surface area of the functional coating. Despite altering the number of cycles, this

value seemed to remain constant. As regards to surface composition, Raman spectroscopy reveals that oxygen-deficiency was present on the coating material.

c) Functional application

The review related to metal oxide gas sensor gave detailed deliberations as regards to their sensing mechanisms. Rutile-TiO_2 surfaces have considerable stability due to inexistence of dipole moment, although its planes are charged. Thus, receptor function is supported by a scenario that eases adsorption of gas molecules. Anyhow, the role of oxygen vacancies in metal oxide gas sensors should be discussed. Correlation of oxygen vacancies in SnO_2 sensors using NO_2 as target gas has already been published by other authors [16]. It was remarked a prevalence of oxygen ionosorption. In particular, strongly bonded oxygen species were attributed to the existence of reduced surfaces. Effectiveness of sensing sites may be determined by: i) continuous adsorption and desorption (being function of gas concentration, energy of the interaction and working temperature) and; ii) net charge exchange between metal oxide and adsorbed species. Then, it was reported that bridging oxygen vacancies can influence the energy exchange and charge transfer between solid surface and gas. In this way, reduced surface of APS TiO_{2-x} may also be able to provide this situation.

Micro-Raman spectroscopy shown in figure 18 reports the difference of the surface of rutile and APS TiO_{2-x} coating caused by its sub-stoichiometry. Thus, receptor function was boosted by surface stability of crystallographic planes of rutile such as (1 1 0) and the presence of bridging oxygen vacancies, which could also improve the output signal of the device (represented in figures 2 and 3 of Paper 2 and figure 5 of Paper 6).

*Paper 1: A review on fabrication, sensing mechanisms and performance of metal oxide gas sensors.
Paper 6: New procedures for building-up the active layer of gas sensors on flexible polymers.

Crystallite size of the starting powder had an average value much above of nanostructured materials, which plays a big disadvantage. Those metal oxides that have a crystallite diameter much larger than the thickness of the space charge layer (zone depleted of charge carriers caused by adsorbed species) could hardly be sensitive to surface interactions with the gas phase. Therefore, if a microstructured coating must have successful sensitivities in front of a gas, it must increase their capacity of adsorbing reactive species (receptor function) and ease the interaction of inner grains (approachability) due to output signal governed by the space charge region is low (transducer function).

Regarding approachability, measured porosity rounded 5-8% and average thickness of the coated spots was approximately 25 microns. This means that specific surface for carrying out electrochemical reactions between current supplied and adsorbed gases was higher. In this manner, inner grains of the coating were also playing a role.

Thus, it was confirmed that despite using microstructured metal oxides, APS can provide highly adsorbing surfaces capable to approach inner grains to the interaction with medium. This pronouncement can be also transferred to other applications where these necessities are required. Therefore, it was decided to keep the work with APS TiO_{2-x} and apply it as the functional component in a metal oxide gas sensor. Results obtained in Paper 6 demonstrated high capacity of this active layer to provide defined and reproducible outputs when a target gas (NH_3) surrounds the material even down to 12,5 ppm concentration. This statement demonstrated the accomplishment of the starting challenge of this thesis; developing the active layer of gas sensors by Atmospheric Plasma Spray using titanium dioxide feedstock. Furthermore, it was built-up on a flexible polymer, which gave a framework that enhances its industrial application.

*Paper 6: New procedures for building-up the active layer of gas sensors on flexible polymers

Figures 9, 10 and 11 (section 5.1.3.a) compile the experiments of sensing response in front of radiation. Measurements of UV-light sensitivity showed that resistance baseline increased after irradiating the coating with intensities above 125%. Partial re-oxidation of oxygen vacancies could be occurring in these experimental conditions. Higher intensities would be favouring the oxidation of reduced Ti^{3+} sites. As a consequence, there was a loss of donor levels from the valance band to the conducting band, which led to a decrease in the electrical conductivity of the sample. Calorimetry of APS TiO_{2-x} coating reported a limitation of its operation up to 350° C. It is supposed that completely oxidized rutile may lead to lower sensing capability of the device regarding gas sensors due to loss of oxygen vacancies at the surface of the active layer. On the other hand, totally oxidized nanostructured TiO_2 gas sensors are well-known and have good responses in front of a target gas [17]. Although in these cases there is no presence of oxygen vacancies (neither in-plane nor bridging), nanostructured nature of the material may boost transducer function.

Spraying parameters selected in the deposition of titanium sub-oxide coatings, the disposition that provided flexibility to the system and its performance as gas sensors was protected by a Trade Secret (Protected on 7th March, 2013).

7.3 Cold Gas Spray

Paper 8 and 10 demonstrated that nano-TiO_2 powders can be used in CGS for building-up homogeneous coatings (powder C426-D). However, this powder did not flow appropriately and the main pipe that connected the feeder with the spraying gun was obstructed. Despite this material clogged the CGS feeding system, it was successfully deposited on steel substrates that were previously coated with an APS TiO_{2-x} layer. Nevertheless, this only happened during the first instants when the powder flowed. Figure 21 shows an image of the intermittent coating and cross-section area.

As regards to spraying conditions for building-up this coating, starting hypothesis were faced to supply enough energy for easing possible chemical bonding mechanisms but without breaking the particles at the impact. Thus, low pressures and temperatures were selected so as to reach relatively low nitrogen velocities (table 10 – Appendix). From the different purposed conditions, no significant conclusions were obtained, excluding that it seemed that particles had the capacity of getting adhered but also of being easily detached when in-flight particles impacted nearby.

*Paper 8: Improved photocatalytic nanostructured anatase coatings obtained by Cold Gas Spray.
Paper 10: Enhancing the bioactivity of polymeric implants by means of Cold Gas Spray coatings.

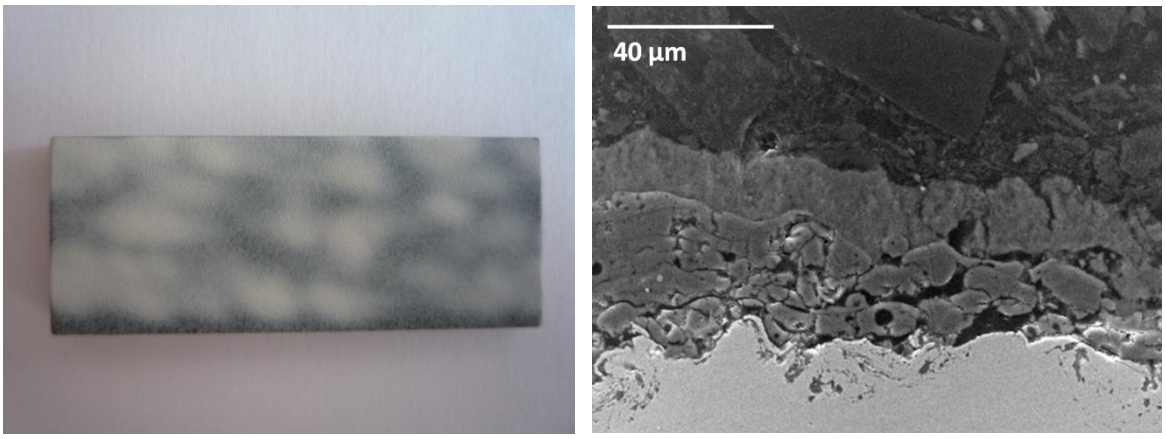

Figure 21. Left: image of APS TiO_{2-x} layer on stainless steel coated by C426-D, with poor flowability. Right: cross-section image of the multilayered coating.

7.3.1 Photocatalysts

a) Coating development

- CGS Cu/nano-TiO_2 coatings

Blend with copper provided the required flowability for avoiding the clogging of the feeder. As it has been mentioned before, nano-TiO_2 powder was adhered at low spraying conditions. On the other hand, copper usually requires higher energetic conditions for being deposited (table 11 – Appendix). According both upper and lower limit, wide operation window was firstly purposed. Pressure and temperature were stepwise increased from lower level to higher values. Using equations 6-25 is possible to estimate nitrogen velocity for the distinct spraying conditions. Figure 22 correlates starting temperature with N_2 velocity (data available in table 11 – Appendix).

Paper 7 discussed above mentioned values and its repercussion on coating development. 50% in vol. blended powders were successfully deposited when applying outlet N_2 velocity between 870 and 970 m/s. The coverage of the top surface by means of nano-TiO_2 particles was attributed to spraying conditions. However, much more reasoning should be provided for demonstrating this statement. It is not clear that for given nitrogen stream velocity, smaller particles with lower density (TiO_2 compared to Cu) should impact *later* to the substrate. Therefore, other mechanisms could be occurring during the flight of the powders. Blended powders were not mechanically alloyed; they were simply mixed. It is possible that metallic and metal oxide particles could be colliding among them in the nozzle. Then, hard titanium dioxide particles would be incrusted into the surface of larger copper particles. Finally, metallic particles covered by TiO_2 could impact onto the substrate surface providing plastic deformation and assuring the presence of the photocatalytic material at the top surface of the coating.

More experiments related to blends based on functional hard materials with ductile powders so as to build-up coatings by CGS should be carried out in order to discriminate particle velocities or demonstrate the existence of the above discussed mechanism.

Once spraying conditions were appropriately adjusted, stainless steel cylinders were coated for its further application as photocatalysts. Cylinders were vertically placed on the spraying plate and subjected to a rotation velocity of 239 rpm and ascending gun velocity of 2,98 mm/s. Nozzle had to be directed precisely to the centre of the cylinder in order to avoid tangential trajectories of the stream because it could lead to coating decohesion.

*Paper 7: Developing photocatalytic Copper/nano-Anatase coatings by Cold Gas Spray.

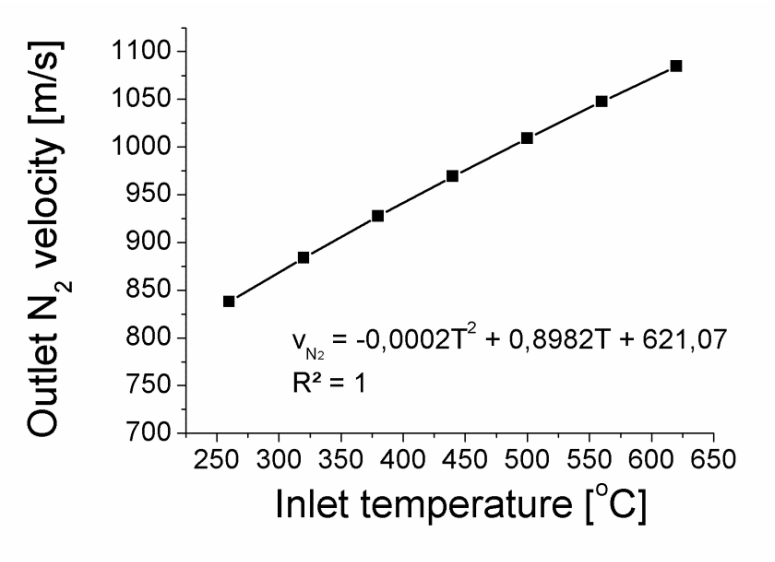

Figure 22. N_2 velocity at the outlet of the nozzle.

- CGS Nano-TiO_2 coatings

C426-D blended with microstructured powder was also used as feedstock. It was decided to coat directly stainless steel substrates as it was done with Cu/nano-TiO_2 powders. However, the coatings were not properly bonded. Figure 23 shows an image of weakly coated stainless steel with micro- and nano-anatase powders. It can be observed that it was not possible to coat the substrate and even total detachment was found.

Figure 23. Inadequately coated stainless steel substrate by CGS nano-TiO_2.

Surface composition and geometry may play a key role in the adhesion of nano-TiO_2. After providing substrate composition that could ease the interaction with sprayed particles, coatings were successfully built-up. In order to clarify these findings, the following mechanisms are purposed:

1. Holes and valleys of APS TiO_{2-x} coatings at its top surface entrapped impacting nano-TiO_2 particles that together with released energy of the stream could develop chemical bonds with the substrate and among particles. Mechanism similar to ceramic sintering could happen. First, densification step is carried out; nanostructured particles are compacted on the geometry of APS TiO_{2-x} roughness. Space among particles, namely porosity, is reduced. Then, sintering mechanisms may occur such as diffusion of atoms at the top surface of the crystallites that could bridge the impacting particles, developing the formation of the coating. This statement would be in agreement with other authors [18,19]. Thickness was limited to certain value despite increasing the number of cycles. Roughness of the surface may have decreased as long as APS TiO_{2-x} was coated with nano-TiO_2 particles, which led to loss of holes and valleys that provided the geometry for entrapping nanostructured particles.

2. A second system can be also reasoned. Temperature required for sintering nanostructured titanium dioxide particles is reported to be at approximately 600° C [20]. Starting N_2 stream temperature in these experiments was much below this value and it was reduced as long as the gas flowed through the nozzle. Therefore, thermal conditions for favouring sintering seemed far away. On the other hand, intimate contact either between the particles and the substrate or among the particles was achieved. Particles could be adhered due to physical bonding. Therefore, electrostatic interactions would be in command to maintain the coating compacted, which could explain the measured weak microhardness (Paper 8).

3. Combination of mechanism 1 and 2. As explained in mechanism 2, supplied temperature could be low enough to make impossible sintering process. Nevertheless, taking into account the quick impact process (tens of nanoseconds) it is assumed that the kinetic energy of the particle becomes a source of thermal energy. Numerous investigations support the existence of a possible localized fusion at the interface particle/substrate and particle/coating, under certain conditions when using metallic powders and substrates [21]. This melting at local level would favour the formation of a metallurgical bond between the deposited particles and the substrate-coating, and therefore, improved adhesion. Then, some particles could achieve enough kinetic energy that released sufficient heat for easing sintering in precise areas. On the other hand, other particles were attached simply by physical bonding due to they reached intimate contact.

In any case, novel process in ceramic engineering could source from this study, which has proved to be capable to deposit hard nanostructured particles in solid state by means of providing enough kinetic energy and temperature. Stainless steel cylinders were firstly coated by APS TiO_{2-x} coating. Then, it was repeated the same step selected with Cu/nano-TiO_2 feedstock regarding circular spraying. In this case, it was even more important to adjust nitrogen stream towards the centre of the cylinder. Deposited nano-TiO_2 particles were easily detached from cylinder surface when N_2 stream impacted tangentially to the cylinder.

*Paper 8: Improved photocatalytic nanostructured anatase coatings obtained by Cold Gas Spray.

b) Key-properties evaluation

Characterization of starting TiO_2 feedstock (C426-D) confirmed that it was based on pure crystalline anatase with a crystallite size ranged between 20 and 100 nm. These materials have outstanding properties as a photocatalyst and are well-known in the industrial and scientific community. Concretely, anatase has a band gap of 3,2 eV and when irradiated with UV-light (**λ**= 320 nm) an electron is excited from balance band to conducting band [22]. Separated electron-hole pairs can be available for oxidation-reduction reactions. Then, adsorbed water is dissociated on anatase surface and OH· radicals are formed at reduction potential of 2,85 V. Besides, oxygen is reduced at -0,13 eV. Subsequently, these reactive species are in command to degrade different adsorbed contaminants.

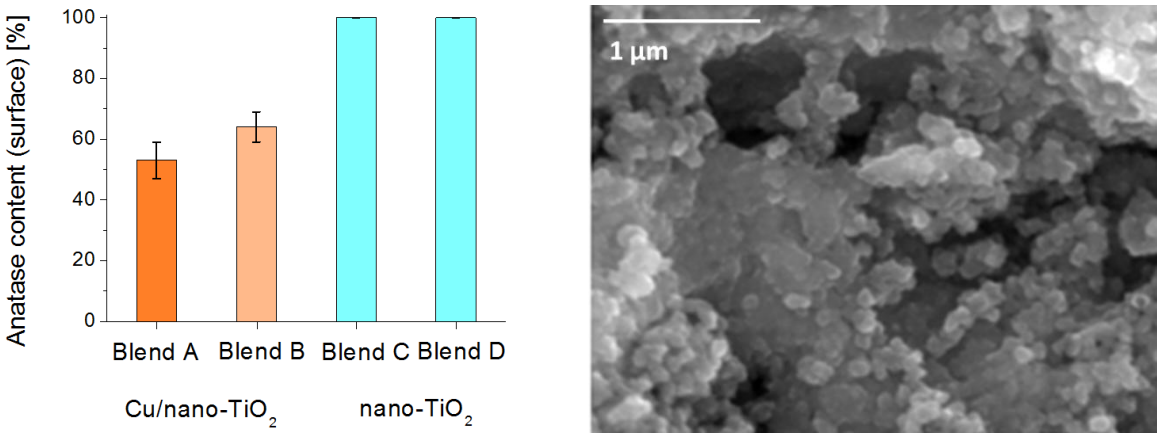

Figure 24. Left: amount of anatase at the top surface of the coatings. Right: Characteristic top surface micrograph (FESEM) of nanostructured anatase in CGS coatings.

Thenceforth, it could be assured that top surfaces that had the presence of nanostructured anatase would provide a coating material with exceptional capacity of degrading contaminants due to its photocatalytic performance and large specific area, where the interaction is carried out.

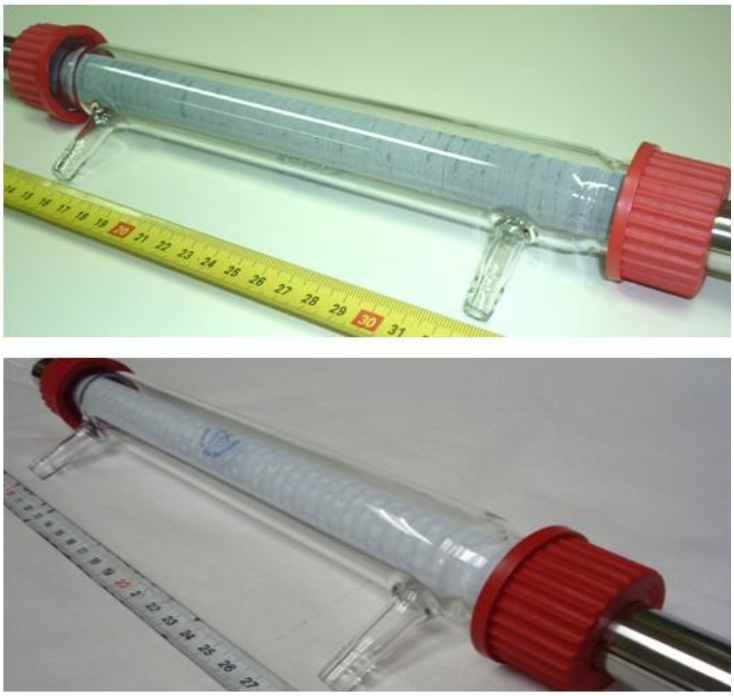

Figure 25. Above: CGS Cu/nano-TiO_2 photocatalyst into the glass reactor. Below: CGS nano-TiO_2 photocatalyst into the glass reactor.

After developing above discussed spraying conditions, the amount of substrate surface coated by nanostructured anatase was the chief parameter to control and optimize (figure 24). Blends with copper provided between 40 and 70 % of anatase at the top surface of the coating; these photocatalysts were used in gaseous phase. On the other hand, both blends obtained by mixing C426-D

with microstructured anatase completely covered steel substrates previously coated with APS TiO_{2-x}.

Figure 25 shows both CGS Cu/nano-TiO_2 and CGS nano-TiO_2 photocatalysts placed into the glass reactor used in the photodegradation of the different contaminants.

c) Functional application

Key application of TS TiO_2 photocatalysts is the removal of contaminants in wastewaters. This is a highly concerning problem in society and significant improvements from Research, Development and Innovation synergies are expected. Therefore, CGS Cu/nano-TiO_2 coatings were applied for degrading phenol in aqueous phase. Interesting degradation rates were obtained demonstrating adequate performance as photocatalyst. However, some traces of copper were found at the outlet of the reactor, which is extremely dangerous due to the presence of copper in water is harmful and severely regulated by environmental standards. Thus, these coating materials may not be used in liquid phase, but are accepted for being used in gaseous phase.

Then, gaseous toluene was selected as gaseous contaminant (Paper 7). High adsorption without degradation of the target gas was caused by the amount of coating material and its enhanced adsorption capability (copper surface). This proved some statements reviewed in Paper 2. The presence of metallic clusters such as Al, Cu or noble metals may increase the capacity of adsorbing gases when combined at the top surface of a metal oxide. Copper could ease the adsorption of reactive oxygen anions and also target gases for subsequently displacing them to the metal oxide active surface. This phenomenon is known as the spill-over effect in metal oxide gas sensors.

*Paper 7: Developing photocatalytic Copper/nano-Anatase coatings by Cold Gas Spray.
Paper 2: A review on fabrication, sensing mechanisms and performance of metal oxide gas sensors.

Previous trials showed this phenomenon before irradiating with UV-light, where starting concentration of 2,5 ppm was reduced at the outlet of the reactor to 0,75 ppm in 100 minutes without degrading toluene gas. Anyhow, tests with UV-light successfully degraded the contaminant proving its adequate performance.

Pure TiO_2 coatings applied in photocatalytic degradation of phenol in liquid phase gave outstanding results (Paper 8). Final performance improved the behaviour of sol-gel commercial standard P25® coatings. Different considerations can be taken into account for discussing this outcome. Degradation mechanisms of organic compounds by photochemical processes that use TiO_2 as photocatalysts are deeply influenced by grain size and co-existence of certain percentages of rutile and anatase, which control adsorption kinetics, surface reactivity and desorption rates. These differences according C426-D and P25® may be in command to provide distinct results as photocatalysts. Since the investigation of degrading mechanisms of pollutants depending on TiO_2 nanostructure and composition is not in the scope of this thesis, increased performances of CGS nano-TiO_2 coatings compared to sol-gel P25® may not be entirely explained. It is noteworthy to mention that lower APS TiO_{2-x} bond coat may act as current collector, which could supply photogenerated electrons and holes more homogeneously through the photocatalyst, which would also increase the differences obtained in both coatings.

*Paper 8: Improved photocatalytic nanostructured anatase coatings obtained by Cold Gas Spray.

Formic acid was also selected as contaminant for being degraded and again CGS nano-TiO_2 coatings had a superior performance compared to sol-gel P25®. In this case, CGS nano-TiO_2 showed larger deviations among results. On the other hand, sol-gel P25® had precise performance after doing several repetitions. This was attributed to the presence of the acid functional group. CGS nano-TiO_2 coatings could be more sensitive towards H^+, $HCOO^-$ adsorption, reactivity and desorption kinetics. Again, CGS nano-TiO_2 photocatalyst showed enhanced performances compared to sol-gel P25®.

Spraying parameters selected in the deposition of Cu/nano-TiO_2 and nano-TiO_2 coatings, blending procedure for providing flowability to CGS powders and its performance as photocatalysts was protected by a Trade Secret (Protected on 2nd May, 2013).

7.3.2 Biomedical applications

a) Coating development

Different spraying conditions were used for coating PEEK with nano-TiO_2 powder (blend D, table 5) but unsatisfactory results were obtained. Titanium dioxide particles simply bounced on the polymer substrate and slightly stained its surface. As it has been explained before, CGS coatings are usually built-up due to plastic deformation of impacting particles. In some cases, ductility of the substrate leads to its plastic deformation and favour the deposition of hard particles. It was first considered to provide temperature to the substrate by means of external heaters such as air streams or infrared lamps. However, this was quickly dismissed because of thermal softening could lead to changes in the composition of PEEK and undesired outcomes in its biocompatibility. Thus, other feasible possibilities had to be thoughtful.

Findings in pure TiO_2 coatings obtained by means of CGS in photocatalytic applications confirmed that substrate surface had a key role in terms of composition and geometrical disposition. Following this statement, it was decided to reproduce same adhesion mechanisms. The direct move could have

been coating PEEK with APS TiO_{2-x}. However, as far as the author was concerned, titanium sub-oxide performance as biocompatible material was not reported to be capable to enhance PEEK bioactivity. Then, it was decided to use titanium layer as bond coat deposited by Cold Gas Spray.

Titanium is among metals a hard material and relatively high energetic conditions are used for its deposition in CGS technology. Starting selected parameters provided too much heat to the polymer (table 13 – Appendix). Then, excessive softening in the surface led to large quantities of mechanically embedded particles (figure 1b Paper 9). Again, this was extremely undesired due to: i) excessive thermal contribution could lead to changes in the composition of the polymer and; ii) softening of the polymer cannot supply enough hardness for favouring plastic deformation of impacting metallic particles.

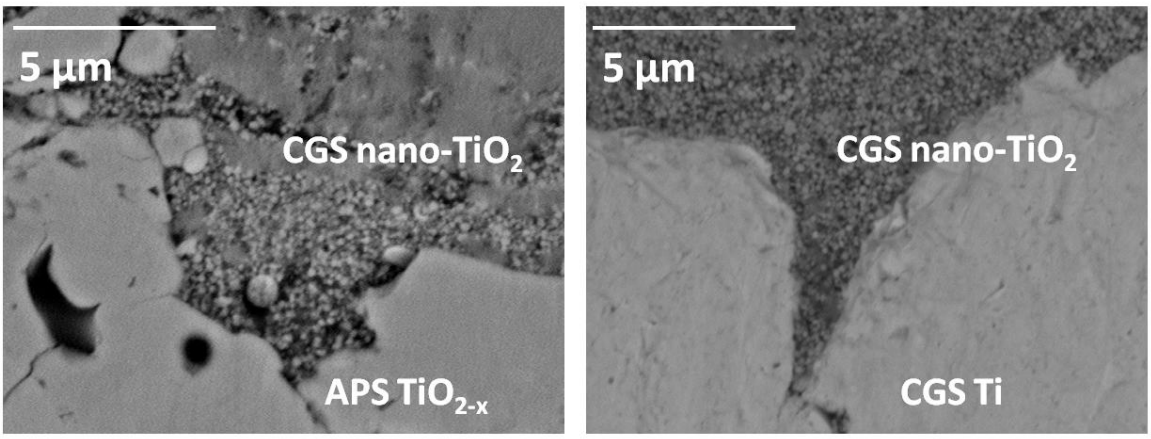

Figure 26. Left: CGS nano-TiO_2 on APS TiO_{2-x} bond coat for photocatalytic applications. Right: CGS nano-TiO_2 on CGS Ti bond coat for biomedical applications.

*Paper 9: Cold Gas Spray titanium coatings onto a biocompatible polymer.

Two opposite interests were found. Temperature was required for accelerating Ti particles, which also favour their plastic deformation at the impact. On the other hand, temperature provided by the nitrogen stream could soften the polymer, which would decrease substrate hardness needed for easing Ti deposition and could also modify PEEK composition. Anyhow, successful results were found when adequately balancing gun velocity, stand-off distance and inlet N_2 temperature. Concretely, inlet temperature was reduced and stand-off distance was increased. At these conditions, it was supposed that substrate could provide enough hardness for assuring that Ti particles could appropriately deform and adhere onto the polymer without influencing the composition of the polymer. Once again, similar phenomena studied in APS TiO_{2-x} onto Kapton was perceived. Spraying distances were increased so as to avoid substrate degradation (in this case softening). Gun velocities were reduced so as to increase the amount of impacting particles, which led to thick homogeneous and well-bonded coatings.

Afterwards, CGS nano-TiO_2 coatings were deposited onto CGS Ti bond coat on PEEK using the same spraying parameters selected for coating APS TiO_{2-x} bond coat in photocatalytic applications. Experimental results and characterization of the samples got back mechanisms 1, 2 and 3 explained in section 6.2.1.a. Figure 26 shows a narrow hole at the top surface of CGS Ti bond coat where nano-TiO_2 particles are adhered, which clearly reminded micrographs related to nano-TiO_2 photocatalysts onto APS TiO_{2-x} bond coat.

b) Key-properties evaluation

As regards to main concerning properties of the coatings in this application, it was first considered the amount of coated surface by means of CGS process. Anyhow, observation by confocal microscopy and scanning electron microscopy determined that PEEK substrates were completely covered by titanium and nanostructured anatase. This confirmed that further functional tests would represent exclusively the behaviour of each material: original PEEK, CGS Ti and

CGS nano-TiO_2, without influences occasioned by partial coating. Then, surface micro-roughness had to be adequately measured (figure 27).

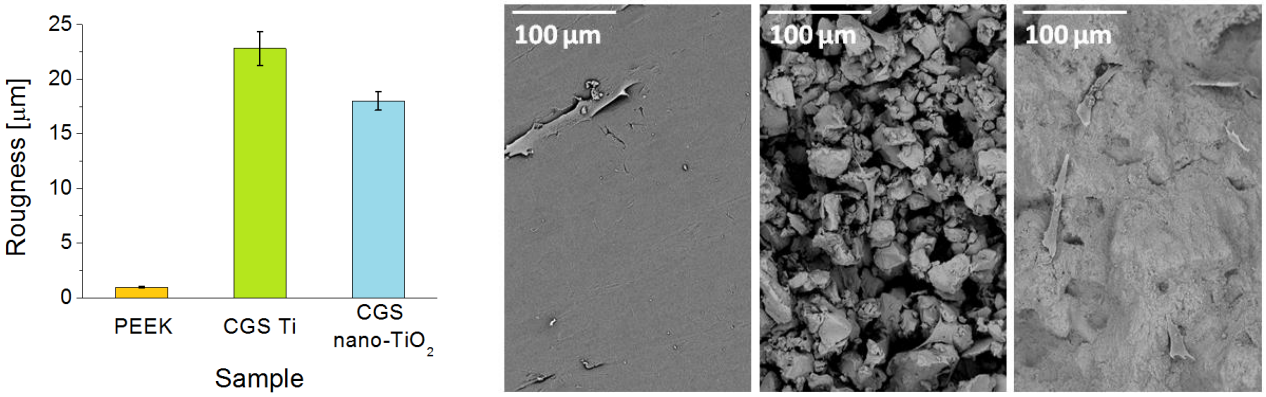

Figure 27. Left: Roughness values for PEEK, CGS Ti and CGS nano-TiO_2. Right: Top surface micrographs of for PEEK, CGS Ti and CGS nano-TiO_2 respectively, some adhered cells are also visible.

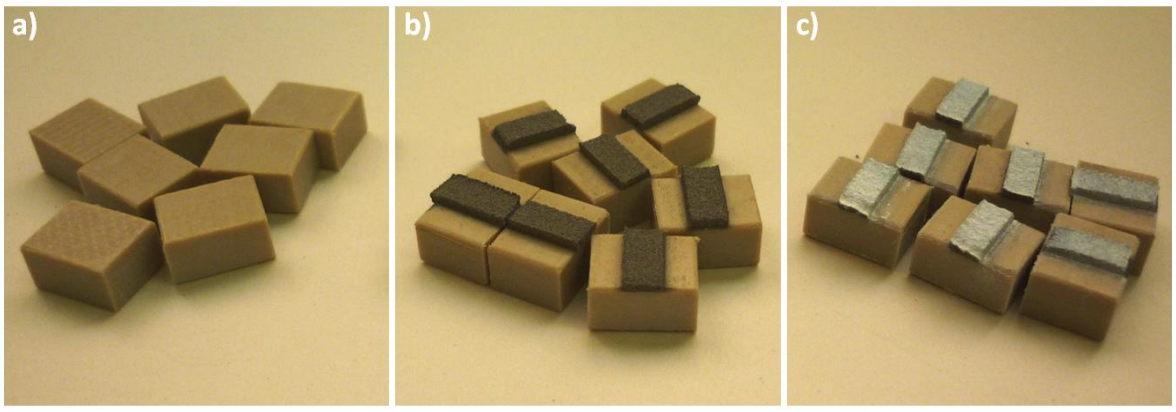

Figure 28. a) 10x8x5mm PEEK pieces, b) CGS Ti layers and c) CGS nano-TiO_2 coatings.

Initial biocompatible polymer was almost completely flat. Roughness of CGS Ti layers was sharp. Successful spraying conditions for achieving these thick, homogeneous and well-bonded layers caused low plastic deformation to the *last* impacting particles. Feedstock material that was firstly deposited was very deformed by secondary impinging particles, which developed a reduced porosity closer to the interface between coating and substrate. On the other hand, particles closer to the top surface of the coating did not receive the impact of arriving particles and their deformation was lower. This led a surface with a higher roughness. Finally, coating with nano-TiO_2 particles led to smoother surfaces. Nanostructured anatase filled holes and valleys present at the rough surface of CGS Ti bond coat. Then, roughness value decreased, although it was still being significantly above starting PEEK. Figure 28 shows an image of some starting PEEK pieces (10x8x5mm), CGS Ti layers onto PEEK and CGS nano-TiO_2 coatings onto Ti.

c) Functional application

Starting hypothesis related to functional application of CGS nano-TiO_2 coatings as biomedical implants was the enhanced capability of nanostructured titanium dioxide surfaces for adsorbing proteins that ease adhesion of cells on the biomaterial. Cell cultures were studied on PEEK, CGS Ti layers on PEEK and CGS nano-TiO_2 coatings. Concretely, it was measured cell adhesion, proliferation and differentiation after 1, 3 and 7 days of assay. Regarding cell adhesion and proliferation, either Ti or nano-TiO_2 coating surfaces exhibited boosted performances compared to PEEK after 7 days. However, no significant differences were observed between coated implants. These unexpected results disagree with initial supposition. Nanostructured titanium dioxide did increase neither cell adhesion nor proliferation compared to titanium. According protein adhesion mechanisms, this outcome may be explained by following statements:

1. Thin oxide film at the top surface of titanium crystallites may be taken into deep consideration. It is well-known that this layer provides recognized biocompatibility to Ti implants. However, thickness of this layer and crystalline

composition should be clarified so as to improve Ti and TiO_2 functional application on PEEK.

2. Hydrophobic and hydrophilic properties of the coatings may be also playing a role here. The capacity of surface implant to attract cell suspension could interfere in final results in some way.

3. Nano and micro-roughness could compete in a certain way for favouring cell adhesion. Nanostructured anatase had larger specific areas, which increased active centres for adsorbing proteins. Nevertheless, these surfaces were less rough in micro-sized scale than CGS Ti layers (figure 1 in Paper 9). Figure 6 in Paper 10 shows details how a cell may be attached in these pronounced valleys formed at the top surface of CGS Ti layers. Therefore, micro-textured Ti surface may not be ignored in terms of cell adhesion and proliferation.

Cell differentiation after 7 days of assay showed extremely increased results for CGS nano-TiO_2 coatings compared to CGS Ti and original PEEK. New formed cells were easily differentiated on anatase, which could be caused by a scenario governed by nanotextures that resembled biological environments. Besides this, it is reported that high crystalline TiO_2 have higher biocompatibilities [23]. Then, lack of crystalline grains in oxide film formed on Ti may reduce cell differentiation. Furthermore, CGS Ti bond coat had lower performance compared to PEEK. Direct correlations were not found for explaining these results, especially after observing enhanced behaviour of CGS Ti layer related to cell adhesion and proliferation.

*Paper 9: Cold Gas Spray titanium coatings onto a biocompatible polymer.
Paper 10: Enhancing the bioactivity of polymeric implants by means of Cold Gas Spray coatings.

8. Conclusions

With the present thesis, Coatings based on Titanium Dioxide have been obtained by means of Thermal Spray Technologies proving their performance in different fields such as electrodes for batteries, gas and radiation sensors, photocatalysts and biomedical applications. From this study, the following statements can be concluded:

8.1 With regard to TiO_{2-X} APS coatings

1. Plasma rich in argon with low amount of hydrogen had higher temperatures but low capacity of transferring this energy to TiO_2 particles. Optimal stand-off distances and plasma intensities reduced coefficient of thermal expansion (CTE) mismatch between TiO_2 coating and ceramic tile substrates, leading to coatings with electric resistivity from around $1{,}7 \cdot 10^{-1}$ to $6{,}0 \cdot 10^{-2}$ **Ω**·cm.

2. CTE mismatch between stainless steel substrates and APS TiO_{2-x} layers was successfully reduced by means of nitrogen cooling and optimum feed rates, which produced coatings with bonding strength up to around 67 MPa and lacking delamination or presence of cracks in its cross-section.

3. Lower energetic conditions were obtained by means of optimum stand-off distances and nitrogen cooling, metallic substrates such as thin stainless steel and aluminium films were properly coated showing the lowest electric resistivity of the Thesis (around 10^{-3} **Ω**·cm).

4. Extremely delicate electrode materials such as carbon-polymer composites were properly coated with APS TiO_{2-x} layers avoiding the damage of the substrate.

5. APS TiO_{2-x} coatings were effectively deposited onto Ni foams; filaments of the Ni foam network were 3-dimensionally coated without damaging the substrate.

6. APS TiO_{2-x} coated stainless steel were applied as electrodes in media such as sulphuric acid, methanesulphonic acid and potassium hydroxide increasing the applied voltage by around 32%, 85% and 35% respectively compared to uncoated samples. Furthermore, 0.2 V of difference between deposition and dissolution of Pb in a soluble lead acid flow battery using uncoated electrodes was reduced to 0.1 V, which was attributed to better electrical conductivity of the coated electrodes.

7. Flexible polymeric film commonly used in electronics with 50 microns of thickness (Kapton®) was effectively coated by means of APS TiO_{2-x} for its further application as gas sensor using optimal stand-off distances that avoided thermal degradation of the substrate. Intermediate number of cycles onto Kapton® made possible to achieve a coating-substrate system with certain flexibility and electric contact between printed electrodes.

8. APS TiO_{2-x} coatings had a surface with considerable amount of oxygen vacancies, which may boost Receptor Function of the sensor, easing adsorption of gaseous reactive species. Furthermore, porosity contained in the thickness of the coating may favour the access to the internal grains, which enhanced its Approachability.

9. APS TiO_{2-x} coatings deposited onto flexible polymer had positive and reproducible response in front of NH_3 gas concentrations ranged between 12.5 and 100 ppm. Besides, the active coatings had positive and reproducible response when irradiating the samples with UV light (λ= 365nm), blue LED light (λ= 453nm) and red LED light (λ= 530nm).

8.2 With regard to CGS coatings

10. Nano-TiO_2 powder designed for being deposited by means of CGS process was blended with copper powder and microstructured TiO_2 powder in order to obtain blends with satisfactory flowability, which avoided the clogging of the feeding system.

11. CGS Cu/nano-TiO_2 coatings were adequately bonded onto stainless steel; copper acted as ductile agent for easing adhesion of hard photoactive ceramic particles when impacting onto the substrate. Besides, nanostructured anatase was present at the top surface of the coating assuring the photocatalytic process.

12. CGS nano-TiO_2 coatings were appropriately bonded on substrates that had certain affine chemical composition and surface geometry; APS TiO_{2-x} coatings were previously deposited onto stainless steel and nano-anatase particles were then sprayed and entrapped on holes and valleys at the top surface of the bond coat, which favoured the building-up of the coating.

13. CGS Cu/nano-TiO_2 coatings had large capacity of adsorbing species in gaseous phase and completely degraded 25 ppm of toluene after 30 min of UV-light irradiation. CGS nano-TiO_2 coatings increased the performance of sol-gel photocatalysts based on commercial P25® by around 24% (after 90 min) and 71% (after 75 min) respectively in the degradation of phenol (10 ppm) and formic acid (10 ppm) in aqueous phase.

14. Thick homogeneous well-bonded Titanium coatings were deposited onto Polyetheretherketone (PEEK) biocompatible using spraying conditions that avoided thermal softening of the polymer, favouring plastic deformation of metallic particles at the impact.

15. PEEK substrates were successfully coated with CGS nano-TiO_2 using a bond coat based on titanium that was previously deposited for entrapping nanostructured particles of anatase on the valleys and holes of the metallic top surface.

16. After 7 days of cell cultures, nanostructured anatase coatings onto PEEK increased cell viability, cell proliferation and cell differentiation by around 92%, 49% and 185% respectively.

8.3 With regard to general juncture

17. Novel nanostructured TiO_2 powders designed for being applied in Cold Gas Spray (CGS) can provide new opportunities in established lines of research for photocatalytic and biomedical applications.

18. Low electric resistivity of APS TiO_{2-x} coatings is of special interest for its application as electrodes in conventional, bi-polar or redox flow batteries.

19. Thermal Spray technologies can be feasibly used for developing metal oxide gas sensors accomplishing the sensing mechanisms that are required for a proper operation of the device.

20. Obtained coatings using APS or CGS were applied as-sprayed for its use as electrodes, gas and radiation sensors, photocatalysts and biomedical implants. No further steps such as thermal or chemical treatments after Thermal Spray processes were carried out for enhancing their performance.

21. Through this Thesis, it has been demonstrated that titanium dioxide toghether with Atmospheric Plasma Spray and Cold Gas Spray offer a new procedure for unseating conventional coating techniques in the development of electrodes, gas and radiation sensors, photocatalysts and biomedical applications due to its high performance cost-effective production, large capacity of manufacturing, brief operation times and environmentally friendly features.

9. Future trends

Findings accomplished during this Thesis have open defined lines of Research, Development and Innovation. Next moves have been already selected for being the continuation of the obtained results:

1. Fabrication of a battery. Improved performances of APS TiO_{2-x} electrodes have released the possibility of developing a bi-polar battery. Thus, APS would be used not just for building-up functional components of these devices, but also other items such as insulator layers, bi-polar walls or the container.

2. Use of APS TiO_{2-x} coatings as counter-electrodes in Dye Sensitized Solar Cells. Results related to electrical conducting layers obtained onto ceramic tiles that are generally used in construction suggested the possibility of developing these cells for either domestic or industrial application.

3. Apply gas and radiation sensors in smart clothes. Positive responses of the active layer have encouraged searching for experienced partners in this field so as to scale-up the product.

4. Scale-up findings obtained in photocatalytic CGS nano-TiO_2 coatings to a plant built in the University of Las Palmas de Gran Canaria, which operates by means of 4 reactors with length of 1 meter and 15 cm of diameter.

5. Combine micro- and nanostructured anatase with different metals such as copper or aluminium in mechanical alloying process. In this way, cermet powders based on hard active metal oxide and ductile metal could be obtained and sprayed by CGS. Thus, metal would provide plastic deformation for easing the adhesion of the particle with the presence of anatase. Study the performance of these coatings as photocatalysts.

6. Make use of titanium dioxide powder with photocatalytic activity in the range of visible light. Study the feasibility of depositing these powders by CGS and its capacity of degrading contaminants in front of solar light instead of UV light.

7. Transfer the findings related to deposition of nanostructured anatase to: i) Dye Sensitized Solar Cells, fabricate the active layer of solar cells onto conducting glass and polymers and; ii) superhydrophobic surfaces, study contact angle of water droplets.

8. Combine micro- and nanostructured hydroxyapatite with nano-TiO_2 and Ti in mechanical alloying process. In this way, cermet powders based on hard ceramic, metal oxide and ductile metal could be obtained and sprayed by CGS. Thus, metal would provide plastic deformation for easing the adhesion of the particle with the presence of nanostructured hydroxyapatite and anatase. Study the performance of these coatings as biomedical implants.

10. Acknowledgements

I appreciate to Prof. Guilemany his guidelines and support in the development of the Thesis. Together with Dr. G. Cano I want to express my sincere gratitude for giving me the possibility to join the Thermal Spray Centre. A special acknowledgement to Mr. Gómez for his expertise and efforts on technical aspects of the spraying experiments and Dr Dosta, Dr Miguel and Dr. Torrell for sharing with me their know-how in thermal spray processes. I can not forget the help received from the rest of the staff of CPT and from my colleagues, PhD students, master students and many more people involved to the Centre.

Furthermore, I want to transmit my respect and admiration for all partners in this Thesis. Dr. Albert Cirera, Mr. Albert Monereo and Mr. Giovanni Vescio for measurements related to gas and radiation sensors (group MIND), Dr. Brian Mellor, Dr. Richard Wills and Miss. Maria Kourasi for their dedication in electrochemical experiments (University of Southampton), Mrs. Cristina Fernández and Mrs. Rosa Maria Espino for all their efforts on measuring photocatalytic activities and Miss. Hortensia Melero and Dr. Natàlia G. Giralt for the cell tests.

11. References

11.1 Specific references

[1] G. V. Samsonov. The Oxide Handbook. IFI/Plenum Press (1982) ISBN: 978-1-4615-9599-1.

[2] L.-M. Berger. Titanium oxide – new opportunities for an established coating material. Intern. Therm. Spray Conf. Proceed. (2010).

[3] F. Millot, M.G. Blanchin, R. Tétot, J.F. Marucco, B. Poumellec, C. Picard, B. Touzeli. High Temperature Nonstoichiometric Rutile TiO_{2-x}. Progr. Solid State Chem., 17 (1987) pp. 263.

[4] H. Gruber, E. Krautz. Magnetoresistance and Conductivity in the Binary System Titanium-Oxygen. Phys. Stat. Sol. 75, 2 (1983) pp. 511.

[5] F.C. Walsh, R.G.A. Wills. The continuing development of Magnéli phase titanium sub-oxides and Ebonex® electrodes. Electr. Acta 55 (2010) pp. 6342.

[6] E. Pfender, J. Heberlein. Heat Transfer Processes and Modeling of Arc Discharges. Adv. Heat Transfer 40 (2007) pp. 345.

[7] L. Pawlowski. Science and Engineering of thermal spray coatings". John Wiley & Sons, Ltd. (1998) ISBN: 978-0-471-49049-4.

[8] F. M. White. Fluid Mechanics. McGraw Hill (2006) ISBN: 0073309206.

[9] K. K. Sahu, T. C. Alex, D. Mishra, A. Agrawal. An overview on the production of pigment grade titania from titania-rich slag. Waste. Manage. Res. 24 (2006) pp. 74.

[10] U. Diebold, M. Li, O. Dulub, E. L. D. Hebenstreit, W. Hebenstreit. The Relationship between Bulk and Surface Properties of Rutile TiO_2(110) Surf. Rev. Lett. 5-6 (2000) pp. 613.

[11] S. Bakardjieva, J. Subrt, V. Stengl, M. Dianez, M. Savagues. Photoactivity of anatase-rutile TiO_2 nanocrystalline mixtures obtained by heat treatment of

homogeneously precipitated anatase. App. Cat. B: Env. (2005) pp. 193.

[12] P.C.S. Hayfield. Development of a New Material - Monolithic Ti_4O_7 Ebonex Ceramic. Royal Soc. Chem. (2002) ISBN: 0-85404-984-3.

[13] N. Bundaleski, A. G. Silva, U. Schröder, C. Moutinho, D. Teodoro. Adsorption dynamics of water on the surface of TiO_2 (110). J. Phy.: Conf. Series 257 (2010) pp. 12008.

[14] U. Diebold. The surface science of titanium dioxide. Surf. Sci. Rep. 48 (2003) pp. 53.

[15] M. D. Gernon, M. Wu, T. Buszta, P. Janney. Environmental benefits of methanesulfonic acid: comparative properties and advantages. Green Chem. 1 (1999) pp. 127.

[16] M. Epifani, J. D. Prades, E. Comini, E. Pellicer, M. Avella, P. Siciliano, G. Faglia, A. Cirera, R. Scotti, F. Morazzoni, J. R. Morante. The Role of Surface Oxygen Vacancies in the NO_2 Sensing Properties of SnO_2 nanocrystals. J. Phys. Chem. C 112, 49 (2008) pp. 19540.

[17] E. Traversa, M. L. Di Vona, S. Licoccia, M. Sacerdoti, M. C. Carotta, L. Crema, G. Martinelli. Sol-Gel Processed TiO_2-Based Nano-Sized Powders for Use in Thick-Film Gas Sensors for Atmospheric Pollutant Monitoring. J. Sol-Gel Sci. Tech 22, 1-2 (2001) pp. 167.

[18] S.-Q. Fan, C.-J. Li, C.-X. Li, G.-J. Liu, G.-J. Yang, L.-Z. Zhang. Preliminary Study of Performance of Dye-Sensitized Solar Cell of Nano-TiO_2 Coating Deposited by Vacuum Cold Spraying. Mat. Trans. 47, 7 (2006) pp. 1703.

[19] S.-Q. Fan, C.-J. Li, G.-J. Yang, L.-Z. Zhang, J.-C. Gao, Y.-X. Xi. Fabrication of Nano-TiO_2 Coating for Dye-Sensitized Solar Cell by Vacuum Cold Spraying at Room Temperature. J. Therm. Spray Tech. 16, 5-6 (2007) pp. 893.

[20] H. Hahn, J. Logas, and R.S. Averback. Sintering characteristics of nanocrystalline TiO_2. J. Mater. Res. 5, 3 (1990) pp. 609.

[21] M. Villa, S. Dosta, A.List, F. Gärtner, T. Klassen, J.M.Guilemany. Ti6Al4V cold gas sprayed coatings: Impact morphologies, splat adhesion and

correlations to coating microstructures. Intern. Therm. Spray Conf. Proceed. (2013).

[22] A. Wold. Photocatalytic Properties of TiO_2. Chem. Mater. 5 (1993) pp. 280-283.

[23] L. Zhao, J. Chang, W. Zhai. Effect of Crystallographic Phases of TiO_2 on Hepatocyte Attachment, Proliferation and Morphology. J. Biomater. Appl. 19 (2005) pp. 237.

11.2 General references

Paper 1: References from [1] to [110]

Paper 2: References from [1] to [86]

Paper 3: References from [1] to [7]

Paper 4: References from [1] to [6]

Paper 5: References from [1] to [19]

Paper 6: References from [1] to [16]

Paper 7: References from [1] to [10]

Paper 8: References from [1] to [16]

Paper 9: References from [1] to [11]

Paper 10: References from [1] to [28]

12. Appendix

Table 1. Starting spraying parameters:

Plasma Intensity / stand-off distance [A/mm]	Ar/H_2 flow ratio	Carrier gas / Feeder [l/g]	Gun Velocity [mm/s]	Plasma temp. [° C]
6-8	2-3	3-4	400-600	~$11{,}5 \cdot 10^3$

Table 2. Constant spraying parameters (Paper 3):

Number of cycles	Ar/H_2 flow ratio	Carrier gas / Feeder [l/g]	Gun Velocity [mm/s]
4	2-3	3-4	400-600

Table 3. Parameters in the factorial design of experiments (Paper 3):

Nomenclature	Plasma Intensity / stand-off distance [A/mm]
1A, 2A	5,5-6
1B,2B	5-5,5
1C, 2C	4,5-5
1D, 2C	4-4,5

Table 4. Parameters in the factorial design of experiments, studying Ar/H_2 ratio (Paper 3):

Plasma Intensity / stand-off distance [A/mm]	Ar/H_2 flow ratio	Carrier gas / Feeder [l/g]	Gun Velocity [mm/s]	Plasma temp. [° C]
4-4,5	2-6	3-4	400-600	~$11,8 \cdot 10^3$
4-4,5	4-9	3-4	400-600	~$12,2 \cdot 10^3$
4-4,5	8-12	3-4	400-600	~$12,7 \cdot 10^3$
4-4,5	35-45	3-4	400-600	~$13,0 \cdot 10^3$

Table 5. Spraying parameters (Paper 4):

Plasma Intensity / stand-off distance [A/mm]	Ar/H_2 flow ratio	Carrier gas / Feeder [l/g]	Gun Velocity [mm/s]	Plasma temp. [° C]
4-4,5	35-45	3-4	600-800	~$13,0 \cdot 10^3$

Table 6. Spraying parameters (Paper 5):

Plasma Intensity / stand-off distance [A/mm]	Ar/H_2 flow ratio	Carrier gas / Feeder [l/g]	Gun Velocity [mm/s]	Plasma temp. [° C]
4-4,5	35-45	3-4	600-800	~$13,0 \cdot 10^3$
2,5-3	35-45	5,5-6	400-600	~$13,0 \cdot 10^3$

*Substrates were cooled with N_2.

Table 7. Constant spraying parameters (Paper 6):

Plasma Intensity [A]	Ar/H_2 flow ratio	Carrier gas / Feeder [l/g]	Gun Velocity [mm/s]
400-600	35-45	3-4	1000-1200

Table 8. Parameters in the factorial design of experiments (Paper 6):

Nomenclature	Stand-off distance / Number of cycles [mm]
1A, 2A	24-28
1B,2B	18-22
1C, 2C	12-16
1D, 2C	8-12

Table 9. CGS spraying conditions for embedding TiO_2 particles onto aluminium.

Temperature / Pressure [° C/bar]	Stand-off distance [mm]	Substrate preparation	N_2 velocity [m/s]
18-20	10-40	Polished	1132

Table 10. CGS spraying conditions for deposition TiO_2 particles APS TiO_{2-X} bond coat.

Material	Temperature / Pressure [° C/bar]	Stand-off distance [mm]	Substrate preparation	N_2 velocity [m/s]
nano-TiO_2 (Blend D)	25-27	10-40	APS TiO_{2-x}	830

Table 11. CGS spraying conditions for nano-TiO_2 and copper (Paper 7).

Material	Temperature / Pressure [° C/bar]	Stand-off distance [mm]	Substrate preparation	N_2 velocity [m/s]
nano-TiO_2	25-27	10-40	APS TiO_{2-x}	830
Copper	13-15	10-40	Grit-blasted	1010

Table 12: Starting spraying conditions for depositing nano-TiO_2 (C426-D) and copper powder.

Temperature / Pressure [° C/bar]	Stand-off distance [mm]	Substrate preparation
28-30	10-30	Grit-blasted
24-26	10-30	Grit-blasted
22-24	10-30	Grit-blasted
20-22	10-30	Grit-blasted
19-21	10-30	Grit-blasted
18-20	10-30	Grit-blasted
17-19	10-30	Grit-blasted

Table 13. Titanium particles onto PEEK substrates (Paper 9).

Temperature / Pressure [° C/bar]	Stand-off distance [mm]	Gun velocity [mm/s]	N_2 velocity [m/s]
16-18	10-40	250-500	1010

Table 14. Titanium particles onto PEEK substrates (Paper 9,10).

Temperature / Pressure [° C/bar]	Stand-off distance [mm]	Gun velocity [mm/s]	N_2 velocity [m/s]
20-22	10-40	100-250	941

Resum

Recobriments d'òxid de titani obtinguts per Projecció Tèrmica i la seva aplicació funcional.

1. Consideracions inicials

La principal motivació d'aquesta Tesi es basa en obtenir superfícies funcionals d'òxid de titani mitjançant Atmospheric Plasma Spray (APS) i Cold Gas Spray (CGS). Recobriments amb aquesta composició han estat habitualment dipositats a través d'aquestes tecnologies aplicant-los com a superfícies passives, on el seu principal rol consistia en protegir un substrat contra fenòmens d'abrasió, erosió o corrosió. En canvi, també és possible produir superfícies actives de TiO_2, és a dir, recobriments que en certes condicions puguin donar una determinada resposta.

Per tal d'identificar les llacunes en la recerca realitzada per altres centres i portar a terme línies de treball interessants que contribueixin a l'estat de l'art, es va realitzar una gran revisió bibliogràfica. Com a conclusió, es va trobar un especial interès en: 1) l'ús de recobriments de sub-òxid de titani obtinguts per APS com elèctrodes; 2) la fabricació de recobriments nano-estructurats d'anatasa mitjançant CGS per la seva aplicació com a foto-catalitzadors i; 3) implants biomèdics. Addicionalment, en el començament del doctorat es va proposar produir la capa activa d'un sensor de gasos d'òxid metàl·lic mitjançant APS i TiO_2 com a matèria prima. Per tant, es va realitzar una segona revisió bibliogràfica centrada en quins son els mecanismes principals de detecció de gasos d'aquests dispositius, les tècniques d'obtenció de capes sensibles més utilitzades i la capacitat de resposta d'aquestes. Així doncs, la recerca d'aquesta Tesi va girar al voltant de les 4 principals aplicacions a desenvolupar: 1/ Elèctrodes per a bateries; 2/ Sensors de gasos; 3/ Foto-catalitzadors i; 4/ Aplicacions biomèdiques.

2. Objectius

Per tal d'obtenir capes actives en les aplicacions anteriorment esmentades, els següents objectius varen ser assolits:

1. Estudiar els resultats més importants obtinguts per altres autors pel que fa a la fabricació de capes actives de TiO_2 mitjançant tècniques de Projecció Tèrmica. Establir noves oportunitats.

2. Revisar la fabricació de sensors de gas d'òxid metàl·lic i la possibilitat de produir-los a través de tecnologies de Projecció Tèrmica i a partir de TiO_2.

3. Entendre els mecanismes involucrats en la detecció de gasos i la possibilitat d'arribar a respostes comercials a través de tecnologies de Projecció Tèrmica i a partir de TiO_2.

4. Fabricar recobriments de TiO_2 mitjançant APS i estudiar transformacions de fases no desitjades.

5. Potenciar les propietats elèctriques dels recobriments de sub-òxid de titani sobre rajoles ceràmiques.

6. Recobrir substrats d'acer inoxidable i estudiar el seu comportament en bateries simulades.

7. Recobrir materials comercials estàndards com làmines fines d'acer inoxidable i d'alumini, materials compostos de polímer-carboni i escumes de níquel.

8. Estudiar la fabricació de sensors d'òxid metàl·lic sobre polímer fi i flexible a través d'APS i utilitzant TiO_2 com a matèria prima. Evitar la degradació tèrmica del polímer.

9. Desenvolupar una geometria superficial i disposició del recobriment APS que permeti certa flexibilitat. Testar la resposta del gas davant gas i radiació.

10. Estudiar pols nano-estructurades d'anatasa dissenyades per ser utilitzades per CGS.

11. Preparar mescles de pols nano-TiO_2 amb pols de Cu. Estudiar la seva fluïdesa i utilitzar-les mitjançant CGS. Potenciar la presència d'anatasa a la superfície del recobriment.

12. Recobrir tubs d'acer inoxidable i estudiar la degradació de toluè en fase gasosa.

13. Preparar mescles de pols nano-TiO_2 amb pols micro-TiO_2. Estudiar la seva fluïdesa en l'equip CGS i utilitzar diversos substrats.

14. Recobrir tubs d'acer inoxidable i estudiar la degradació de fenol i àcid fòrmic en fase aquosa.

15. Recobrir polímers biocompatibles amb l'objectiu d'augmentar la seva bioactivitat. Estudiar el comportament de les cèl·lules vives sobre el material.

3 Procediment experimental

3.1 Atmospheric Plasma Spray

En la projecció tèrmica per plasma atmosfèric, l'ús d'un arc elèctric d'alta intensitat genera un plasma d'alta temperatura que escalfa i accelera partícules de pols cap a un substrat amb l'objectiu de formar un recobriment. Com s'aprecia en la figura 1, la pols s'injecta radialment, es disposa d'un sistema de refrigeració per aigua i els cabals s'injecten de forma axial fluint a través de l'arc elèctric on es genera el plasma fins sortir de la pistola.

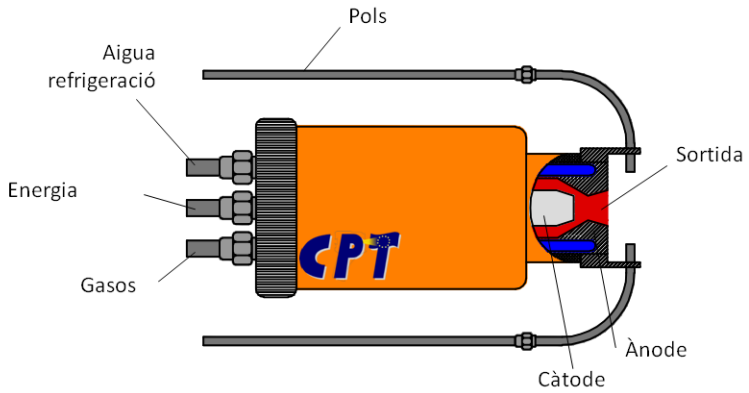

Fig. 1. Esquema de la pistola de APS amb els punts més significatius del procés.

Es pot operar amb diferents composicions de gasos per a formar el plasma, com Ar o bé mescles de Ar+H_2, Ar+He o bé Ar+H_2+He. En la present tesi es varen emprar argó i hidrogen per a la formació del plasma. La variació en les condicions del feix degut a diferents composicions dels gasos per plasma, genera un rang d'interaccions diferents amb les partícules.

S'ha emprat un sistema de detecció de temperatura i velocitat de partícula en el "temps de vol" conegut com Oseir Spraywatch 3.1® . Aquest utilitza una càmera per crear imatges digitals de l'aspersió de les partícules a partir de milers de petits fotodetectors que cobreixen un determinat volum d'espai. Les imatges son preses en temps de exposició molt curts per poder detenir les partícules a alta velocitat i processar-les mitjançant un software informàtic. Aquest identifica individualment les partícules en les imatges mesurant la posició, direcció, temperatura i velocitat.

3.2 Cold Gas Spray

Per altre banda, Cold Gas Spray no requereix altes temperatures per a dipositar partícules de pols i formar un recobriment. Les partícules queden adherides sobre la superfície del substrat degut a la seva deformació plàstica en el impacte. Aquesta tecnologia permet accelerar la pols a elevades velocitats i assegurar la deformació plàstica de materials durs com el titani. La figura 2 indica un esquema de la pistola.

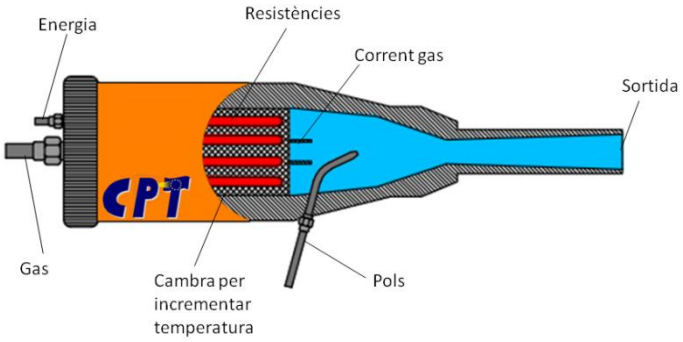

Fig. 2. Esquema de la pistola de CGS.

4. Òxids de titani

El diòxid de titani cristal·litza en tres principals estructures: anatasa, rútil i brookita. Aquest material és habitualment utilitzat com a capa protectora de substrats fàcilment oxidables degut al seu baix cost i alta estabilitat química. L'anatasa i el rútil han sigut fases molt aplicades com a foto-catalitzadors a

causa de la gran capacitat que tenen de generar el parell forat-electró al ésser irradiades amb llum UV. La figura 3 mostra el diagrama de fases, les fases reduïdes també estan incloses.

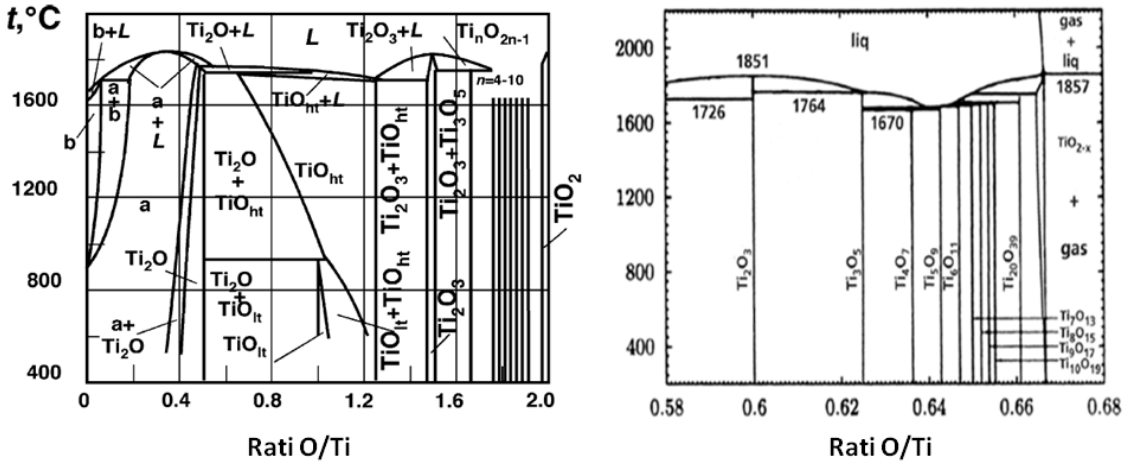

Figura 3. Esquerra: diagrama de fases del sistema Ti-O. Dreta: fases reduïdes del TiO_2.

El rútil té una gran capacitat d'acumular vacants d'oxigen en la seva estructura. Això comporta la creació d'un nivell donador a la banda de conducció, és a dir, un increment de la conductivitat elèctrica del sòlid. La taula 1 recopila els valors de resistivitat elèctrica per al TiO_2 i els òxids reduïts. Estequiometries definides per sota del diòxid de titani son conegudes com fases de Magnéli (Ti_nO_{2n-1}, n=4-10), on la resistivitat més baixa la té la fase Ti_4O_7. Diòxid de titani lleugerament reduït també conegut com sub-òxids de titani (TiO_{2-x}, $x < 10^{-2}$) també presenten resistivitats molt baixes essent per tant d'elevat interès.

Taula 1: Resistivitat elèctrica de TiO_2 i òxids reduïts.

Fase titani-oxigen	TiO_2	Ti_8O_5	Ti_6O_{11}	Ti_5O_9+Ti_6O_{11}	Ti_5O_9
Resistivitat [Ω·cm]	10^{13}	$4{,}0\cdot10^{-2}$	$1{,}6\cdot10^{-2}$	$2{,}0\cdot10^{-3}$	$1{,}6\cdot10^{-3}$

Fase titani-oxigen	Ti_4O_7+Ti_5O_9	Ti_4O_7	Ti_3O_5+Ti_4O_7	Ti_3O_5
Resistivitat [Ω·cm]	$3{,}0\cdot10^{-3}$	$9{,}7\cdot10^{-4}$	$2{,}4\cdot10^{-3}$	$1{,}6\cdot10^{-3}$

Així doncs, des del sistema Ti-O es possible arribar a diferents materials que poden ser de gran interès: i) eficients superfícies foto-catalítiques i; ii) material ceràmic amb baixa resistència elèctrica.

5. Resultats i discussió

A continuació es presenten els resultats més significatius de la tesi amb la pertinent discussió dividits en funció de la tècnica de projecció utilitzada.

5.1 Atmospheric Plasma Spray

5.1.2 Elèctrodes

a) Fabricació dels recobriments

- Substrats ceràmics

Inicialment, es va projectar pols d'anatasa. Es va observar que l' hidrogen utilitzat en la formació del plasma que accelera les partícules cap el substrat tenia la capacitat de reduir el diòxid de titani a sub-òxids de titani. Aquest fet, es poc desitjat quan es projecta TiO_2 mitjançant APS. No obstant, aquesta composició en forma de recobriment pot ser d'alt interès en aplicacions electroquímiques. Per tant, es va va projectar una pols basada en TiO_2 y certa quantitat de fases de Magnéli (figura 4) sobre substrats ceràmics amb l'objectiu de estudiar la dependència dels paràmetres de projecció sobre la resistivitat elèctrica del recobriment.

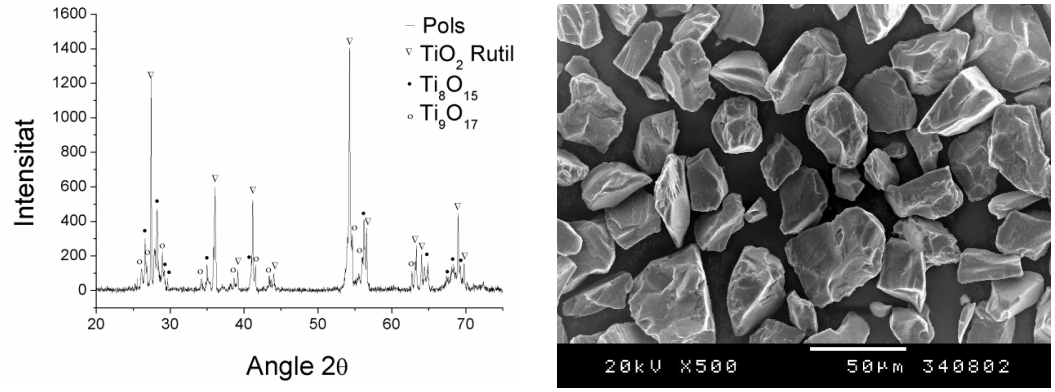

Figura 4. Esquerra: difractograma de raigs-X de la pols. Dreta: Micrografia SEM de la pols.

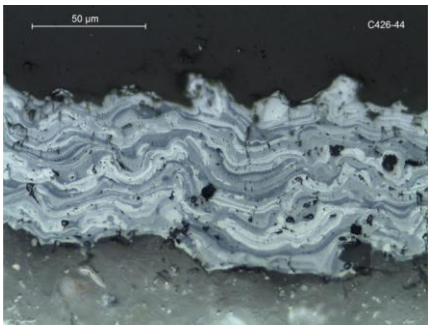

Figura 5. Secció transversal d'un recobriment APS TiO_{2-x} sobre substrat ceràmic.

Es va elaborar un disseny d'experiments per tal de conèixer la influència de intensitat del plasma i distància de projecció. Concretament, els nivells estudiats varen ser 4 per la distància de projecció (en nivell ascendent: 1A, 1B, 1C i 1D) i 3 per a la intensitat del plasma (2A, 2B i 2C).

Es va observar una forta dependència de les condicions de projecció amb el número d'esquerdes verticals en la secció transversal del recobriment. A més, la resistivitat elèctrica també es veia significativament afectada pel número

d'esquerdes. Per tant, la temperatura de la partícula va ser mesurada mitjançant l'equip Spraywatch correlacionant el número d'esquerdes i la resistivitat elèctrica de cada mostra. La figura 6 presenta els resultats.

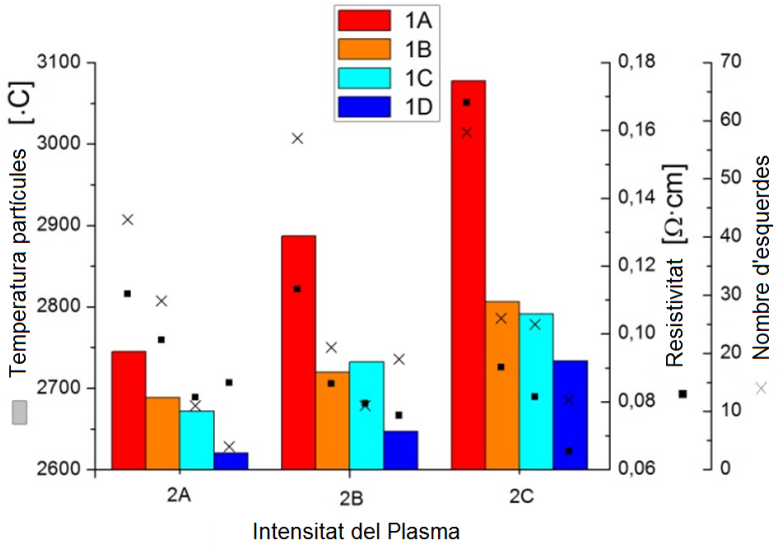

Figura 6. Temperatura de les partícules respecte les condicions de projecció. Número d'esquerdes i resistivitat associada a cada mostra.

A mesura que la temperatura de partícula decreix, també ho fa el número d'esquerdes i la resistivitat elèctrica. Això es deu a la diferència del coeficient d'expansió tèrmica del material ceràmic amb l'òxid de titani. A mesura que les condicions son més energètiques, la temperatura de les partícules creix. Al augmentar la temperatura de les partícules, la diferència en el coeficient d'expansió tèrmica fa que la tensió acumulada incrementi. Aquest fet comporta una quantitat d'energia que el material no pot acumular i la allibera en forma d'esquerdes. Finalment, aquestes actuen com a resistència a la corrent elèctrica, augmentant el valor de la resistivitat elèctrica. A partir d'aquí, la recerca es va centrar en buscar condicions menys energètiques que reduïssin el nombre d'esquerdes en la secció transversal de les mostres obtingudes.

Es va reduir la quantitat d'hidrogen present en el feix de plasma per tal de decréixer la temperatura. Es va aconseguir reduir la temperatura de les partícules i conseqüentment el número d'esquerdes. No obstant, el valor de la resistència elèctrica va decréixer. Aquest fet es va atribuir a que feixos amb menys quantitat d'hidrogen tenen menys capacitat de reduir el diòxid de titani a sub-òxid de titani. Per tant, la quantitat de vacants d'oxigen baixa i la resistivitat elèctrica puja. La figura 7 presenta les dades.

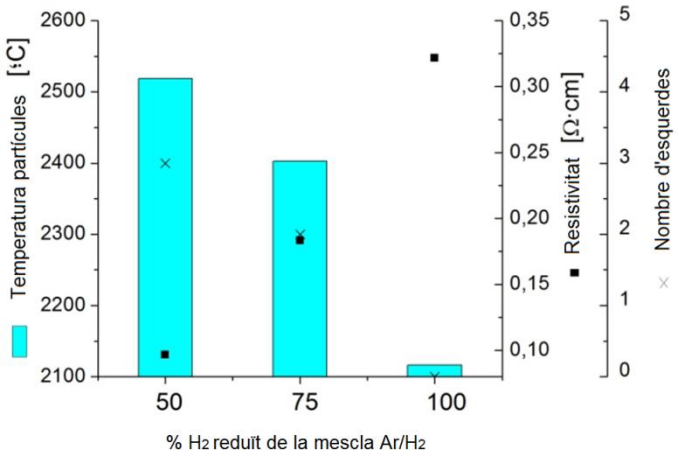

Figura 6. Temperatura de les partícules respecte les condicions de projecció. Número d'esquerdes i resistivitat associada a cada mostra.

- Substrats metàl·lics (acer inoxidable)

Després de comprovar la fabricació reproduïble i controlada de recobriments APS TiO_{2-x} amb resistivitats elèctriques de l'ordre de 0,33 Ω·cm, es va decidir recobrir substrats d'acer inoxidable ja que aquest material és emprat com elèctrodes en diferents dispositius electroquímics. Malauradament, la diferència del coeficient d'expansió tèrmica entre l'acer i el diòxid de titani és encara més pronunciada. Els primers resultats varen mostrar resultats molt pobres on els recobriments tenien una gran quantitat d'esquerdes. Per tal de mitigar aquest efecte, es varen buscar condicions menys energètiques partint dels òptims obtinguts en les projeccions sobre rajola ceràmica. Després de diferents proves,

s'utilitzà nitrogen com a refrigerant sobre el substrat. Aquest recurs dona la possibilitat de mantenir el substrat a una temperatura constant i més reduïda, fent decréixer la dilatació i contracció del material i reduint l'acumulació de tensions. A més, es va utilitzar una càrrega de matèria prima superior a l'anterior. Al haver-hi més quantitat de pols en el feix de plasma, la temperatura d'aquesta decreix. D'aquesta forma l'energia global del sistema es veu reduïda i també fa decréixer l'acumulació de tensions.

Les mostres obtingudes al aplicar aquestes variacions varen mostrar una bona adherència i seccions transversals lliures d'esquerdes. Diferents cicles es varen realitzar, la figura 7 mostra els diferents espessors.

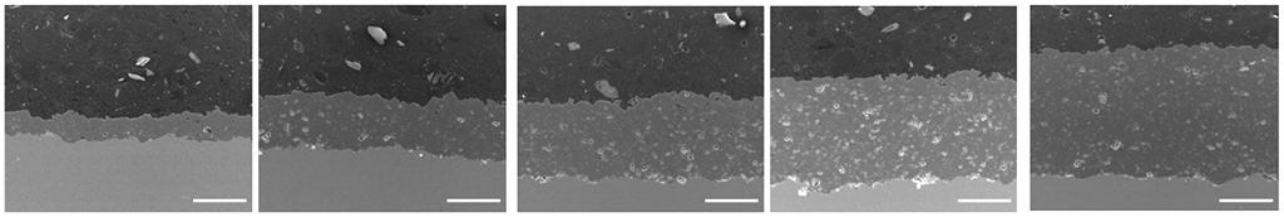

Figura 7. Mostres amb diferents espessors (l'escala representa 100 μm).

- Substrats basats en elèctrodes

Amb l'objectiu d'aproximar el més aviat possible els recobriments APS TiO_{2-x} a la aplicació real en bateries, es van utilitzar substrats estàndards utilitzats com elèctrodes. Concretament, aquests materials foren: i) làmines d'acer inoxidable; ii) làmines d'alumini; iii) material compost de polímer i carboni i; iv) escumes de níquel.

Per tal de recobrir les làmines d'acer inoxidable d'un gruix de 1 mm, es varen utilitzar les projeccions optimitzades obtingudes en els recobriments sobre substrats d'acer inoxidable gruixuts explicats en l'anterior secció (condicions d'alta energia, CAE). La rugositat fou de gran importància; va caldre augmentar la rugositat a través d'una etapa de granallat ja que les mostres obtingudes

sobre les làmines llises originals es descohesionaven completament. Un cop augmentada la rugositat, de nou la diferència dels materials al dilatar-se a causa del calor subministrat pel procés de projecció va comportar mostres amb gran quantitat d'esquerdes en la secció transversal. En aquest cas, per tal d'obtenir recobriments apropiadament adherits sobre els substrats, es va mantenir el nitrogen de refrigeració i s'utilitzaren distàncies de projecció més llargues (condicions de baixa energia, CBE). Al realitzar aquestes modificacions, CBE van recobrir amb èxit les làmines d'acer inoxidable i les d'alumini (figura 8).

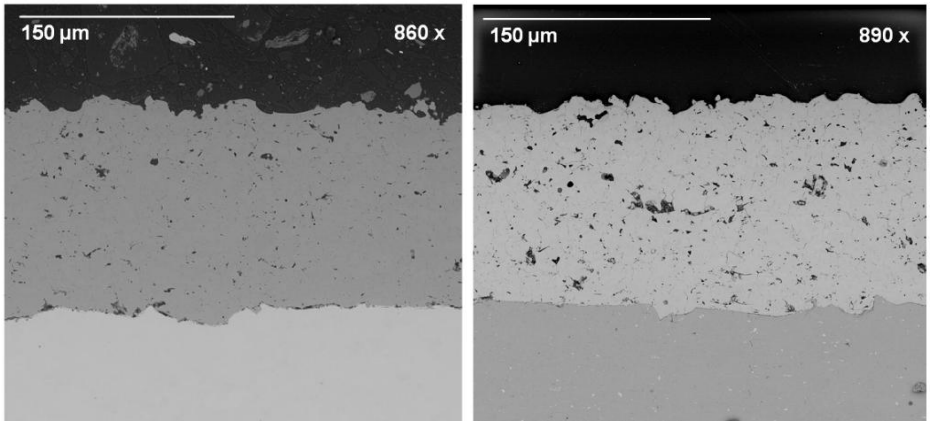

Figura 8. Esquerra: recobriment APS TiO_{2-x} sobre acer inoxidable. Dreta: recobriment APS TiO_{2-x} sobre alumini.

Pel que fa els compostos de polímer-carboni, augmentar la rugositat fou una etapa crítica. Aquests substrats tenen una naturalesa molt fràgil i el procés de granallat es massa agressiu esquerdant i trencant les peces. Es va tenir que granallar a baixa pressió per generar certa rugositat. Posteriorment es va tornar a projectar la pols mitjançant APS utilitzant els paràmetres CBE aconseguint recobriments ben adherits sobre els substrats (figura 9)

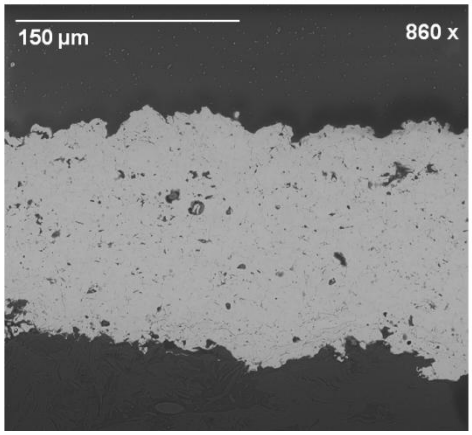

Figura 9. Recobriment APS TiO_{2-x} sobre el compost de polímer i carboni.

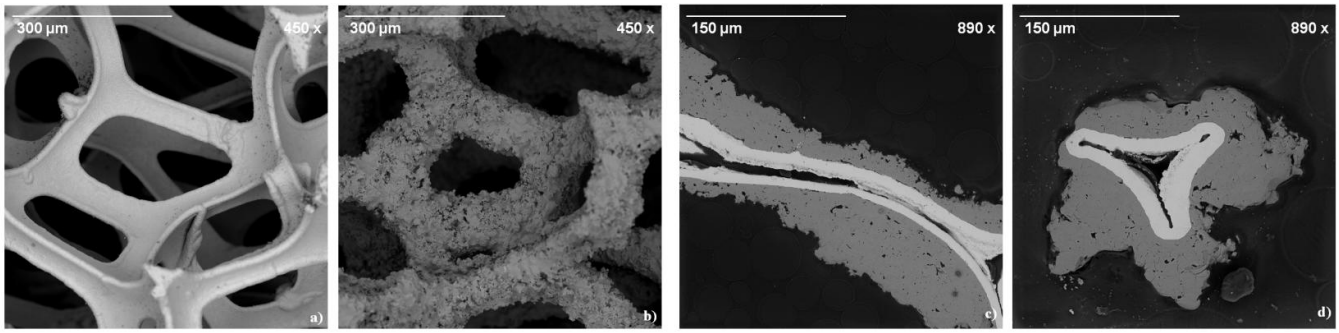

Figura 10. a) escuma original, b) escuma recoberta. c),d) seccions transversals dels filaments recoberts.

L'escuma de níquel va presentar moltes dificultats en relació a la subjecció dels substrats sobre el suport. Els filaments que composen l'escuma son molt delicats i agafar amb força la peça la deforma. Arribant a una subjecció adequada i utilitzant els paràmetres CBE de nou es va recobrir aquest substrat obtenint bons resultats. Al projectar per ambdós costats de l'escuma va ser

possible recobrir completament els filaments. La figura 10 mostra l'escuma original i la recoberta.

El fet d'aconseguir un recobriment al voltant del filament es atribuït al següent procés. Les partícules foses impacten sobre el filament i es divideixen en d'altres més petites desviant la seva trajectòria. Aquestes s'adhereixen sobre els laterals dels filaments i es solidifiquen. Al donar la volta al substrat i repetir el procés és possible obtenir un recobriment que envolti tot el filament.

b) Propietats i característiques fonamentals

La resistivitat elèctrica fou un paràmetre a optimitzar constantment durant l'obtenció de recobriments APS TiO_{2-x} per la seva aplicació com elèctrodes. Els valors corresponents als diferents materials recoberts es presenten en la figura 11. Com s'observa, la resistivitat elèctrica més elevada es va trobar en les mostres obtingudes sobre rajola ceràmica, mentre que la més baixa es va obtenir al recobrir la làmina fina d'acer inoxidable. Evidentment les propietats del substrat varen condicionar aquestes mesures, fent que la conductivitat global del sistema augmenti a mesura que la conductivitat elèctrica del substrat incrementa.

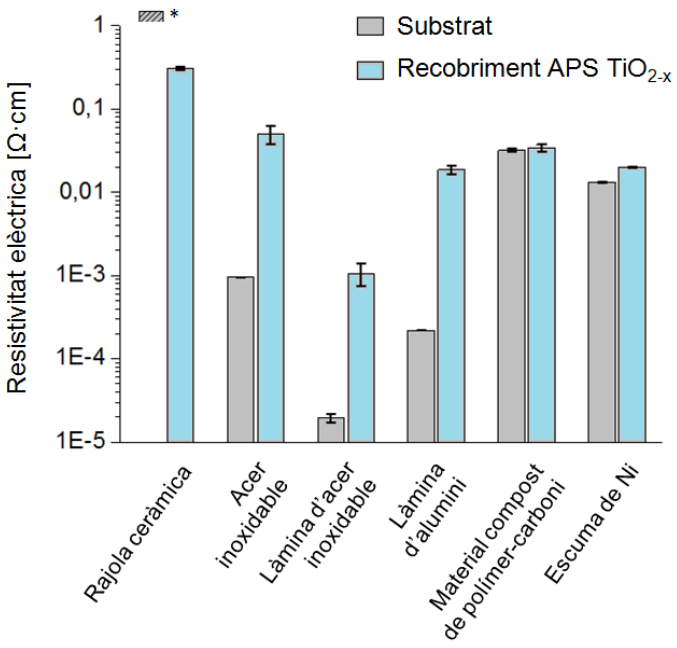

Figura 11. Resistivitat elèctrica dels recobriments APS TiO_{2-x} sobre els diferents substrats (*fora del rang de mesura).

A partir de l'estudi dels diferents paràmetres de projecció es pot assegurar que en els rangs analitzats la resistivitat elèctrica dels recobriments APS TiO_{2-x} decreix al reduir la temperatura de partícula, és a dir, reduir la intensitat del plasma, augmentar la distància de projecció i augmentar l'alimentació de la pols. Quan aquestes condicions es varen utilitzar, la tensió acumulada en el sistema substrat-recobriment fou inferior, la propagació d'esquerdes va disminuir i la resistivitat elèctrica va decréixer.

c) Resposta funcional

Es va estudiar el comportament com elèctrode dels recobriments obtinguts sobre acer inoxidable gruixut. Voltamogrames cíclics es van dur a terme per tal d'observar la limitació del potencial elèctric aplicat en els recobriments causada per l'evolució d'hidrogen i d'oxigen en diferents medis com àcid sulfúric, àcid

metansulfònic i hidròxid de potassi. A continuació es presenten les corresponents corbes (figura 12).

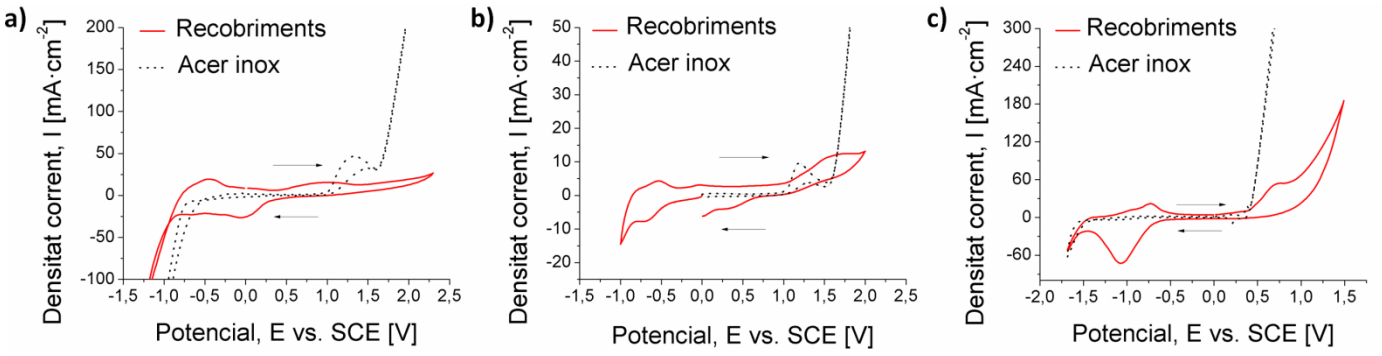

Figura 12. Voltametries cícliques d'elèctrodes d'acer inoxidable recoberts per APS TiO_{2-x} i elèctrodes originals en a) àc. Sulfúric, b) àc. Metansulfònic i c) hidròxid de potassi.

Els resultats mostren un augment en el potencial aplicat al recobrir els elèctrodes d'acer amb les capes d'APS TiO_{2-x}. El fet de poder augmentar el potencial evitant l'evolució d'hidrogen i d'oxigen és un resultat significatiu ja que permet augmentar la potència de la bateria. Addicionalment, es va analitzar el comportament dels recobriments sobre làmines fines d'alumini.

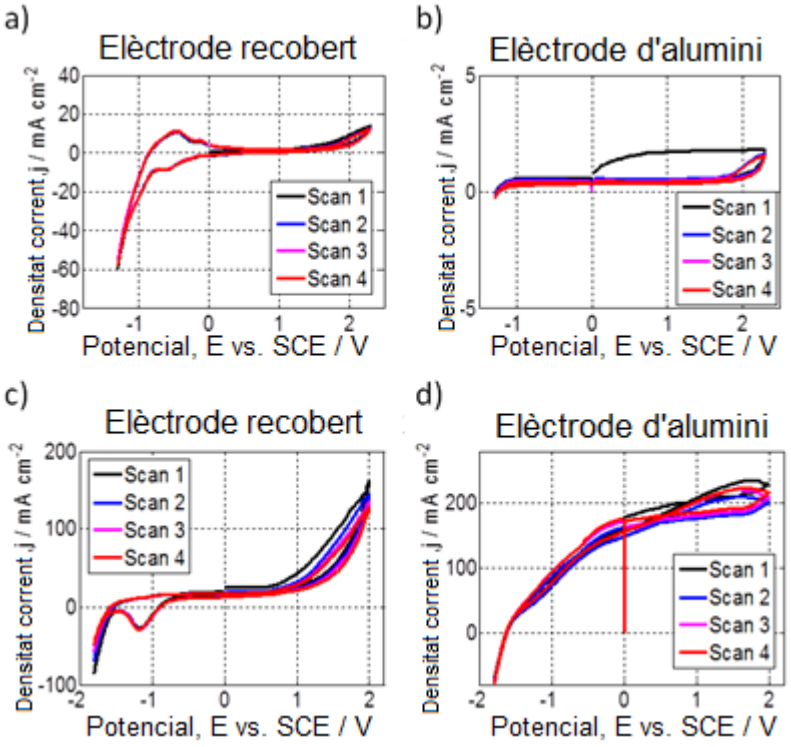

Figura 13. Voltametries cícliques d'elèctrodes d'alumini recoberts per APS TiO_{2-x} i elèctrodes originals en a) àc. Sulfúric, b) àc. Metansulfònic i c) hidròxid de potassi.

5.1.2 Sensors de gasos

a) Fabricació dels recobriments

Per tal d'aportar i contribuir més a l'estat de l'art referent als sensors de gasos basats en una capa activa d'òxid metàl·lic, es va decidir dipositar el recobriment sobre una làmina polimèrica de 50 µm de gruix molt utilitzada en circuits electrònics flexibles. Les primeres projeccions varen partir dels paràmetres CBE utilitzats en els recobriments sobre elèctrodes. No obstant, el polímer va quedar totalment degradat. Aquest inconvenient es va resoldre al augmentar les

distàncies de projecció, obtenint recobriments ben adherits i evitant la degradació del substrat.

b) Propietats i característiques fonamentals

Obtenir una capa activa de TiO_2 mitjançant APS que pugui permetre certa flexibilitat al sistema sense descohesionar-se i tingui una bona sensibilitat és un objectiu prou complex. Un número elevat de cicles produeix recobriments amb massa gruix i es trenquen al flexionar el substrat. Per altre banda, a mesura que es redueix el nombre de cicles es troben zones no recobertes en el recobriment fins que arribat cert valor no es disposa de contacte elèctric entre els elèctrodes del sensor. En canvi, números intermedis de cicles van aportar contacte elèctric entre elèctrodes i el fet d'intercalar zones recobertes amb zones sense recobrir va suposar obtenir una disposició geomètrica que aportava flexibilitat al dispositiu. La figura 14 mostra la secció transversal i micrografia superficial del recobriment on s'observa l'heterogeneïtat de la mostra.

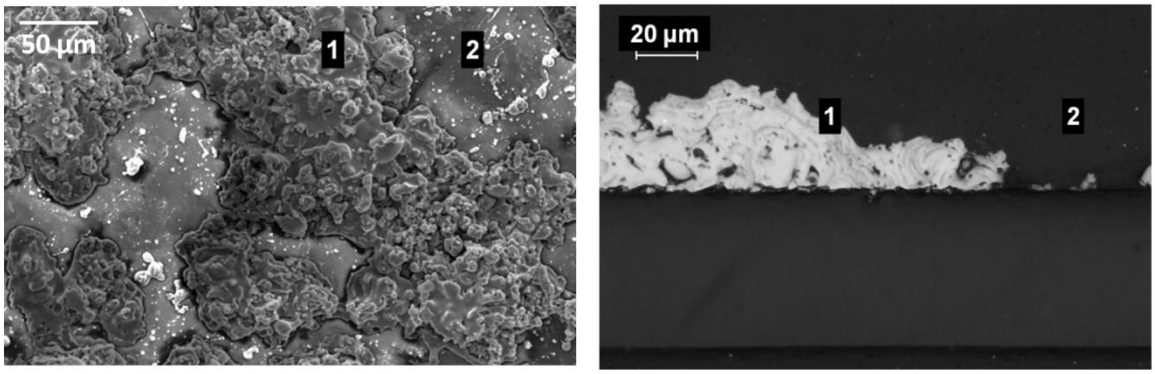

Figura 14. Esquerra: superfície de la mostra. Dreta: secció transversal del recobriment.

En aquesta aplicació la composició del recobriment també juga un paper fonamental. De la mateixa forma que en el cas dels elèctrodes, els recobriments

dipositats per APS estaven basats en rútil amb gran quantitat de vacants d'oxigen. La figura 15 mostra l'espectre Raman del recobriment comparat amb pols de rútil.

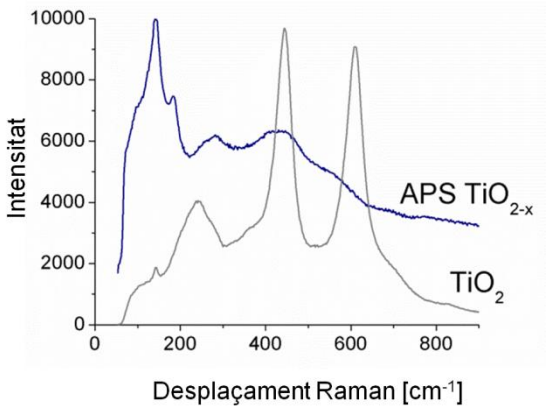

Figura 15. Espectres Raman del recobriment i del rútil.

c) Resposta funcional

El motiu pel qual es va decidir fer ús de recobriments de sub-òxid de titani obtinguts per APS com la capa activa d'un sensor de gasos fou de nou l'existència de gran quantitat de vacants d'oxigen en la superfície del material. Tot i no ser un material nano-estructurat, motiu pel que la funció transductor es veu reduïda, les vacants d'oxigen incrementen la funció receptor del sensor. Cada vacant actua com un centre d'adsorció de les espècies reactives gasoses i del gas objectiu. A més, la porositat del material fa augmentar la superfície específica del sòlid, incrementant la interacció del recobriment funcional amb l'ambient. Es va analitzar la resposta del recobriment APS TiO_{2-x} obtingut sobre el polímer en front de NH_3 gas i els resultats varen mostrar respostes positives i reproduïbles des de 10 fins 100 ppm (figura 16)

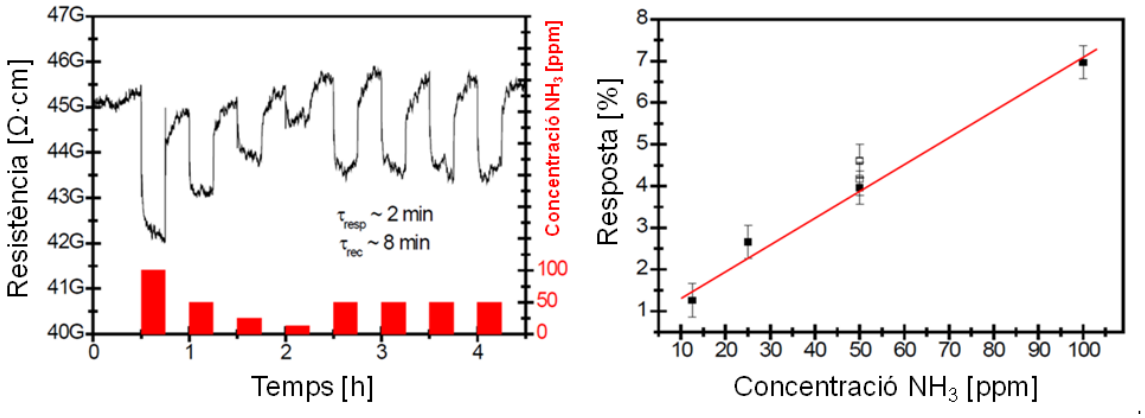

Figura 16. Resposta a diferents i constants concentracions.

5.2 Cold Gas Spray

5.2.1 Foto-catalitzadors

a) Fabricació dels recobriments

Es va utilitzar una pols nano-estructurada d'anatasa (C426-D) dissenyada per ser dipositada mitjançant CGS. Les primeres proves van ratificar que la pols s'adheria satisfactòriament sobre substrats d'acer en els que prèviament s'havia projectat APS TiO_{2-x}. No obstant, C426-D obturava els conductes del sistema d'alimentació a causa de la gran capacitat d'aglomerar-se fent impossible el seu ús com a matèria prima en aquesta tecnologia. Per tal de resoldre aquest inconvenient, es va mesclar aquesta pols amb pols de Cu comportant els següents resultats: i) la pols de Cu amb bona fluïdesa aconseguia arrossegar la pols nano-TiO_2 sense obturar el sistema d'alimentació i; ii) el coure actua com agent plàstic a l'impactar i afavoreix l'adhesió de les partícules dures d'òxid sobre el substrat. Les mescles van ser al 50% Vol. (mescla A) i 30% Vol de Cu (mescla B).

Les primeres probes projectant C42-D mentre la pols va fluir van mostrar que les partícules nano-estrucutrades d'anatasa s'adherien en condicions energètiques relativament baixes. En canvi, el coure que és habitualment molt emprat en CGS, utilitza condicions energètiques intermèdies. Per tant, es van

optimitzar els paràmetres buscant un òptim entre ambdós condicions de projecció. Finalment, es va aconseguir formar un recobriment en el que les partícules d'anatasa eren presents a la superfície de la capa formada en algunes condicions, assegurant el procés foto-catalític (figura 17).

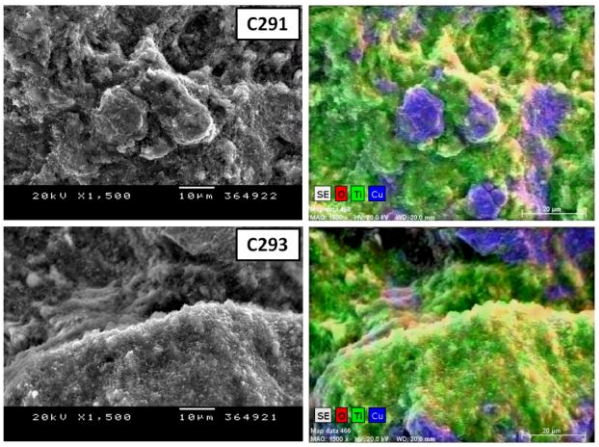

Figura 17. Superfície del recobriment CGS Cu/nano-TiO_2 referent a les mostres C291 i C293 (verd: TiO_2, blau: Cu).

Per altre banda, també es va mesclar la pols C426-D amb pols micro-estructurada de TiO_2. Les mescles van ser al 50% Vol. (mescla C) i 30% Vol de micro-TiO_2 (mescla D).De nou, la pols resultant va fluir adequadament sense obturar els conductes que van des l'alimentació fins a la pistola CGS. Es va utilitzar un substrat d'acer inoxidable prèviament recobert amb una capa de APS TiO_{2-x} amb l'objectiu de maximitzar l'afinitat de la pols amb el substrat en el impacte (figura 18). Tot i ser un procés on les partícules s'adhereixen en estat sòlid, fou possible produir un recobriment pur de nano-TiO_2. Tres diferents mecanismes poden explicar aquest fet: 1) les partícules nano-estructurades queden atrapades en la micro-textura de la superfície de la capa APS TiO_{2-x} i s'adhereixen degut a la difusió d'àtoms de la superfície de les partícules a la superfície de la capa de sub-òxid i entre les partícules. Aquest procés seria semblant al de la sinterització d'un material ceràmic. 2) Les partícules arriben a

un contacte íntim entre elles i amb el substrat i queden adherides per forces electrostàtiques sense enllaç químic. 3) Una combinació de tots dos; una de les hipòtesis de CGS es la possibilitat de micro-fusions de les partícules en el impacte. Per tant, és possible que les partícules arribin un contacte íntim entre elles i amb el substrat i tot tenint en compte l'energia alliberada en el impacte s'hi doni la difusió d'àtoms en la superfície dels materials. D'altre banda, algunes partícules quedarien adherides per forces electrostàtiques.

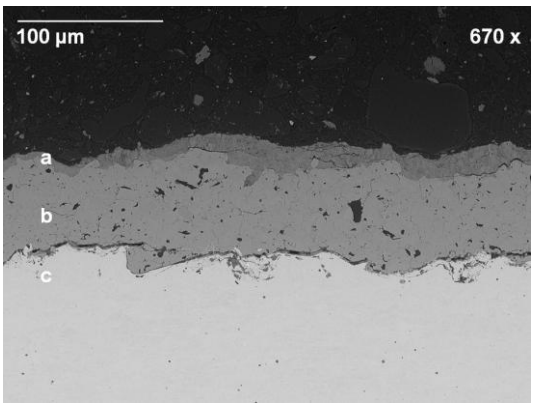

Figura 18. a) Recobriment CGS nano-TiO_2, b) capa APS TiO_{2-x} i c) acer inoxidable.

b) Propietats i característiques fonamentals

La característica fonamental a optimitzar en aquests recobriments fou la quantitat d'anatasa present a la superfície del recobriment, ja que és l'espècie responsable de dur a terme el procés foto-catalític (figura 19).

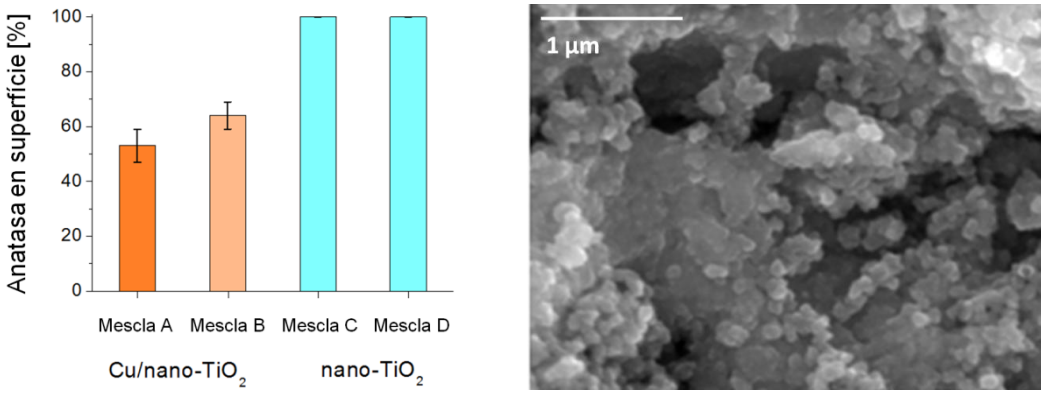

Figura 19. Esquerra: anatasa en superfície. Dreta: micrografia FE-SEM de l'anatasa nano-estructurada.

c) Resposta funcional:

Les figures 20 i 21 mostren respectivament la degradació de toluè en fase gasosa utilitzar en el recobriment CGS Cu/nano-TiO_2 y la degradació de fenol i àcid fòrmic al fer ús del recobriment CGS nano-TiO_2.

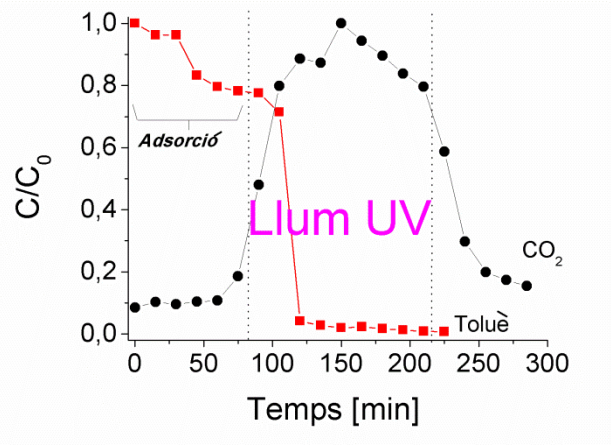

Figura 20: degradació de toluè.

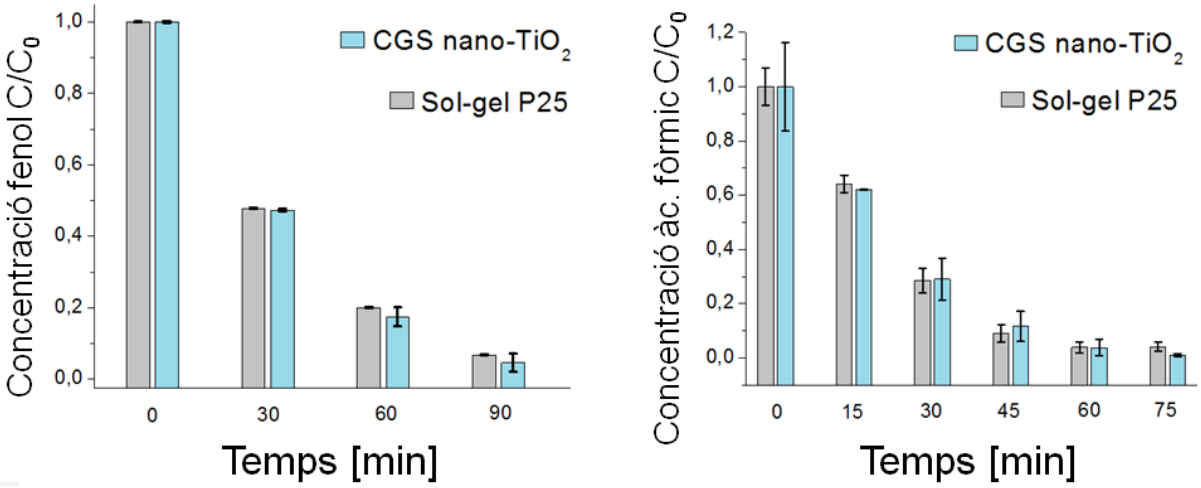

Figura 21: degradació de fenol (esquerra) i àc. Fòrmic (dreta), inclou comparació amb sol-gel P25®.

El toluè fou degradat amb menys de 30 min d'acció de llum UV i el recobriment va mostrar una gran capacitat d'adsorbir el contaminant en la seva superfície. Pel que fa fenol i àc. fòrmic el recobriment CGS nano-TiO_2 va superar la capacitat de degradació del recobriment sol-gel basat en l'estàndard comercial P25®.

5.2.2 Aplicacions biomèdiques

a) Fabricació dels recobriments

Es varen utilitzar substrats de PEEK (polyetheretherketone) com a polímers biocompatibles amb l'objectiu de recobrir-los de nano-TiO_2 mitjançant CGS per augmentar la seva bioactivitat. No obstant, no va ser possible dipositar la pols d'anatasa sobre aquest material. Per tant, es va utilitzar un altre material projectat prèviament per a facilitar l'adhesió de les partícules nano-TiO_2. En aquest cas, fou pols de Ti (figura 22). Posteriorment, es va projectar la pols nano-estructurada i es va repetir el procés observat en els recobriments emprats com

a foto-catalitzadors. Les partícules de TiO_2 quedaven atrapades en la superfície de la capa prèviament projectada.

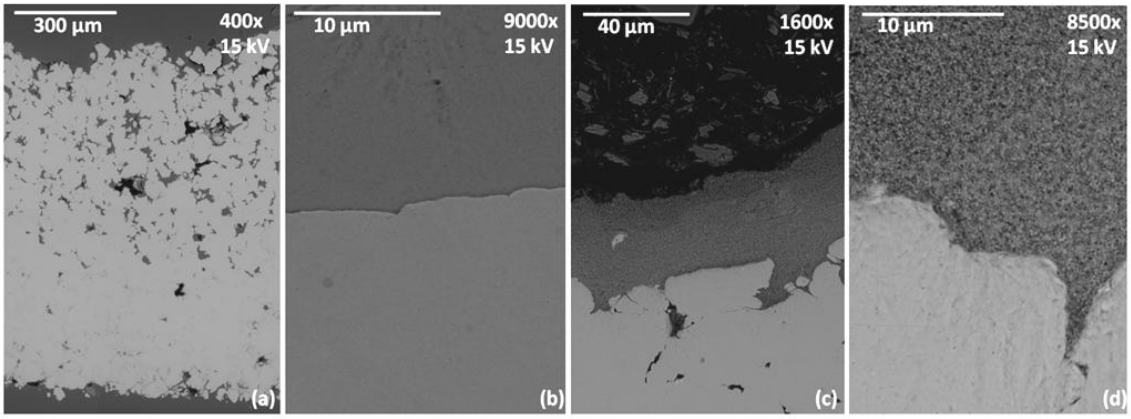

Figura 22: a) secció transversal Ti sobre PEEK i b) interfase. c) secció transversal TiO_2 sobre Ti i d) interfase.

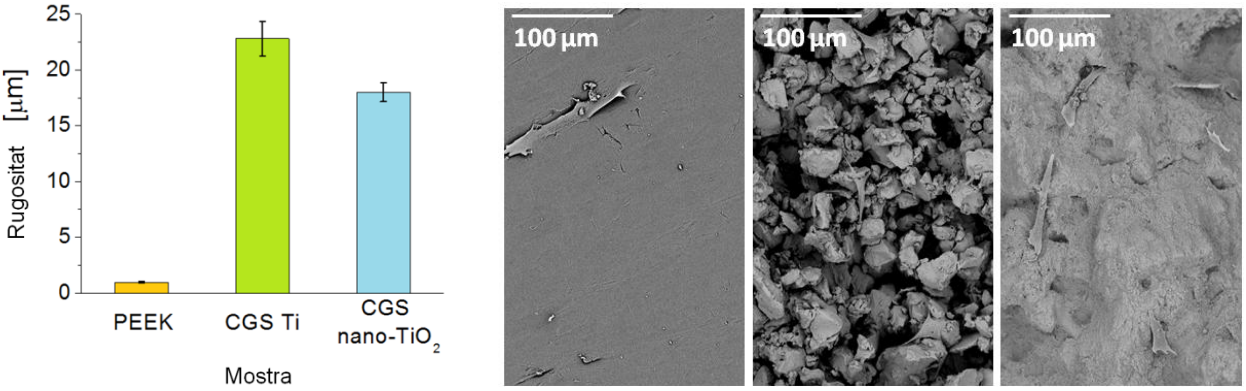

Figura 23. Esquerra: Rugositat dels diferents materials. Dreta: superfície de PEEK, CGS Ti and CGS nano-TiO_2.

b) Propietats i característiques fonamentals

En aquesta aplicació la rugositat fou d'especial interès ja que juga un paper clau en la interacció amb les cèl·lules (figura 23).

c) Resposta funcional

Es va mesurar la viabilitat, proliferació i diferenciació d'osteoblasts passats 1, 3 i 7 dies pel que fa el PEEK, CGS Ti sobre PEEK i finalment CGS nano-TiO_2 dipositat sobre el Ti. La figura 24 mostra l'evolució dels resultats. Passat 7 dies de cultiu cel·lular les mostres de polímer recobertes amb TiO_2 nano-estructurat milloren significativament el comportament del material en tots tres assajos. Aquests resultats s'atribueixen a la capacitat que té l'òxid metàl·lic nano-estructurat d'adsorbir proteïnes que posteriorment fomenten l'adhesió de les cèl·lules. El titani dipositat per CGS també va mostrar molt bons resultats. Cal dir que la biocompatibilitat del titani ve donada per la fina capa d'òxid que té a la superfície. Diferències entre ambdós materials podrien venir donades per l'efecte de la micro-rugositat i la nano-rugositat.

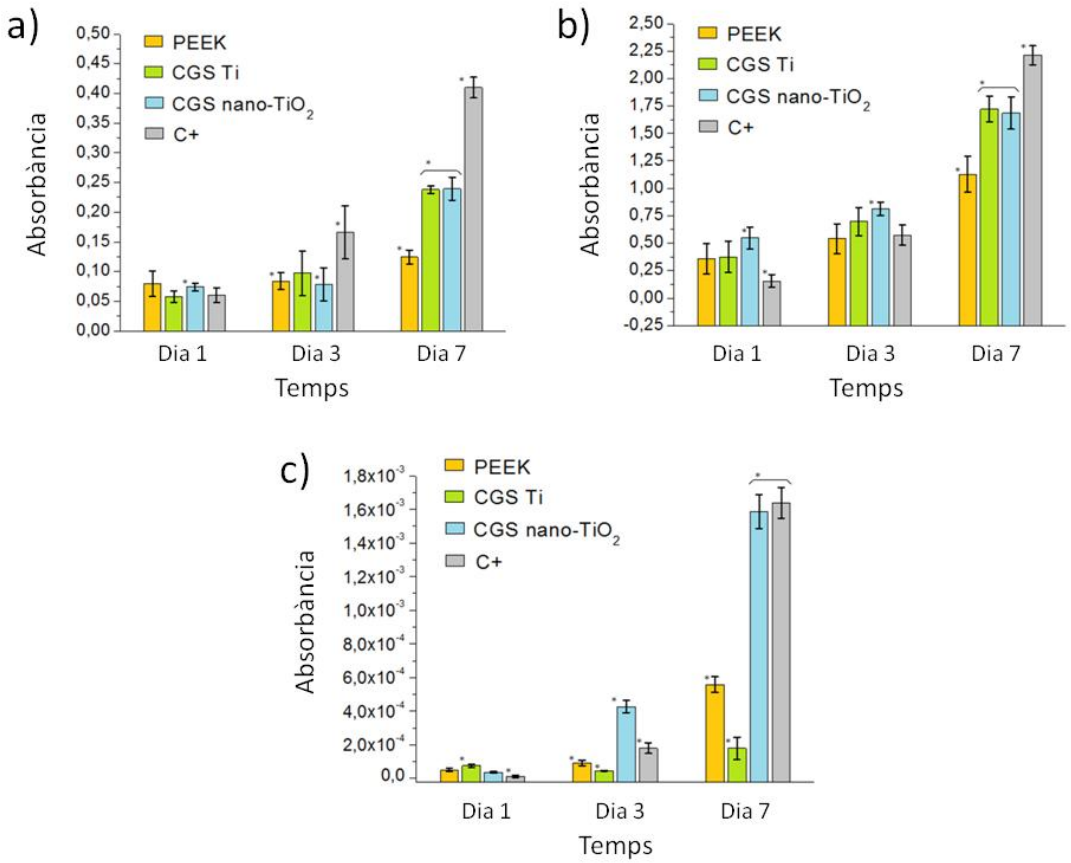

Figura 24. a) viabilitat cel·lular, b) proliferació cel·lular i c) diferenciació cel·lular. L'asterisc marca dades amb diferències significatives.

6 Conclusions

En la present Tesi, recobriments funcionals d'òxid de titani han sigut dipositats mitjançant Atmospheric Plasma Spray i Cold Gas Spray per la seva aplicació com elèctrodes per a bateries, sensors de gasos, foto-catalitzadors i implants. D'aquest estudi, s'obtenen les següents conclusions:

1/ Plasma ric en argó amb baix contingut d'hidrogen va tenir majors temperatures però menor capacitat de transferir energia a les partícules. Distàncies de projecció òptimes i intensitats de plasma varen reduir l'efecte de la

diferència en els coeficients d'expansió tèrmica (CET) entre el recobriment i el substrat ceràmic, resultant en una resistivitat elèctrica aproximadament des $1,7 \cdot 10^{-1}$ fins $6,0 \cdot 10^{-2}$ $\Omega \cdot$cm.

2/ L'efecte de la diferència del CET entre els substrats d'acer inoxidable i els recobriments APS TiO_{2-x} va ser adequadament reduït utilitzant nitrogen de refrigeració i tasses d'alimentació òptimes produint recobriments amb una adherència de fins 67 MPa sense la presència d'esquerdes en la secció transversal.

3/ Condicions d'energia baixes obtingudes a través de distàncies de projecció òptimes, van recobrir adequadament làmines fines d'acer inoxidable i alumini resultant en les resistivitats elèctriques més baixes de la tesi (aprox. 10^{-3} $\Omega \cdot$cm).

4/ Elèctrodes molt delicats com materials compostos de polímer i carboni van ser adequadament recoberts amb capes APS TiO_{2-x} sense fer malbé les peces.

5/ Recobriments APS TiO_{2-x} van ser adequadament dipositats sobre espumes de Ni; els filaments de l'escuma van ser completament recoberts.

6/ Acer inoxidable recobert amb capes APS TiO_{2-x} es van emprar com elèctrodes mostrant un increment en el voltatge aplicat respecte els substrats originals d' aproximadament 32%, 85% i 35% en àcid sulfúric, àcid metansulfònic i hidròxid potàssic respectivament.

7/ Films polimèrics flexibles van ser adequadament recoberts amb capes APS TiO_{2-x} pel seu ús com a sensors de gasos a través de distàncies de projecció òptimes que varen evitar la degradació del substrat. Nombres intermedi de cicles de projecció van permetre un sistema amb certa flexibilitat i contacte elèctric entre elèctrodes.

8/ Els recobriments APS TiO_{2-x} disposaven d'una gran quantitat de vacants d'oxigen que potencien la funció receptor, facilitant l'adsorció d'espècies reactives gasoses. A més, la porositat interna incrementa l'accés dels grans interns, que potencia la funció proximitat.

9/ Els recobriments APS TiO_{2-x} sobre el polímer flexible varen tenir una resposta positiva i reproduïble en front de NH_3 en concentracions des 12,5 fins a 100 ppm. A més, també va tenir resposta satisfactòria en front de radiació (λ = 365, 453, 530 nm).

10/ Pols nano-TiO_2 dissenyada per ésser dipositada per Cold Gas Spray (CGS) va ser mesclada amb coure i TiO_2 micro-estructurat per tal d'obtenir mescles amb bona fluïdesa evitant la obturació del sistema d'alimentació.

11/ Recobriments CGS Cu/nano-TiO_2 van ser adequadament dipositats sobre acer inoxidable; el coure va actuar com agent dúctil, facilitant l'adhesió de les partícules foto-actives dures en el impacte. A més, l'anatasa estava present a la superfície del recobriment, assegurant el procés foto-catalític.

12/ Recobriments CGS nano-TiO_2 van ser adequadament dipositats sobre substrats que varen tenir certa afinitat química i geometria superficial; recobriments APS TiO_{2-x} varen ser dipositats prèviament sobre acer inoxidable i les partícules nano-estructurades d'anatasa es varen veure atrapades en la rugositat superficial del recobriment APS.

13/ Recobriments CGS Cu/nano-TiO_2 tenen una gran capacitat d'adsorbir espècies gasoses i varen degradar completament 25 ppm de toluè després de irradiar el foto-catalitzador amb llum UV durant 30 minuts. Recobriments CGS nano-TiO_2 varen incrementar la capacitat de degradació dels foto-catalitzadors sol-gel basats en P25® en un 24% (90 min) i 71% (75 min) pel que fa respectivament la degradació (10 ppm) de fenol i àcid fòrmic.

14/ Recobriments de Ti ben adherits i de gran gruix varen ser dipositats sobre el polímer biocompatible PEEK (polyetheretherketone) utilitzant condicions de projecció que varen evitar estovar el polímer, afavorint la deformació plàstica de les partícules metàl·liques.

15/ Recobriments CGS nano-TiO_2 van ser dipositats sobre substrats PEEK els quals prèviament s'havien recobert amb Ti; les partícules nano-estructurades d'anatasa varen quedar adherides en la superfície rugosa del recobriment CGS Ti.

16/ Després de 7 dies cultius cel·lulars, les mostres de PEEK recobertes amb CGS nano-TiO_2 varen incrementar la viabilitat cel·lular, proliferació cel·lular i diferenciació cel·lular en aproximadament un 92%, 49% i 185% respectivament.

17/ A través d'aquesta tesi s'ha demostrat que les superfícies de sub-òxid de titani i diòxid de titani nano-estructurat obtingudes a través de Atmospheric Plasma Spray i Cold Gas Spray ofereixen un nou procediment per desbancar

convencionals tècniques en el desenvolupament d'elèctrodes, sensors de gasos i radiació, foto-catalitzadors i superfícies bioactives gràcies a la seva eficiència, baix cost, gran capacitat de producció, breus temps d'operació i característiques més tolerants amb el medi ambient.